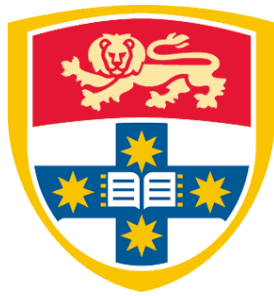


# **The development and applications of ceragenins and bone-binding antimicrobials to prevent osteomyelitis in orthopaedic patients**



THE UNIVERSITY OF  
**SYDNEY**

**Aiken DAO**

**A thesis submitted for the degree of Doctor of Philosophy in Medicine**

Kids Research, The Children's Hospital at Westmead  
Westmead Institute for Medical Research, Westmead Hospital  
Garvan Institute of Medical Research, St Vincent's Hospital  
Sydney Medical School, Faculty of Medicine and Health, University of Sydney

**2022**

# Certificate of Originality

I, Aiken Dao, hereby declare that this submission is my own work. To the best of my knowledge, it contains no materials previously published or written by another person, nor materials to which a substantial extent has been accepted for the award of any other degrees or diploma at Sydney Medical School, the University of Sydney, or any other educational institutes, except where due acknowledgement is made in this thesis. Any contribution made to the research by others whom I have worked with at the University of Sydney or elsewhere is explicitly acknowledged in the thesis.

I also declare that the intellectual content of this thesis is the product of my own work, except to the extent that assistance from others in the study design and conception or style, presentation and linguistic expression is acknowledged.

A handwritten signature in black ink, appearing to read 'Aiken', with a long horizontal flourish extending to the right.

**Aiken Dao**

# Declaration of Contributions

The work presented in this thesis was conducted during my full-time candidature to fulfil the Doctor of Philosophy (Medicine) requirements through the Sydney Medical School, Faculty of Medicine and Health, University of Sydney.

Unless otherwise stated, all experiments were conducted by me at the Orthopaedic Research and Biotechnology Unit, Kids Research, Children's Hospital at Westmead and other stated institutes.

I completed the drafting of published manuscripts included in this thesis and the thesis itself with guidance from my co-authors and supervisors (A/Prof Aaron Schindeler and Prof David Little). Initial experimental conception and thesis editing were conducted in conjunction with my supervisors. Our listed authors have approved all included publications presented in manuscript format.

The final thesis was proofread by my supervisors (A/Prof Schindeler and Prof Little) and several co-supervisors and colleagues, including Prof Paul Savage, Dr Behnam Akhavan, A/Prof Justin Beardsley, Dr Lucinda Lee, Dr Alexander Wykes, Dr Emily Vasiljevski, Dr Alexandra O'Donohue and Ms Helen Power.

A/Prof Schindeler wrote the initial project ethics, and I was involved in writing modifications and new applications thereafter with A/Prof Schindeler. Ethics were approved by the CMRI/CHW Animal Ethics Committee. All animal orders and maintenance were done with assistance from the transgenic animal facility's manager and technicians (Kids Research and Garvan Institute of Medical Research).

In Chapter 1, all literature reviews were conducted by me. Dr Rebecca Mills, A/Prof Michelle McDonald and my supervisors contributed to the substantive editing.

In Chapter 2, the animal surgeries were performed by me, Prof Little and Dr Justin Bobyn with the assistance of Dr Vasiljevski and Dr O'Donohue.

In Chapter 3, Dr Akhavan and his team (School of Physics, University of Sydney) completed the ion-assisted plasma polymerisation surface coating. Dr Bobyn and I completed animal surgeries. The supplementary data (Table 3.1 and Figures S3.1-S.3.3) were unpublished data from Mr Denis Sylvester for his honours project (2018). I contributed to the study design and data analysis. A/Prof Schindeler contributed to the conception of the study.

In Chapter 4, the synthesis of BBA-1 was conducted by Prof Savage (Brigham Young University) and Dr Sumedh Kamble (University of Sydney). Dr Bobyn and I conducted the animal surgeries. I developed the multiple myeloma-related bone infection animal models with A/Prof McDonald at the Garvan Institute of Medical Research. A/Prof Schindeler and A/Prof McDonald contributed to the conception of the study.

# Publications related to this thesis

Throughout this thesis, several reviews and studies have been published or are in the process of being peer-reviewed/published. These original publications are presented in manuscript format.

## Chapter 1 (Section 1.2): Review Article

**DAO, A.**, MILLS, R. J., KAMBLE, S., SAVAGE, P. B., LITTLE, D. G. & SCHINDELER, A. 2020. The application of ceragenins to orthopedic surgery and medicine. *J Orthop Res*, 38, 1883-1894.

## Chapter 1 (Section 1.3): Review Article

**DAO, A.**, MCDONALD, M. M., SAVAGE, P. B., LITTLE, D. G. & SCHINDELER, A. 2022. Preventing osteolytic lesions and osteomyelitis in multiple myeloma. *J Bone Oncol*, 37, 100460

## Chapter 2: Research Article

**DAO, A.**, O'DONOHUE, A. K., VASILJEVSKI, E., BOBYN, J. D., LITTLE, D. G. & SCHINDELER, A. 2023. Murine models of orthopedic infection featuring *Staphylococcus aureus* biofilm. *J Bone and Joint Infect* (Accepted)

## Chapter 3: Research Article

**DAO, A.**, GAITANOSI, C., KAMBLE, S., SHARIFAHMADIAN, O., TAN, R. P., WISE, S. G., CHEUNG, T. L. Y., BILEK, M., SAVAGE, P. B., SCHINDELER, A. & AKHAVAN, B. 2023. Antibacterial plasma polymer coatings on 3D materials for orthopedic applications. *ACS Applied Mat & Interfaces* (Submitted)



## Other publications not related to this thesis

Publications not related to the submission of this thesis, but to which I was a first/co-author during my candidature.

### Other Publications

KAMBLE, S., VALTCHEV, P., **DAO, A.**, PELRAS, T., ROGERS, M. J., SAVAGE, P. B., DEHGHANI, F. & SCHINDELER, A. 2021. Synthesis and Characterization of Bone Binding Antibiotic-1 (BBA-1), a Novel Antimicrobial for Orthopedic Applications. *Molecules*, 26.

MIRKHALAF, M., **DAO, A.**, SCHINDELER, A., LITTLE, D. G., DUNSTAN, C. R. & ZREIQAT, H. 2021a. Personalized Baghdadite scaffolds: stereolithography, mechanics and in vivo testing. *Acta Biomater*, 132, 217-226.

MIRKHALAF, M., GOLDSMITH, J., REN, J., **DAO, A.**, NEWMAN, P., SCHINDELER, A., WOODRUFF, M. A., DUNSTAN, C. R. & ZREIQAT, H. 2021b. Highly substituted calcium silicates 3D printed with complex architectures to produce stiff, strong and bioactive scaffolds for bone regeneration. *Applied Materials Today*, 25, 101230.

O'DONOHUE, A., **DAO, A.**, BOBYN, J., MUNNS, C. F., LITTLE, D. G., SCHINDELER, A. 2022. Modelling anabolic and anti-resorptive therapies for fracture healing in a mouse model of osteogenesis imperfecta. *J Orthop Res*, DOI: 10.1002/jor.25414.

**DAO, A.**, KIM, H. Y., GARNHAM, K., KIDD, S., SATI, H., PERFECT, J., SORRELL, T., HARRISON, ... ALFFENAAR, J-W., MORRISSEY, O., CHEN, S. C-A. & BEARDSLEY, J. 2023. *Med Myco*, Cryptococcosis — a Systematic Review to Inform the World Health Organization Priority List of Fungal Pathogens.

**DAO, A.**, KIM, H. Y., KIDD, S., HALLIDAY, C., ... SATI, H., ALFFENAAR, J-W., OLADELE, R., MORRISSEY, O., RICKERTS, V., BEARDSLEY, J. & ALASTRUEY, A. 2023. *Med Myco*, Histoplasmosis — a Systematic Review to Inform the World Health Organization Priority List of Fungal Pathogens.

PARAMBATH, S#, **DAO, A#.**, KIM, H.Y., ... ALFFENAAR, J-W. & BEARDSLEY, J. 2023. *Med Myco*, *Candida albicans* — a Systematic Review to Inform the World Health Organization Priority List of Fungal Pathogens.

MORRISSEY, O., KIM, H. Y., SATI, H., ... **DAO, A.**, ALFFENAAR, J-W. & BEARDSLEY, J. 2023. *Med Myco*, Mucorales — a Systematic Review to Inform the World Health Organization Priority List of Fungal Pathogens.

# Acknowledgements

I would like to gratefully acknowledge the assistance from several individuals and organisations who have contributed to the production of this thesis. First and foremost, I would like to thank my supervisors, Associate Professor Aaron Schindeler and Professor David Little, for their encouragement, patience, and advocacy during my term in the Orthopaedics Department at the Children's Hospital at Westmead. I appreciate that Aaron's leadership and criticism have provided invaluable guidance to my project and my development as an academic and medical researcher, whereas David's passion and experience in orthopaedic surgery have greatly inspired and influenced me to become a great physician and specialist in the future.

Recognition must also go to my co-supervisor at the Garvan Institute of Medical Research, Associate Professor Michelle McDonald, and our co-operators, Professor Paul Savage and Dr Behnam Akhavan. Without their contribution and support, this research project would not be possible. Also, I would like to offer general thanks to the University of Sydney, The Children's Hospital at Westmead, St Vincent's Hospital, the National Centre for Immunisation Research and Surveillance (NCIRS) and the World Health Organization (WHO) for the opportunities and their support for the scholarships, studentships, and employments during my doctoral candidature. Without them, my PhD completion would be impossible. Special thanks must also go to the original members of the Orthopaedic Research and the Bioengineering and Molecular Medicine (BAMM) team: Professor Craig Munns, Associate Professor Andrew Biggin, Dr Rebecca Mills, Dr Justin Bobyn, Dr Tegan Cheng, Dr Lucinda Lee, Dr Sumedh Kamble, Dr Emily Vasiljevski, Dr Alexandra O'Donohue, and Ms Hoai-Lan Mai. I benefited from their expertise and generous assistance throughout my candidature.

I would also thank Associate Professor Wendy Gold, Associate Professor Justin Beardsley, Professor Tania Sorrell, Professor Ben Marais, Dr Giselle Manalo, Dr Archana Koirala, Dr Rama Kandasamy, Professor Wieland Meyer, Associate Professor Mark Douglas and Associate Professor Nicholas Wood for their benevolent mentorships, inspiration, and support during the most challenging time of my study. And my appreciation to the nurses, Ms Lisa Paleyo, Ms Veronica Abruzzo, Ms Deidre Brogan, and our facility manager Ms Kim Hewitt. Working with them has been an honour and privilege, and I have learned much from them throughout the last few years.

In my personal life, I want to express my thankfulness to my best friends, Dr Jordan Gabriels, Dr Chin Goh, Dr Ben Varley, Dr Raed Altulayhi, Dr Patricio Munoz, Mr André Grech, Mr Rhett Marchant, Mr Gregory Dziaduch, Mr Jake Bozzo, Mr Alexander MacDonald, Mr Patryk Urban, Mr James Loveday, Mr Vasco Rocha, Mr Heron Chu, Mr Nathan Tam, Mr Oscar Chiu, Mr Sacca Antara, Mr Jeffrey Tandean, Mr Vincent Yang, Mr Sean Ji, Mr Kevin Chen, Mr Kelvin Kwun, and Mr Kent Kwun, for their tremendous support throughout my journey.

Finally, I thank my family for their care and support, especially my beloved younger brother, Alexandra Dao. Thank you, Alex, for being in my life. You are the best brother I could ever wish for, and I would share every moment of my success with you. And last, I express my deepest gratitude to my parents, grandparents, aunts and uncles, other siblings and cousins, and the rest of my family. I love them all for their lifetime of unconditional love and everything they have done and sacrificed for me.

# Abstract

Bone infection remains a high-burden disease in orthopaedic and trauma patients with fractures and implantations. Osteomyelitis is difficult to cure in clinical settings, especially if antimicrobial resistance or biofilm is involved, which may prolong the treatments with antibiotics and require multiple surgeries, severely affecting the patients' quality of life and mobility. Osteomyelitis can lead to osteonecrosis, septicaemia, amputation, multi-organ dysfunction, and death in severe cases.

Preclinical models are essential for efficacy testing to develop new prophylactic and therapeutic interventions. Previously bone infection models in rats involved fractures and implantations, making it complicated to perform. In this study, we have developed and optimised murine models with a tibial drilled hole (TDH) and needle insertion surgery (NIS) that are reliable, reproducible, and cost-effective for studying implant-related and biofilm bone infections and efficacy testing.

Ceragenins (CSAs) are a novel class of broad-spectrum antimicrobials that mimic the activities of antimicrobial peptides. They are effective against bacterial, viral, fungal, and parasitic infections with low minimum inhibitory concentrations (MICs) and minimum bactericidal concentrations (MBCs). CSAs can also penetrate biofilm and kill antimicrobial-resistant bacteria, such as methicillin-resistant *Staphylococcus aureus* (MRSA) and methicillin-resistant *Staphylococcus epidermidis* (MRSE). In recent years, CSA-131 has been approved by the FDA for endotracheal tube coating to prevent infection in intubated and critical patients. In our study, we applied CSA-90 (which belongs to the same family as CSA-131) to implant coating and prevented osteomyelitis in a mouse model and demonstrated the osteogenic properties of CSA-90, which promotes bone healing and reunion of the bone defects.

CSA-90 has been classified as a potential drug to prevent and treat osteomyelitis. However, conventional methods of antibiotic delivery to the bone are inefficient. To increase the bone-binding property of CSA-90, we invented a new molecule by attaching alendronate (bisphosphonate) to CSA-90 and named it bone-binding antimicrobial-1 (BBA-1). *In vitro*, we determined the bone-binding properties of BBA-1 and confirmed its antimicrobial activities against *S. aureus*. Later, we conducted a preclinical trial to test the *in vivo* efficacy of BBA-1 and showed that BBA-1 could prevent osteomyelitis in mice and has low cytotoxicity.

Multiple myeloma (MM) is an aggressive cancer of plasma cells. Although chemotherapy, corticosteroids, and radiation therapy manage multiple myeloma, MM has no cure. Most MM patients (>90%) suffer myeloma-skeletal disease, including local osteolytic lesions and osteomyelitis. Thus, we dedicate the clinical application of BBA-1 to MM patients. To pursue clinical trials, preclinical trials must be conducted. In our attempts, we proposed a feasible murine model that can induce bone infections in MM mice and elucidated how MM patients will benefit from BBA-1.

# Abbreviations

AAOS	American Academy of Orthopedic Surgeons
ABS	Absorbance
AHO	Acute haematogenous osteomyelitis
ALP	Alkaline phosphatase
AMP	Antimicrobial peptide
AMR	Antimicrobial-resistant
ASCT	Autologous stem-cell transplantation
ATCC	American Type Culture Collection
AuNP	Gold nanoparticle
AuP	Peanut-shaped gold nanoparticles
AuR	Rod-shaped gold nanoparticles
AuS	Star-shaped gold nanoparticles
BBA	Bone-binding antimicrobial
Bcc	<i>Burkholderia cepacia</i> complex
BMP-2	Bone morphogenetic proteins-2
BPs	Bisphosphonates
BV	Bone volume
B2M	Beta-2-microglobulin
CAP/CAMP	Cationic antimicrobial peptides
CDC	Centers for Disease Control and Prevention
CFU	Colony-forming unit
CKD	Chronic kidney disease
CNS/CONS	Coagulase negative staphylococci
CSA	Ceragenins
CT	Computed tomography
CV	Crystal violet
DAIR	Debridement, antibiotic therapy and implant retention
DFO	Diabetic foot osteomyelitis
DFU	Diabetic foot ulcer
DiD	1'-dioctadecyl-3,3,3',3'-tetramethylindodicarbocyanine
Dkk-1	Dickkopf-1
DM	Diabetes mellitus
ESPID	European Society for Paediatric Infectious Disease
ETT	Endotracheal tube
FCS	Foetal calf serum
FDA	Food and Drug Administration
FPRL1	Formyl peptide receptor-like 1
HA	Hydroxyapatite
HCM	Hypercalcaemia of malignancy
H&E	Haematoxylin and eosin
hMSCs	Human mesenchymal stem cells
hOBs	Human osteoblasts
IAFF	Infection after fracture fixation
I&D	Irrigation and debridement
IL-2	Interleukin-2
IMiDs	Immunomodulatory agents
IP	Intraperitoneal

IPP	Ion-assisted plasma polymerisation
IRI	Implant-related infection
IV	Intravenous
IDSA	Infectious Diseases Society of America
KB	Kirby-Bauer
LB	Lysogeny broth
LDH	Lactate dehydrogenase
LL-37	Cathelicidin
MAR	Mineral apposition rate
MBC/MBCs	Minimum bactericidal concentration(s)
MBD	Myeloma bone disease
MDE	Myeloma defining events
MGS	Mouse Grimace Scale
MGUS	Monoclonal gammopathy of undetermined significance
MIC/MICs	Minimum inhibitory concentration(s)
Micro-CT	Micro-computed tomography
MM	Multiple myeloma
MNP	Magnetic nanoparticles
MRI	Magnetic resonance imaging
MRONJ	Medication-related osteonecrosis of the jaw
MRSA	Methicillin-resistant <i>Staphylococcus aureus</i>
MRSE	Methicillin-resistant <i>Staphylococcus epidermidis</i>
MSSA	Methicillin susceptible/sensitive <i>Staphylococcus aureus</i>
NDMM	Newly diagnosed multiple myeloma
NF/NFs	Nanofiber(s)
NIS	Needle insertion surgery
NP/NPs	Nanoparticle(s)
OD	Optical density
PAM	Pamidronate
PCR	Polymerase chain reaction
PDMS	Polydimethylsiloxane
PEG-PAM	Poly(ethylene glycol)-polyallyl mercaptan
PHPT	Primary hyperparathyroidism
PI	Proteasome inhibitor
PJI	Prosthetic joint infections
PMMA	Poly(methyl-methacrylate)
PP	Plasma polymerisation
PTH	Parathyroid hormone
rhBMP-2	Recombinant human bone morphogenetic protein-2
RF	Radio frequency
RISS	Revised international staging system
ROI	Region of interest
ROS	Reactive oxygen species
RRMM	Refractory multiple myeloma
SA	<i>Staphylococcus aureus</i>
SC	Subcutaneous
Scl-Ab	Antisclerostin antibody
SDS	Sodium dodecyl sulphate
SMM	Smouldering multiple myeloma
SNP	Silver nanoparticle

SRE	Skeletal-related events
SS/SSt	Stainless-steel
SSI	Surgical site infection
TDH	Tibial-drilled hole
TGF- $\beta$	Transforming growth factor- $\beta$
Thal	Thalidomide
Ti	Titanium
TMP-SMX	Trimethoprim-sulfamethoxazole
TSB	Tryptic soya broth
VCd	Bortezomib-cyclophosphamide-dexamethasone
VISA	Vancomycin-intermediate <i>Staphylococcus aureus</i>
VR	Lenalidomide
VRd	Dexamethasone
VRSA	Vancomycin-resistant <i>Staphylococcus aureus</i>
VTd	Bortezomib-thalidomide-dexamethasone
Xen36	Bioluminescent Xen36 <i>Staphylococcus aureus</i>
XDR	Extensively drug resistance
XR	X-ray
ZA	Zoledronic acid
ZOI	Zone of inhibition

# LIST OF FIGURES

## Chapter 1: Introduction

### Section 1.2

Figure 1: The chemical structure of CSA-8, CSA-13, CSA131 and CSA-90 .....	27
--	----

## Chapter 2: Murine models of orthopaedic infection featuring *Staphylococcus aureus* biofilm

Figure 1: [Study 1B] The bone infection rate in the TDH models .....	61
Figure 2: [Study 1B] XR images of TDH and NIS.....	62
Figure 3: [Study 2] The bone infection rate of TDH and NIS models.....	63
Figure 4: [Study 2] The bacterial loads (ABS 600 nm) of TDH and NIS models .....	64
Figure 5: [Study 2] Micro-CT reconstructions of uninfected and infected tibiae .....	65
Figure 6: [Study 2] The regenerate bone volumes of TDH and NIS models.....	66
Figure 7: [Study 2] Histology sections .....	67
Figure S1: The proposed protocol of free bacterial culture for local inoculation .....	70
Figure S2: The proposed protocol of biofilm culture for local inoculation .....	72
Figure S3: The proposed protocol of the NIS-biofilm bone infection model .....	75
Figure S4: The proposed protocol of the NIS-pin bone infection model.....	76

## Chapter 3: Ion-assisted plasma polymerisation and CSA-90 coating for orthopaedic implants

Figure 3.1: Schematic illustration of a retrofitted plasma polymerisation chamber .....	86
Figure 3.2: A schematic of the <i>in vitro</i> assay.....	87
Figure 3.3: The bacterial loads (ABS 600) of silica beads and Kirshner-wire <i>in vitro</i> assays .....	91
Figure 3.4: Semi-quantitative analysis of relative bacterial loads in bones .....	93
Figure 3.5: Xray of the tibiae (No coating vs. PP vs. PP + CSA-90) .....	94
Figure 3.6: Micro-CT reconstructions and Regenerate Bone Volume .....	95
Figure 3.7: H&E-stained histology sections.....	96
Figure S3.1: The CFU counts of uncoated and PP-coated titanium (Ti) foils.....	101
Figure S3.2: The CFU counts of uncoated and PP-coated stainless-steel (SSt) foils .....	101
Figure S3.3: Kirby-Bauer susceptibility test incorporating CSA-90 of Ti and SSt foils.....	102

## Chapter 4: Testing BBA-1 in vivo to prevent osteomyelitis and myeloma bone

Figure 4.1: The process of synthesising BBA-1 .....	137
Figure 4.2: [Study 4A] The infection rate of soft tissue, bone, and blood .....	145
Figure 4.3: [Study 4A] The regenerate bone volumes .....	146
Figure 4.4: [Study 4A] The micro-CT reconstructions of the tibiae .....	146
Figure 4.5: [Study 4B] The radiographs (XR) of NIS and MM-cell injected tibiae.....	148
Figure 4.6: [Study 4B] An IVIS scanned image of a mouse injected with Xen36 <i>S. aureus</i> .....	148



# TABLE OF CONTENTS

<i>Certificate of Originality .....</i>	<i>I</i>
<i>Declaration of Contributions .....</i>	<i>II</i>
<i>Publications related to this thesis.....</i>	<i>III</i>
<i>Other publications not related to this thesis .....</i>	<i>IV</i>
<i>Acknowledgements .....</i>	<i>V</i>
<i>Abstract .....</i>	<i>VI</i>
<i>Abbreviations .....</i>	<i>VII</i>
<i>List of Figures .....</i>	<i>X</i>

## Chapter 1: Introduction

<b>Chapter 1.....</b>	<b>1</b>
<b>Executive Summary.....</b>	<b>1</b>
<b>Section 1.1: Clinical Complexity and Burden of Osteomyelitis.....</b>	<b>2</b>
1.1.1: Aetiology and classification of osteomyelitis .....	2
1.1.2. The causative pathogens of osteomyelitis .....	3
1.1.3. Open fractures and implant-related osteomyelitis.....	3
1.1.4. Biofilm infection and chronic osteomyelitis.....	4
1.1.5. Diabetic foot-related osteomyelitis.....	4
1.1.6. Acute haematogenous osteomyelitis.....	5
1.1.7. Osteomyelitis related to myeloma bone disease.....	5
1.1.8. Diagnosis of osteomyelitis.....	6
1.1.9. Antibiotic therapies for osteomyelitis .....	7
1.1.10. Surgical interventions for osteomyelitis.....	8
1.1.11. Prophylaxis and prevention for osteomyelitis .....	10
1.1.12. Conclusion .....	11
<b>Section 1.2: The application of ceragenins to orthopaedic surgery and medicine .....</b>	<b>22</b>
Publication Manuscript: The application of ceragenins to orthopedic surgery and medicine .....	23
Abstract .....	23
1.1. Joint and bone infections are an increasing issue for orthopedic care .....	23
1.2. Causative organisms of bone infections .....	24
1.3. Antibiotic prophylaxis and treatment for bone infections .....	24
2.1. CSAs are broad-spectrum antimicrobials derived from cholic acid .....	25
2.2. The CSA-13 sub-class of antimicrobials .....	27
3.1. The antimicrobial effects of CSAs against orthopedic pathogens .....	28
3.2. <i>In vivo</i> antimicrobial activity of CSAs in orthopedic models .....	28
3.3. Osteogenic properties of CSAs .....	30
3.4. Bone delivery systems and implant coatings for CSAs.....	30
Conclusion .....	31
<b>Section 1.3: Preventing osteolytic lesions and osteomyelitis in multiple myeloma .....</b>	<b>35</b>
Publication Manuscript: Preventing osteolytic lesions and osteomyelitis in multiple myeloma .....	36
Abstract .....	36
1. The disease burden of multiple myeloma .....	36
2. Clinical interventions for multiple myeloma .....	37

3. Osseous lesions and associated complications in myeloma bone disease .....	37
4. Conventional and emerging treatments for myeloma bone disease.....	38
4.1. Bisphosphonates prevent bone disease in NDMM patients .....	38
4.2. Denosumab prevents skeletal-related events in MM patients .....	41
4.3. Bortezomib stimulates osteoblast growth and differentiation.....	42
4.4. Chemotherapies for osteolytic lesions are ineffective .....	42
4.5. Interleukin-2 does not prevent myeloma bone disease .....	42
5. MM lytic lesions as a risk factor for osteomyelitis .....	43
6. Discussion .....	43
7. Conclusion .....	46

## Chapter 2: Murine models of orthopaedic infection featuring *Staphylococcus aureus* biofilm

<b>Chapter 2.....</b>	<b>49</b>
Publication Manuscript: Murine models of orthopedic infection featuring <i>Staphylococcus aureus</i> biofilm.....	50
Abstract .....	50
1. Introduction .....	51
2. Methods.....	51
2.1. Bacterial and Biofilm Culture .....	51
2.2. Animal husbandry and ethics .....	52
2.3. Study Design .....	52
2.4. Surgery and Anesthesia .....	52
2.5. X-ray and Post-Surgical Monitoring .....	53
2.6. Specimen Collection and Bacterial Assay .....	53
2.7. Radiographic Analysis .....	53
2.8. Paraffin Histology.....	54
2.9. Statistical Analyses.....	54
3. Results.....	54
3.1. TDH surgery led to fracture when holes were generated in the tibial midshaft .....	54
3.2. Metal surfaces and biofilms are essential to achieve high infection rates in the TDH model.....	54
3.3. NIS is a less complex procedure than TDH .....	55
3.4. Establishing reproducible murine models of bone defect infection .....	55
4. Discussion .....	56
5. Conclusion .....	57
Appendix: Supplementary Protocol .....	68

## Chapter 3: Ion-assisted plasma polymerisation and CSA-90 coating for orthopaedic implants

<b>Chapter 3.....</b>	<b>78</b>
<b>Section 3.1: Introduction .....</b>	<b>79</b>
3.1.1. Implant-related osteomyelitis is a clinical challenge .....	79
3.1.2. The current limitations on drug delivery systems and implant coatings.....	80
3.1.3. Preclinical models for implant-related infections .....	82
3.1.4. IPP technology and its potential clinical applications .....	83
3.1.5. Ceragenins (CSAs) as bioactive molecules for IPP coating .....	84
3.1.6. Aims and hypotheses.....	84
<b>Section 3.2: Materials and Methods .....</b>	<b>84</b>
3.2.1. Materials.....	84
3.2.2. Ion-assisted plasma polymerisation on silica beads and metal pins.....	85
3.2.3. Beads and antimicrobial coating for in vitro assay .....	86

3.2.4. Covalent attachment of CSA-90 on stainless-steel pins .....	87
3.2.5. Bacterial culture .....	87
3.2.6. Animal ethics and study design .....	88
3.2.7. Preclinical orthopaedic surgical model with implantation.....	88
3.2.8. Specimen collection and analysis .....	89
3.2.9. Histology .....	89
3.2.10. Statistical analysis.....	90
<b>Section 3.3: Results .....</b>	<b>90</b>
3.3.1. IPP biofunctionalised 3D surfaces for antimicrobial coating .....	90
3.3.2. IPP+CSA-90 coating reduces bacterial loads in bones and soft-tissues .....	92
3.3.3. IPP + CSA-90 coating reduced bone loss and promote bone healing .....	93
<b>Section 3.4: Discussion .....</b>	<b>97</b>
<b>Section 3.5: Conclusion .....</b>	<b>100</b>
<b>Section 3.6 Supplementary Data.....</b>	<b>101</b>
<b>Appendix .....</b>	<b>108</b>
Manuscript: Antibacterial plasma polymer coatings on 3D materials for orthopedic applications.....	108

## Chapter 4: Testing BBA-1 in vivo to prevent osteomyelitis and myeloma bone

<b>Chapter 4.....</b>	<b>135</b>
<b>Section 4.1: Introduction .....</b>	<b>136</b>
4.1.1. The clinical challenges of using intravenous antibiotics to treat osteomyelitis .....	136
4.1.2. The generation of bone-binding antimicrobials.....	137
4.1.3. Developing a MM-related bone infection murine model .....	138
<b>Section 4.2: Methods .....</b>	<b>139</b>
4.2.1. Study 4A design: in vivo testing of BBA-1 in an orthopaedic model.....	139
4.2.2. Study 4B design: development of a MM infection model .....	140
4.2.3. Bacterial and biofilm culture .....	140
4.2.4. Cell culture and injection.....	141
4.2.5. Animal husbandry and ethics .....	141
4.2.6. Surgery and anaesthesia .....	141
4.2.7. Surgical or post-surgical bacterial inoculation .....	142
4.2.8. X-ray and IVIS imaging and monitoring.....	142
4.2.9. Specimen Collection and Bacterial Assay .....	143
4.2.10. Radiographic Analysis and Paraffin Histology .....	143
4.2.11. Statistical Analyses .....	144
<b>Section 4.3: Results .....</b>	<b>144</b>
4.3.1. BBA-1 showed limited in vivo antimicrobial activities and osteogenic property .....	144
4.3.2. The pilot trial of modelling bone infection in MM mice .....	147
<b>Section 4.4: Extended Discussion .....</b>	<b>149</b>
4.4.1. Study 4A: BBA-1 requires further trials and development .....	149
4.4.2. Study 4B: MM-related bone infection model development.....	151
4.4.3. Future iterative development and refinement of a MM-bone infection model .....	152
4.4.4. Preclinical testing of BBA-1 using the MM-related bone infection model .....	154
<b>Section 4.5: Conclusion .....</b>	<b>155</b>

## Chapter 5: Discussion

Chapter 5.....	159
----------------	-----

<b>Section 5.1: Key findings .....</b>	<b>159</b>
5.1.1. Development of a reliable murine bone infection model for preclinical trials.....	159
5.1.2. Plasma polymerisation has utility in producing antimicrobial coatings.....	159
5.1.3. Synthetic bone binding antimicrobial is functional.....	160
<b>Section 5.2: Major limitations.....</b>	<b>160</b>
5.2.1. NIS models need optimisation and testing new variables .....	160
5.2.2. IPP coating with ceragenins require further investigations and clinical trials .....	162
5.2.3. The MM-related bone infection model demands amendments and development .....	163
<b>Section 5.3: Results from parallel studies.....</b>	<b>165</b>
5.3.1. The applications of ceragenins for infectious diseases.....	165
5.3.2. The potentials of ceragenins as anticancer agents .....	168
<b>Section 5.4: Future directions .....</b>	<b>169</b>
5.4.1. Antibiotic susceptibility and resistance surveillance.....	169
5.4.2. Optimising animal models for preclinical trials.....	170
5.4.3. Determining the orthopaedic applications of CSA-131.....	171
5.4.4. Exploring the combined effects of BBAs and CSA-coated implants.....	172
5.4.5. Understanding the underlying osteogenic mechanisms of CSAs and BBAs.....	173
<b>Conclusion .....</b>	<b>174</b>

# 1. Introduction

## Executive Summary

My thesis focuses on preclinical modelling of osteomyelitis and their potential treatments. The central hypotheses of this project are that the ceragenin, CSA-90, and the derivative novel bone binding antimicrobial, BBA-1, have considerable potential to prevent bone infection. This introductory chapter is separated into three parts:

**Section 1.1** provides a brief overview of the clinical complexity and burden of osteomyelitis, including diagnosis, treatment, and prevention.

**Section 1.2** describes the potential utility of the ceragenins in treating orthopaedic infection (this is a published review paper).

**Section 1.3** focuses on myeloma bone disease (MBD), which is purported to be an underappreciated cause of bone infection. This is relevant to subsequent attempts in the thesis to model infection associated with MBD (this is a published review paper).

## 1.1. Clinical Complexity and Burden of Osteomyelitis

This section provides a brief overview of subjects relevant to the subsequent experimental research. This narrative review focuses on understanding the causes of bone infection and approaches that can be used for diagnosis, prevention, and treatment.

### 1.1.1. Aetiology and classification of osteomyelitis

Osteomyelitis, or bone infection, is mainly caused by bacterial invasion into the skeleton <sup>1</sup>. Osteomyelitis is a major clinical challenge in orthopaedic surgery, with an incidence of 22 per 100,000 person/year in the United States and occurs more commonly in men than in women <sup>2</sup>. While the incidence remains relatively stable among children and young adults, it triples among individuals older than 60 years of age <sup>2-7</sup>. Immunocompromised (e.g., cancer and HIV/AIDS) and diabetic patients are also at higher risk for developing bone infections <sup>8-11</sup>.

In 1970, Waldvogel proposed a classification system based on the source of infection <sup>12,13</sup>, and there are three main types of osteomyelitis:

1. Osteomyelitis resulting from the spread from a contiguous source (e.g., surgical contamination or trauma),
2. Osteomyelitis occurring secondary to vascular insufficiency or neuropathy (e.g., diabetic foot ulcers), and
3. Acute haematogenous osteomyelitis (AHO) derived from bacteraemia.

Osteomyelitis can also be further categorised as acute, chronic, diabetic foot-related, and implant-related. The clinical management of osteomyelitis varies according to these classifications <sup>12</sup>, but treatment can be invariably time-consuming and expensive <sup>13</sup>. Once the bone infection is established, appropriate treatment may require a multidisciplinary approach, multiple surgeries and long courses of antibiotics <sup>13</sup>.

This prolonged treatment can lead to significant financial loss and economic burden for the healthcare system and patients <sup>14</sup>. The cost of managing musculoskeletal infections varies widely, although infections that require surgical intervention (e.g., osteomyelitis and septic arthritis) have higher costs than those without intervention (e.g., septic bacteraemia or surgical site infections). In the United States alone, orthopaedic infections cost 8.6 billion USD annually, and diabetic foot osteomyelitis (DFO) can cost the healthcare system up to 9-13 billion USD per annum <sup>15-17</sup>. Naturally, the costs of treating bone infections vary in different countries due

to their healthcare systems and economies. However, to date, there are no systematic reviewed data to address the incidence and financial burden of osteomyelitis in Australia or globally.

### 1.1.2. The causative pathogens of osteomyelitis

The causative pathogens in osteomyelitis are not always identified; 70-90% of positive culture cases involve *Staphylococcus aureus*<sup>14</sup>. The proportion of these caused by methicillin-resistant *Staphylococcus aureus* (MRSA) is increasing globally<sup>18,19</sup>. Osteomyelitis is mainly caused by bacterial invasion into the bone from injuries or open fractures, with *Staphylococcus* species and *Streptococcus* species being the predominant aetiology of open fractures and post-traumatic bone infections. In implant-related osteomyelitis, *Pseudomonas aeruginosa* and *Escherichia coli* are seen more frequently. Coagulase negative staphylococci (CNS) and *Corynebacterium sp.* are more frequent in diabetic-foot osteomyelitis (DFO)<sup>20-27</sup>.

In paediatric patients, most cases of osteomyelitis are secondary to haematogenous spread from transient bacteraemia, which is often a result of otitis media and pharyngitis<sup>28</sup>. Acute Haematogenous Osteomyelitis (AHO) is sometimes linked to osteoarticular infections caused by *S. aureus*, *Streptococcus pyogenes*, and *Streptococcus pneumoniae*. However, in recent years, *Kingella kingae* has also been reported as a major cause of osteoarticular infection in paediatrics. This pathogen can cause paediatric bacteraemia and represents the leading infectious cause of osteomyelitis and septic arthritis in children aged 6 to 48 months<sup>29-36</sup>. Other causes of bone infections include bacteria of the genus *Mycobacterium*<sup>37-41</sup>, Group B *Streptococcus* (e.g., *Streptococcus agalactiae*) and anaerobic bacteria like *Haemophilus influenzae* type B and *Salmonella*<sup>18,42-45</sup>. In rare cases, fungal pathogens such as *Candida*, *Cutibacterium*, *Bartonella*, *Histoplasma*, *Cryptococcus*, *Blastomyces* and *Coxiella* can also cause osteomyelitis<sup>46-58</sup>.

### 1.1.3. Open fractures and implant-related osteomyelitis

Open fractures are often the result of high-energy trauma and may be associated with life-threatening injuries with high morbidity and mortality<sup>59-61</sup>. Bones, tendons, nerves, and articular cartilage may be exposed and subject to damage. Fracture wounds can then become susceptible to deep local-site infections due to contamination of the site with microorganisms or the introduction of foreign bodies into the wound.<sup>62</sup> Infection rates of 12-13% are found in open fracture patients<sup>63</sup> and occur predominantly in Gustilo and Anderson type III fractures<sup>64</sup>.

In severe cases, open fractures can also lead to chronic osteomyelitis, non-union, loss of function, or limb loss. One of the most challenging complications in trauma surgery is infection after fracture fixation (IAFF) <sup>65</sup>. IAFF may result in permanent functional loss or even amputation of the affected limb in patients who may otherwise be expected to achieve complete, uncomplicated recovery.

In the past decade, the problem of implant-related bone infections has garnered increasing attention in both clinical and basic laboratory research <sup>66-75</sup>. As prosthetic joint infections (PJIs) are one of the most severe complications of joint replacement surgery, many studies have focused on this area <sup>67,68,70</sup>. PJIs almost always necessitate surgical intervention and prolonged courses of intravenous and oral antibiotics <sup>76-78</sup>. Strong collaboration between all involved medical and surgical specialists (e.g., orthopaedic surgeons, plastic surgeons, infectious disease specialists, and other physicians) is a critical component of patient care and clinical management for PJI and IAFF <sup>68</sup>. Treatment for post-trauma surgery and implant-related osteomyelitis is challenging and continues to lead to recalcitrant clinical outcomes.

### **1.1.4. Biofilm infection and chronic osteomyelitis**

Biofilm bone infections can be challenging to treat and eradicate with antimicrobials, which often struggle to penetrate through a biofilm matrix effectively <sup>79,80</sup>. A biofilm is a community of bacteria enclosed in a self-produced exopolysaccharide matrix that adheres to a biotic or abiotic surface. Biofilm infection may also lead to implant failure, deep tissue infection, haematogenous infection (e.g., bacteraemia and sepsis), and chronic osteomyelitis (e.g., ulcer and diabetic foot osteomyelitis) <sup>81-83</sup>. Such complications can lead to negative outcomes for the patient, including multiple revision surgeries to correct implants or surgical debridement to remove infected and necrotic bone tissues <sup>84-86</sup>. In some cases, severe osteomyelitis can lead to amputation, prolonged hospitalisation, and intravenous antibiotic treatment (up to six months or longer) <sup>87-90</sup>. Even if the infection is resolved, poor healing can lead to long-term impairments and life-long disability <sup>91,92</sup>.

### **1.1.5. Diabetic foot-related osteomyelitis**

Diabetes mellitus (DM) increases the risk of foot infection and diabetic foot ulcer (DFU), which may progress to diabetic foot osteomyelitis (DFO) <sup>93,94</sup>. This is reflected in the elderly population, in which the increased incidence of osteomyelitis is driven by DM <sup>2</sup>. DFU is a micro-vascular complication associated with neuropathy, peripheral arterial diseases, foot



deformities, and infections <sup>95</sup>. Diabetic foot infection is the most common diabetic complication, affecting 60% of DFUs, which leads to hospitalisation and amputation in 20-30% of cases. DFO typically involves the forefoot and develops by contiguous spread from overlying soft tissue and penetration through cortical bone and into the medullary cavity <sup>96,97</sup>. DFO is complex and challenging to treat and has a high relapse rate <sup>98</sup>. Difficulties arise from a range of host factors and associated challenges, including the absence of well-defined diagnostic criteria, inconclusive test results and the frequent requirement of surgical intervention and treatment with antibiotics <sup>99</sup>. Although DFO is usually caused by bacterial infection, DFUs are also susceptible to fungal infections, especially in immunocompromised individuals <sup>44,45,52</sup>. Clinically, over 50% of DFO cases lead to minor or major amputation <sup>89,96,100</sup>. The most frequent causes of amputation in individuals with DFUs are ischemia and infection, which critically impact the life expectancy and quality of life of these patients <sup>101</sup>.

### **1.1.6. Acute haematogenous osteomyelitis**

Acute haematogenous osteomyelitis (AHO) needs timely management. AHO in children is usually caused by bacterial seeding that develops due to transient bacteraemia. It can result from otitis media, pharyngitis, and repeated from above causes <sup>28</sup>. AHO continues to present a significant clinical challenge due to its complex pathogenesis. Children with AHO and musculoskeletal infections may also experience involvement and complications of additional systems, including chronic osteomyelitis (1.7%), avascular necrosis, growth disturbance (1.8%), pathological fractures (1.7%), deep vein thrombosis (0.4-6%), septic pulmonary embolism, pneumonia, empyema, endocarditis, bacteraemia, and septic shock <sup>28</sup>. While AHO in children is usually curable, the evolving epidemiology of the disease as immunisation practices and patterns of bacterial resistance change continues to raise challenges to clinicians, demanding greater vigilance in clinical practice <sup>102</sup>. In rare severe cases, surgical debridement and amputation may be necessary, causing physical disabilities and emotional challenges in children <sup>103,104</sup>.

### **1.1.7. Osteomyelitis related to myeloma bone disease**

Multiple myeloma (MM) is a haematological malignancy of plasma cells and the second most common hematologic cancer in adults <sup>105-107</sup>. Myeloma bone disease (MBD) is a devastating complication of MM, causing high morbidity and mortality <sup>108,109</sup>. Enhanced bone loss in MM is associated chiefly with the axial skeleton and pelvis (e.g., diffuse osteopenia, focal lytic bone

lesions, spinal cord compression, pathological fractures, hypercalcemia, renal insufficiency, and bony pain)<sup>110</sup>. Nearly 85% of MM patients will have some degree of osteopenia at diagnosis, and 80-90% of patients will develop osteolytic bone lesions as the disease progresses<sup>111,112</sup>. The severity of bone destruction also correlates with tumour burden and prognosis<sup>109,113</sup>. Although myeloma-related osteomyelitis is not common, most infections are associated with the vertebra, particularly in the lumbar region, meaning they are especially difficult to manage as amputation is not possible and debridement is challenging<sup>114-117</sup>. It is speculated based on clinical evidence that if osteolytic lesions are left untreated, MM patients may be prone to bone infections (elaborated upon in **Section 1.3**).

#### 1.1.8. Diagnosis of osteomyelitis

Prompt diagnosis of the condition is the key to managing osteomyelitis. However, the current diagnostic tools do not always allow early detection, which is critical for timely management, particularly if the disease is associated with traumatic injuries and post-traumatic infections<sup>118</sup>. Obtaining appropriate specimens for culture is essential for selecting empirical and definitive antimicrobial therapies<sup>96</sup>. Successful diagnosis often requires an intimate knowledge of pathological mechanisms and the microorganisms most common in each. The diagnostic approach to osteomyelitis is very similar among different types and usually involves a combination of clinical examination, supportive blood testing, and appropriate radiography<sup>119</sup>. A diagnostic biopsy of infected bone can be used to identify the causative organism and surgical intervention can also assist diagnosis when necessary<sup>1</sup>.

The diagnostic tests for PJI are not always accurate and reliable. Apart from microbiological testing, a histological study of periprosthetic tissue and intraoperative inspection can sometimes assist with the diagnosis<sup>70</sup>. In recent years, polymerase chain reaction (PCR) test has become more accessible and commonly used in orthopaedics to diagnose patients with unknown infection<sup>120</sup>. A sinus tract in communication with the prosthesis, and identical pathogens present in two separate periprosthetic tissue or fluid samples, is definitive evidence of PJI. Other features may include the growth of virulent organisms from a single culture or the finding of acute inflammation by periprosthetic tissue histopathology<sup>68,70,121,122</sup>.

Diagnosis in children is most often associated with the pathogen *S. aureus*. However, the incidence of *Kingella kingae* and MRSA infections has been increasing<sup>123,124</sup>. Paediatric osteomyelitis primarily affects the lower extremities and long bones, i.e., the femur (~23-29%), tibia (~19-23%), humerus (~5-13%), pelvis (~3-14%) and calcaneus (~4-11%)<sup>125</sup>. Magnetic

resonance imaging (MRI) is the most effective diagnostic imaging modality for paediatric patients as MRI has high sensitivity and specificity for bone and soft tissue <sup>123</sup>. While medical history, physical examination, blood culture and serology test results can also assist diagnosing paediatric osteomyelitis <sup>32,34,126</sup>, bone biopsy may be necessary to increase the diagnostic yield<sup>127</sup>. Although molecular testing of microbial DNA in sonication fluid allows early detection with higher sensitivity than conventional bacterial cultures, PCR-based methods are costly and not always available for routine diagnostics <sup>128,129</sup>. However, PCR can detect *K. kingae* more easily in children aged less than four years with osteoarticular infections <sup>3</sup>.

### 1.1.9. Antibiotic therapies for osteomyelitis

The clinical treatment for osteomyelitis is dependent on the type. As each condition has its own risks and challenges, the clinical guidelines also vary based on evidence of efficacy. Treatment for osteomyelitis in adults can also differ from children. There are three fundamental approaches to managing clinical osteomyelitis: targeted antimicrobial therapy, source control and correction of medical comorbidities <sup>1</sup>. Source control entails debridement of necrotic bone, drainage and irrigation of abscessed tissue, and removal of infected hardware if feasible. Correction of hyperglycaemia and amelioration of peripheral vascular disease are critical components of successful therapy in patients with chronic wounds or osteomyelitis <sup>1</sup>.

Empirical therapy, or medical treatment based on clinical experience, is a mainstay of osteomyelitis care for patients who are suspected to have severe or disseminated disease, and patients with unknown aetiology (e.g., pending source cultures or infeasible to obtain one) <sup>1</sup>. However, the therapy decision is dependent on various factors, and it may be altered by patient history or disease severity, and there are still regional differences based on prevalence and resistance patterns of pathogens. Flucloxacillin and cefazolin are commonly used in clinical practice to treat osteomyelitis in children <sup>130,131</sup>. Clindamycin is another bacteriostatic choice for empirical antibiotic coverage of suspected *S. aureus* osteomyelitis if patients are grossly ill, but its utility can be limited by resistance patterns. Antibiotic susceptibility trends in paediatric *S. aureus* isolates indicate a trend toward increased clindamycin resistance in methicillin-susceptible *S. aureus* (MSSA) strains <sup>132</sup>.

For MRSA implant-associated osteomyelitis, the IDSA (Infectious Diseases Society of America) recommends empirical therapy with an intravenous agent (vancomycin or daptomycin) combined with oral rifampin for the initial two weeks, followed by rifampin with another oral antibiotic (e.g., fluoroquinolone, trimethoprim-sulfamethoxazole, tetracycline, or

clindamycin) for a further three to six months <sup>124</sup>. Long-term suppressive oral antibiotic therapy is recommended for those patients in whom debridement and hardware removal are not feasible. For paediatric AHO, the IDSA currently recommends empirical vancomycin therapy and the consideration of IV clindamycin for patients who do not have ongoing bacteraemia and in hospitals where clindamycin resistance is historically low <sup>124</sup>. Minimum duration of four to six weeks is recommended. The European Society for Paediatric Infectious Disease (ESPID) has published clinical practice guidelines for paediatric osteomyelitis. Prompt initiation of empirical therapy after cultures is highly recommended with regimens targeting both MSSA and MRSA (i.e., clindamycin with or without an anti-staphylococcal beta-lactam) in regions where MRSA prevalence is higher than 10-15% of all *S. aureus* infections <sup>133</sup>.

For children with severe infection or at high risk of clindamycin-resistant MRSA, vancomycin is preferred with or without the inclusion of clindamycin or an anti-staphylococcal beta-lactam. A first-generation cephalosporin such as cefazolin should be included for children under five, to cover *Kingella kingae* infections. The duration of therapy should be three to four weeks, with an early switch to oral antibiotics guided by susceptibility patterns and clinical improvement of the patient <sup>133</sup>. In addition, there is now compelling data suggesting that prolonged intravenous therapy is not superior to oral therapy for AHO and may lead to more complications <sup>134,135</sup>.

For native vertebral osteomyelitis, empirical treatments should include vancomycin to cover *Staphylococci*, *Streptococci*, combined with a third- or fourth-generation cephalosporin to cover Gram-negative bacilli <sup>136</sup>. initial, empirical therapy should be tailored based on culture results and treatment should include targeted parenteral or highly bioavailable oral antibiotics for six weeks.

For DFO, IDSA recommends an initial parenteral regimen followed by prolonged oral therapy <sup>101</sup>. Wounds without confirmed soft tissue or bone infections do not require antibiotic therapy. Mild and moderate infections need empiric therapy covering Gram-positive cocci. Severe infections caused by drug-resistant bacteria should use broad-spectrum antimicrobials targeting aggressive Gram-negative aerobes and obligate anaerobes <sup>95</sup>.

### 1.1.10. Surgical interventions for osteomyelitis

Surgery often has a unique and imperative role in improving the local environment during bone infection through debridement of the devitalized tissue, decompression of the bacterial burden,

and enhancement of antibiotic delivery. General indications for operative intervention include the presence of a subperiosteal or soft tissue abscess, osseous sequestrum (dead bone), or signs of chronic infection such as in the sinus tract <sup>137</sup>. Other indications may include unresponsive antibiotic treatment or concurrent septic joint arthritis <sup>138-140</sup>.

For bone infections that involve bacterial biofilm, abscess formation, and necrotic bone, IV antibiotics are mostly ineffective due to poor penetration. Surgical debridement of necrotic and nonviable tissues is usually required to improve antibiotic delivery <sup>132,141-144</sup>.

For diabetic ulcers, debridement is reserved for deeply progressed wounds involving the bone. The standard practices in DFU management include surgical debridement, dressing to facilitate a moist wound environment and exudate control <sup>145-149</sup>. Wound debridement involves the removal of all necrotic and devitalised tissue that is incompatible with healing and the surrounding callus. This process aids in granulation tissue formation and re-epithelialization and reduces plantar pressures at callus areas <sup>101</sup>. Debridement is also crucial for infection control, as dead tissue can act as a nidus for bacterial proliferation and biofilm formation <sup>150</sup>. The IDSA and the Wound Healing Society recommend sharp debridement (removing unhealthy or dead tissue by cutting it off) over topical debridement agents (i.e., autolytic dressing or biological debridement) <sup>101,149</sup>. Sharp debridement has also been found to be efficacious in several clinical trials <sup>151-153</sup>.

In orthopaedic trauma, the key is management of open fractures with a high risk of infection. Urgent irrigation and debridement are necessary to prevent infection and promote healing <sup>154-156</sup>. Early surgical intervention and stabilisation of the fracture are critical for damage control in a trauma setting <sup>157,158</sup>.

For implant-related osteomyelitis like PJI, two-stage exchange arthroplasty is the gold standard when the infection is chronic. The procedure involves the placement of a temporary antibiotic spacer with a period of intravenous antibiotics followed by reconstruction when the infection is deemed to be eradicated <sup>159,160</sup>. However, failure rates of two-stage revision and irrigation and debridement (I&D) with component retention are generally high due to biofilm contamination <sup>144,161-163</sup>. Typical PJI can be managed with debridement, antibiotic therapy, and implant retention (DAIR) <sup>142</sup>. Therefore, treatment often requires an interdisciplinary team with infectious diseases specialists and microbiologists in collaboration with orthopaedic surgeons.

### 1.1.11. Prophylaxis and prevention for osteomyelitis

Since antibiotic treatments are not always effective, and surgical intervention can sometimes fail, prophylaxis and prevention measures are essential. Antimicrobial prophylaxis and surgical debridement are standard practices and conventional interventions to prevent infectious complications following traumatic injury <sup>164</sup>. For open fractures, first-generation cephalosporins can significantly reduce the risk of infection when used in combination with prompt, modern orthopaedic fracture wound management <sup>61</sup>.

Since *S. aureus* causes most bone infections, active antibacterial agents against Gram-positive microorganisms are uniformly recommended in all relevant post-trauma clinical guidelines <sup>61,165-168</sup>. However, the addition of fluoroquinolones and aminoglycosides to expanded Gram-negative coverage is also important for extremity injury cases <sup>164</sup>, and should be considered based on clinical judgements.

Antibiotic-laden poly(methyl-methacrylate), also known as PMMA or bone cement, can deliver antibiotics locally and prevent osteomyelitis with surgery. Antibiotics are added to the PMMA powder before the start of polymerisation. A typical mix includes 1 g of vancomycin and 1 g of gentamicin or tobramycin per bag of PMMA. High viscosity Palacos cement is recommended due to its superior elution properties. However, the antibiotic elution is limited to only a few days <sup>169,170</sup>. The advantages include local delivery of high doses of antibiotics, filling dead space, and maintaining soft tissue tension. The disadvantage, however, is that it requires additional surgery to remove, which poses a substantial risk of infection<sup>81</sup>.

For DFU/DFO, inappropriately treating wounds with antibiotics as a precaution for missed infections can cause several adverse effects, including antibacterial resistance <sup>148</sup>. Hydrogels are specialised dressings used to facilitate wound healing. They are made of insoluble polymers and bind a relatively large volume of water, which can be donated to the wounded tissue. The polymer matrix can absorb wound exudate, keeping the wound at an optimal moisture level for cells, facilitating autolytic debridement and assisting the breakdown of necrotic tissue through endogenous proteolytic enzymes <sup>171</sup>.

For implant-related osteomyelitis like PJI, prevention is slightly more complicated. Numerous strategies have been employed, including implant surface fabrication and incorporation of antibiotics into the implant <sup>172</sup>. Antibiotic-impregnated cement can also be used to prevent infections. However, these methods have distinctive limitations and disadvantages. For example, traditional iodine and nano-particulate silver implant coatings have shown uncontrollable release and cytotoxicity to bone cells. Bone cement is limited to use with

cemented implants or as a temporary spacer and require an additional surgery for removal. Antibiotic-loaded implant coatings like hydroxyapatite (HA) are disadvantaged by burst drug-release due to the weak binding between the HA surface and loaded drugs <sup>173</sup>. Additionally, coating orthopaedic implants with standard antibiotics like clindamycin, gentamicin and vancomycin may increase the prevalence of antimicrobial resistance in clinical settings and hence reduce the effectiveness of future antibiotic treatment.

Coating intramedullary rods with antibiotic PMMA cement is another strategy for preventing implant-related osteomyelitis. It has been shown to increase stability and improve outcomes for infected non-union long bones <sup>174</sup>. However, burst drug-release and low release capacity remain fundamental problems. While incorporating silica or other fillers may enhance antibiotic elution from PMMA cement, this approach also reduces the mechanical strength, which is critical for weight-bearing bone cement <sup>175</sup>. Another development is the use of calcium polyphosphate gel formulated PMMA cement. This method managed to reduce the initial burst release of vancomycin and tobramycin and extended the release for 25 weeks. The improved antibiotic release was due to the strong ionic binding of the embedded drugs with the calcium polyphosphate gel and exhibited no detrimental effects on the mechanical properties <sup>176</sup>.

Newer developments for implant coatings include plasma polymerisation, biodegradable polymer coatings and nanofibers (NFs). They can be used as controllable means to deliver antibiotics in a sustained fashion, minimising toxicity (local or systemic) associated with high antibiotic concentrations <sup>172,177-180</sup>. One study shows that doxycycline doped (PCL<sup>Col</sup>/PVA<sup>HA</sup>) coaxial NFs can sustainably release the drug for one month. In a preclinical trial, doxycycline doped rods inhibited *S. aureus* infection and enhanced osseointegration for up to eight weeks. Further clinical validation, however, is required <sup>181</sup>.

### 1.1.12. Conclusion

In conclusion, osteomyelitis is a high-burden disease with high morbidity and mortality. In severe cases, bone infections can lead to amputation and permanent disability, affecting quality of life and causing financial losses to patients. The current diagnostic tools for osteomyelitis require collecting appropriate specimens and radiography, but these methods are not always accurate and reliable. The gold standard of treatment for osteomyelitis is prolonged antibiotic treatment and surgical intervention. However, empirical treatment is often based on clinical experience rather than susceptibility test results and has low efficacy if antimicrobial resistance occurs. Surgical debridement can cause secondary infections, which are associated with

implant failure if bacterial biofilms or orthopaedic implants are involved. While various measures prevent orthopaedic infections, intravenous antibiotics are ineffective against biofilm formation. Therefore, a novel broad-spectrum antimicrobial with antibiofilm properties and bactericidal activities with low resistance like ceragenins will be advantageous in preventing osteomyelitis.

### References

1. Urish KL, Cassat JE. Staphylococcus aureus Osteomyelitis: Bone, Bugs, and Surgery. *Infection and immunity* 2020; **88**(7).
2. Kremers HM, Nwojo ME, Ransom JE, Wood-Wentz CM, Melton LJ, 3rd, Huddleston PM, 3rd. Trends in the epidemiology of osteomyelitis: a population-based study, 1969 to 2009. *The Journal of bone and joint surgery American volume* 2015; **97**(10): 837-45.
3. Castellazzi L, Mantero M, Esposito S. Update on the Management of Pediatric Acute Osteomyelitis and Septic Arthritis. *International journal of molecular sciences* 2016; **17**(6).
4. Dartnell J, Ramachandran M, Katchburian M. Haematogenous acute and subacute paediatric osteomyelitis: a systematic review of the literature. *The Journal of bone and joint surgery British volume* 2012; **94**(5): 584-95.
5. Loh R, Phua M, Shaw CL. Management of paediatric acute mastoiditis: systematic review. *The Journal of laryngology and otology* 2018; **132**(2): 96-104.
6. Jaul E. Assessment and management of pressure ulcers in the elderly: current strategies. *Drugs & aging* 2010; **27**(4): 311-25.
7. Wiegand S, Berner R, Schneider A, Lundershausen E, Dietz A. Otitis Externa. *Deutsches Arzteblatt international* 2019; **116**(13): 224-34.
8. Hern JD, Almeyda J, Thomas DM, Main J, Patel KS. Malignant otitis externa in HIV and AIDS. *The Journal of laryngology and otology* 1996; **110**(8): 770-5.
9. Vassilopoulos D, Chalasani P, Jurado RL, Workowski K, Agudelo CA. Musculoskeletal infections in patients with human immunodeficiency virus infection. *Medicine* 1997; **76**(4): 284-94.
10. Medaris LA, Ponce B, Hyde Z, et al. Cryptococcal osteomyelitis: a report of 5 cases and a review of the recent literature. *Mycoses* 2016; **59**(6): 334-42.
11. Cross GB, Le Q, Webb B, et al. Mycobacterium haemophilum bone and joint infection in HIV/AIDS: case report and literature review. *International journal of STD & AIDS* 2015; **26**(13): 974-81.
12. Maffulli N, Papalia R, Zampogna B, Torre G, Albo E, Denaro V. The management of osteomyelitis in the adult. *The surgeon : journal of the Royal Colleges of Surgeons of Edinburgh and Ireland* 2016; **14**(6): 345-60.
13. Lew DP, Waldvogel FA. Osteomyelitis. *Lancet (London, England)* 2004; **364**(9431): 369-79.
14. Howard-Jones AR, Isaacs D. Systematic review of duration and choice of systemic antibiotic therapy for acute haematogenous bacterial osteomyelitis in children. *Journal of paediatrics and child health* 2013; **49**(9): 760-8.
15. Geraghty T, LaPorta G. Current health and economic burden of chronic diabetic osteomyelitis. *Expert review of pharmacoeconomics & outcomes research* 2019; **19**(3): 279-86.
16. Xi W, Hegde V, Zoller SD, et al. Point-of-care antimicrobial coating protects orthopaedic implants from bacterial challenge. *Nature Communications* 2021; **12**(1): 5473.



17. Hirshberg J, Rees RS, Marchant B, Dean S. Osteomyelitis related to pressure ulcers: the cost of neglect. *Advances in skin & wound care* 2000; **13**(1): 25-9.
18. Hartemann-Heurtier A, Senneville E. Diabetic foot osteomyelitis. *Diabetes & metabolism* 2008; **34**(2): 87-95.
19. Guo Y, Song G, Sun M, Wang J, Wang Y. Prevalence and Therapies of Antibiotic-Resistance in Staphylococcus aureus. *Frontiers in cellular and infection microbiology* 2020; **10**: 107.
20. Chapman PR, Choudhary G, Singhal A. Skull Base Osteomyelitis: A Comprehensive Imaging Review. *AJNR American journal of neuroradiology* 2021; **42**(3): 404-13.
21. Pliska NN. Pseudomonas Aeruginosa as the Main Causative Agent of Osteomyelitis and its Susceptibility to Antibiotics. *Drug research* 2020; **70**(6): 280-5.
22. Chien HI, Yang KC, Liu WC, Ho YY, Tsai WH, Chen LW. Haematogenous Klebsiella pneumoniae osteomyelitis. *International orthopaedics* 2021; **45**(7): 1693-8.
23. Prokesch BC, TeKippe M, Kim J, Raj P, TeKippe EM, Greenberg DE. Primary osteomyelitis caused by hypervirulent Klebsiella pneumoniae. *The Lancet Infectious diseases* 2016; **16**(9): e190-e5.
24. Lienard A, Hosny M, Jneid J, et al. Escherichia coli Isolated from Diabetic Foot Osteomyelitis: Clonal Diversity, Resistance Profile, Virulence Potential, and Genome Adaptation. *Microorganisms* 2021; **9**(2).
25. Matsuura H, Sue M, Takahara M, Kuninaga N. Escherichia coli rib osteomyelitis. *QJM : monthly journal of the Association of Physicians* 2019; **112**(1): 35-6.
26. Padhiary SK, Srivastava G, Panda S, Subudhi S, Lenka S. E.coli Associated Extensive Bilateral Maxillary Osteomyelitis: A Rare Case Report. *Journal of clinical and diagnostic research : JCDR* 2013; **7**(10): 2380-2.
27. Yamashita T, Arata J, Kumakiri M, Kaito S, Yoon Y. Reconstruction of E. coli Osteomyelitis of Costa: A Case Report. *Plastic and reconstructive surgery Global open* 2021; **9**(2): e3413.
28. Funk SS, Copley LA. Acute Hematogenous Osteomyelitis in Children: Pathogenesis, Diagnosis, and Treatment. *Orthop Clin North Am* 2017; **48**(2): 199-208.
29. Alvares PA, Mimica MJ. Osteoarticular infections in pediatrics. *Jornal de pediatria* 2020; **96 Suppl 1**: 58-64.
30. Coulin B, Demarco G, Spyropoulou V, et al. Osteoarticular infection in children. *The bone & joint journal* 2021; **103-b**(3): 578-83.
31. DeMarco G, Chargui M, Coulin B, et al. Kingella kingae Osteoarticular Infections Approached through the Prism of the Pediatric Orthopedist. *Microorganisms* 2021; **10**(1).
32. Samara E, Spyropoulou V, Tabard-Fougère A, et al. Kingella kingae and Osteoarticular Infections. *Pediatrics* 2019; **144**(6).
33. Yagupsky P. Kingella kingae: carriage, transmission, and disease. *Clinical microbiology reviews* 2015; **28**(1): 54-79.
34. Nguyen JC, Rebsamen SL, Tuite MJ, Davis JM, Rosas HG. Imaging of Kingella kingae musculoskeletal infections in children: a series of 5 cases. *Emergency radiology* 2018; **25**(6): 615-20.
35. Yagupsky P. Diagnosing Kingella kingae infections in infants and young children. *Expert review of anti-infective therapy* 2017; **15**(10): 925-34.
36. Laurent E, Petit L, Maakaroun-Vermeesse Z, Bernard L, Odent T, Grammatico-Guillon L. National epidemiological study reveals longer paediatric bone and joint infection stays for infants and in general hospitals. *Acta paediatrica (Oslo, Norway : 1992)* 2018; **107**(7): 1270-5.
37. Al Farsi F, Al Adawi B, Ba Tahir H, et al. Mycobacterium farcinogenes osteomyelitis of the proximal tibia: A case report. *IDCases* 2021; **25**: e01194.

38. Jaime-Villalonga A, Saul Z, Miljkovic G. Mycobacterium arupense finger osteomyelitis: Case report. *International journal of infectious diseases : IJID : official publication of the International Society for Infectious Diseases* 2020; **92**: 226-7.
39. McGee AW, Jr., Dean CS, Ignatiuk A, Savelli C, Kleck CJ. Mycobacterium phlei Vertebral Osteomyelitis. *Journal of the American Academy of Orthopaedic Surgeons Global research & reviews* 2019; **3**(12).
40. Momodu, II, Savaliya V. Osteomyelitis. StatPearls. Treasure Island (FL): StatPearls Publishing

Copyright © 2022, StatPearls Publishing LLC.; 2022.

41. Moral MZ, Desai K, Arain AR, O'Leary RE, Haddad SF, Lawrence JP. Mycobacterium abscessus-associated vertebral osteomyelitis in an immunocompetent patient: a rare case report and literature review. *Spinal cord series and cases* 2019; **5**: 53.
42. Ahmed EF, Gad GF, Soliman WE, El-Asady RS, Hasaneen AM, Abdelwahab SF. Prevalence of methicillin-resistant coagulase-negative staphylococci among Egyptian patients after surgical interventions. *Tropical doctor* 2021; **51**(1): 40-4.
43. Al-Bakri AG, Bulatova NR, Younes NA, et al. Characterization of staphylococci sampled from diabetic foot ulcer of Jordanian patients. *Journal of applied microbiology* 2021; **131**(5): 2552-66.
44. Anafo RB, Atiase Y, Dayie N, et al. Methicillin-Resistant Staphylococcus aureus (MRSA) Infection of Diabetic Foot Ulcers at a Tertiary Care Hospital in Accra, Ghana. *Pathogens (Basel, Switzerland)* 2021; **10**(8).
45. Dörr S, Freier F, Schlecht M, Lobmann R. Bacterial diversity and inflammatory response at first-time visit in younger and older individuals with diabetic foot infection (DFI). *Acta diabetologica* 2021; **58**(2): 181-9.
46. Bariteau JT, Waryasz GR, McDonnell M, Fischer SA, Hayda RA, Born CT. Fungal osteomyelitis and septic arthritis. *The Journal of the American Academy of Orthopaedic Surgeons* 2014; **22**(6): 390-401.
47. Buijs SB, Weehuizen JM, Oosterheert JJ, van Roeden SE. Chronic Q fever vertebral osteomyelitis, an underrecognized clinical entity. *Infectious diseases (London, England)* 2021; **53**(4): 241-2.
48. Cherry CC, Kersh GJ. Pediatric Q Fever. *Current infectious disease reports* 2020; **22**(4).
49. Dorfman K, Eran A, Ghanem-Zoubi N. Q Fever Vertebral Osteomyelitis Complicating Vertebroplasty. *Rambam Maimonides medical journal* 2021; **12**(1).
50. Ghanem-Zoubi N, Karram T, Kagna O, Merhav G, Keidar Z, Paul M. Q fever vertebral osteomyelitis among adults: a case series and literature review. *Infectious diseases (London, England)* 2021; **53**(4): 231-40.
51. Virk A, Mahmood M, Kalra M, et al. Coxiella burnetii Multilevel Disk Space Infection, Epidural Abscess, and Vertebral Osteomyelitis Secondary to Contiguous Spread From Infected Abdominal Aortic Aneurysm or Graft: Report of 4 Cases Acquired in the US and Review of the Literature. *Open forum infectious diseases* 2017; **4**(4): ofx192.
52. Ghioldi ME, Dealbera ED, Chemes LN, Caballero GA, Del Vecchio JJ. Cryptococcus neoformans osteomyelitis of the calcaneus: Case report and literature review. *SAGE open medical case reports* 2021; **9**: 2050313x211027094.
53. Jain D, Najjar M, Azher Q, Bachuwa G. Cryptococcal sternal osteomyelitis in a healthy woman: a review of Cryptococcus neoformans. *BMJ case reports* 2013; **2013**.
54. Matsuki T, Miyamoto S, Yamashita T. Cryptococcal osteomyelitis of the Zygomatic bone: a case report. *BMC infectious diseases* 2020; **20**(1): 399.

55. Krishnamoorthy M, Othman NAN, Hassan NEB, Hitam SB. Candida Skull Base Osteomyelitis: a Case Report and Literature Review. *Acta medica (Hradec Kralove)* 2020; **63**(2): 82-5.
56. Lopez R, Hunter AR, Geoghegan O, Demertzi E. Candida parapsilosis osteomyelitis. *BMJ case reports* 2014; **2014**.
57. McLeod N, Fisher M, Lasala PR. Vertebral osteomyelitis due to Candida species. *Infection* 2019; **47**(3): 475-8.
58. Minervini F, Kestenholtz PB, Fritsche E, Franchi A. Candida Albicans Osteomyelitis after Chest Wall Blunt Trauma: A Case Report. *Case reports in surgery* 2021; **2021**: 9987317.
59. Zalavras CG. Prevention of Infection in Open Fractures. *Infectious disease clinics of North America* 2017; **31**(2): 339-52.
60. Court-Brown CM, Bugler KE, Clement ND, Duckworth AD, McQueen MM. The epidemiology of open fractures in adults. A 15-year review. *Injury* 2012; **43**(6): 891-7.
61. Hauser CJ, Adams CA, Jr., Eachempati SR. Surgical Infection Society guideline: prophylactic antibiotic use in open fractures: an evidence-based guideline. *Surgical infections* 2006; **7**(4): 379-405.
62. Zalavras CG, Patzakis MJ. Open Fractures: Evaluation and Management. *JAAOS - Journal of the American Academy of Orthopaedic Surgeons* 2003; **11**(3).
63. Fernandes Mde C, Peres LR, de Queiroz AC, Jr., Lima JQ, Jr., Turíbio FM, Matsumoto MH. Open fractures and the incidence of infection in the surgical debridement 6 hours after trauma. *Acta ortopedica brasileira* 2015; **23**(1): 38-42.
64. Halawi MJ, Morwood MP. Acute Management of Open Fractures: An Evidence-Based Review. *Orthopedics* 2015; **38**(11): e1025-33.
65. Metsemakers WJ, Kuehl R, Moriarty TF, et al. Infection after fracture fixation: Current surgical and microbiological concepts. *Injury* 2018; **49**(3): 511-22.
66. Beam E, Osmon D. Prosthetic Joint Infection Update. *Infectious disease clinics of North America* 2018; **32**(4): 843-59.
67. Mercuri LG. Prevention and detection of prosthetic temporomandibular joint infections-update. *International journal of oral and maxillofacial surgery* 2019; **48**(2): 217-24.
68. Osmon DR, Berbari EF, Berendt AR, et al. Diagnosis and management of prosthetic joint infection: clinical practice guidelines by the Infectious Diseases Society of America. *Clinical infectious diseases : an official publication of the Infectious Diseases Society of America* 2013; **56**(1): e1-e25.
69. Tande AJ, Gomez-Urena EO, Berbari EF, Osmon DR. Management of Prosthetic Joint Infection. *Infectious disease clinics of North America* 2017; **31**(2): 237-52.
70. Tande AJ, Patel R. Prosthetic joint infection. *Clinical microbiology reviews* 2014; **27**(2): 302-45.
71. Canbek U, Akgun U, Soylemez D, Canbek TD, Aydogan NH. Incomplete atypical femoral fractures after bisphosphonate use in postmenopausal women. *Journal of orthopaedic surgery (Hong Kong)* 2019; **27**(3): 2309499019875262.
72. Jiang N, Wang BW, Chai YM, et al. Chinese expert consensus on diagnosis and treatment of infection after fracture fixation. *Injury* 2019; **50**(11): 1952-8.
73. Metsemakers WJ, Kortram K, Morgenstern M, et al. Definition of infection after fracture fixation: A systematic review of randomized controlled trials to evaluate current practice. *Injury* 2018; **49**(3): 497-504.
74. Metsemakers WJ, Smeets B, Nijs S, Hoekstra H. Infection after fracture fixation of the tibia: Analysis of healthcare utilization and related costs. *Injury* 2017; **48**(6): 1204-10.
75. Wiratnaya IGE, Nugraha HK, Kawiya IKS, Subawa IW, Sutheno A. Arthroscopic debridement for infection after fracture fixation (IAFF) of the ankle: A case report. *International journal of surgery case reports* 2022; **91**: 106772.

76. Zimmerli W, Trampuz A, Ochsner PE. Prosthetic-joint infections. *The New England journal of medicine* 2004; **351**(16): 1645-54.
77. Darouiche RO. Treatment of infections associated with surgical implants. *The New England journal of medicine* 2004; **350**(14): 1422-9.
78. Sia IG, Berbari EF, Karchmer AW. Prosthetic joint infections. *Infectious disease clinics of North America* 2005; **19**(4): 885-914.
79. Cobb LH, McCabe EM, Priddy LB. Therapeutics and delivery vehicles for local treatment of osteomyelitis. *Journal of orthopaedic research : official publication of the Orthopaedic Research Society* 2020; **38**(10): 2091-103.
80. Walter G, Kemmerer M, Kappler C, Hoffmann R. Treatment algorithms for chronic osteomyelitis. *Deutsches Arzteblatt international* 2012; **109**(14): 257-64.
81. Masters EA, Trombetta RP, de Mesy Bentley KL, et al. Evolving concepts in bone infection: redefining "biofilm", "acute vs. chronic osteomyelitis", "the immune proteome" and "local antibiotic therapy". *Bone research* 2019; **7**: 20.
82. Morgenstern M, Post V, Erichsen C, et al. Biofilm formation increases treatment failure in Staphylococcus epidermidis device-related osteomyelitis of the lower extremity in human patients. *Journal of orthopaedic research : official publication of the Orthopaedic Research Society* 2016; **34**(11): 1905-13.
83. Rao N, Ziran BH, Lipsky BA. Treating osteomyelitis: antibiotics and surgery. *Plastic and reconstructive surgery* 2011; **127 Suppl 1**: 177s-87s.
84. Bury DC, Rogers TS, Dickman MM. Osteomyelitis: Diagnosis and Treatment. *American family physician* 2021; **104**(4): 395-402.
85. Dekker AP, Uzoho C, Scammell B. Do Antibiotic-impregnated Calcium Sulfate Beads Improve the Healing of Neuropathic Foot Ulcers With Osteomyelitis Undergoing Surgical Debridement? *Wounds : a compendium of clinical research and practice* 2019; **31**(6): 145-50.
86. Hatzenbuehler J, Pulling TJ. Diagnosis and management of osteomyelitis. *American family physician* 2011; **84**(9): 1027-33.
87. Boffeli TJ, Luer SA, Brett KM, Chang HC. A Review of Consecutive Cases to Identify the Rate of Underlying Osteomyelitis in Patients Undergoing Surgical Treatment of Gangrene of the Forefoot and Impact of Acute Infection on Outcome Following Amputation. *The Journal of foot and ankle surgery : official publication of the American College of Foot and Ankle Surgeons* 2022; **61**(2): 286-92.
88. Grady JF, Winters CL. The Boyd amputation as a treatment for osteomyelitis of the foot. *Journal of the American Podiatric Medical Association* 2000; **90**(5): 234-9.
89. Miller W, Berg C, Wilson ML, Heard S, Knepper B, Young H. Risk Factors for Below-the-Knee Amputation in Diabetic Foot Osteomyelitis After Minor Amputation. *Journal of the American Podiatric Medical Association* 2019; **109**(2): 91-7.
90. Nizamani R, Heisler S, Chrisco L, Campbell H, Jones SW, Williams FN. Osteomyelitis Increases the Rate of Amputation in Patients With Type 2 Diabetes and Lower Extremity Burns. *Journal of burn care & research : official publication of the American Burn Association* 2020; **41**(5): 981-5.
91. J. F, M. M, D. S. THE FINANCIAL BURDEN OF TREATING OSTEOMYELITIS IN THE UK. *Orthopaedic Proceedings* 2019; **101-B**(SUPP\_14): 65-.
92. Shirley R, Fazekas J, McNally M, Ramsden A. Costs and remuneration of osteomyelitis treatment involving free flaps: implications of return to theatre. *J Bone Joint Infect* 2018; **3**(1): 15-9.
93. Mutluoglu M, Lipsky BA. Diabetic foot osteomyelitis. *CMAJ : Canadian Medical Association journal = journal de l'Association medicale canadienne* 2016; **188**(17-18): E535.

94. Chatzipapas C, Karaglani M, Papanas N, Tilkeridis K, Drosos GI. Local Antibiotic Delivery Systems in Diabetic Foot Osteomyelitis: A Brief Review. *The review of diabetic studies : RDS* 2021; **17**(2): 75-81.
95. Pitocco D, Spanu T, Di Leo M, et al. Diabetic foot infections: a comprehensive overview. *European review for medical and pharmacological sciences* 2019; **23**(2 Suppl): 26-37.
96. Lázaro Martínez JL, García Álvarez Y, Tardáguila-García A, García Morales E. Optimal management of diabetic foot osteomyelitis: challenges and solutions. *Diabetes, metabolic syndrome and obesity : targets and therapy* 2019; **12**: 947-59.
97. Lipsky BA, Aragón-Sánchez J, Diggle M, et al. IWGDF guidance on the diagnosis and management of foot infections in persons with diabetes. *Diabetes/metabolism research and reviews* 2016; **32** Suppl 1: 45-74.
98. Berendt AR, Peters EJ, Bakker K, et al. Diabetic foot osteomyelitis: a progress report on diagnosis and a systematic review of treatment. *Diabetes/metabolism research and reviews* 2008; **24** Suppl 1: S145-61.
99. Lipsky BA, Berendt AR, Deery HG, et al. Diagnosis and treatment of diabetic foot infections. *Clinical infectious diseases : an official publication of the Infectious Diseases Society of America* 2004; **39**(7): 885-910.
100. Lázaro-Martínez JL, Tardáguila-García A, García-Klepzig JL. Diagnostic and therapeutic update on diabetic foot osteomyelitis. *Endocrinología, diabetes y nutrición* 2017; **64**(2): 100-8.
101. Lipsky BA, Berendt AR, Cornia PB, et al. 2012 Infectious Diseases Society of America clinical practice guideline for the diagnosis and treatment of diabetic foot infections. *Clinical infectious diseases : an official publication of the Infectious Diseases Society of America* 2012; **54**(12): e132-73.
102. Yeo A, Ramachandran M. Acute haematogenous osteomyelitis in children. *BMJ (Clinical research ed)* 2014; **348**: g66.
103. Loucas CA, Brand SR, Bedoya SZ, Muriel AC, Wiener L. Preparing youth with cancer for amputation: A systematic review. *Journal of psychosocial oncology* 2017; **35**(4): 483-93.
104. McQuerry J, Gammon L, Carpiaux A, et al. Effect of Amputation Level on Quality of Life and Subjective Function in Children. *Journal of pediatric orthopedics* 2019; **39**(7): e524-e30.
105. Neuse CJ, Lomas OC, Schliemann C, et al. Genome instability in multiple myeloma. *Leukemia* 2020; **34**(11): 2887-97.
106. Shah UA, Mailankody S. Emerging immunotherapies in multiple myeloma. *BMJ (Clinical research ed)* 2020; **370**: m3176.
107. Terpos E, Raje N, Croucher P, et al. Denosumab compared with zoledronic acid on PFS in multiple myeloma: exploratory results of an international phase 3 study. *Blood Adv* 2021; **5**(3): 725-36.
108. Sonmez M, Akagun T, Topbas M, et al. Effect of pathologic fractures on survival in multiple myeloma patients: a case control study. *J Exp Clin Cancer Res* 2008; **27**(1): 11.
109. Panaroni C, Yee AJ, Raje NS. Myeloma and Bone Disease. *Current osteoporosis reports* 2017; **15**(5): 483-98.
110. Yeh HS, Berenson JR. Treatment for myeloma bone disease. *Clinical cancer research : an official journal of the American Association for Cancer Research* 2006; **12**(20 Pt 2): 6279s-84s.
111. Terpos E, Ntanasis-Stathopoulos I, Dimopoulos MA. Myeloma bone disease: from biology findings to treatment approaches. *Blood* 2019; **133**(14): 1534-9.

112. Mai EK, Miah K, Bertsch U, et al. Bortezomib-based induction, high-dose melphalan and lenalidomide maintenance in myeloma up to 70 years of age. *Leukemia* 2021; **35**(3): 809-22.
113. Hjertner Ø, Standal T, Børset M, Sundan A, Waage A. Bone disease in multiple myeloma. *Medical oncology (Northwood, London, England)* 2006; **23**(4): 431-41.
114. Desikan R, Barlogie B, Sethi R, et al. Infection--an underappreciated cause of bone pain in multiple myeloma. *Br J Haematol* 2003; **120**(6): 1047-50.
115. Roque R, Machado L, Flor D, Cunha F. Oligosecretory multiple myeloma: a devastating presentation of a difficult diagnosis. *BMJ case reports* 2021; **14**(4).
116. Yu SF, Lui CC, Pei SN, Liu JW, Cheng TT. Unsuspected multiple myeloma presenting as Escherichia coli infectious spondylitis: a case report. *Int J Rheum Dis* 2010; **13**(4): e55-8.
117. Park SS, Lee SE, Min CK. Emphysematous osteomyelitis due to Escherichia coli in multiple myeloma. *Blood Res* 2016; **51**(4): 224.
118. Stahel PF, Mauffrey C. Post-traumatic osteomyelitis: an unresolved conundrum in orthopedic trauma surgery. *European journal of trauma and emergency surgery : official publication of the European Trauma Society* 2016; **42**(4): 395-6.
119. Schmitt SK. Osteomyelitis. *Infectious disease clinics of North America* 2017; **31**(2): 325-38.
120. O'Rourke S, Meehan M, Bennett D, et al. The role of real-time PCR testing in the investigation of paediatric patients with community-onset osteomyelitis and septic arthritis. *Ir J Med Sci* 2019; **188**(4): 1289-95.
121. Parvizi J, Zmistowski B, Berbari EF, et al. New definition for periprosthetic joint infection: from the Workgroup of the Musculoskeletal Infection Society. *Clinical orthopaedics and related research* 2011; **469**(11): 2992-4.
122. Parvizi J, Gehrke T, Chen AF. Proceedings of the International Consensus on Periprosthetic Joint Infection. *The bone & joint journal* 2013; **95-b**(11): 1450-2.
123. Gornitzky AL, Kim AE, O'Donnell JM, Swarup I. Diagnosis and Management of Osteomyelitis in Children: A Critical Analysis Review. *JBJS reviews* 2020; **8**(6): e1900202.
124. Liu C, Bayer A, Cosgrove SE, et al. Clinical practice guidelines by the infectious diseases society of america for the treatment of methicillin-resistant Staphylococcus aureus infections in adults and children. *Clinical infectious diseases : an official publication of the Infectious Diseases Society of America* 2011; **52**(3): e18-55.
125. Peltola H, Pääkkönen M. Acute osteomyelitis in children. *The New England journal of medicine* 2014; **370**(4): 352-60.
126. Crone AM, Wanner MR, Cooper ML, Fox TG, Jennings SG, Karmazyn B. Osteomyelitis of the ribs in children: a rare and potentially challenging diagnosis. *Pediatric radiology* 2020; **50**(1): 68-74.
127. Zhorne DJ, Altobelli ME, Cruz AT. Impact of antibiotic pretreatment on bone biopsy yield for children with acute hematogenous osteomyelitis. *Hospital pediatrics* 2015; **5**(6): 337-41.
128. Choi SH, Sung H, Kim SH, et al. Usefulness of a direct 16S rRNA gene PCR assay of percutaneous biopsies or aspirates for etiological diagnosis of vertebral osteomyelitis. *Diagnostic microbiology and infectious disease* 2014; **78**(1): 75-8.
129. Dodwell ER. Osteomyelitis and septic arthritis in children: current concepts. *Current opinion in pediatrics* 2013; **25**(1): 58-63.
130. Street M, Puna R, Huang M, Crawford H. Pediatric Acute Hematogenous Osteomyelitis. *Journal of pediatric orthopedics* 2015; **35**(6): 634-9.
131. Preiss H, Kriechling P, Montrasio G, et al. Oral Flucloxacillin for Treating Osteomyelitis: A Narrative Review of Clinical Practice. *J Bone Jt Infect* 2020; **5**(1): 16-24.

132. Sutter DE, Milburn E, Chukwuma U, Dzialowy N, Maranich AM, Hospenthal DR. Changing Susceptibility of *Staphylococcus aureus* in a US Pediatric Population. *Pediatrics* 2016; **137**(4).
133. Saavedra-Lozano J, Falup-Pecurariu O, Faust SN, et al. Bone and Joint Infections. *The Pediatric infectious disease journal* 2017; **36**(8): 788-99.
134. Spruiell MD, Searns JB, Heare TC, et al. Clinical Care Guideline for Improving Pediatric Acute Musculoskeletal Infection Outcomes. *Journal of the Pediatric Infectious Diseases Society* 2017; **6**(3): e86-e93.
135. Wood JB, Johnson DP. Prolonged intravenous instead of oral antibiotics for acute hematogenous osteomyelitis in children. *Journal of hospital medicine* 2016; **11**(7): 505-8.
136. Berbari EF, Kanj SS, Kowalski TJ, et al. 2015 Infectious Diseases Society of America (IDSA) Clinical Practice Guidelines for the Diagnosis and Treatment of Native Vertebral Osteomyelitis in Adults. *Clinical infectious diseases : an official publication of the Infectious Diseases Society of America* 2015; **61**(6): e26-46.
137. Orr HW. The treatment of acute osteomyelitis by drainage and rest. 1927. *Clinical orthopaedics and related research* 2006; **451**: 4-9.
138. Song KM, Sloboda JF. Acute hematogenous osteomyelitis in children. *The Journal of the American Academy of Orthopaedic Surgeons* 2001; **9**(3): 166-75.
139. Peltola H, Unkila-Kallio L, Kallio MJ. Simplified treatment of acute staphylococcal osteomyelitis of childhood. The Finnish Study Group. *Pediatrics* 1997; **99**(6): 846-50.
140. LaMont RL, Anderson PA, Dajani AS, Thirumoorathi MC. Acute hematogenous osteomyelitis in children. *Journal of pediatric orthopedics* 1987; **7**(5): 579-83.
141. Urish KL, Bullock AG, Kreger AM, Shah NB, Jeong K, Rothenberger SD. A Multicenter Study of Irrigation and Debridement in Total Knee Arthroplasty Periprosthetic Joint Infection: Treatment Failure Is High. *The Journal of arthroplasty* 2018; **33**(4): 1154-9.
142. Shah NB, Hersh BL, Kreger A, et al. Benefits and Adverse Events Associated With Extended Antibiotic Use in Total Knee Arthroplasty Periprosthetic Joint Infection. *Clinical infectious diseases : an official publication of the Infectious Diseases Society of America* 2020; **70**(4): 559-65.
143. Ma D, Mandell JB, Donegan NP, et al. The Toxin-Antitoxin MazEF Drives *Staphylococcus aureus* Biofilm Formation, Antibiotic Tolerance, and Chronic Infection. *mBio* 2019; **10**(6).
144. Urish KL, DeMuth PW, Kwan BW, et al. Antibiotic-tolerant *Staphylococcus aureus* Biofilm Persists on Arthroplasty Materials. *Clinical orthopaedics and related research* 2016; **474**(7): 1649-56.
145. Bandyk DF. The diabetic foot: Pathophysiology, evaluation, and treatment. *Seminars in vascular surgery* 2018; **31**(2-4): 43-8.
146. Chastain CA, Klopfenstein N, Serezani CH, Aronoff DM. A Clinical Review of Diabetic Foot Infections. *Clinics in podiatric medicine and surgery* 2019; **36**(3): 381-95.
147. de Oliveira AL, Moore Z. Treatment of the diabetic foot by offloading: a systematic review. *Journal of wound care* 2015; **24**(12): 560, 2-70.
148. Everett E, Mathioudakis N. Update on management of diabetic foot ulcers. *Annals of the New York Academy of Sciences* 2018; **1411**(1): 153-65.
149. Lavery LA, Davis KE, Berriman SJ, et al. WHS guidelines update: Diabetic foot ulcer treatment guidelines. *Wound repair and regeneration : official publication of the Wound Healing Society [and] the European Tissue Repair Society* 2016; **24**(1): 112-26.
150. Braun L, Kim PJ, Margolis D, Peters EJ, Lavery LA. What's new in the literature: an update of new research since the original WHS diabetic foot ulcer guidelines in 2006. *Wound repair and regeneration : official publication of the Wound Healing Society [and] the European Tissue Repair Society* 2014; **22**(5): 594-604.

151. Game FL, Apelqvist J, Attinger C, et al. Effectiveness of interventions to enhance healing of chronic ulcers of the foot in diabetes: a systematic review. *Diabetes/metabolism research and reviews* 2016; **32 Suppl 1**: 154-68.
152. Elraiyyah T, Domecq JP, Prutsky G, et al. A systematic review and meta-analysis of débridement methods for chronic diabetic foot ulcers. *Journal of vascular surgery* 2016; **63**(2 Suppl): 37S-45S.e1-2.
153. Hinchliffe RJ, Valk GD, Apelqvist J, et al. A systematic review of the effectiveness of interventions to enhance the healing of chronic ulcers of the foot in diabetes. *Diabetes/metabolism research and reviews* 2008; **24 Suppl 1**: S119-44.
154. Bhandari M, Jeray KJ, Petrisor BA, et al. A Trial of Wound Irrigation in the Initial Management of Open Fracture Wounds. *The New England journal of medicine* 2015; **373**(27): 2629-41.
155. Anglen JO. Wound irrigation in musculoskeletal injury. *The Journal of the American Academy of Orthopaedic Surgeons* 2001; **9**(4): 219-26.
156. Mundi R, Chaudhry H, Niroopan G, Petrisor B, Bhandari M. Open Tibial Fractures: Updated Guidelines for Management. *JBJS reviews* 2015; **3**(2).
157. Pape HC, Tornetta P, 3rd, Tarkin I, Tzioupis C, Sabeson V, Olson SA. Timing of fracture fixation in multitrauma patients: the role of early total care and damage control surgery. *The Journal of the American Academy of Orthopaedic Surgeons* 2009; **17**(9): 541-9.
158. Pape HC, Halvachizadeh S, Leenen L, Velmahos GD, Buckley R, Giannoudis PV. Timing of major fracture care in polytrauma patients - An update on principles, parameters and strategies for 2020. *Injury* 2019; **50**(10): 1656-70.
159. Kildow BJ, Springer BD, Brown TS, Lyden E, Fehring TK, Garvin KL. Long Term Results of Two-Stage Revision for Chronic Periprosthetic Hip Infection: A Multicenter Study. *Journal of clinical medicine* 2022; **11**(6).
160. Kildow BJ, Springer BD, Brown TS, Lyden ER, Fehring TK, Garvin KL. Long Term Results of Two-Stage Revision for Chronic Periprosthetic Knee Infection: A Multicenter Study. *The Journal of arthroplasty* 2022; **37**(6s): S327-s32.
161. Hersh BL, Shah NB, Rothenberger SD, Zlotnicki JP, Klatt BA, Urish KL. Do Culture Negative Periprosthetic Joint Infections Remain Culture Negative? *The Journal of arthroplasty* 2019; **34**(11): 2757-62.
162. Ma D, Shanks RMQ, Davis CM, 3rd, et al. Viable bacteria persist on antibiotic spacers following two-stage revision for periprosthetic joint infection. *Journal of orthopaedic research : official publication of the Orthopaedic Research Society* 2018; **36**(1): 452-8.
163. Urish KL, DeMuth PW, Craft DW, Haider H, Davis CM, 3rd. Pulse lavage is inadequate at removal of biofilm from the surface of total knee arthroplasty materials. *The Journal of arthroplasty* 2014; **29**(6): 1128-32.
164. Lloyd BA, Murray CK, Shaikh F, et al. Early infectious outcomes after addition of fluoroquinolone or aminoglycoside to posttrauma antibiotic prophylaxis in combat-related open fracture injuries. *J Trauma Acute Care Surg* 2017; **83**(5): 854-61.
165. Hoff WS, Bonadies JA, Cachecho R, Dorlac WC. East Practice Management Guidelines Work Group: update to practice management guidelines for prophylactic antibiotic use in open fractures. *J Trauma* 2011; **70**(3): 751-4.
166. Jaeger M, Maier D, Kern WV, Südkamp NP. Antibiotics in trauma and orthopedic surgery -- a primer of evidence-based recommendations. *Injury* 2006; **37 Suppl 2**: S74-80.
167. Gosselin RA, Roberts I, Gillespie WJ. Antibiotics for preventing infection in open limb fractures. *Cochrane Database Syst Rev* 2004; **2004**(1): Cd003764.
168. Lane JC, Mabvuure NT, Hindocha S, Khan W. Current concepts of prophylactic antibiotics in trauma: a review. *Open Orthop J* 2012; **6**: 511-7.



169. Slane J, Gietman B, Squire M. Antibiotic elution from acrylic bone cement loaded with high doses of tobramycin and vancomycin. *Journal of orthopaedic research : official publication of the Orthopaedic Research Society* 2018; **36**(4): 1078-85.
170. Stevens CM, Tetsworth KD, Calhoun JH, Mader JT. An articulated antibiotic spacer used for infected total knee arthroplasty: a comparative in vitro elution study of Simplex and Palacos bone cements. *Journal of orthopaedic research : official publication of the Orthopaedic Research Society* 2005; **23**(1): 27-33.
171. Dumville JC, O'Meara S, Deshpande S, Speak K. Hydrogel dressings for healing diabetic foot ulcers. *Cochrane Database Syst Rev* 2013; **2013**(7): Cd009101.
172. Simchi A, Tamjid E, Pishbin F, Boccaccini AR. Recent progress in inorganic and composite coatings with bactericidal capability for orthopaedic applications. *Nanomedicine : nanotechnology, biology, and medicine* 2011; **7**(1): 22-39.
173. Cook GE, Markel DC, Ren W, Webb LX, McKee MD, Schemitsch EH. Infection in Orthopaedics. *Journal of orthopaedic trauma* 2015; **29 Suppl 12**: S19-23.
174. Conway J, Mansour J, Kotze K, Specht S, Shabtai L. Antibiotic cement-coated rods: an effective treatment for infected long bones and prosthetic joint nonunions. *The bone & joint journal* 2014; **96-b**(10): 1349-54.
175. Shen SC, Ng WK, Shi Z, Chia L, Neoh KG, Tan RB. Mesoporous silica nanoparticle-functionalized poly(methyl methacrylate)-based bone cement for effective antibiotics delivery. *Journal of materials science Materials in medicine* 2011; **22**(10): 2283-92.
176. Song W, Seta J, Kast RE, et al. Influence of Particle Size and Soaking Conditions on Rheology and Microstructure of Amorphous Calcium Polyphosphate Hydrogel. *Journal of the American Ceramic Society* 2015; **98**(12): 3758-69.
177. Hegde V, Park HY, Dworsky E, et al. The Use of a Novel Antimicrobial Implant Coating In Vivo to Prevent Spinal Implant Infection. *Spine* 2020; **45**(6): E305-e11.
178. Akhavan B, Bakhshandeh S, Najafi-Ashtiani H, et al. Direct covalent attachment of silver nanoparticles on radical-rich plasma polymer films for antibacterial applications. *Journal of materials chemistry B* 2018; **6**(37): 5845-53.
179. Croes M, Akhavan B, Sharifahmadian O, et al. A multifaceted biomimetic interface to improve the longevity of orthopedic implants. *Acta biomaterialia* 2020; **110**: 266-79.
180. Zhang BG, Myers DE, Wallace GG, Brandt M, Choong PF. Bioactive coatings for orthopaedic implants-recent trends in development of implant coatings. *International journal of molecular sciences* 2014; **15**(7): 11878-921.
181. Song W, Yu X, Markel DC, Shi T, Ren W. Coaxial PCL/PVA electrospun nanofibers: osseointegration enhancer and controlled drug release device. *Biofabrication* 2013; **5**(3): 035006.

## **1.2. The application of ceragenins to orthopaedic surgery and medicine**

This section provides an extensive review of literature concerning CSAs and their orthopaedic applications in preventing and treating antimicrobials. This review article has been peer reviewed and published in the Journal of Orthopaedic Research (IF: 3.62). It is included here in manuscript format.

### **Reference:**


**Dao A**, Mills RJ, Kamble S, Savage PB, Little DG, Schindeler A. The application of ceragenins to orthopedic surgery and medicine. J Orthop Res. 2020 Sep;38(9):1883-1894. doi: 10.1002/jor.24615. Epub 2020 Feb 10. PMID: 31994754.

### **Statement of Contribution:**

AD and AS conceptualized the article; AD conducted the review, data extraction and prepared the tables; AD and AS wrote, RJM, SK, PBS and DGL reviewed, and edited the manuscript. All authors read and approved the final manuscript.

## REVIEW

# The application of ceragenins to orthopedic surgery and medicine

Aiken Dao<sup>1,2</sup> | Rebecca J. Mills<sup>1,2</sup> | Sumedh Kamble<sup>1,2</sup> | Paul B. Savage<sup>1,3</sup>  |  
David G. Little<sup>1,2</sup>  | Aaron Schindeler<sup>1,2</sup> 

<sup>1</sup>Orthopaedic Research & Biotechnology Unit, The Children's Hospital at Westmead, Sydney, NSW, Australia

<sup>2</sup>The Discipline of Child and Adolescent Health, Faculty of Medicine, University of Sydney, Sydney, NSW, Australia

<sup>3</sup>Department of Chemistry and Biochemistry, Brigham Young University, Provo, Utah

## Correspondence

Aaron Schindeler, Orthopaedic Research & Biotechnology, Research Building, The Children's Hospital at Westmead, Locked Bag 4001, Westmead, NSW 2145, Australia.  
Email: [aaron.schindeler@sydney.edu.au](mailto:aaron.schindeler@sydney.edu.au)

## Abstract

Osteomyelitis and infections associated with orthopedic implants represent a significant burden of disease worldwide. Ceragenins (CSAs) are a relatively new class of small-molecule antimicrobials that target a broad range of Gram-positive and Gram-negative bacteria as well as fungi, viruses, and parasites. This review sets the context of the need for new antimicrobial strategies by cataloging the common pathogens associated with orthopedic infection and highlighting the increasing challenges of managing antibiotic-resistant bacterial strains. It then comparatively describes the antimicrobial properties of CSAs with a focus on the CSA-13 family. More recently developed members of this family such as CSA-90 and CSA-131 may have a particular advantage in an orthopedic setting as they possess secondary pro-osteogenic properties. In this context, we consider several new preclinical studies that demonstrate the utility of CSAs in orthopedic models. Emerging evidence suggests that CSAs are effective against antibiotic-resistant *Staphylococcus aureus* strains and can prevent the formation of biofilms. There remains considerable scope for developing CSA-based treatments, either as coatings for orthopedic implants or as local or systemic antibiotics to prevent bone infection.

## KEYWORDS

bone, cationic selective antimicrobial, cationic steroid antimicrobial, ceragenin, CSA, orthopedics, osteomyelitis, prosthetic joint infection

## 1 | JOINT AND BONE INFECTIONS

### 1.1 | Joint and bone infections are an increasing issue for orthopedic care

Prosthetic joint infection (PJI) is a significant clinical problem worldwide, and one that is set to increase as arthroplasty is performed to keep an aging population active. Patients are now living longer with their implants, and surgeons are feeling more confident in offering arthroplasty to younger patients, resulting in an increased number of procedures being performed.

However, despite pre-operative patient optimization, meticulous surgical technique, and routine systemic antibiotic prophylaxis, the incidence rate of PJI continues to rise.<sup>1</sup> According to the US National Inpatient Sample, the PJI incidence rate in the United States expressed as a percentage of the total number of arthroplasties performed, increased from 1.9% to 2.2% for hip arthroplasties and from 2.1% to 2.2% for knee arthroplasties per annum between 2001 and 2009.<sup>2</sup> While the frequency of infection following elective orthopedic surgery is not particularly high (1.5–2.5%), the rates of reinfection are significantly higher. Approximately 20% to 25% of revision arthroplasty was due to implant infections.<sup>3,4</sup> Also, the management

and treatment for PJI can be complicated and incredibly difficult to eradicate. Once an infection has been established it would require a multispecialty approach, multiple surgeries and long courses of intravenous antibiotics to cure.<sup>1</sup>

Osteomyelitis is often seen in the context of trauma, particularly with high-energy open fractures.<sup>5</sup> It has been estimated that 5% to 10% of orthopaedic trauma patients are affected by implant-related infections,<sup>6</sup> ranging from ~1% for the surgical fixation of closed low-energy fractures such as distal radius and ankle fractures, to >30% for complex open tibial fractures in patients with multiple comorbidities.<sup>7</sup> Besides, vertebral osteomyelitis is also a severe form of bone infection in adults with an incident rate of 4.8 per 100 000, accounts for 3% to 5% of all cases of osteomyelitis.<sup>8</sup>

Acute hematogenous osteomyelitis (AHO) is seen mainly within the pediatric population,<sup>9,10</sup> with an incidence of two cases per 10 000.<sup>11</sup> The most common sites of osteomyelitis in children are the metaphyseal regions of the long bones, including the femur (27%), tibia (22%), and humerus (12%).<sup>12</sup> On the other hand, chronically infected nonunions of fractures can cause significant pain and disability,<sup>5</sup> whereas relapsing and persistent infection may require multiple invasive procedures and extended courses of antibiotics to attempt curative treatment.<sup>13</sup> With prompt diagnosis and treatment, children generally respond well to systemic antibiotics, and surgical intervention is rarely required. However, amongst the adult population, the largest group of patients affected by chronic osteomyelitis are diabetics suffering from diabetic foot osteomyelitis and lower limb ulcers.<sup>14</sup> This immunocompromised group is at high risk of developing life-threatening sepsis and not infrequently require serial amputation, alongside intravenous antibiotics to manage their chronic osteomyelitis.

Although PJI only happens in a minority of arthroplasty cases, it represents a significant burden to the patient and community with severe clinical outcomes and high healthcare expenditure.<sup>1</sup> The cost of treating implant-associated infections and osteomyelitis varies widely among countries. In the United States, the cost per case of two-stage revision septic hip arthroplasty was approximately US \$90 000 to \$100 000, and the cost for knee arthroplasty was approximately US \$75 000.<sup>15</sup> Moreover, the government pays at least 1.6 billion USD to cover the expense of the excess hospital charges to treat PJIs and will exceed 1.62 billion USD by 2020 in the United States alone.<sup>16</sup>

As healthcare systems face increasing economic pressure worldwide, there is substantial interest in reducing the incidence of joint and bone infections and developing novel strategies for both prophylaxis and treatment.

## 1.2 | Causative organisms of bone infections

While many bone infections are polymicrobial, and often the causative organism is never identified, *Staphylococcus aureus* (70-90%) remains the most prevalent causative agent of acute and chronic osteomyelitis.<sup>17,18</sup> Due to the clinical use of penicillin, osteomyelitis

caused by methicillin-resistant *S. aureus* (MRSA) has also increased,<sup>19</sup> even though methicillin-sensitive *S. aureus* (MSSA) is still the most common pathogenic organism of PJI.<sup>2</sup>

In the United States, it was estimated that 25% to 32% of infections after fracture fixation were caused by MRSA.<sup>7</sup> While vancomycin-resistant *S. aureus* (VRSA) is not a common cause of osteomyelitis, since 2002, there have been a number of confirmed VRSA infection cases involving soft tissue and bone, and one case of PJI in the United States.<sup>20</sup> This suggests that VRSA can be a cause for future concern as vancomycin-resistance represents a troubling evolution of microbial drug resistance.

PJI caused by *S. aureus* and MRSA is difficult to cure due to the formation and persistence of the bacteria in biofilm adherent to the prosthesis surface.<sup>21</sup> Other etiologies are coagulase-negative staphylococci (CONS), enterococci, gram-negative bacilli, and anaerobic bacteria, including *Haemophilus influenzae* type B, *Salmonella*, *Streptococcus agalactiae*, and *Escherichia coli*.<sup>7,22</sup>

Post-traumatic osteomyelitis is either caused by skin commensals or direct contamination at the time of injury.<sup>23</sup> *Staphylococci* and *Streptococci* are again the predominant pathogens while *Pseudomonas aeruginosa* and *E. coli* can cause implant-related osteomyelitis.<sup>7,18</sup> Furthermore, *Mycobacterium*, *Cutibacterium*, *Bartonella*, *Histoplasma*, *Cryptococcus*, *Blastomyces*, *Candida*, and *Coxiella* are less frequent but possible pathogens to cause osteomyelitis in infected patients.<sup>24-27</sup>

In pediatrics, the majority of osteomyelitis cases are secondary to hematogenous spread. AHO is sometimes linked to osteoarticular infections caused by *S. aureus*, *Streptococcus pyogenes*, and *Streptococcus pneumoniae*.<sup>28-30</sup> *Kingella kingae* has recently been recognized as a cause of pediatric bacteremia and represents the leading pathogen causing osteomyelitis and septic arthritis in children aged 6 to 48 months.<sup>31-34</sup> Fortunately, most AHO cases respond well to current antibiotic treatments, and advances in pharmacology have led to significant reductions in associated mortality.

## 1.3 | Antibiotic prophylaxis and treatment for bone infections

Prophylactic antibiotics have a recognized efficacy in reducing the number of postsurgical infections in orthopaedic patients. For elective orthopaedic procedures, prophylactic antibiotics are routinely given at induction of anesthesia. A wide variety of broad-spectrum antimicrobials are in use with different dosing regimens.<sup>35</sup> Recommendations from the American Academy of Orthopaedic Surgeons (AAOS) and CDC place the optimal timing of prophylactic treatment at 1 hour before a surgical procedure. If vancomycin and fluoroquinolones are used, the treatment should be extended to 2 hours due to their longer infusion time.<sup>36</sup>

Cefazolin is the most commonly used prophylactic antibiotic in the management of open fractures. Patients receiving antibiotics within 60 minutes of injury have a quarter of the risk of infection compared to patients receiving antibiotics after 90 minutes.<sup>23</sup> For fractures, coverage for Gram-positive bacteria is essential in type I

and type II open fractures, whereas the addition of Gram-negative coverage is necessary for type III open fractures. Open fracture wounds at risk for fecal or clostridial contamination are advocated to be treated with penicillin. For type I and type II open fractures, prophylactic treatment can be discontinued by 24 hours after wound closure. For type III open fractures, antibiotic discontinuation is specified to be 72 hours after an injury or 24 hours after wound closure or coverage.<sup>23</sup>

For established infections, the microbial culture is a common starting point for identifying suitable antibiotic strategies. An early decision is whether surgery is required to debride the area of pathogens or remove any contaminated implants. For infected metalwork, surgical excision is considered the gold standard and is needed to eradicate biofilms. Clinical decision-making as to whether a one-stage or two-stage reconstruction is employed can be case dependent, but regardless all operations are followed by an extended course of systemic antibiotics.<sup>37</sup>

The rationale for the aggressive removal of contaminated implants is the presence of a biofilm. A biofilm is a polysaccharide or protein matrix produced by bacterial colonies, and its function is to prevent the host immune system and systemic antibiotics from attacking the bacteria. Biofilms develop preferentially on inert surfaces and dead tissues, including medical devices and fragments of dead bones and respond poorly to systemic antimicrobial treatments as the biofilm acts as a relatively impermeable barrier to many antibiotics. Bacteria within the biofilm shift to a less active state, lowering their susceptibility to antibiotics by up to 1000-fold.<sup>37–41</sup> Biofilm implant-related infection and antimicrobial-resistant infection can cost the healthcare system up to 3 billion US dollars individually per year in the United States.<sup>42–44</sup> Therefore, it is not only a significant cause of morbidity but also increases economic loss.

In the absence of contaminated implants, osteomyelitis can be managed by 6 days of intravenous antibiotics and followed by 6 weeks of antimicrobial therapy orally.<sup>17</sup> Vancomycin, combined with gentamicin or rifampin, is usually used to treat adult osteomyelitis, although third-generation cephalosporin, aminoglycoside, fosfomycin, and glycopeptides are also commonly used in pediatrics.<sup>45</sup> The purpose of such combined therapy is to broaden coverage to include vancomycin-intermediate *S. aureus* (VISA).<sup>10</sup> Other treatment options include clindamycin, nafcillin/methicillin, and dicloxacillin, but it has been shown that clindamycin is more effective than semi-synthetic penicillin due to the prevalence of MRSA and methicillin-resistant bacteria in osteomyelitis patients.<sup>17</sup> The treatment and prognosis of acute osteomyelitis can be different in infants and very young children, as the infection may progress more rapidly, and they are more susceptible to fatal complications.

The emergence of antibiotic resistance is leading to increased morbidity and mortality. The prolonged and arbitrary use of antibiotics is the predisposing factors for the emergence of multi-drug resistant bacteria. Despite advances in orthopedic surgery, such antibiotic-resistant bacteria remain challenging to prevent and to treat, and the incident rates are increasing.<sup>46</sup> *S. aureus* is particularly prone to acquiring antibiotic resistance, as the acquisition of the

*mecA* gene encoding a unique penicillin-binding protein can reduce its affinity for  $\beta$ -lactam and decrease cell wall synthesis even in the presence of penicillin, cephalosporin, and carbapenem.<sup>47</sup> Thus, a challenge for orthopedic pharmacology is the development of innovative, broad-spectrum antimicrobials for infection prophylaxis and treatment, to prevent or reduce perioperative-related infections.

## 2 | CERAGENINS

### 2.1 | CSAs are broad-spectrum antimicrobials derived from cholic acid

Ceragenins (CSAs) are a class of novel synthetic antibiotics developed from cholic acid by the addition of amine groups and other functional side chains.<sup>48</sup> They mimic the bactericidal activities of cationic antimicrobial peptides (CAPs) that are a part of the innate immune system, such as LL-37 to have bacteriostatic and bactericidal actions.<sup>49,50</sup> Part of their initial conceptualization involved mimicking the amphiphilic properties of CAPs. However, unlike CAPs, CSAs do not have peptide bonds and thus cannot be degraded by proteases at the sites of infection and have a longer half-life in the body than CAPs. CSAs are simpler to synthesize on a large scale than CAPs,<sup>49,51,52</sup> making their preparation more cost-effective and attractive for antimicrobial therapy than conventional broad-spectrum antibiotics.

The antimicrobial activities of CSAs are known to involve direct interaction with negatively charged membrane molecules of bacteria, including phosphatidylglycerol and lipid A lipopolysaccharides, which then lead to bacterial cell membrane permeabilization and depolarization.<sup>48,51,53</sup> However, the precise mechanism remains to be elucidated. CSAs selectively bind to bacterial membranes over eukaryotic cell membranes, attributed to their lipid A binding properties.<sup>51,54</sup> Although some CSAs (eg, CSA-13) may have less potency vs Gram-negative bacteria due to their high phosphatidylethanolamine content,<sup>55</sup> many other CSAs have shown broad-spectrum antimicrobial activities against different species of Gram-positive and Gram-negative bacteria,<sup>50,56,57</sup> fungi,<sup>58</sup> enveloped viruses,<sup>59</sup> and parasites.<sup>60,61</sup> Nevertheless, the precise mechanisms of action and whether they may differ between Gram-positive and Gram-negative microbes are an area for future study.

The minimum inhibitory concentrations (MICs) and minimum bactericidal concentrations (MBCs) of CSAs against various pathogens were tested and compared to other antimicrobial agents, such as erythromycin, cefepime, ciprofloxacin, doxycycline, piperacillin, tobramycin, colistin, metronidazole, ampicillin, meropenem, and other antimicrobial peptides.<sup>48,51,52,62,63</sup> While CSAs have equivalent antibacterial efficacy to other clinical antibiotics, multiple studies have indicated they can be superior to other antibiotics in penetrating and eradicating biofilms.<sup>49,51</sup> For example, CSA-8, CSA-13, CSA-31, CSA-38, and CSA-44 were found to have a significantly lower minimum biofilm eradication concentration than erythromycin and doxycycline. Another study showed that CSA-13, CSA-90, and

**TABLE 1** Microorganisms susceptible to CSAs in in vitro studies

Organisms	CSAs known to be effective	References
<i>Acinetobacter baumannii</i>	13	62,64
<i>Aspergillus fumigatus</i>	131, 192	65
<i>Bacillus anthracis</i>	13	66
<i>Bacillus subtilis</i>	8, 13, 54	57,66
<i>Bacteroides fragilis</i>	13, 131	52
<i>Bacteroides thetaiotaomicron</i>	13, 131	52
<i>Bacteroides stercoris</i>	13, 131	52
<i>Candida albicans</i>	8, 13, 44, 131, 138, 142, 144, 192	58,65,67
<i>Candida auris</i>	44, 131	68,69
<i>Candida dublieusis</i>	13, 44, 131, 138	67
<i>Candida glabrata</i>	8, 13, 44, 131, 138, 142, 192	58,67
<i>Candida kefyr</i>	8, 13, 44, 131, 138, 142, 192	58
<i>Candida krusei</i>	8, 13, 44, 131, 138, 142, 192	58,67
<i>Candida parapsilosis</i>	13, 44, 131, 138	67
<i>Candida tropicalis</i>	13, 44, 131, 138	67
<i>Caulobacter crescentus</i>	8	66
<i>Clostridium difficile</i>	8, 13, 131	70
<i>Clostridium perfringens</i>	13, 131	52
<i>Cryptococcus neoformans</i>	131, 192	65
<i>Escherichia coli</i>	13, 54, 131	48,63,66,71,72
<i>Enterococcus faecalis</i>	13, 90, 92	73
<i>Haemophilus influenzae</i>	13, 90, 92	73
<i>Helicobacter pylori</i>	13, 90, 92	73,74
<i>Klebsiella pneumoniae</i>	13, 44, 131, 138, 142	48
<i>Legionella pneumophila</i>	8, 13, 31, 38, 44, 131, 138	75
<i>Leishmania major</i>	13	60
<i>Moraxella catarrhalis</i>	13, 90, 92	73
<i>Neisseria meningitidis</i> (B)	13, 90, 92	73
<i>Neisseria meningitidis</i> (C)	13, 90, 92	73
<i>Peptostreptococcus anaerobius</i>	13, 131	52,66,70,73
<i>Porphyromonas ginivalis</i>	13	73
<i>Prevotella bivia</i>	13, 131	52
<i>Prevotella disiens</i>	13, 131	52
<i>Prevotella melaninogenica</i>	13, 131	52
<i>Prevotella oralis</i>	13, 131	52

**TABLE 1** (Continued)

Organisms	CSAs known to be effective	References
<i>Propionibacterium acnes</i>	13, 131	52
<i>Pseudomonas aeruginosa</i>	13, 44, 90, 131, 134, 136, 138, 192	51,64,71,73,76–83
<i>Salmonella typhi</i>	13	48
<i>Staphylococcus aureus</i>	8, 13, 25, 44, 54, 90, 92, 131, 134, 136, 138, 142, 144, 145, 192	50,64,66,73,78,82
<i>Staphylococcus epidermidis</i>	13, 90, 92	73
<i>Streptococcus gordonii</i>	13	84
<i>Streptococcus mitis</i>	13	84
<i>Streptococcus mutans</i>	13, 90, 92	73,84
<i>Streptococcus oralis</i>	13	84
<i>Streptococcus pneumoniae</i>	13, 90, 92	73,84
<i>Streptococcus pseudopneumoniae</i>	13	84
<i>Streptococcus pyogenes</i>	8, 13, 90, 92	66,73,84
<i>Streptococcus salivarius</i>	13, 90, 92	73
<i>Streptococcus sanguinis</i>	13, 90, 92	73,84
<i>Trypanosoma cruzi</i>	13	60
<i>Trichomonas vaginalis</i>	13, 44, 131, 138	61

CSA-131 can reduce the number of live bacteria in the biofilm of *P. aeruginosa*, *Klebsiella pneumoniae*, and *S. aureus* at 100 µg/mL, and bacteria that were treated by CSAs had significantly less matrix substance production.<sup>56</sup> Another study suggested that CSA-13 and CSA-131 significantly inhibited biofilm formation by *Bacteroides fragilis* at a lower concentration than metronidazole.<sup>52</sup> Table 1 summarizes the microorganisms that were shown to be susceptible to CSAs.

CSAs have been generated with a variety of physicochemical properties. For instance, CSA-44 is a degradable CSA with a half-life in aqueous solution to pH 7 of 37 days. Breakdown products include cholic acid, beta-alanine, and octanol. CSA-44 can be prepared at a large scale, and its degradation products can be readily measured from biological fluids.<sup>75</sup> CSA-44 demonstrates antimicrobial activities for multiple *Candida* spp., including *Candida auris* and *Candida albicans*, as well as many bacterial strains.

It has been speculated that bacteria and fungi are unlikely to develop resistance against CSAs, as this would require massive alterations to the plasma membrane.<sup>51,56,68,85</sup> In one study, three critical pathogens (*S. aureus*, *P. aeruginosa*, and *Acinetobacter baumannii*) were tested for MICs following serial exposure to ciprofloxacin, colistin, vancomycin, and CSA-13. In results, all bacteria became highly

resistant to ciprofloxacin (after <20 passages), colistin, and vancomycin (after 20–30 passages), except CSA-13; there was only a minimal increase of MICs of CSA-13 in all bacteria after 30 passages.<sup>64</sup> Additionally, continual exposure to colistin had little or no effect on the MICs with CSA-131, suggesting that CSAs are effective against colistin-resistant bacteria.<sup>85</sup> Indeed, a study showed that prolonged exposure of Gram-negative bacteria to chlorhexidine reduces susceptibility to colistin but not to AMPs and CSAs.<sup>86</sup> One potential mechanism hypothesized for bacteria to acquire CSA resistance is via modification of the lipid A portion of lipopolysaccharide; lipid A is a prime target of both colistin and CSAs.

## 2.2 | The CSA-13 sub-class of antimicrobials

The CSA-13 sub-class of CSAs (CSA-13, CSA-90, and CSA-131) has been a focus of development in terms of biomedical applications. This

sub-class shares structural similarity to CSA-8 (Figure 1), which displays a broad-spectrum activity against Gram-positive bacteria but is less effective against Gram-negative bacteria than other CSAs.<sup>50,51,62</sup> CSA-13 is a prototypical member of the CSA antibiotic class, and a large number of studies have characterized its broad-spectrum efficacy and antimicrobial mechanism. CSA-13 exhibits structural similarity to CSA-8 but contains an amine group at C24. CSA-131 is closely related to CSA-13, and they share similar bactericidal activities. CSA-90 is distinctive with the double lipid chains from the amine at C24. CSA-138 is in the same class, although it has not been widely investigated.

CSA-13, CSA-90, and CSA-131 are particularly effective against several high burden pathogens, including *S. aureus*,<sup>50</sup> MRSA,<sup>49</sup> VRSA,<sup>50</sup> *P. aeruginosa*,<sup>51</sup> *Clostridium difficile*,<sup>70</sup> *Helicobacter pylori*,<sup>74</sup> *S. pneumoniae*,<sup>84</sup> *K. pneumoniae*,<sup>56</sup> and several anaerobic pathogens, such as *B. fragilis* and *Propionibacterium acnes*.<sup>52</sup> Additionally, CSA-13 exerts a high affinity for the external layers of *Bacillus subtilis* spores

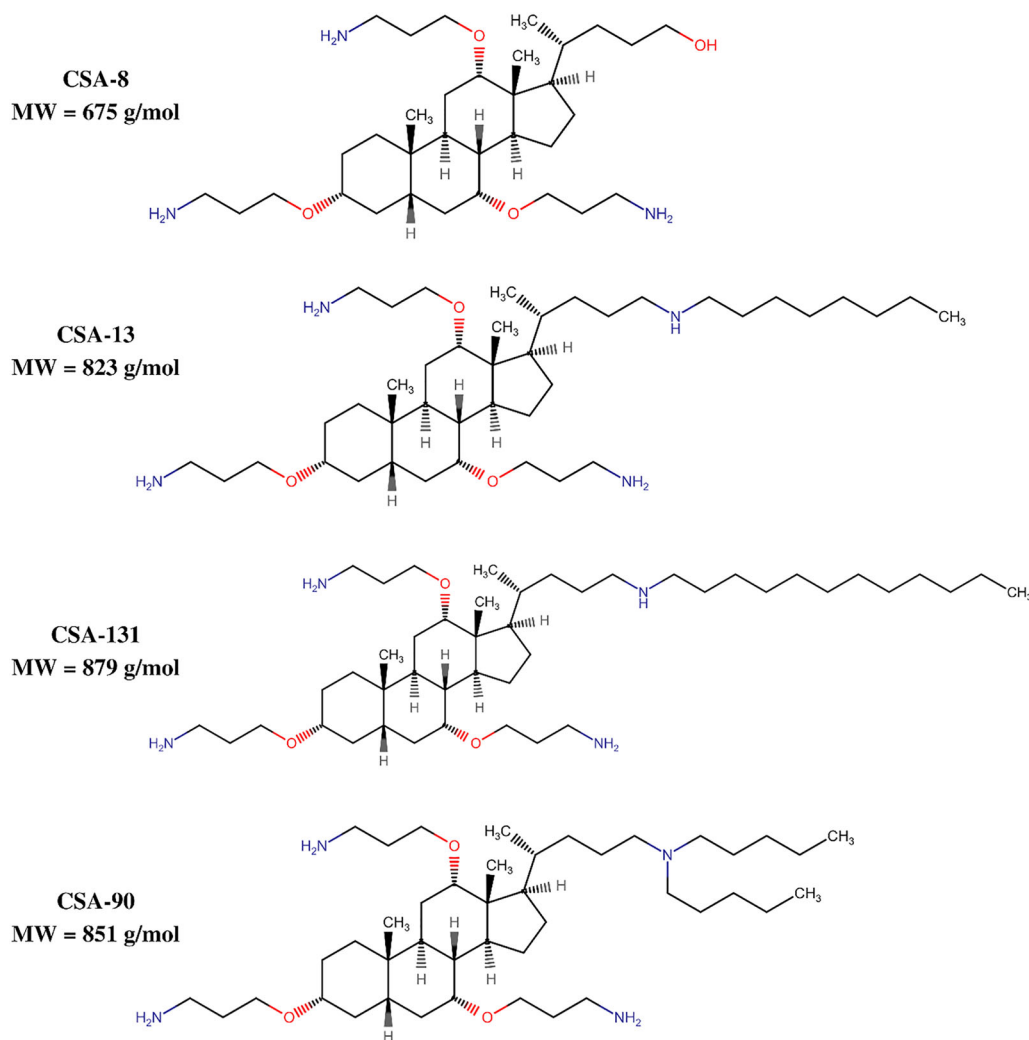


**FIGURE 1** The chemical structures of CSA-8, CSA-13, CSA-131, and CSA-90. CSA-90 and CSA-131 are closely related to CSA-13, the only difference is that CSA-131 has a longer extended lipid chain from the amine at C24, and CSA-90 has double short lipid chains from the amine at C24. In contrast, CSA-8 does not contain an amine group at C24, replaced by a hydroxyl group [Color figure can be viewed at [wileyonlinelibrary.com](http://wileyonlinelibrary.com)]



and increase the permeability of the outer and inner spore membrane. Although *B. subtilis* is considered part of the normal gut flora and does not usually cause clinical infections, the model had sufficiently demonstrated the sporicidal effects of CSA-13.

CSA-131 is not only effective against bacterial species but can also prevent the growth of the yeast *C. auris*.<sup>68,69</sup> The scanning electron microscopic images showed that the fungal cells were morphologically disrupted after being exposed to CSA-131 (25 mg/L or above), and it would kill the fungal cells in biofilms at higher concentrations.<sup>68</sup> Similar results were found in *C. albicans*, *Cryptococcus neoformans*, and *Aspergillus fumigatus* with similar concentrations of CSA-131 and CSA-13.<sup>65</sup> Meanwhile, a study found that CSA-13 and CSA-131 eradicate orthopoxviral infections in Kupffer cells by disrupting the envelope and internal structure of the vaccinia virus.<sup>59</sup> Lastly, CSA-13, CSA-131, and CSA-138 can kill metronidazole-resistant *Trichomonas vaginalis*,<sup>61</sup> whereas CSA-8 and CSA-13 are toxic to *Trypanosoma cruzi* and *Leishmania major*.<sup>60</sup>

The utility of CSA-13 sub-class members may be enhanced by the co-administration of other antimicrobial agents. CSA-13 was able to increase the activity of erythromycin against various gram-negative pathogenic bacteria (eg, *E. coli*, *Salmonella typhi*, *Pseudomonas spp.*, and *Klebsiella spp.*) isolated from clinical patients (37). Another study showed the rapid bactericidal activity of CSA-13 and synergism with colistin in the CSA-13-colistin combination group while no antagonism was observed.<sup>76</sup> A recent study has found synergistic interactions of CSA-13 and CSA-138 with fluconazole, in the context of *Candida spp.* treatment.<sup>58</sup> Subsequently, CSAs have also been shown to exhibit a synergistic effect with cefepime and ciprofloxacin.<sup>62,76</sup>

CSAs may benefit wound-healing by the promotion of local blood vessel formation. Some cationic antimicrobial peptides have been shown to initiate angiogenesis via an agonistic action on formyl peptide receptor-like 1 (FPRL1) and the prostaglandin E2-EP3.<sup>80</sup> In an in vitro angiogenesis model CSA-13 and CSA-192 stimulated cell migration, while CSA-13, CSA-90, and CSA-142 stimulated tube formation.<sup>56</sup> Tube formation was linked to the expression of vascular endothelial growth factor receptor 2.

However, CSA-13 at high doses can have cytotoxic effects on human cells. CSA-13 was found to be hemolytic and can induce lysis in human osteoblasts at concentrations  $\geq 50 \mu\text{g/mL}$ .<sup>84,87</sup> CSAs were also cytotoxic to immortalized human keratinocytes (HaCaTs) at lower concentrations ( $< 10 \mu\text{g/mL}$ ).<sup>73</sup> These effects were possibly due to depolarization and permeabilization characteristics on cell membranes.<sup>68,84</sup> CSA-13 can also increase apoptosis rates. However, this may have beneficial applications in terms of cancer treatment. CSA-13 has similar effects on colon cancer cells (HCT116, HT-29, and DLD-1) and human breast cancer cells (MCF-7 and MDA-MB-21).<sup>80,88</sup> CSA-13 reduced cancer cell growth most effectively at 10 to  $20 \mu\text{g/mL}$  at the G1/S phase. Notably, CAPs can likewise affect apoptosis, with antimicrobial peptide LL-37 increasing the rate of apoptosis of lung epithelial cells.<sup>80,89</sup> In the case of CSA-13, it has been hypothesized the compounds can induce mitochondrial membrane depolarization and apoptosis via a p53-independent pathway and a caspase-independent mechanism. While no adverse cytotoxic

effects were detected after the administration of CSA-13 in pre-clinical (BALB/c mice) models, the anti-cancer effects of CSAs were observed at a relatively low dose.<sup>90</sup>

### 3 | CSAs AND ORTHOPEDIC APPLICATIONS

#### 3.1 | The antimicrobial effects of CSAs against orthopedic pathogens

Orthopedic implant surfaces provide a unique environment for bacteria to attach and colonize that induce bone and implant-related infections. *S. aureus*, *Staphylococcus epidermidis*, and *E. coli* are the most frequent causative agents of osteomyelitis.<sup>91</sup> However, there is a range of other bacteria associated with bone infections. Table 2 highlights the efficacy of CSA-13 sub-class members against the bacteria that commonly cause osteomyelitis and list the associated MIC and MBC values.

*S. aureus* and methicillin-resistant *S. aureus* are significant causative agents of osteomyelitis, and in vitro studies have identified the MIC and MBC values required for treatments.<sup>63,66,68,73,82</sup> Generally, MICs are between 0.4 mg/L and 6.3 mg/L. CSA-13 is effective against most tested pathogens in low dose concentrations (0.4–2.0 mg/L), whereas CSA-90 and CSA-131 have the same MICs but higher MBCs than CSA-13 against most selected pathogens. The CSA-13 sub-class may be less effective against *P. aeruginosa* based on the MIC and MBC values. No data is available on the sensitivities of MRSE and *K. kingae*, which are emerging causative agents of osteomyelitis in children.<sup>9,92</sup>

#### 3.2 | In vivo antimicrobial activity of CSAs in orthopedic models

The first study testing CSAs as a prophylactic agent was performed in an established sheep model of pin-tract infection. The study by Perry et al.<sup>93</sup> aimed to evaluate the efficacy of CSA-13 at preventing infection developing following implantation of a percutaneous bicortical titanium alloy pin in the proximal tibia. The study comprised of two groups where the treatment group received CSA-13 treated polyurethane foam pads around the pin after surgery, whereas the control group received untreated autoclaved foam pads. An oral bolus of tetracycline (0.5–1.5 g) was given to all animals 1 hour before surgery, but no further antibiotics were given to the animals after surgery. In the results, the CSA-13 treated group had one positive blood culture, nine positive soft tissue cultures, and no positive bone culture, whereas the untreated control group had two positive blood cultures, eight positive soft tissue cultures, and three positive bone cultures. Although the Kaplan-Meier curve did not show that CSA-13 treated foam pads significantly reduced the infection rate and mortality, CSA-13 may delay infection during the first 20 days post-surgery.<sup>93</sup> Thus CSA-13 may have utility as a secondary preventive



**TABLE 2** Efficacy of CSA-13, CSA-90, and CSA-131 vs bacterial pathogens that cause osteomyelitis

Organisms	Ceragenins (CSAs)					
	CSA-13		CSA-90		CSA-131	
	MIC, mg/L	MBC, mg/L	MIC, mg/L	MBC, mg/L	MIC, mg/L	MBC, mg/L
Methicillin-susceptible <i>Staphylococcus aureus</i>	0.4-0.8	0.8-1.4	0.7	2.8	0.5-2.0	3.1
Methicillin-resistant <i>Staphylococcus aureus</i>	0.5	1.0	ND	ND	0.5	1.0
Vancomycin-resistant <i>Staphylococcus aureus</i>	1.0-2.0	1.0-2.0	ND	ND	ND	ND
<i>Staphylococcus epidermidis</i>	0.4	0.7	0.7	1.4	ND	ND
Methicillin-resistant <i>Staphylococcus epidermidis</i>	ND	ND	ND	ND	ND	ND
<i>Streptococcus pyogenes</i>	0.7	0.7	0.4	1.4	ND	ND
<i>Streptococcus pneumoniae</i>	0.4	0.7	0.7	1.4	ND	ND
<i>Pseudomonas aeruginosa</i>	3.0	6.0	6.3	6.3	3.1	3.1
<i>Haemophilus influenzae</i>	0.4	0.7	0.7	1.4	ND	ND
<i>Kingella kingae</i>	ND	ND	ND	ND	ND	ND

Note: Data from Expand et al,<sup>63</sup> Expand et al,<sup>66</sup> Hashemi,<sup>68</sup> Leszczynska et al,<sup>73</sup> and Niemirowicz et al.<sup>82</sup>

Abbreviations: MBC, minimal bactericidal concentration (the lowest concentration of an antimicrobial required to kill a particular bacteria); MIC, minimal inhibitory concentration (the lowest concentration of an antimicrobial that will inhibit the visible growth of a microorganism); ND, not determined.

measure. However, this study did not include a positive control group where pin-tract infection could be induced by bacterial inoculation, or a negative control group where oral or IV antibiotics could be given postsurgically. The overall data was inconclusive to determine the CSA-13 efficacy in preventing pin-tract infections.

A follow-up study by Williams et al<sup>94</sup> further investigated the application of CSA-13 in preventing wound infections in a sheep model. Instead of a titanium alloy pin implant, a new osseointegrated implant was used in this study. CSA-13 embedded foam pads could not reduce or eradicate the bacterial colonization and failed to prevent infections at the skin/implant interface and the underlying tissues. It was concluded that the skin surrounding an osseointegrated implant should be sutured to act as a primary biological barrier while CSAs could be used adjunctively to reduce infection risk. A limitation of this paper is that no positive control groups were included, making it unclear whether this infection model would also be recalcitrant to more aggressive existing antimicrobial treatments.

This team next reported on another sheep model featuring a novel CSA-coating system using polydimethylsiloxane (PDMS) and primer (MED-160) on stainless-steel plates,<sup>95</sup> and it was the first open fracture model to feature a CSA coating for treatment. A Gustilo type IIIB open fracture was introduced surgically (with the stripping of a 2 × 5 cm area of periosteum), and infection was introduced via two membranes containing MRSA biofilms. Biofilms were grown on a piece of polyetheretherketone membrane in brain heart infusion broth. Then, to treat, proximal and distal plates were

templated by drilling and placing transcortical screws through each plate onto the bare cortical surface and placed in apposition to the biofilms. CSA-13 produced 100% protection against bone infection and eradicated biofilm on the implant surface based on microbial and histological analyses. The difference was statistically significant compared to the untreated infected group with a 100% infection rate, illustrating that the CSA-13 coating was the cause of prevention.

A porous-coated eluting titanium plug was implanted into the sheep femur to study perioperative device-related infections.<sup>96</sup> Group 1 received the implant and an inoculum of MRSA, and group 2 received a CSA-13 coated implant and the MRSA inoculum. Group 3 and 4 were the non-infected control groups, received only the CSA-13 coated implant and the implant without the CSA, respectively. All group 1 sheep became infected within 6 to 10 days. The CSA-13 containing groups (ie, group 2 and 3) exhibited no bacterial infection until the end of the 12-week study and established skeletal attachment consistent with group 4 that has the uncoated implant. While these data support the utility of CSA-13 in perioperative infection prevention, it may be challenging to translate the design of the porous-coated implant to the uncoated metalwork used in many orthopedic procedures.

CSA-90 was tested in a rat open fracture model with intramedullary fixation that featured local inoculation with *S. aureus* at the time of surgery.<sup>97</sup> Animals were monitored post-surgically for osteolysis, weight loss, poor bone healing, and other evidence of

wound contamination. Rats treated with CSA-90 showed a significant decrease in wound infection, and healing was further improved by adjunctive local recombinant human bone morphogenetic protein-2 (rhBMP-2). Notably, rhBMP-2 alone was insufficient to impact on bone infection, consistent with previous infected non-union models.<sup>98</sup> A follow-up study confirmed CSA-90 was similarly effective at preventing infections developing in fractures inoculated with MRSA and MRSE. However, the 500 µg dose used for prophylaxis proved insufficient for treating established infections, even when combined with aggressive debridement of the wound.<sup>99</sup>

CSA-90 for infection prevention has also been assessed in a rat femoral implant model using press-fit porous titanium implants.<sup>100</sup> In this model of joint infection, *S. aureus* was introduced locally ( $1 \times 10^4$  CFU/mL) or delivered via tail vein injection ( $1 \times 10^5$  CFU/mL). In the absence of treatment, both local and systemic *S. aureus* groups developed infections that led to radiographic evidence of PJI and worsening animal health within 14 days of surgery. CSA-90 treatment increased the median survival in both inoculation groups compared to the untreated animals. Deep tissue cultures also demonstrated a reduced rate of periprosthetic infection with CSA-90. These data support the utility of CSA-90 as an implant coating despite the primitive nature of the drug coating in this system (ie, drip coated and air-dried). Further studies are required to elucidate the optimal release profile and delivery system.

### 3.3 | Osteogenic properties of CSAs

The osteogenic properties of CSAs were first described in sheep models.<sup>49,95</sup> While initial studies focused on the antimicrobial effects of CSAs, it was serendipitously observed that CSA-13 coated pins showed evidence of improved osseointegration. Dynamic bone labeling revealed that the CSA-13 containing groups has a higher mineral apposition rate (MAR) adjacent to the implants than the controls.<sup>96</sup> The osteogenic properties of CSA-13 were further seen in the previously described fracture infection model of William et al,<sup>95</sup> induced with an MRSA biofilm. CSA-13 turned out to increase MAR and impaired bone necrosis.

The mechanism for increased bone seen in this and other studies remains unclear but may be due to indirect or direct effects on bone formation. CSAs may indirectly affect bone healing by the generic promotion of the bone healing response. Antimicrobial peptides (eg, LL-37) can augment wound healing by promoting neovascularization and angiogenesis and can also neutralize endotoxins, decelerating the acute immune response and preventing septic shock. Similar effects have been demonstrated by CSAs.<sup>56,101,102</sup>

CSAs may directly improve osteogenesis by stimulating endogenous osteogenic factors such as BMPs. LL-37 also stimulates BMP-2 expression in cells.<sup>102</sup> Subsequent screening of CSAs by Gianni Rossini and colleagues (Southwest Research Institute, San Antonio, TX) revealed that CSA-90 was able to increase the expression of bone morphogenetic proteins-2 (BMP-2) cell culture by six-fold (unpublished data referenced in<sup>97</sup>). In vitro, CSA-13 and

CSA-90 could increase alkaline phosphatase activity and mineralization in MC3T3-E1 mouse preosteoblasts; both were studied individually and in combination with BMP-2.<sup>97</sup> In vivo, CSA-90 (500 µg) was found to enhance ectopic bone formation by BMP-2 in mice and rats,<sup>99</sup> leading to a six-fold increase in bone volume. Further mechanistic studies are required to elucidate the signaling pathways modulating the upregulation of BMPs and other osteogenic factors in response to CSA-13 class members and identify structural features of this class that make them more osteogenic than other CSAs.

### 3.4 | Bone delivery systems and implant coatings for CSAs

CSAs have potential as local and systemic agents, but their use in bone requires the development of specialized delivery systems. Delivery to sites of bone infection could be achieved by (a) systemic delivery systems, (b) local delivery systems, and (c) coatings on orthopedic implants or medical devices.

As systemic agents, the cytotoxic effects of CSAs make them challenging to use at high doses. Several poloxamers have developed for use as drug carriers to reduce the cytotoxic effects. The poloxamers Pluronic F127 has been most frequently tested because it can form well-defined micelles and sequester CSAs for delivery to targeted tissues.<sup>68</sup> Some studies have shown that the compatibility of Pluronic F127 with CSAs can decrease their cytotoxic properties without impairing antibacterial activities.<sup>68,103,104</sup> Nevertheless, the transient encapsulation of CSAs in micelles are less prone to associate with host membranes and raises the affinity of CSAs for microbial membranes. Subsequently, the dynamic nature of micelles amplifies the membrane selectivity to specific sites where infections occur.<sup>68,104</sup>

Recently, other new systems have been developed with the potential to target bone. Nanoparticles (NPs) can be used as drug carriers to increase drug efficacy, half-life, and selective binding properties. While there have been several studies delivering CSAs via NPs, practical systems targeting bone delivery have yet to be developed.

Silver is an antimicrobial metal, and silver NPs conjugated with CSA-124 (SNP-CSA) was developed as a selective antimicrobial for Gram-positive bacteria. SNP-CSA showed increased adherence to *S. aureus* (Gram-positive) cells than *E. coli* (Gram-negative) cells,<sup>105</sup> but CSAs also show greater antimicrobial activity to Gram-positive organisms over Gram-negative. Magnetic nanoparticles (MNP) have been shown to reduce the cytotoxicity of CSAs but did not interrupt the anti-cancer properties.<sup>88</sup> CSA-13-coated magnetic nanoparticles (MNP-CSA-13) exhibit antibacterial activity and prevent biofilm formation in different body fluids, although less than CSA-13 alone.<sup>80</sup> Nanoparticle coating does significantly reduce the hemolytic activity of CSA-13, and similar results were reported for MNP-CSA-131,<sup>52,82</sup> and reduced the toxicity of CSA-13 to hFOB 1.19 human osteoblasts, even at high concentrations (50 µg/mL).<sup>87</sup> MNP-CSA-13 was also effective against fungal cell adhesion and biofilm formation of *Candida spp.*, which was attributed to the ability of MNPs to penetrate

fungal cell membranes.<sup>87</sup> Notably, MNP-LL-37 was not fungicidal, suggestive of unique interactions between MNPs and CSAs. MNPs have also been proposed as a diagnostic contrast agent for identifying deep tissue infection.<sup>106</sup>

Topical powdered antibiotics have been used for local delivery as an adjunctive treatment for preventing surgical site infections.<sup>107</sup> Antibiotic powders have the advantage of achieving an exceptionally high antibiotic concentration at the surgical site for a sustained duration while minimizing the adverse effects associated with high-dose systemic exposure. Antibiotic powders have particular utility in treating orthopedic injuries with compromised vascularity, which can impede systemic drug delivery. However, local delivery of prophylactic antibiotics is not routinely used due to a lack of reliable evidence-base to support the practice, despite some studies indicating protective effects and cost-effectiveness.<sup>108,109</sup> Based on preclinical studies with CSA-90 applied topically in solution,<sup>99</sup> there is potential for CSAs to be tested via an intra-wound approach in powdered form.

Another local use of antibiotics is loading within poly-methyl methacrylate bone cement. These can be used to fabricate spacers during the two-stage exchange of knee and hip prostheses for the treatment of PJI,<sup>110</sup> and also for the Masquelet technique. Thermal instability is a limitation of many antibiotics, precluding their use within bone cement that is cured using a highly exothermic process. Notably, CSA-90 is thermostable and was active following elution from both calcium sulfate and bone cement.<sup>99</sup>

Hydrogels are ideal vehicles for local antimicrobial delivery as they can hydrate cells and support cell survival by providing an essential matrix for growth. A hydrogel film containing CSA-131 reduced bacterial and fungal colonization on an endotracheal tube,<sup>111</sup> and was fast-tracked by the FDA for clinical testing. Hydrogels combined with CSA-131 and other CSAs (eg, CSA-134 and CSA-138) are effective against *S. aureus* and *P. aeruginosa* biofilms on contact lenses.<sup>78</sup> Although hydrogels generally do not integrate with bone cells or nucleate cell-secreted calcium, an osteoconductive hydrogel has been created using arginine-glycine-aspartic acid (RGD)-alginate/hyaluronate.<sup>112</sup> This compound also enhanced neovascularization and bone formation when the hydrogel was combined with mesenchymal stromal cells, but it has not been explicitly used in conjunction with antimicrobials.

Finally, CSAs may be highly applicable as coatings for implants that are introduced to bone sites, particularly combined with the pro-osteogenic properties of CSA-13 family members. To date, the coating methods have not been particularly sophisticated, such as adding the drug in solution and air drying [107]. Such methods yield burst release with little sustained delivery. Polymer systems are a logical advancement of coating methods due to their biocompatibility, simplicity, and widespread use. In the sheep model, stainless steel plates were hand-dipped in a primer (MED-160), air dried, and then immersed in a dispersion of PDMS with CSA-13, and dried for 7 days.<sup>95</sup> An in vitro elution study showed elution within 30 days, but it is unclear whether this is reflective of in vivo usage. Other polymer systems for CSAs have used polylactic acid.<sup>113</sup> Notably, many polymer systems have acidic breakdown products that lead to osteoclast stimulation and premature bone resorption.

## 4 | CONCLUSION

CSAs are broad-spectrum antimicrobials with high efficacy against various types of bacterial, viral, fungal, and parasitic infections, including the most common causative agents of orthopedic diseases and drug-resistant microorganisms. CSAs can permeate bacterial and fungal biofilms effectively in lower concentrations than other classes of antibiotics, and it is confirmed that CSA coating can reduce biofilm formation and prevent bacterial infections associated with orthopedic implants. Since CSA resistance is less likely to be developed by bacteria through continued exposure, CSAs are highly potent for device and implant coating.

With cytotoxic effects of CSAs only seen at high concentrations, CSA-13 and the CSA-13 sub-class (including CSA-90 and CSA-131) demonstrate wound-healing effects, osteogenic properties, and anti-cancer activities at non-cytotoxic concentrations. CSAs have broad potential to become therapeutics for orthopedics, but further studies will be needed to identify the most suitable roles as topical, local, or systemic agents and as stand-alone or adjunctive treatments.

## AUTHOR CONTRIBUTIONS

AD initially drafted the manuscript with contributions from all other authors. All authors read and approved the final draft of the manuscript.

## ORCID

Paul B. Savage  <http://orcid.org/0000-0002-4642-6109>

David G. Little  <http://orcid.org/0000-0003-3684-9770>

Aaron Schindeler  <http://orcid.org/0000-0002-7757-6281>

## REFERENCES

1. Beam E, Osmon D. Prosthetic joint infection update. *Infect Dis Clin North Am*. 2018;32:843-859.
2. Tande AJ, Patel R. Prosthetic joint infection. *Clin Microbiol Rev*. 2014; 27:302-345.
3. Cataldo MA, Petrosillo N, Cipriani M, Cauda R, Tacconelli E. Prosthetic joint infection: recent developments in diagnosis and management. *J Infect*. 2010;61:443-448.
4. Kapadia BH, Berg RA, Daley JA, Fritz J, Bhav A, Mont MA. Peri-prosthetic joint infection. *Lancet*. 2016;387:386-394.
5. Lew DP, Waldvogel FA. Osteomyelitis. *Lancet*. 2004;364:369-379.
6. Pan C, Zhou Z, Yu X. Coatings as the useful drug delivery system for the prevention of implant-related infections. *J Orthop Surg*. 2018; 13:220.
7. Moriarty TF, Kuehl R, Coenye T, et al. Orthopaedic device-related infection: current and future interventions for improved prevention and treatment. *EFORT Open Rev*. 2017;1:89-99.
8. Issa K, Diebo BG, Faloony M, et al. The epidemiology of vertebral osteomyelitis in the United States from 1998 to 2013. *Clin Spine Surg*. 31:e102-e108.
9. DeRonde KJ, Girotto JE, Nicolau DP. Management of pediatric acute hematogenous osteomyelitis, Part I: antimicrobial stewardship approach and review of therapies for methicillin-susceptible *Staphylococcus aureus*, *Streptococcus pyogenes*, and *Kingella kingae*. *Pharmacotherapy*. 2018;38:947-966.

10. DeRonde KJ, Giroto JE, Nicolau DP. Management of pediatric acute hematogenous osteomyelitis, Part II: a focus on methicillin-resistant *Staphylococcus aureus*, current and emerging therapies. *Pharmacotherapy*. 2018;38:1021-1037.
11. Agarwal A, Aggarwal AN. Bone and joint infections in children: acute hematogenous osteomyelitis. *Indian J Pediatr*. 2016;83:817-824.
12. Funk SS, Copley LA. Acute hematogenous osteomyelitis in children: pathogenesis, diagnosis, and treatment. *Orthop Clin North Am*. 2017;48:199-208.
13. Dym H, Zeidan J. Microbiology of acute and chronic osteomyelitis and antibiotic treatment. *Dent Clin North Am*. 2017;61:271-282.
14. Peled C, Kraus M, Kaplan D. Diagnosis and treatment of necrotising otitis externa and diabetic foot osteomyelitis-similarities and differences. *J Laryngol Otol*. 2018;132:775-779.
15. Haddad FS, Ngu A, Negus JJ. Prosthetic joint infections and cost analysis? *Adv Exp Med Biol*. 2017;971:93-100.
16. Kurtz SM, Lau E, Watson H, Schmier JK, Parvizi J. Economic burden of periprosthetic joint infection in the United States. *J Arthroplasty*. 2012;27:61-65.e1.
17. Howard-Jones AR, Isaacs D. Systematic review of duration and choice of systemic antibiotic therapy for acute haematogenous bacterial osteomyelitis in children. *J Paediatr Child Health*. 2013;49:760-768.
18. Masters EA, Trombetta RP, de Mesy Bentley KL, et al. Evolving concepts in bone infection: redefining "biofilm", "acute vs. chronic osteomyelitis", "the immune proteome" and "local antibiotic therapy". *Bone Res*. 2019;7:20.
19. Ceroni D, Kampouroglou G, Valaikaite R, Anderson D, Salvo D. Osteoarticular infections in young children: what has changed over the last years? *Swiss Med Wkly*. 2014;144:w13971.
20. Antony SJ. Case series describing an outbreak of highly resistant vancomycin *Staphylococcus aureus* (possible VISA/VRSA) infections in orthopedic related procedures in Guatemala. *Infect Disord Drug Targets*. 2014;14:44-48.
21. Aboltins C, Daffy J, Choong P, Stanley P. Current concepts in the management of prosthetic joint infection. *Intern Med J*. 2014;44:834-840.
22. Arnold JC, Bradley JS. Osteoarticular infections in children. *Infect Dis Clin North Am*. 2015;29:557-574.
23. Carver DC, Kuehn SB, Weinlein JC. Role of systemic and local antibiotics in the treatment of open fractures. *Orthop Clin North Am*. 2017;48:137-153.
24. Castellazzi L, Mantero M, Esposito S. Update on the management of pediatric acute osteomyelitis and septic arthritis. *Int J Mol Sci*. 2016;17:17.
25. Harik NS, Smeltzer MS. Management of acute hematogenous osteomyelitis in children. *Expert Rev Anti Infect Ther*. 2010;8:175-181.
26. Zimmermann P, Curtis N. The role of *Cutibacterium acnes* in auto-inflammatory bone disorders. *Eur J Pediatr*. 2019;178:89-95.
27. Dunn RN, Ben Husien M. Spinal tuberculosis: review of current management. *Bone Joint J*. 2018;100-B:425-431.
28. Jaramillo D, Dormans JP, Delgado J, Laor T, St Geme JW. Hematogenous osteomyelitis in infants and children: imaging of a changing disease. *Radiology*. 2017;283:629-643.
29. Kremers HM, Nwojo ME, Ransom JE, Wood-Wentz CM, Melton LJ, Huddleston PM. Trends in the epidemiology of osteomyelitis: a population-based study, 1969 to 2009. *J Bone Joint Surg Am*. 2015;97:837-845.
30. Peltola H, Pääkkönen M. Acute osteomyelitis in children. *N Engl J Med*. 2014;370:352-360.
31. Nguyen JC, Rebsamen SL, Tuite MJ, Davis JM, Rosas HG. Imaging of *Kingella kingae* musculoskeletal infections in children: a series of 5 cases. *Emerg Radiol*. 2018;25:615-620.
32. Yagupsky P. *Kingella kingae*: carriage, transmission, and disease. *Clin Microbiol Rev*. 2015;28:54-79.
33. Yagupsky P. Diagnosing *Kingella kingae* infections in infants and young children. *Expert Rev Anti Infect Ther*. 2017;15:925-934.
34. Laurent E, Petit L, Maakaroun-Vermeze Z, et al. National epidemiological study reveals longer paediatric bone and joint infection stays for infants and in general hospitals. *Acta Paediatr*. 2018;107:1270-1275.
35. Garcia S, Lozano ML, Gatell JM, Soriano E, Ramon R, Sanmiguel JG. Prophylaxis against infection. Single-dose cefonicid compared with multiple-dose cefamandole. *J Bone Joint Surg Am*. 1991;73:1044-1048.
36. Boyle KK, Duquin TR. Antibiotic prophylaxis and prevention of surgical site infection in shoulder and elbow surgery. *Orthop Clin North Am*. 2018;49:241-256.
37. Mears SC, Edwards PK. Bone and joint infections in older adults. *Clin Geriatr Med*. 2016;32:555-570.
38. Mah TF, Pitts B, Pellock B, Walker GC, Stewart PS, O'Toole GA. A genetic basis for *Pseudomonas aeruginosa* biofilm antibiotic resistance. *Nature*. 2003;426:306-310.
39. Costerton JW, Stewart PS, Greenberg EP. Bacterial biofilms: a common cause of persistent infections. *Science*. 1999;284:1318-1322.
40. Chung PY, Toh YS. Anti-biofilm agents: recent breakthrough against multi-drug resistant *Staphylococcus aureus*. *Pathog Dis*. 2014;70:231-239.
41. Archer NK, Mazaitis MJ, Costerton JW, Leid JG, Powers ME, Shirtliff ME. *Staphylococcus aureus* biofilms: properties, regulation, and roles in human disease. *Virulence*. 2011;2:445-459.
42. Zimmerli W. Clinical presentation and treatment of orthopaedic implant-associated infection. *J Intern Med*. 2014;276:111-119.
43. Williams DL, Sinclair KD, Jeyapalina S, Bloebaum RD. Characterization of a novel active release coating to prevent biofilm implant-related infections. *J Biomed Mater Res B Appl Biomater*. 2013;101:1078-1089.
44. Shrestha P, Cooper BS, Coast J, et al. Enumerating the economic cost of antimicrobial resistance per antibiotic consumed to inform the evaluation of interventions affecting their use. *Antimicrob Resist Infect Control*. 2018;7:98.
45. Osei L, El Houmami N, Minodier P, et al. Paediatric bone and joint infections in French Guiana: a 6 year retrospective review. *J Trop Pediatr*. 2017;63:380-388.
46. ter Boo G-JA, Grijpma DW, Moriarty TF, Richards RG, Eglis D. Antimicrobial delivery systems for local infection prophylaxis in orthopedic- and trauma surgery. *Biomaterials*. 2015;52:113-125.
47. Bhattacharya S, Pal K, Jain S, et al. Surgical site infection by methicillin resistant *Staphylococcus aureus*- on decline? *J Clin Diagn Res*. 2016;10:DC32-DC36.
48. Saha S, Savage PB, Bal M. Enhancement of the efficacy of erythromycin in multiple antibiotic-resistant gram-negative bacterial pathogens. *J Appl Microbiol*. 2008;105:822-828.
49. Sinclair KD, Pham TX, Farnsworth RW, et al. Development of a broad spectrum polymer-released antimicrobial coating for the prevention of resistant strain bacterial infections. *J Biomed Mater Res A*. 2012;100:2732-2738.
50. Chin JN, Rybak MJ, Cheung CM, Savage PB. Antimicrobial activities of ceragenins against clinical isolates of resistant *Staphylococcus aureus*. *Antimicrob Agents Chemother*. 2007;51:1268-1273.
51. Chin JN, Jones RN, Sader HS, Savage PB, Rybak MJ. Potential synergy activity of the novel ceragenin, CSA-13, against clinical isolates of *Pseudomonas aeruginosa*, including multidrug-resistant *P. aeruginosa*. *J Antimicrob Chemother*. 2008;61:365-370.
52. Durnas B, Piktet E, Wątek M, et al. Anaerobic bacteria growth in the presence of cathelicidin LL-37 and selected ceragenins delivered as magnetic nanoparticles cargo. *BMC Microbiol*. 2017;17:167.
53. Leszczyńska K, Namiot A, Cruz K, et al. Potential of ceragenin CSA-13 and its mixture with pluronic F-127 as treatment of topical bacterial infections. *J Appl Microbiol*. 2011;110:229-238.



54. Ding B, Yin N, Liu Y, et al. Origins of cell selectivity of cationic steroid antibiotics. *J Am Chem Soc.* 2004;126:13642-13648.
55. Epand RM, Epand RF, Savage PB. Ceragenins (cationic steroid compounds), a novel class of antimicrobial agents. *Drug News Perspect.* 2008;21:307-311.
56. Olekson MA, You T, Savage PB, Leung KP. Antimicrobial ceragenins inhibit biofilms and affect mammalian cell viability and migration in vitro. *FEBS Open Bio.* 2017;7:953-967.
57. Piktel E, Pogoda K, Roman M, et al. Sporidicidal activity of ceragenin CSA-13 against *Bacillus subtilis*. *Sci Rep.* 2017;7:44452.
58. Hacıoglu M, Guzel CB, Savage PB, Tan A. Antifungal susceptibilities, in vitro production of virulence factors and activities of ceragenins against *Candida* spp. isolated from vulvovaginal candidiasis. *Med Mycol.* 2019;57:291-299.
59. Howell MD, Streib JE, Kim BE, et al. Ceragenins: a class of antiviral compounds to treat orthopox infections. *J Invest Dermatol.* 2009; 129:2668-2675.
60. Lara D, Feng Y, Bader J, Savage PB, Maldonado RA. Antitrypanosomatid activity of ceragenins. *J Parasitol.* 2010;96:638-642.
61. Polat ZA, Cetin A, Savage PB. Evaluation of the in vitro activity of ceragenins against *Trichomonas vaginalis*. *Acta Parasitol.* 2016;61: 376-381.
62. Bozkurt-Guzel C, Savage PB, Akcali A, Ozbek-Celik B. Potential synergy activity of the novel ceragenin, CSA-13, against carbapenem-resistant *Acinetobacter baumannii* strains isolated from bacteremia patients. *BioMed Res Int.* 2014;2014:710273-710275.
63. Epand RF, Pollard JE, Wright JO, Savage PB, Epand RM. Depolarization, bacterial membrane composition, and the antimicrobial action of ceragenins. *Antimicrob Agents Chemother.* 2010;54: 3708-3713.
64. Pollard JE, Snarr J, Chaudhary V, et al. In vitro evaluation of the potential for resistance development to ceragenin CSA-13. *J Antimicrob Chemother.* 2012;67:2665-2672.
65. Durnaś B, Wnorowska U, Pogoda K, et al. Candidacidal activity of selected ceragenins and human cathelicidin LL-37 in experimental settings mimicking infection sites. *PLoS One.* 2016;11:e0157242.
66. Epand RF, Savage PB, Epand RM. Bacterial lipid composition and the antimicrobial efficacy of cationic steroid compounds (ceragenins). *Biochim Biophys Acta.* 2007;1768:2500-2509.
67. Bozkurt-Guzel C, Hacıoglu M, Savage PB. Investigation of the in vitro antifungal and antibiofilm activities of ceragenins CSA-8, CSA-13, CSA-44, CSA-131, and CSA-138 against *Candida* species. *Diagn Microbiol Infect Dis.* 2018;91:324-330.
68. Hashemi M, Holden B, Taylor M, et al. Antibacterial and antifungal activities of poloxamer micelles containing ceragenin CSA-131 on ciliated tissues. *Molecules.* 2018;23:596.
69. Hashemi MM, Rovig J, Holden BS, et al. Ceragenins are active against drug-resistant *Candida auris* clinical isolates in planktonic and biofilm forms. *J Antimicrob Chemother.* 2018;73:1537-1545.
70. Wang J, Ghali S, Xu C, et al. Ceragenin CSA13 reduces *Clostridium difficile* infection in mice by modulating the intestinal microbiome and metabolites. *Gastroenterology.* 2018;154:1737-1750.
71. Bucki R, Namiot DB, Namiot Z, Savage PB, Janmey PA. Salivary mucins inhibit antibacterial activity of the cathelicidin-derived LL-37 peptide but not the cationic steroid CSA-13. *J Antimicrob Chemother.* 2008;62:329-335.
72. Wnorowska U, Piktel E, Durnaś B, Fiedoruk K, Savage PB, Bucki R. Use of ceragenins as a potential treatment for urinary tract infections. *BMC Infect Dis.* 2019;19:369.
73. Leszczynska K, Namiot D, Byfield FJ, et al. Antibacterial activity of the human host defence peptide LL-37 and selected synthetic cationic lipids against bacteria associated with oral and upper respiratory tract infections. *J Antimicrob Chemother.* 2013;68:610-618.
74. Leszczyńska K, Namiot A, Fein DE, et al. Bactericidal activities of the cationic steroid CSA-13 and the cathelicidin peptide LL-37 against *Helicobacter pylori* in simulated gastric juice. *BMC Microbiol.* 2009; 9:187.
75. Birteksoz-Tan AS, Zeybek Z, Hacıoglu M, Savage PB, Bozkurt-Guzel C. In vitro activities of antimicrobial peptides and ceragenins against *Legionella pneumophila*. *J Antibiot.* 2019;72:291-297.
76. Bozkurt-Guzel C, Savage PB, Gerciker AA. In vitro activities of the novel ceragenin CSA-13, alone or in combination with colistin, tobramycin, and ciprofloxacin, against *Pseudomonas aeruginosa* strains isolated from cystic fibrosis patients. *Chemotherapy.* 2011;57: 505-510.
77. Bucki R, Sostarec AG, Byfield FJ, Savage PB, Janmey PA. Resistance of the antibacterial agent ceragenin CSA-13 to inactivation by DNA or F-actin and its activity in cystic fibrosis sputum. *J Antimicrob Chemother.* 2007;60:535-545.
78. Gu X, Jennings JD, Snarr J, Chaudhary V, Pollard JE, Savage PB. Optimization of ceragenins for prevention of bacterial colonization of hydrogel contact lenses. *Invest Ophthalmol Vis Sci.* 2013;54: 6217-6223.
79. Bucki R, Niemirowicz K, Wnorowska U, et al. Bactericidal activity of ceragenin CSA-13 in cell culture and in an animal model of peritoneal infection. *Antimicrob Agents Chemother.* 2015;59:6274-6282.
80. Niemirowicz K, Prokop I, Wilczewska A, et al. Magnetic nanoparticles enhance the anticancer activity of cathelicidin LL-37 peptide against colon cancer cells. *Int J Nanomedicine.* 2015;10: 3843-3853.
81. Nagant C, Pitts B, Stewart PS, Feng Y, Savage PB, Dehaye JP. Study of the effect of antimicrobial peptide mimic, CSA-13, on an established biofilm formed by *Pseudomonas aeruginosa*. *Microbiol Open.* 2013;2:318-325.
82. Niemirowicz K, Piktel E, Wilczewska A, et al. Core-shell magnetic nanoparticles display synergistic antibacterial effects against *Pseudomonas aeruginosa* and *Staphylococcus aureus* when combined with cathelicidin LL-37 or selected ceragenins. *Int J Nanomedicine.* 2016; 11:5443-5455.
83. Nagant C, Feng Y, Lucas B, Braeckmans K, Savage P, Dehaye JP. Effect of a low concentration of a cationic steroid antibiotic (CSA-13) on the formation of a biofilm by *Pseudomonas aeruginosa*. *J Appl Microbiol.* 2011;111:763-772.
84. Moscoso M, Esteban-Torres M, Menéndez M, García E. In vitro bactericidal and bacteriolytic activity of ceragenin CSA-13 against planktonic cultures and biofilms of *Streptococcus pneumoniae* and other pathogenic streptococci. *PLoS One.* 2014;9:e101037.
85. Hashemi MM, Rovig J, Weber S, Hilton B, Forouzan MM, Savage PB. Susceptibility of colistin-resistant, gram-negative bacteria to antimicrobial peptides and ceragenins. *Antimicrob Agents Chemother.* 2017;61:61.
86. Hashemi MM, Holden BS, Coburn J, et al. Proteomic analysis of resistance of gram-negative bacteria to chlorhexidine and impacts on susceptibility to colistin, antimicrobial peptides, and ceragenins. *Front Microbiol.* 2019;10:210.
87. Niemirowicz K, Durnaś B, Tokajuk G, et al. Formulation and candidacidal activity of magnetic nanoparticles coated with cathelicidin LL-37 and ceragenin CSA-13. *Sci Rep.* 2017;7:4610.
88. Piktel E, Prokop I, Wnorowska U, et al. Ceragenin CSA-13 as free molecules and attached to magnetic nanoparticle surfaces induce caspase-dependent apoptosis in human breast cancer cells via disruption of cell oxidative balance. *Oncotarget.* 2018;9: 21904-21920.
89. Aarbiou J, Tjallingii GS, Verhoosel RM, et al. Mechanisms of cell death induced by the neutrophil antimicrobial peptides alpha-defensins and LL-37. *Inflamm Res.* 2006;55:119-127.
90. Kuroda K, Fukuda T, Okumura K, et al. Ceragenin CSA-13 induces cell cycle arrest and antiproliferative effects in wild-type and p53 null mutant HCT116 colon cancer cells. *Anti-cancer Drugs.* 2013;24: 826-834.

91. Ceroni D, Grumetz C, Desvachez O, Pusateri S, Dunand P, Samara E. From prevention of pin-tract infection to treatment of osteomyelitis during paediatric external fixation. *J Children's Orthop.* 2016;10: 605-612.
92. Gill SR, Fouts DE, Archer GL, et al. Insights on evolution of virulence and resistance from the complete genome analysis of an early methicillin-resistant *Staphylococcus aureus* strain and a biofilm-producing methicillin-resistant *Staphylococcus epidermidis* strain. *J Bacteriol.* 2005;187:2426-2438.
93. Perry EL, Beck JP, Williams DL, Bloebaum RD. Assessing peri-implant tissue infection prevention in a percutaneous model. *J Biomed Mater Res B Appl Biomater.* 2010;92:397-408.
94. Williams DL, Bloebaum RD, Beck JP, Petti CA. Characterization of bacterial isolates collected from a sheep model of osseointegration. *Curr Microbiol.* 2010;61:574-583.
95. Williams DL, Haymond BS, Beck JP, et al. In vivo efficacy of a sili-conecationic steroid antimicrobial coating to prevent implant-related infection. *Biomaterials.* 2012;33:8641-8656.
96. Sinclair KD, Pham TX, Williams DL, Farnsworth RW, Loc-Carrillo CM, Bloebaum RD. Model development for determining the efficacy of a combination coating for the prevention of perioperative device related infections: a pilot study. *J Biomed Mater Res B Appl Biomater.* 2013;101:1143-1153.
97. Schindeler A, Yu NYC, Cheng TL, et al. Local delivery of the cationic steroid antibiotic CSA-90 enables osseous union in a rat open fracture model of *Staphylococcus aureus* infection. *J Bone Joint Surg Am.* 2015;97:302-309.
98. Chen X, Schmidt AH, Tsukayama DT, Bourgeault CA, Lew WD. Recombinant human osteogenic protein-1 induces bone formation in a chronically infected, internally stabilized segmental defect in the rat femur. *J Bone Joint Surg Am.* 2006;88:1510-1523.
99. Mills R, Cheng TL, Mikulec K, et al. CSA-90 promotes bone formation and mitigates methicillin-resistant *Staphylococcus aureus* infection in a rat open fracture model. *Clin Orthop Relat Res.* 2018;476: 1311-1323.
100. Mills RJ, Boyling A, Cheng TL, et al. CSA-90 reduces periprosthetic joint infection in a novel rat model challenged with local and systemic *Staphylococcus aureus*. *J Orthoped Res.* 2020. <https://doi.org/10.1002/jor.24618>
101. Steinstraesser L, Koehler T, Jacobsen F, et al. Host defense peptides in wound healing. *Mol Med.* 2008;14:528-537.
102. Scott MG, Davidson DJ, Gold MR, Bowdish D, Hancock REW. The human antimicrobial peptide LL-37 is a multifunctional modulator of innate immune responses. *J Immunol.* 2002;169:3883-3891.
103. Hashemi M, Mmuogbulam A, Holden B, et al. Susceptibility of multidrug-resistant bacteria, isolated from water and plants in Nigeria, to Ceragenins. *Int J Environ Res Public Health.* 2018;15:15.
104. Nagant C, Savage PB, Dehay JP. Effect of pluronic acid F-127 on the toxicity towards eukaryotic cells of CSA-13, a cationic steroid analogue of antimicrobial peptides. *J Appl Microbiol.* 2012;112: 1173-1183.
105. Hoppens MA, Sylvester CB, Qureshi AT, et al. Ceragenin mediated selectivity of antimicrobial silver nanoparticles. *ACS Appl Mater Interfaces.* 2014;6:13900-13908.
106. Hoppens MA, Wheeler ZEW, Qureshi AT, et al. Maghemite, silver, ceragenin conjugate particles for selective binding and contrast of bacteria. *J Colloid Interface Sci.* 2014;413:167-174.
107. Chen AF, Fleischman A, Austin MS. Use of intrawound antibiotics in orthopaedic surgery. *J Am Acad Orthop Surg.* 2018;26:e371-e378.
108. Katarincic JA, Fantry A, DePasse JM, Feller R. Local modalities for preventing surgical site infections: an evidence-based review. *J Am Acad Orthop Surg.* 2018;26:14-25.
109. Xie L, Zhu J, Yang M, et al. Effect of intra-wound vancomycin for spinal surgery: a systematic review and meta-analysis. *Orthop Surg.* 2017;9:350-358.
110. Boelch SP, Rueckl K, Fuchs C, et al. Comparison of elution characteristics and compressive strength of biantibiotic-loaded PMMA bone cement for spacers: Copal(R) spacem with gentamicin and vancomycin versus Palacos(R) R+G with vancomycin. *BioMed Res Int.* 2018;2018:4323518.
111. Hashemi MM, Rovig J, Bateman J, et al. Preclinical testing of a broad-spectrum antimicrobial endotracheal tube coated with an innate immune synthetic mimic. *J Antimicrob Chemother.* 2018;73:143-150.
112. Ingavle GC, Gionet-Gonzales M, Vorwald CE, et al. Injectable mineralized microsphere-loaded composite hydrogels for bone repair in a sheep bone defect model. *Biomaterials.* 2019;197:119-128.
113. Bayramov DF, Neff JA. Beyond conventional antibiotics—new directions for combination products to combat biofilm. *Adv Drug Deliv Rev.* 2017;112:48-60.

**How to cite this article:** Dao A, Mills RJ, Kamble S, Savage PB, Little DG, Schindeler A. The application of ceragenins to orthopedic surgery and medicine. *J Orthop Res.* 2020;38: 1883-1894. <https://doi.org/10.1002/jor.24615>

### **1.3. Preventing osteolytic lesions and osteomyelitis in multiple myeloma**

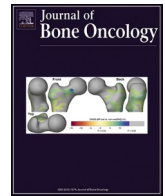
This section provides a comprehensive review of clinical trials and case reports focusing on osteolytic lesions and multiple myeloma-related bone infections. This review article has been peer reviewed and published in the Journal of Bone Oncology (IF: 4.07). It is included here in manuscript format.

#### **Reference:**

**Dao A**, McDonald MM, Savage PB, Little DG, Schindeler A. Preventing osteolytic lesions and osteomyelitis in multiple myeloma. J Bone Oncol. 2022 Oct 28; 37:100460. doi: 10.1016/j.jbo.2022.100460. PMID: 36388641; PMCID: PMC9640986.

#### **Statement of Contribution:**

AD and AS conceptualized the article; AD conducted the systematic review and prepared the tables; AD and AS wrote, MM, PBS and DGL reviewed, and edited the manuscript. All authors read and approved the final manuscript.



## Review Article

## Preventing osteolytic lesions and osteomyelitis in multiple myeloma

Aiken Dao<sup>a,b,c</sup>, Michelle M McDonald<sup>c,e</sup>, Paul B. Savage<sup>d</sup>, David G. Little<sup>a,b</sup>,  
Aaron Schindeler<sup>a,b,\*</sup>

<sup>a</sup> Bioengineering & Molecular Medicine Laboratory, The Children's Hospital at Westmead and the Westmead Institute for Medical Research, Sydney, New South Wales, Australia

<sup>b</sup> Children's Hospital Westmead Clinical School, Faculty of Medicine and Health, University of Sydney, Sydney, New South Wales, Australia

<sup>c</sup> Garvan Institute of Medical Research, Darlinghurst, New South Wales, Australia

<sup>d</sup> Department of Chemistry and Biochemistry, Brigham Young University, Provo, UT, United States

<sup>e</sup> Charles Perkins Centre, Faculty of Medicine and Health, University of Sydney, Camperdown, NSW, Australia

## HIGHLIGHTS

- Myeloma bone disease is a challenging complication of multiple myeloma and one of increasing treatment interest.
- Over 90% of patients develop local osteolytic lesions and skeletal-related events at some point during the progression of the disease.
- Bone lesions can induce severe pain and immobility and can also increase the risk of fractures and osteomyelitis.
- Denosumab can reduce skeletal-related events and bortezomib/1D11 can reduce bone destruction and pathological fractures in multiple myeloma patients.

## ARTICLE INFO

## Keywords:

Multiple myeloma  
Myeloma bone disease  
Osteolytic bone infections  
Osteomyelitis  
Cancer

## ABSTRACT

Multiple myeloma is a hematological malignancy affecting the plasma cells. It is the second most common hematologic cancer in adults. Over 90% of patients develop local osteolytic lesions and skeletal-related events at some point during the progression of the disease. Bone lesions can induce severe pain and immobility and can also increase the risk of fractures and osteomyelitis. Skeletal complications are associated with poor clinical outcomes, affecting quality of life and mortality. Current standards of care for myeloma, e.g., autologous stem-cell transplantation (ASCT) and chemotherapy, do not lessen the risk of adverse events in bone. Once bone lesions are present, bone-targeted interventions are limited, with bone antiresorptive drugs being a mainstay of treatment. This review highlights the growing literature surrounding osteolytic lesions and bone infections associated with multiple myeloma and assesses current and emerging treatments. Emerging evidence from clinical trials suggests that denosumab can reduce skeletal-related events, and the potential application of bortezomib/1D11 can reduce bone destruction and pathological fractures in MM patients. Once established, bone lesions are prone to develop osteomyelitis – especially in immunocompromised individuals. Antibiotics and surgical interventions have been used to manage bone infections in most reported cases. As the bone infection risk associated with MM bone lesions become more evident, there is scope to improve patient management by mitigating this risk with prophylactic antimicrobial therapy.

## 1. The disease burden of multiple myeloma

Multiple myeloma (MM) is a currently incurable hematological malignancy affecting the plasma cells. It is the second most common hematologic cancer in adults, accounting for 10 % of hematologic malignancies and 1 % of all cancers [1]. The incidence rate of MM

worldwide is estimated to be 21 per 1,000,000, and ~150,000 individuals are newly diagnosed every year worldwide [2,3]. The mortality of MM accounts for 1 % of all cancer-related deaths and an estimated 72,000 people die from MM annually [4].

Multiple myeloma features clonal proliferation of B-lymphocyte-derived plasma cells in the bone marrow that leads to progressive

\* Corresponding author at: Bioengineering & Molecular Medicine Laboratory, The Children's Hospital at Westmead, Research Building, Locked Bag 4001, Westmead, New South Wales 2145, Australia.

E-mail address: [aaron.schindeler@sydney.edu.au](mailto:aaron.schindeler@sydney.edu.au) (A. Schindeler).

<https://doi.org/10.1016/j.jbo.2022.100460>

Received 28 June 2022; Received in revised form 16 October 2022; Accepted 27 October 2022

Available online 28 October 2022

2212-1374/Crown Copyright © 2022 Published by Elsevier GmbH. This is an open access article under the CC BY-NC-ND license (<http://creativecommons.org/licenses/by-nc-nd/4.0/>).



immune dysfunction. MM typically starts as a monoclonal gammopathy of undetermined significance (MGUS) or smouldering multiple myeloma (SMM), both of which can be asymptomatic [5]. At present, MM is still considered a single disease, but clinically, it is a collection of several different cytogenetically distinct plasma cell malignancies. Patients with MM can develop a range of complications including anemia, immune dysfunction, renal impairment and osteolytic bone lesions before ultimately succumbing to their disease [6].

MM is often identified coincidentally following blood testing for general symptoms, such as bone pain. A diagnostic confirmation is achieved through serum biochemistry, blood cell counts, serum or urine tests or a bone marrow biopsy for monoclonal M–protein production or free light chains [7]. The criteria for the diagnosis of multiple myeloma requiring therapy are 10 % or more plasma cells in the bone marrow, abnormal immunoglobulins in the blood/urine and the presence of one or more myeloma defining events (MDE), including hypercalcemia, renal failure, anemia, and lytic bone lesions [8].

In general, the prognosis of multiple myeloma is poor despite the advancement of anti-myeloma therapy. According to the revised international staging system (RISS), there are three stages of multiple myeloma. In stage one, patients' levels of albumin, beta-2-microglobulin (B2M) and lactate dehydrogenase (LDH) are normal, and it is most treatable at this stage. However, most patients are diagnosed in stage two, in which case, their albumin level is low, B2M level may increase, and more than half of these patients will live seven years or more past the start of treatment. In the advanced stage three, patients will have high B2M and/or LDH levels, suggesting the disease is widespread and more than half of patients in this stage will survive for another three and a half years [9,10]. The rate of SRE and bone lytic lesions is also high, and it is often lytic disease or fracture that provokes a late-stage diagnosis. Overall, only 50.7 % of MM patients were alive five years post diagnosis, mostly due to the under detection and difficulties to diagnose MM until it has progressed. In addition, only approximately 5 % of MM patients are diagnosed at an early stage. Their five-year survival rate is higher (71 %) than later-stage diagnosis (48 %).

## 2. Clinical interventions for multiple myeloma

Conventional chemotherapy for MM uses melphalan, an alkylating agent, and prednisone [11], and it has been the gold standard conditioning regimen for decades. Currently, MM patients are typically treated with approximately-three to four cycles of induction therapy with bortezomib (an antineoplastic agent), lenalidomide (an immunomodulatory drug), and dexamethasone (VRd) prior to stem cell harvest. In the presence of acute renal failure, other bortezomib-containing regimens such as bortezomib-thalidomide-dexamethasone (VTd) or bortezomib-cyclophosphamide-dexamethasone (VCD) can be used instead of VRd. However, the low-dose dexamethasone regimen (40 mg once a week) is generally preferred with chemotherapies to minimize toxicity [12].

After harvest, patients can either undergo frontline autologous stem cell transplantation (ASCT) or resume induction therapy delaying ASCT until first relapse. ASCT can prolong patient survival and has become the standard of care for treating newly diagnosed multiple myeloma in young and select, fit, elderly patients [13]. Still, not all MM patients are suitable candidates for ASCT. One of the key clinical challenges is to critically assess the patient's overall health to ensure a balance between risks and benefits [14].

Since patients can become refractory to their initial treatment, multiple therapeutic options have been developed and can improve long-term outcomes. Combined therapies with thalidomide, lenalidomide, bortezomib and dexamethasone have been shown to significantly improve the five-year related overall survival from 29 % to 35 % over the past 20 years [15–19]. Meanwhile, trials with immunomodulatory drugs (e.g., pomalidomide), proteasome inhibitors (e.g., carfilzomib and ixazomib), histone deacetylase inhibitor, CD38-targeting monoclonal

antibodies and B-lymphocyte mutation antigen CAR T-lymphocyte therapy have also shown promising outcomes [20–24].

Thalidomide slows blood vessel growth around the abnormal plasma cells (anti-angiogenesis), and it is an effective and well-tolerated front-line chemotherapy for MM [25]. As an initial treatment to prepare patients for autologous stem-cell transplantation, thalidomide in combination with dexamethasone resulted in higher response rates than the combination of vincristine, doxorubicin, and dexamethasone or dexamethasone alone [25,26]. Clinical trials have shown prolonged progression-free survival rate and improved depth of response when combinations of conventional (e.g. melphalan and prednisone) and novel therapies (e.g. thalidomide or lenalidomide) are applied [15,27–31].

Subsequently, daratumumab (16 mg/kg), an IgG-kappa monoclonal antibody targeting CD38, is approved as monotherapy in patients with heavily pre-treated relapsed or refractory multiple myeloma (RRMM) and in combination with bortezomib/dexamethasone or lenalidomide/dexamethasone [32].

Since many MM patients become refractory to treatment and relapses are likely to occur in all cases, clinical trials are constantly focusing on testing new chemotherapeutics and refining immunotherapies. Although the treatment of multiple myeloma is rapidly evolving, and there are many options available, daratumumab is to some extent the final treatment option for MM. In contrast to the extensive developments in anti-tumor therapeutics, therapeutic management of myeloma-induced skeletal-related events remain under-researched. Given the increased survival rates we have achieved with tumor targeted therapies, this is becoming more pertinent as this increases the time frame during which skeletal related events such as fracture can occur. Therefore, there is significant potential to reduce the burden of disease and improve the patient experience by specifically addressing the osseous lesions and resulting complications [33].

## 3. Osseous lesions and associated complications in myeloma bone disease

Myeloma bone disease (MBD) is a common and devastating complication of multiple myeloma and a major cause of increased morbidity and mortality [34,35]. The clinical features of MM are enhanced bone loss mainly associated with the axial skeleton and pelvis, such as diffuse osteopenia, focal lytic bone lesions, spinal cord compression, pathological fractures, hypercalcemia, renal insufficiency, and bony pain [36]. Indeed, at least 85 % of MM patients show some degree of osteopenia at diagnosis, and the severity of bone destruction typically correlates with tumor burden and prognosis [35,37]. Moreover, 80–90 % of patients will develop osteolytic bone lesions as their cancer progresses, which can negatively affect quality of life and worsen survival prospects [38,39].

As the low sensitivity of skeletal survey in identifying lytic bone lesions in MM patients has necessitated the use of more sophisticated imaging approach, whole-body low-dose CT (WBLDCT) is recommended as the imaging modality of choice for the initial assessment of MM-related lytic bone lesions [40]. Meanwhile, MRI is the gold standard imaging modality for detecting bone marrow involvement and to rule out spinal cord compression in MM patients [41]. In contrast, XR, PET/CT and MIBI imaging are not recommended for routine use in the management of myeloma patients but can still provide valuable prognostic data to assess the response to therapy and warrant clarification of previous imaging findings in selected cases [42].

Clinical data suggest that bone pain is common in MM patients (63 %) and most patients (74 %) had two or more bone lesions at initiation of first-line treatment [43]. Pain can be intense, but the focal lytic lesions can also lead to bone deformation, spinal cord compression and concomitant height loss, and pathological fractures. However, in the early stage, MM patients were often asymptomatic and underdiagnosed until initial orthopedic symptoms associated with bone pain occur. In

some cases, the pain and fractures precede osteoclastic-activating growth factors, driving further osteopenia and lesions. The cytokine release and the lack of osteoblastic response are also contributed to deterioration [44].

Mechanistically, osteolytic lesions and bone pain are caused by bone marrow infiltration by malignant plasma cells and expansion within the bone microenvironment [45]. Most lesions are localized to the spine, spinal discs, ribs, skull, or pelvis. Bone destruction in MM is multifactorial, resulting from an interaction of bone marrow stromal cells and myeloma tumour cells within the microenvironment of the bone marrow [44]. MM is often characterized by a loss of synchronization between bone formation and resorption, associated with an excess osteoclasts and reduced osteoblast activity [35,36].

The pathogenic mechanism of MM involves the interaction between multiple signaling pathways and cell types (Fig. 1). In brief, tumor cells that enter and colonize the bone microenvironment propagate osteolytic lesions by increasing osteoclast activation and differentiation [46]. Tumor cells express receptor activator of NF- $\kappa$ B ligand (RANKL) and macrophage inflammatory protein-1 $\alpha$  (MIP-1 $\alpha$ , CCL3), which stimulate differentiation of osteoclast progenitors in the bone marrow into mature osteoclasts. Local expression of parathyroid hormone-related protein (PTHrP), IL-6, along with stromal cell-derived factor-1 (SDF-1 or CXCL12), osteopontin, and matrix metalloproteinase 13 (MMP13) can further promote bone turnover by osteoblasts and osteoclasts. MIP-1 $\alpha$ , PTHrP and IL-8 upregulate RANKL in stromal cells, further stimulating osteoclastogenesis indirectly. Additionally, Dkk1 and IL-7 from multiple myeloma cells can suppress osteoblast differentiation from mesenchymal stromal progenitors. These alterations in bone turnover led to the initiation of the well described vicious cycle in which osteoclast resorption of bone matrix releases pro-tumorigenic factors such as TGF $\beta$ , osteopontin and GDF15, stimulating further MM cell expansion in bone [47,48]. Overall, this results in a positive feedback loop of tumor proliferation and bone destruction.

#### 4. Conventional and emerging treatments for myeloma bone disease

Nearly 30 % of patients with multiple myeloma have pathological fractures in the spine and long bones [52]. If the patients are not treated in a timely fashion, these can lead to long-term or permanent disability

and severely impact their quality of life. Patients with a single bone lesion, a negative bone marrow biopsy, and no paraproteinemia in serum had a better survival probability [53]. In these conditions, surgical intervention can strengthen and support the weak section of the bone. However, surgical treatment in patients with multiple myeloma is mostly limited to a palliative approach. Although osteolytic lesions and skeletal diseases are common in multiple myeloma patients, studies focusing on treating osteolytic lesions in multiple myeloma are limited. Only several clinical trials in the past twenty years focused on treatment in MM patients with orthopedic measures. To examine the clinical evidence for the current therapies to treat bone lesions or osteomyelitis, we conducted a semi-systematic search for clinical trials in the English literature using the PubMed database was conducted. All searches were limited to January 2000-December 2021. We used medical subject headings (MeSH) and keyword terms in the title/abstract, and the final search used the terms “multiple myeloma AND bone lesion OR osteolytic lesions OR osteomyelitis OR bone infection” and filtered for “clinical trials” only. Additional clinical trials that were found relevant to the subject were manually added to the list. Clinical trial findings are summarized chronologically in Table 1.

##### 4.1. Bisphosphonates can prevent bone disease in NDMM patients

Bisphosphonates (BPs) are bone antiresorptives with a long history of clinical use, particularly for treating cancers that have metastasized to the bone [66]. Pamidronate and zoledronic acid (ZA) are third-generation nitrogen-containing BPs with a high potency [67]. When given by intravenous infusion, these agents can preserve skeletal integrity and minimize the impact of MBD [68]. This can reduce the risk of complications caused by pathologic fracture, spinal cord compression and hypercalcemia due to persistent osteolytic lesions [69]. Numerous clinical trials have demonstrated the efficacy of bisphosphonates (BPs) in preventing skeletal-related events in newly diagnosed multiple myeloma (NDMM) patients [33,56,57,59,60,64]. The application of high-dose BPs has been linked to osteonecrosis of the jaw and are contraindicated when dental procedures are required [70]. However, they can represent an invaluable tool for the management of osteolytic lesions.

One of the more notable studies to highlight the utility of BPs in the management of MM was the comprehensive and randomized MRC

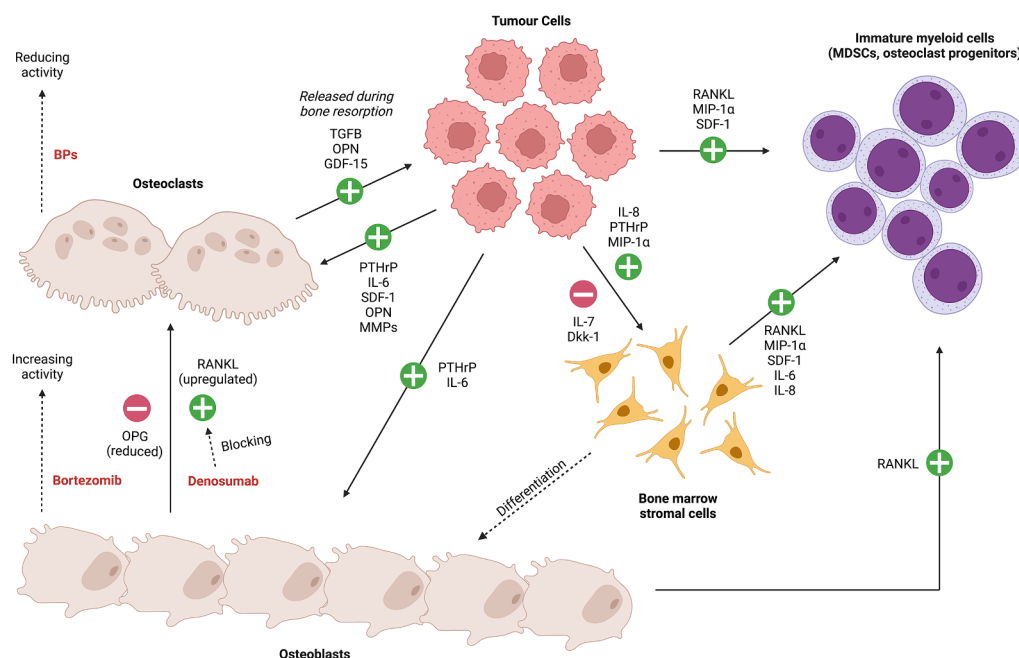


**Fig. 1.** Interactions of tumor cells and drug activities with osteoblasts, osteoclasts bone marrow stromal cells and immature myeloid cells. The schematic incorporates points of drug intervention including bisphosphonates (BPs) to reduce osteoclastic activity [49]; Denosumab a neutralizing antibody inhibitor of RANKL that suppresses osteoclastogenesis [50]; and first-in-class proteasome inhibitor (PI) bortezomib that can increase vitamin D receptor (VDR) signaling and markers of osteoblast differentiation [51]. Notably, no therapeutic approach will eliminate the lytic bone lesions caused by MM and can still have progression of skeletal disease if the osteolytic lesions are left untreated [36].

**Table 1**

Summary of clinical trials focused on treatment in MM patients with bone defect measures (Jan 2000- Dec 2021).

References	Cohort	Phase	Study design	Treatment groups and medications	Outcomes
Barlogie et al. 2008 [54]	76 adult patients with smoldering multiple myeloma SMM)	II	Survival surveillance and cohort study	Thalidomide (200 mg/d) with monthly pamidronate (PAM)	No SMM patients had hypercalcemia more than 2.625 mM (10.5 mg/dL). No patients developed hypercalcemia or bone lesions after treatment. 36 % of patients required reduced dosing due to peripheral neuropathy. Other side effects include neutropenia and dizziness (8 %), fatigue, thrombocytopenia, and cardiovascular events (7 %).
Rajkumar et al. 2010 [15]	445 adult patients with MM	ND	Open label, randomized controlled trial	High dose group: lenalidomide (25 mg) on days 1–21 plus dexamethasone 40 mg on days 1–4, 9–12, and 17–20 of a 28-day cycle Low dose group: lenalidomide (25 mg) given on the same schedule with dexamethasone 40 mg on days 1, 8, 15, and 22 of a 28-day cycle	149 patients (67 %) in the high-dose group had bone disease at baseline compared with 127 (57 %) of 222 in the low-dose group. No improvement in bone disease incidence between the high-dose (67 %) and low-dose (57 %) groups. Lenalidomide plus low-dose dexamethasone is associated with better short-term survival, and with lower toxicity than lenalidomide plus high-dose dexamethasone.
Gimsing et al. 2010 [55]	504 patients of any age with untreated symptomatic multiple myeloma	III	Double-blind, multi-center, randomized controlled trial	Group 1: received pamidronate (30 mg) monthly Group 2: pamidronate (90 mg) monthly	Median time to first skeletal-related event in patients was 9.2 month in the 90 mg and 10.2 months in the 30 mg group. Eight patients in the 90 mg group developed osteonecrosis of the jaw compared to only two patients in the 30 mg group. Pamidronate 90 mg per month was not superior to a dose of 30 mg for prevention of skeletal events or for improvement of QOL in patients with NDMM. No further inhibition of the osteoclast by bisphosphonates can be achieved by higher doses.
Morgan et al. 2012 [56]	1960 patients with NDMM	ND	Randomized trial	Intensive treatment pathway: Group 1: CLO + CVAD Group 2: ZA + CVAD Group 3: CLO + CTD Group 4: ZA + CTD Non-intensive treatment pathway: Group 5: CLO + MP Group 6: ZA + MP Group 7: CLO + CTDA Group 8: ZA + CTDA	Patients who received attenuated oral cyclophosphamide, thalidomide, and dexamethasone (CTDA) had better responses and lower SRE rates than melphalan and prednisolone (MP). Zoledronic acid (ZA) improved the overall survival (OS) compared with clodronate (CLO) independently of gender, stage, or myeloma subtype, most profoundly in patients with baseline bone disease or other SREs. In patients treated for more than two years, ZA improved OS compared with CLO from randomization. Thalidomide-containing regimens had better efficacy than traditional regimens, and ZOL demonstrated greater benefits than CLO.
Witzig et al. 2013 [57]	68 adult MM patients	III	Randomized trial	Group 1: Thalidomide (Thal)/Zoledronic acid (ZA) Group 2: Zoledronic acid only	The risk of progression to active MM significantly reduced with a combination of Thal and ZA. The time to progression (TTP) was superior for Thal/ZA (n = 35) patients compared with ZA alone (n = 33). In the first year, 86 % of Thal/ZA patients were progression free compared with 55 % on ZA alone. The overall response rate after the first year was 37 % for Thal/ZA with a median duration of response of 3.3 years, but there were no confirmed responses to ZA alone. The addition of Thal to standard ZA treatment produces anti-tumor responses whereas ZA alone does not. No significant difference of osteolytic bone lesions (2 %) in both groups.
Miguel et al. 2013 [58]	455 adult patients with refractory or relapsed multiple myeloma	III	Multicentre, open label, randomized trial	Group 1: pomalidomide + low-dose dexamethasone Group 2: high-dose dexamethasone	Pomalidomide plus low-dose dexamethasone resulted in significantly longer progression-free survival and overall survival, and a greater number of responses compared with high-dose

(continued on next page)

Table 1 (continued)

References	Cohort	Phase	Study design	Treatment groups and medications	Outcomes
					dexamethasone in patients. The median PFS was 4.0 months in the low-dose dexamethasone group compared with 1.9 months in the high-dose group. Clinical data showed that high-dose dexamethasone resulted fewer infections and infestations (53 % vs 68 %), back pain (16 % vs 20 %) and bone pain (13 % vs 17 %).
García-Sanz et al. 2015 [59]	100 adult patients with MM	IV	Prospective, open-label, randomized trial	Group 1: Zoledronic acid (4 mg, IV, every-four weeks) Group 2: No zoledronic acid	ZA shows no anti-tumor effect but reduces the risk of progression with symptomatic bone disease and skeletal complications. There were fewer skeletal-related events in the treated group than in the untreated control group. Progressive osteolytic bone lesions, spinal cord compression and hypercalcemia were observed in 16 % of patients in the ZA group, and 41 % in the control group ( $P = 0.005$ ). The pattern of relapses was different for treated versus control patients, including progressive bone disease (8 vs 20), anemia (24 vs 18), renal dysfunction (1 vs 2), and plasmacytomas (1 vs 1).
Diel et al. 2015 [60]	3822 adult patients with multiple myeloma	III	Double-blind, active-controlled, randomized trial	Group 1: Denosumab (120 mg, IV) every-four weeks Group 2: Zoledronic Acid (4 mg, IV) every-four weeks	Denosumab delayed hypercalcaemia of malignancy (HCM), representing a 37 % reduction in the hazard ratio (HR) compared with zoledronic acid and reduced the risk of developing recurrent HCM by 52 %. Fewer patients receiving denosumab compared with zoledronic acid experienced an HCM event. Denosumab treatment was more efficacious than treatment with zoledronic acid in delaying or preventing HCM in advanced MM and other cancers.
Moreau et al. 2018 [61]	578 adult patients with relapsed and refractory multiple myeloma	III	Multi-center, randomized trial	Group 1: Carfilzomib once a week (70 mg/m <sup>2</sup> ) with dexamethasone Group 2: Carfilzomib twice a week (27 mg/m <sup>2</sup> ) with dexamethasone	Once weekly carfilzomib and dexamethasone had significantly improved progression-free survival, higher overall response, and deeper responses compared with patients who received twice weekly carfilzomib with dexamethasone. No difference in the incidence of bone lesions (77 % presence).
Raje et al. 2018 [33]	1718 adult patients with NDMM	III	Multi-center, double-blind, randomized, controlled trial	Group 1: subcutaneous denosumab (120 mg) with intravenous placebo every 4 weeks Group 2: intravenous zoledronic acid (4 mg; dose adjusted for renal function at baseline) with subcutaneous placebo every 4 weeks	Denosumab was non-inferior to zoledronic acid in the prevention of skeletal-related events. The greater progression-free survival with denosumab than with zoledronic acid. Denosumab had an improved renal adverse event profile. The risk of osteonecrosis of the jaw is an adverse reaction of denosumab and zoledronic acid, there was no significant difference in incidence between the two groups. The most common grade 3 or higher treatment-emergent adverse events for denosumab and ZA were neutropenia, thrombocytopenia, anemia, febrile neutropenia, and pneumonia. Denosumab could be an additional option for the standard of care for patients with MM-related bone diseases.
Terpos et al. 2019 [62]	59 adult patients with MM	I	Open-label prospective study	Lenalidomide (VR) (25 mg) Bortezomib (0.7–1.3 mg/m <sup>2</sup> ) Valacyclovir (500 mg) Trimethoprim/sulfamethoxazole (800 mg/160 mg)	Four cycles of VR consolidation without dexamethasone after ASCT in NDMM patients improved the depth of response and survival outcomes with a manageable safety profile. 58 % of patients improved their response status after ASCT, but 39 % patients following VR consolidation had further deepened response. Stringent complete response rate increased to 51 % after VR from 24 % post-ASCT. A favorable effect on bone remodeling and skeletal-related events (SRE) incidence was observed in the absence of bisphosphonates.

(continued on next page)

Table 1 (continued)

References	Cohort	Phase	Study design	Treatment groups and medications	Outcomes
					VR consolidation is an effective, dexamethasone- and bisphosphonate-free approach that offers long overall survival with improvements on bone metabolism and no SREs.
Fazzi et al. 2020 [63]	44 adult patients with MM	II	Multi-center, single arm trial	IL-2 (SC, $2 \times 10^6$ IU) Zoledronic acid (IV, 4 mg)	The median time to progression was 22.5 months. Treatment was well-tolerated without grade 3 or 4 toxicities. IL-2 and zoledronate may have activity against myeloma possibly through the activation of $\gamma\delta$ T-lymphocytes. The clinical benefit does not support the use of maintenance treatment with IL-2/zoledronate in myeloma patients after autologous bone marrow transplantation.
Huang, et al. 2020 [64]	1718 adult patients with MM	III	Double-blinded, randomized trial	Group 1: Denosumab 120 mg (SC) Group 2: Zoledronic acid 4 mg (IV)	The most common adverse events reported in either group (denosumab, zoledronic acid) were diarrhea, nausea, and pyrexia. Treatment-emergent renal toxicity occurred in 9/102 (denosumab) and 20/92 (zoledronic acid) patients. Fewer patients in the denosumab group developed first on-study SRE compared with the zoledronic acid group. Results support denosumab as an additional treatment for standard of care for NDMM Asian patients.
Diamond et al. 2021 [65]	108 adult patients with MM	II	Single-arm, single center	Oral lenalidomide (10 mg) was given on days 1–21 of a 28-day cycle continuously, until progression or intolerance, for up to 5 years on protocol Aspirin was required for thrombophylaxis	Median follow-up was 40.7 months. At 60 months, progression-free survival was 64 %. The most common adverse events of grade 3 or higher were decreased lymphocyte count in 48 (44 %) patients and decreased neutrophil count in 47 (44 %) patients. One death occurred on study due to sepsis and heart failure but was unrelated to the treatment. The treatment had several adverse reactions, including fractures (3–6 %) and bone/other infections (5–34 %).

Myeloma IX trial [56]. A cohort of nearly 2000 patients were dosed with IV ZA versus oral Clodronate in combination with a variety of other drugs (see Table 1). The primary outcome of overall survival was significantly improved with ZA as a preferred agent over clodronate (the historical treatment of choice [71]). A secondary conclusion was that the combination of ZA with thalidomide yielded better efficacy than other traditional regimens.

Gimsing et al (2010) cited a pre-publication of these findings to justify their efforts to refine a BP dose given by monthly infusion to prevent bone disease in NDMM patients [55]. Their study was double-blinded and compared the incidence of skeletal-related events in patients who received 30 mg and 90 mg of pamidronate. While there was a small difference in median time to the first skeletal event, they concluded overall the safety benefits of the lower pamidronate dose made it the superior treatment. Critically, the higher dose was linked to an increase in osteonecrosis of the jaw and a lack of improvement in quality of life. A limitation to this trial was the reliance on historical placebo control data showing the efficacy of BP treatment alone.

Another notable study showed that BPs can prevent bone disease in MM patients presenting with an asymptomatic biochemical relapse after a prior response to standard therapy [59]. While early monotherapy with ZA produced no anti-tumor effects, it nevertheless reduced the risk of progression to symptomatic bone disease and skeletal complications. Only 16 % of ZA-treated patients (4 mg IV/4 weeks, 12 doses) developed osteolytic bone lesions, spinal cord compression and hypercalcemia – significantly lower than the control group (41 %,  $p = 0.005$ ). The pattern of relapses was also different for treated versus control patients, including progressive bone disease, anemia, renal dysfunction, and

plasmacytomas. However, follow-up was limited in patients that remained asymptomatic and did not show progression after one year of ZA treatment.

BPs are currently listed as a non-therapeutic intervention for pain management in MM and the International Myeloma Working Group has recommended that BPs should be considered in all MM patients receiving first-line antimyeloma therapy regardless of the presence of osteolytic bone lesions on conventional radiography [72]. Comorbidities associated with chronic kidney disease or dental complications can contraindicate their use, although this is not unique to MM and is a consideration for all patients potentially receiving bisphosphonates [70,73]. Under such circumstances, other emerging agents such as denosumab may have considerable potential.

#### 4.2. Denosumab can prevent skeletal-related events in MM patients

Denosumab is a monoclonal antibody that binds and blocks the activity of RANKL. It is approved by the FDA for the management of MBD and prevention of skeletal-related events (e.g. bone pain and fractures) secondary to MM [74]. It is now considered as an alternative therapy for MM patients with renal impairment where BPs may be contraindicated [75].

The efficacy of denosumab has been tested in multiple clinical trials [33,60,64]. Overall, these studies showed that denosumab (120 mg) was more effective than ZA (4 mg) in preventing skeletal-related events (SRE) and controlling hypercalcemia of malignancy (HCM). However, the cost and accessibility of the antibody therapy must be considered in contrast to more conventional BP therapies.



Among MM patients, hypercalcemia of malignancy (HCM) is common (30–80 %) and associated with a poor prognosis. Diel et al. (2015) conducted a phase III randomized trial ( $n = 3822$ ) to compare the activity of denosumab and ZA for delaying and preventing HCM in patients with MM [60]. Denosumab treatment significantly delayed the time to first onset HCM compared with ZA treatment. The higher efficacy of denosumab treatment was observed as early as six months and continued through to the end of the study. Denosumab also reduced the risk of recurrent HCM by 52 %, suggesting it may be superior to BPs to manage hypercalcemia in advanced MM patients. However, the overall rates of adverse events (AEs) and serious adverse events (SAEs) were similar between the denosumab and ZA treatment groups. This study did include non-MM patients (e.g., breast cancer and other solid tumors), which could have confounded these findings.

Still, the superiority of denosumab over ZA was further supported by additional studies in terms of preventing skeletal-related events (SRE) and controlling hypercalcemia of malignancy (HCM) [33,64]. As previously noted, chronic kidney disease is a contraindication for BP use, and it was speculated that denosumab may be a better treatment option under such conditions. Indeed, Raje et al. (2018) reported an improved renal adverse event profile and greater progression-free survival rate with denosumab [33]. Similarly, Huang et al. (2020) found that there were fewer patients with treatment-emergent renal toxicity in the denosumab group versus the ZA group, however, the absolute numbers were low (9/102, 9 % vs 20/92, 22 %) [64]. In contrast, the risk of osteonecrosis of the jaw not significantly different between denosumab and ZA arms. While the study was well designed and powered, recruitment was highly skewed towards Asian patients with MM. It also excluded patients with compromised kidney function (a creatinine clearance of less than 30 mL/min) as treatment assignment was blinded, although this might represent a key target patient subgroup in terms of future clinical treatment. Both studies concluded that denosumab could be considered an additional option for managing patients with MM-related bone diseases.

As a treatment option, denosumab may be limited by its so-called “rebound phenomenon” that occurs upon discontinuation [76]. This is associated with a sharp increase in osteoclast number and activity that can lead to a profound increase in localized or systemic bone turnover. Thus, the suspension of denosumab in the absence of any alternative antiresorptive treatment may lead to adverse outcomes in some patients.

#### 4.3. Bortezomib stimulates osteoblast growth and differentiation

Bortezomib is an anti-cancer medication used to treat MM and some lymphomas and acts on the proteasome (a mechanism important for maintaining the immortality of myeloma cells). It is often used in combination with other agents, such as lenalidomide, dexamethasone, melphalan and/or prednisone [77]. There is potential for bortezomib to improve outcomes after autologous stem cell transplantation and it has been tested in combination with naldomide, valacyclovir, and trimethoprim/sulfamethoxazole [62]. However, bortezomib has also been suggested to upregulate vitamin D receptor signaling, which can directly stimulate osteoblast growth and differentiation [51]. Bortezomib has also been indicated to inhibit osteoclastogenesis and osteoclast activity, the other side of bone metabolism equation [62,78].

The bone anabolic effects of bortezomib have been suggested to lead to repair of lytic lesions in some patients, even in the absence of BPs. Following stem cell transplantation, one study reported a favorable effect of bortezomib-based induction and lenalidomide (VR) consolidation on bone remodeling and SREs [62]. This featured a normalization in circulating bone markers including RANKL/OPG ratios and serum sclerostin. Notably, this trial eschewed the use of other classical bone-affecting therapies such as BPs and dexamethasone but was limited to only transplant-eligible NDMM patients.

It is unclear whether other next-generation proteasome inhibitors (such as carfilzomib and ixazomib [79]) will produce similar bone-

benefits to bortezomib in the bone compartment. While there is potential for these drugs to be effective MM therapeutics [80–82], there is a critical lack of mechanistic studies addressing effects on myeloma progression versus direct impact on osteolytic lesions.

#### 4.4. Chemotherapy does not reduce the formation of osteolytic lesions

Although chemotherapy remains the frontline treatment for MM, there is little evidence that it positively impacts on the progression of MBD and any established osteolytic lesions.

Miguel et al. (2013) recommended pomalidomide plus low-dose dexamethasone to be used in patients with refractory or relapsed and refractory MM who had failed previous treatments of bortezomib and lenalidomide [58]. This was based on their findings that median progression-free survival was 4.0 months in the low-dose dexamethasone group compared with 1.9 months in the high-dose group. While the high vs low-dose dexamethasone did not significantly affect many bone-related adverse events (e.g., back pain and bone pain), the overall rate of infections and infestations was extremely high (68 %). The study did not report what percentage affected the bone, but it does point to an overall higher infection risk associated with MM.

A small but randomized trial reported the progression to active MM was significantly reduced with thalidomide treatment [57]. However, unless combined with ZA, thalidomide on its own did not prevent the acquisition of osteolytic bone lesions. While the sample size was small, the findings are consistent with the concept that many anti-cancer agents are ineffective against MBD. In another trial, comparison of high-dose versus low-dose lenalidomide and dexamethasone showed no improvement in the incidence of bone disease [15]. This study had greater numbers and showed difference in short-term survival with low-dose treatment such that the high-dose group was transitioned to the lower therapy after the 1-year interim analysis. While the MBD analysis was limited, the early mortality in the first four months with high-dose therapy suggests that even short courses carry significant risk, though the study did not mandate thromboprophylaxis or antibiotic prophylaxis.

Diamond et al. (2021) also tested oral lenalidomide (10 mg) given on days 1–21 of a 28-day cycle continuously until progression or intolerance for up to five years in patients with multiple myeloma. It was evident that the treatment had several adverse reactions, which may associate with fractures (3–6 %) and bone or other infections (5–35 %) [65]. The most common adverse events of grade 3 or worse were decreased lymphocyte count in 48 (44 %) patients and decreased neutrophil count in 47 (44 %) patients. At 60 months, progression-free survival was 64 %. One death occurred on study due to sepsis and heart failure; though this was unrelated to treatment, it further illustrates the vulnerability of MM patients to infections. While this was a single-center study it achieved sufficient recruitment to adequately power its primary endpoint.

In another randomized trial, Moreau et al. (2018) tested the efficacies of once (70 mg/m<sup>2</sup>) and twice weekly (27 mg/m<sup>2</sup>) carfilzomib with dexamethasone (40 mg, weekly) in patients with relapsed and refractory MM to bortezomib or ixazomib. The trial found no difference in the incidence of bone lesions between both groups, and the treatments did not reduce bone pain or skeletal events in NDMM patients [61]. However, once weekly carfilzomib and dexamethasone had significantly improved progression-free survival, higher overall response, and deeper responses compared with patients who received twice weekly carfilzomib with dexamethasone. Nonetheless, this study was not double-blinded and allowed for the possibility of selection bias.

#### 4.5. Interleukin-2 does not prevent myeloma bone disease

In 2020, a phase II trial determined the efficacy of interleukin-2 (IL-2) combined with zoledronate (4 mg). It shows that IL-2/zoledronate activates T-lymphocytes against myeloma cells in MM patients. Whilst

the treatment is feasible in terms of adverse events, it is challenging for patients to have numerous visits to the hospital. The clinical benefits observed in terms of time to progression also did not support the use of maintenance treatment with IL-2/zoledronate as a treatment option in myeloma patients after autologous bone marrow transplantation [63]. No clinical data indicated that IL-2 could prevent bone diseases in MM patients.

However, the idea of immunotherapy for myeloma bone disease may still be valid as multiple preclinical *in vivo* studies have identified some proteins (e.g., sclerostin, parathyroid hormone, and BMP) that play a crucial role in myeloma bone disease progression, and are prone to be therapeutic targets [83–88]. Clinical studies exploring such potential will be discussed later in this review.

## 5. MM lytic lesions as a risk factor for osteomyelitis

MM patients that are immunocompromised by chemotherapy, transplantation or steroid medications can be susceptible to infections. However, the medical literature rarely highlights the risks of bone infection associated with myeloma bone disease. While the literature to date chiefly consists of case reports rather than rigorous prospective trials, the anecdotal evidence would suggest that this may be an area of clinical concern that justifies further investigation. Moreover, when osteomyelitis effects a cancerous bone lesion, the clinical outcomes are often poor.

Consequently, we conducted a literature search on PubMed database looking for clinical case reports of osteomyelitis in multiple myeloma patients. All searches were limited to January 2000–December 2021. We used medical subject headings (MeSH) and keyword terms in the title/abstract, and the final search used the terms “multiple myeloma AND bone lesion OR osteolytic lesions OR osteomyelitis OR bone infection” and filtered for “case reports” only. Additional reports that were found relevant to the subject were manually added to the list. All case reports were summarized in Table 2.

Various bacterial pathogens have been reported to cause osteomyelitis in multiple myeloma patients, including *Staphylococcus aureus* and coagulase-negative *Staphylococci* [89], *Streptococcus pneumoniae* [89,93], *Escherichia coli* [90,92], *Haemophilus quentini* [94]. Most reported infections were associated with vertebra, particularly in the lumbar region.

Desikan et al. (2003) reported three cases of spondylodiscitis and epidural abscesses in MM patients. *Staphylococci* and *Streptococci* were found in culture [89]. One 72-year-old male patient received discectomy and corpectomy of C4–C5 vertebrae along with arthrodesis of the C3–C6 vertebrae. Another 56-year-old male patient received a partial laminectomy of L4–L5 to evacuate the epidural abscess, and then received intravenous vancomycin for six weeks with no recurrence of vertebral infections. The third case, a 61-year-old male patient had spondylodiscitis of the L5–S1 disc space. The patient received intravenous vancomycin for one month and had no recurrence of pain. Evaluations were normal for the next three years.

Roque et al. (2021) reported a 57-year-old man with lumbar pain, paraplegia and fever was diagnosed with spondylodiscitis. MRI identified a mass extending from the intervertebral disc D9 to the vertebral canal with a numerous adjacent osteolytic lesion. A plasmacytoma was later confirmed by a biopsy of D9, suggesting skeleton osteolytic lesions caused by multiple myeloma [96]. In the end, a short course of radiation therapy and high-dose corticosteroids were used to treat the patient.

Yu et al. (2010) revealed a case of a 57-year-old female patient with IgG kappa gammopathy with tenderness and knocking pain over the lumbar area (L2) [90]. Blood culture later confirmed an *E. coli* infection and a CT-guided biopsy at the L2 vertebra confirmed infectious spondylitis. The patient was first treated with intravenous oxacillin, and then switched to cefazolin and cefuroxime. The patient was free of recurrent back pain and fever six months after, and was subsequently treated with melphalan, dexamethasone and thalidomide for MM [90]. Park et al.

(2016) also reported a 74-year-old female patient with Fever and diffuse abdominal pain and septic shock [92]. Chest CT showed emphysematous osteomyelitis on her T6 vertebra, and blood culture was positive for *E. coli*.

Although most MM patients with osteomyelitis were above 50 years of age, osteomyelitis sometimes occurred in younger patients. Webber et al. (2017) reported a 25-year-old male patient with femoral pyomyositis, hypercalcemia, mild anemia [93]. The patient was later diagnosed with IgG kappa multiple myeloma, and *Streptococcus pneumoniae* was identified. The patient received zoledronate for hypercalcemia and completed a four-week course of IV ceftriaxone for the infection. He also received bortezomib-lenalidomide-dexamethasone therapy and autologous bone marrow transplant for MM. One year later, the swelling and the pain were resolved.

Apart from bacteria, other invasive fungal pathogens can also cause bone infections in MM patients. Mohan et al. (2016) and Sassine et al. (2021) reported two individual cases of osteomyelitis associated with *Lasiodiplodia* and *Cryptococcus neoformans* in MM patients [91,95]. A 69-year-old male patient had relapsed refractory MM and was admitted for chemotherapy and ASCT was infected with *Lasiodiplodia*. In the end, the infection was treated with amputation and antifungal medications (oral voriconazole alone after 14 days of liposomal amphotericin B). In the other case, a 77-year-old male patient had multiple myeloma treated with lenalidomide developed a slowly progressive right upper thigh pain with no antecedent trauma or known history of osteolytic lesions. Tissue cultures and bone histology later identified Cryptococcosis. The patient had then received intravenous liposomal amphotericin B (5 mg/kg daily) for one week and was discharged on a high dose (800 mg/day) of oral fluconazole. Nailing of the femur was conducted to prevent fracture and following a switch to oral voriconazole (300 mg twice daily) for three months.

Despite the high patient impact of these complications, it must be recognized that only ten published case reports of osteomyelitis associated with MBD were identified and most were single cases only. Moreover, many did not fully address the management or outcomes. In the absence of unbiased clinical data longitudinally tracking infection comorbid with MBD it is not possible to gauge the relative infection risk associated with osteolytic lesions.

## 6. Discussion

Multiple myeloma is a malignant tumor of plasma cells that involves the bone marrow and can cause severe lytic bone damage in the axial skeleton and pelvis. Primary bone tumors and lesions are commonly found in the spine, pelvis, skull, sternum, and ribs [97]. Skeletal complications caused by multiple myeloma are associated with considerable pain in patients, increased mortality, and low quality of life.

Infection is the leading cause of morbidity and mortality in patients with multiple myeloma (MM) [98]. Although osteomyelitis is not the most common form of infections among MM patients, osteolytic bone lesions and profound immunodeficiency can increase the risk of developing bone infections in immunosuppressive MM patients. In severe cases, infection results in life-threatening complications, including bacteremia, organ failures, septic shock, or even death [99]. While bone infections are manageable in most reported cases with broad spectrum antibiotics, prolonged hospitalization, antibiotic treatment, and additional surgeries could significantly increase the burden of disease and severely affect the prognosis with increased mortality. Also, drug-resistant bacterial infection has been reported [91], and can potentially be a major threat to MM patients in the future.

Subsequently, clinical trials focusing on antimicrobial prophylaxis in multiple myeloma are limited, and the data are inconsistent. Oken et al. (1996) showed that administering trimethoprim-sulfamethoxazole (TMP-SMX) for the first two months of initial chemotherapy is effective, inexpensive prophylaxis for early bacterial infection in multiple myeloma [100]. However, Vesole et al. (2012) contradictorily reported

**Table 2**

Summary of case reports focused on treatment of bone infections in MM patients (Jan 2000- Dec 2021).

References	Patient details	Medical history, sign, and symptoms	Infection site and causative pathogens	Treatments and clinical outcomes
Desikan, et al. (2003) [89]	72, Male	Stage IIA kappa light-chain disease, received 140 mg/m <sup>2</sup> melphalan after induction therapy with 40 mg of dexamethasone Had a history of oxacillin-resistant <i>Staphylococcus aureus</i> infection, treated with intravenous vancomycin Three months later, readmitted with significant right shoulder pain and required intravenous morphine	Spondylodiscitis with prevertebral and epidural abscesses causing impingement of the cervical cord Blood culture was positive for <i>S. aureus</i>	Received discectomy and corpectomy of C4 and C5 vertebrae along with arthrodesis of the C3-C6 vertebrae.
Desikan, et al. (2003) [89]	56, Male	Stage IIIA IgG lambda multiple myeloma Received induction therapy and tandem transplants Recurrence of MM with severe low back pain	An MRI scan revealed spondylodiscitis of disc L4-L5 with an associated epidural abscess. Culture of the epidural abscess showed positive for <i>Streptococcus pneumoniae</i> with intermediate resistance to penicillin.	A partial laminectomy of L4 was performed to evacuate the epidural abscess. Received intravenous vancomycin for six weeks, and no recurrence of vertebral infection was observed. The patient suffered respiratory infections and died of progressive disease one year later.
Desikan, et al. (2003) [89]	61, Male	VAD refractory stage IIIB kappa light-chain myeloma received combination chemotherapy with dexamethasone, thalidomide, cisplatin, adriamycin, cyclophosphamide and etoposide (DT-PACE) for stem cell procurement. Developed fever, complained of localized pain and tenderness of the lower back before admission for stem cell transplant. The back pain worsened during the post-transplant neutropenic period.	An MRI revealed spondylodiscitis of the L5-S1 disc space. A CT-guided aspirate was positive for coagulase-negative <i>Staphylococci</i> .	Received intravenous vancomycin for one month. The patient had no recurrence of pain. Evaluations were normal for the next three years.
Yu et al. (2010) [90]	57, Female	IgG kappa gammopathy (subsequent diagnosis of myeloma), had 3-week history of chill and low back pain. No history of trauma. The patient also had mild tenderness and knocking pain over the lumbar area. The MRI of spine demonstrated hyperintensity at the L2 body with a pre-vertebral abscess, suspected spondylitis.	Blood culture revealed <i>Escherichia coli</i> , and a CT-guided biopsy at the L2 vertebra confirmed infectious spondylitis.	First treated with intravenous oxacillin, then switched to cefazolin and cefuroxime. Neurological deficit was alleviated after eight weeks of antibiotic therapy. The patient was free of recurrent back pain and fever six months after discharge, and was subsequently treated with melphalan, dexamethasone and thalidomide for MM.
Mohan et al. (2016) [91]	69, Male	Relapsed refractory MM, admitted for chemotherapy and autologous stem cell transplant (ASCT). He was diagnosed with MM and had been heavily treated in the past including three prior ASCTs. He was admitted for velcade, dexamethasone, thalidomide, adriamycin, cytoxan, and etoposide administration days 1 to 4, with one dose of melphalan and ASCT on day 6. He developed new onset atrial fibrillation with acute renal failure, and the neutropenic phase was further complicated with sepsis caused by vancomycin- and daptomycin-resistant <i>Enterococcus faecium</i> bacteremia. The infection was successfully treated with quinapristin-dalfopristin.	<i>Lasiodiplodia</i> On day 6 post ASCT, the patient reported new swelling and erythema of the third right toe. Physical examination showed hemorrhagic bullae around the nail with reddish discoloration of the entire third right toe and minimal oedema.	Successfully treated with amputation and antifungal medications (oral voriconazole alone after 14 days of liposomal amphotericin B).
Park et al. (2016) [92]	74, Female, Korean	Fever and diffuse abdominal pain and septic shock Multiple myeloma, had 2 cycles of chemotherapy with thalidomide-cyclophosphamide-dexamethasone for relapsed MM after previous chemotherapy with bortezomib-melphalan-prednisolone and lenalidomide-dexamethasone	<i>Escherichia coli</i> in blood culture Chest computed tomography (CT) showed incidental intraosseous gas in her sternum and T6 vertebra, suggesting emphysematous osteomyelitis	Meropenem and supportive treatment The patient recovered and was discharged 20 days later.
Webber et al. (2017) [93]	25, Male	Femoral pyomyositis, hypercalcemia, mild anaemia, and elevated inflammatory markers. Diagnosed with IgG kappa multiple myeloma.	<i>Streptococcus pneumoniae</i> Femoral pyomyositis	Received zoledronic acid therapy for hypercalcemia. Completed a 4-week course of IV ceftriaxone. Received bortezomib-lenalidomide-dexamethasone (VRd)

(continued on next page)



Table 2 (continued)

References	Patient details	Medical history, sign, and symptoms	Infection site and causative pathogens	Treatments and clinical outcomes
				therapy and autologous bone marrow transplant. One year later, the swelling and the leg/thigh pain had resolved.
Cohen et al. (2019) [94]	56, Male	Undiagnosed multiple myeloma with severe sepsis associated with pneumonia, meningitis, polyarthritis, and osteomyelitis	<i>Haemophilus quentini</i>	Not determined.
Sassine, et al. (2021) [95]	77, Male	Had multiple myeloma treated with lenalidomide, developed a slowly progressive right upper thigh pain with no antecedent trauma or known history of osteolytic lesions. PET-CT showed a right proximal femoral diaphysis lesion with cortical destruction and intensely avid FDG uptake.	Tissue cultures positive for <i>Cryptococcus neoformans</i> . Bone histology was consistent with cryptococcosis. Serum positive for cryptococcal antigen.	Received intravenous liposomal amphotericin B (5 mg/kg daily) for one week and was discharged on a high dose (800 mg/d) of oral fluconazole. Had nailing of the femur to prevent fracture, following a switch to oral voriconazole (300 mg twice daily) for three months.
Roque et al. (2021) [96]	57, Male	Had lumbar pain, paraplegia, and fever. Diagnosed with spondylodiscitis. MRI identified a mass extending from D9 to the vertebral canal with numerous adjacent osteolytic lesions. A plasmacytoma was confirmed by C9's biopsy.	<i>B. melitensis</i>	A short course of radiation therapy and high-dose corticosteroids were used to treat the patient.

that prophylactic treatment with TMP-SMX and Ciprofloxacin (500 mg) or Ofloxacin (400 mg) did not decrease the incidence of serious bacterial infections ( $\geq$  grade 3) within the first two months of treatment. Later, the clinical trials of Drayson et al. (2019) tested the addition of prophylactic levofloxacin to active myeloma treatment during the first 12 weeks of therapy, and the results showed reduction of febrile episodes and mortality compared with the placebo group without increasing health care-associated infections, suggesting that prophylactic levofloxacin may be beneficial for patients with NDMM undergoing antimyeloma therapy [99]. However, none of the clinical trials focused on preventing osteomyelitis in MM patients. There is also a knowledge gap in the efficacy of prophylactic antimicrobial use for reducing morbidity and mortality of bone infections in MM patients.

Pain induced by vertebral fracture in multiple myeloma are common with additional causes such as spondylolysis deformans, osteochondrosis, stenosis of the spinal canal and intervertebral nerve compression [101]. IV antibiotic and surgical interventions, such as discectomy, decompression, and debridement, are used to manage spondylodiscitis and epidural abscesses. Whereas amputation is used to manage osteonecrosis in the long bones [89,93]. Multiple case reports have shown that the vertebra and vertebral discs are highly susceptible to infections in patients aged over 50 [89,90,96]. Therefore, future studies should focus on etiology of vertebral infections in MM patients to reduce disease burden, improve prognosis and prevent severe complications.

While fungal osteomyelitis is rarely encountered, it is often difficult to culture and diagnose. The clinical case reports highlighted that there were certain risks factors associated with immunocompromised patients and fungal osteomyelitis that can lead to severe consequences (e.g., amputation and length antifungal treatment) [91,95]. The studies of fungal osteomyelitis in multiple myeloma patients are minority. Nevertheless, fungal pathogens should not be overlooked in MM patients when diagnosing osteomyelitis.

Multiple myeloma patients frequently develop tumor-induced bone destruction, but no therapy eliminates the tumor or fully reverses bone loss. Agents that prevent bone resorption like BPs and denosumab can effectively reduce the risk of skeletal-related events and myeloma bone disease in NDMM patients. Conventionally, zoledronate was widely prescribed as a prophylaxis to prevent local osteolytic lesions, but recent trials suggested that denosumab is a better alternative with high efficacy. However, cumulative doses of BPs and denosumab are associated with serious adverse reactions and medication-related osteonecrosis of

the jaw (MRONJ) [102]. Therefore, administration and treatment must be carefully monitored, and dentist consultation is warranted.

On the other hand, Wnt signaling pathway such as Dkk-1 may be responsible for inhibiting osteoblast activities [103,104]. Fulciniti, et al. (2009) identified anti-Dkk-1 monoclonal antibody (BHQ880) as a potential therapeutic agent for multiple myeloma. The pro-anabolic effect and anti-myeloma activity of anti-Dkk-1 neutralizing antibodies was determined in *in vitro* and *in vivo* preclinical trials [105–107]. Later, a phase 1B clinical trial showed that BHQ880 in combination with zoledronate and anti-myeloma therapy was well tolerated and may be eligible for patients with relapsed or refractory multiple myeloma [108].

Furthermore, studies show that sclerostin, a glycoprotein that is exclusively secreted by osteocytes, is also involved in the regulation of bone metabolism. It affects the activity of BMPs and inhibits Wnt/ $\beta$ -catenin metabolic pathway in bone cells [86]. Sclerostin is also an early marker of relapse in multiple myeloma and can be targeted for therapies [83,84]. In preclinical models, the deletion of SOST gene (encoding sclerostin) prevented MM-induced bone disease, and the administration of anti-sclerostin antibody (Scl-Ab) increased bone mass and decreases osteolysis in immune-competent mice with established MM [85]. Subsequently, treatment with anti-sclerostin antibody combined with zoledronic acid also displayed higher bone mass and fracture resistance than zoledronic acid alone [87]. The combination therapy of anti-sclerostin antibody and the proteasome inhibitor carfilzomib also show potent anti-myeloma activity with positive effects on bone disease [109].

Preclinical trials also indicated that transforming growth factor- $\beta$  (TGF- $\beta$ ) inhibition can induce the repair of lytic lesions in mice bearing myeloma [110]. Such findings have raised the clinical potential for combined therapy with bortezomib/1D11 with zoledronate [111–113]. Nyman et al. (2016) found that although monotherapy with TGF- $\beta$  inhibitors is unlikely to be beneficial, a combined therapy of 1D11 (an anti-TGF- $\beta$  antibody inhibiting TGF- $\beta$  signaling) with bortezomib (a proteasome inhibitor) can reduce bone destruction and pathological fractures in MM patients [114]. Substantial clinical trials should continue to optimize its efficacy and establish clinical guidelines for this therapy.

Although bone morphogenetic protein (BMP) signaling was not reported to be dysregulated in myeloma bone disease previously, a study found that BMP upregulated signaling in stromal progenitor cells [88], and the *in vivo* murine model later confirmed that inhibiting BMP

signaling using a small molecule BMP receptor antagonist or a BMP1a-FC receptor ligand trap could prevent trabecular and cortical bone loss caused by myeloma without increasing the tumor burden. It was hypothesized that BMP inhibition can directly reduce osteoclastogenesis, increase osteoblasts and bone formation and suppress bone marrow sclerostin levels. This study highlighted the possibility of targeting the BMP pathway to prevent myeloma-induced bone disease.

Finally, there are many other factors released by bone resorption further promote MM cell growth perpetuating the vicious cycle of malignant cell expansion and bone destruction. For example, the receptor activator of NF- $\kappa$ B ligand (RANKL), may influence osteoclast activation [115,116]. Serum parathyroid hormone (PTH) level was also found to be associated with risk factors and clinical outcome in MM patients with extensive bone disease [117]. As primary hyperparathyroidism (PHPT) is the most common cause of non-neoplastic hypercalcemia in MM patients, it was suspected that high secretion of PTH may have a negative impact on MM associated bone disease and MM progression [118]. Future trials and continuous studies investigating these pathological pathways may be critical for finding novel interventions to treat myeloma bone diseases.

## 7. Conclusion

Immunocompromised multiple myeloma patients with bone defects are susceptible to fractures and substantial osteomyelitis, increasing mortality and the burden of disease. For antiresorptive agents, denosumab has advantages over conventional zoledronate therapy in preventing myeloma bone disease, particularly in some patient subgroups. Chemotherapy agents like lenalidomide and carfilzomib do not reduce bone pain and osteolytic lesions, whereas a robust anti-myeloma agent like bortezomib can reduce the tumor area, and the anti-TGF- $\beta$  antibody 1D11 can improve bone repair and bone quality in multiple myeloma. Emerging clinical data suggest that trimethoprim-sulfamethoxazole and levofloxacin can be used as a prophylaxis for bone infections, although further clinical trials are needed. Despite these advances, MM remains incurable, and patients continue to suffer from bone lesions and fractures. While bone infection is not the most common complication of MBD, persistent local osteolytic lesions possess an underlying risk of progression to osteomyelitis. Indeed, the lack of studies testing the connection between MBD and bone infection represent an opportunity to undertake retrospective reviews of the clinical data and prospective trials. This may identify a need for new prophylaxis strategies to prevent bone infection as well as improved clinical guidelines for the treatment of infected bone lesions.

## Declaration of Competing Interest

The authors declare that they have no known competing financial interests or personal relationships that could have appeared to influence the work reported in this paper.

## References

- [1] C.J. Neuse, O.C. Lomas, C. Schliemann, et al., Genome instability in multiple myeloma, *Leukemia* 34 (11) (2020) 2887–2897.
- [2] U.A. Shah, S. Mailankody, Emerging immunotherapies in multiple myeloma, *Bmj* 370 (2020), m3176.
- [3] E. Terpos, N. Raje, P. Croucher, et al., Denosumab compared with zoledronic acid on PFS in multiple myeloma: exploratory results of an international phase 3 study, *Blood Adv* 5 (3) (2021) 725–736.
- [4] P.G. Richardson, J.P. Laubach, R.L. Schlossman, et al., The Medical Research Council Myeloma IX trial: the impact on treatment paradigms, *Eur J Haematol* 88 (1) (2012) 1–7.
- [5] N.W.C.J. van de Donk, C. Pawlyn, K.L. Yong, Multiple myeloma, *The Lancet* 397 (10272) (2021) 410–427.
- [6] F. Gay, A. Palumbo, Management of disease- and treatment-related complications in patients with multiple myeloma, *Med Oncol* 27 (Suppl 1) (2010) S43–S52.
- [7] S.V. Rajkumar, Multiple myeloma: 2020 update on diagnosis, risk-stratification and management, *Am J Hematol* 95 (5) (2020) 548–567.
- [8] O. Landgren, S.V. Rajkumar, New Developments in Diagnosis, Prognosis, and Assessment of Response in Multiple Myeloma, *Clin Cancer Res* 22 (22) (2016) 5428–5433.
- [9] A. Palumbo, H. Avet-Loiseau, S. Oliva, et al., Revised International Staging System for Multiple Myeloma: A Report From International Myeloma Working Group, *J Clin Oncol* 33 (26) (2015) 2863–2869.
- [10] A.J. Cowan, D.J. Green, M. Kwok, et al., Diagnosis and Management of Multiple Myeloma: A Review, *Jama* 327 (5) (2022) 464–477.
- [11] S.V. Rajkumar, Treatment of multiple myeloma, *Nat Rev Clin Oncol* 8 (8) (2011) 479–491.
- [12] S.V. Rajkumar, Multiple myeloma: Every year a new standard? *Hematol Oncol* 37 Suppl 1 (Suppl 1) (2019) 62–65.
- [13] R. Al Hamed, A.H. Bazarbachi, F. Malard, J.L. Harousseau, M. Mohty, Current status of autologous stem cell transplantation for multiple myeloma, *Blood Cancer J* 9 (4) (2019) 44.
- [14] G. Ricciuti, A. Falcone, N. Cascavilla, G. Martinelli, C. Cerchione, Autologous stem cell transplantation in multiple myeloma, *Panminerva Med* 62 (4) (2020) 220–224.
- [15] S.V. Rajkumar, S. Jacobus, N.S. Callander, et al., Lenalidomide plus high-dose dexamethasone versus lenalidomide plus low-dose dexamethasone as initial therapy for newly diagnosed multiple myeloma: an open-label randomised controlled trial, *Lancet Oncol* 11 (1) (2010) 29–37.
- [16] S. Singhal, J. Mehta, R. Desikan, et al., Antitumor activity of thalidomide in refractory multiple myeloma, *N Engl J Med* 341 (21) (1999) 1565–1571.
- [17] M. Dimopoulos, A. Spencer, M. Attal, et al., Lenalidomide plus dexamethasone for relapsed or refractory multiple myeloma, *N Engl J Med* 357 (21) (2007) 2123–2132.
- [18] P.G. Richardson, B. Barlogie, J. Berenson, et al., A phase 2 study of bortezomib in relapsed, refractory myeloma, *N Engl J Med* 348 (26) (2003) 2609–2617.
- [19] H. Eda, L. Santo, G. David Roodman, N. Raje, Bone Disease in Multiple Myeloma, *Cancer treatment and research* 169 (2016) 251–270.
- [20] I. Ntanasis-Stathopoulos, M. Gavriatopoulou, E. Kastritis, E. Terpos, M. A. Dimopoulos, Multiple myeloma: Role of autologous transplantation, *Cancer Treat Rev* 82 (2020), 101929.
- [21] T. Choi, Is autologous stem cell transplantation still relevant for multiple myeloma? *Curr Opin Hematol* 26 (6) (2019) 386–391.
- [22] R.D. Parrondo, S. Ailawadhi, T. Sher, A.A. Chanan-Khan, V. Roy, Autologous Stem-Cell Transplantation for Multiple Myeloma in the Era of Novel Therapies, *JCO Oncol Pract* 16 (2) (2020) 56–66.
- [23] M. Gentile, F. Morabito, M. Martino, et al., Chemotherapy-based regimens in multiple myeloma in 2020, *Panminerva Med* 63 (1) (2021) 7–12.
- [24] M.T. Petrucci, F. Vozella, The Anti-CD38 Antibody Therapy in Multiple Myeloma, *Cells* 8 (12) (2019).
- [25] F. Cavallo, M. Boccadoro, A. Palumbo, Review of thalidomide in the treatment of newly diagnosed multiple myeloma, *Ther Clin Risk Manag* 3 (4) (2007) 543–552.
- [26] M. Cavo, E. Zamagni, P. Tosi, et al., First-line therapy with thalidomide and dexamethasone in preparation for autologous stem cell transplantation for multiple myeloma, *Haematologica* 89 (7) (2004) 826–831.
- [27] M. Dimopoulos, H. Quach, M.V. Mateos, et al., Carfilzomib, dexamethasone, and daratumumab versus carfilzomib and dexamethasone for patients with relapsed or refractory multiple myeloma (CANDOR): results from a randomised, multicentre, open-label, phase 3 study, *Lancet* 396 (10245) (2020) 186–197.
- [28] M. Attal, P.G. Richardson, S.V. Rajkumar, et al., Isatumixab plus pomalidomide and low-dose dexamethasone versus pomalidomide and low-dose dexamethasone in patients with relapsed and refractory multiple myeloma (ICARIA-MM): a randomised, multicentre, open-label, phase 3 study, *Lancet* 394 (10214) (2019) 2096–2107.
- [29] P.M. Voorhees, J.L. Kaufman, J. Laubach, et al., Daratumumab, lenalidomide, bortezomib, and dexamethasone for transplant-eligible newly diagnosed multiple myeloma: the GRIFFIN trial, *Blood* 136 (8) (2020) 936–945.
- [30] M.V. Mateos, J. Bladé, S. Bringhen, et al., Melflufen: A Peptide-Drug Conjugate for the Treatment of Multiple Myeloma, *J Clin Med* 9 (10) (2020).
- [31] S. Zweegman, B. van der Holt, U.H. Mellqvist, et al., Melphalan, prednisone, and lenalidomide versus melphalan, prednisone, and thalidomide in untreated multiple myeloma, *Blood* 127 (9) (2016) 1109–1116.
- [32] K. Weisel, A. Spencer, S. Lentzsch, et al., Daratumumab, bortezomib, and dexamethasone in relapsed or refractory multiple myeloma: subgroup analysis of CASTOR based on cytogenetic risk, *J Hematol Oncol* 13 (1) (2020) 115.
- [33] N. Raje, E. Terpos, W. Willenbacher, et al., Denosumab versus zoledronic acid in bone disease treatment of newly diagnosed multiple myeloma: an international, double-blind, double-dummy, randomised, controlled, phase 3 study, *Lancet Oncol* 19 (3) (2018) 370–381.
- [34] M. Sonmez, T. Akagun, M. Topbas, et al., Effect of pathologic fractures on survival in multiple myeloma patients: a case control study, *J Exp Clin Cancer Res* 27 (1) (2008) 11.
- [35] C. Panaroni, A.J. Yee, N.S. Raje, Myeloma and Bone Disease, *Current osteoporosis reports* 15 (5) (2017) 483–498.
- [36] H.S. Yeh, J.R. Berenson, Treatment for myeloma bone disease, *Clin Cancer Res* 12 (20 Pt 2) (2006) 6279s–s6284.
- [37] Ø. Hjertner, T. Standal, M. Børset, A. Sundan, A. Waage, Bone disease in multiple myeloma, *Med Oncol* 23 (4) (2006) 431–441.
- [38] E. Terpos, I. Ntanasis-Stathopoulos, M.A. Dimopoulos, Myeloma bone disease: from biology findings to treatment approaches, *Blood* 133 (14) (2019) 1534–1539.

- [39] E.K. Mai, K. Miah, U. Bertsch, et al., Bortezomib-based induction, high-dose melphalan and lenalidomide maintenance in myeloma up to 70 years of age, *Leukemia* 35 (3) (2021) 809–822.
- [40] L.A. Mouloupos, V. Koutoulidis, J. Hillengass, et al., Recommendations for acquisition, interpretation and reporting of whole body low dose CT in patients with multiple myeloma and other plasma cell disorders: a report of the IMWG Bone Working Group, *Blood Cancer Journal* 8 (10) (2018) 95.
- [41] K.M. Treitl, J. Ricke, A. Baur-Melnyk, Whole-body magnetic resonance imaging (WBMRI) versus whole-body computed tomography (WBCT) for myeloma imaging and staging, *Skeletal Radiology* (2021).
- [42] M. Dimopoulos, E. Terpos, R.L. Comenzo, et al., International myeloma working group consensus statement and guidelines regarding the current role of imaging techniques in the diagnosis and monitoring of multiple Myeloma, *Leukemia* 23 (9) (2009) 1545–1556.
- [43] M.V. Mateos, L. Fink, N. Koneswaran, et al., Bone complications in patients with multiple myeloma in five European countries: a retrospective patient chart review, *BMC cancer* 20 (1) (2020) 170.
- [44] T.S. Miceli, K. Colson, B.M. Faïman, K. Miller, J.D. Tariman, Maintaining bone health in patients with multiple myeloma: survivorship care plan of the International Myeloma Foundation Nurse Leadership Board, *Clin J Oncol Nurs* 15 Suppl(0) (2011) 9–23.
- [45] A. Valentin-Opran, S.A. Charhon, P.J. Meunier, C.M. Edouard, M.E. Arlot, Quantitative histology of myeloma-induced bone changes, *British journal of haematology* 52 (4) (1982) 601–610.
- [46] N. Kovacic, P.I. Croucher, M.M. McDonald, Signaling between tumor cells and the host bone marrow microenvironment, *Calcified tissue international* 94 (1) (2014) 125–139.
- [47] P.I. Croucher, M.M. McDonald, T.J. Martin, Bone metastasis: the importance of the neighbourhood, *Nat Rev Cancer* 16 (6) (2016) 373–386.
- [48] K.N. Weilbaecher, T.A. Guise, L.K. McCauley, Cancer to bone: a fatal attraction, *Nat Rev Cancer* 11 (6) (2011) 411–425.
- [49] S.H. Tella, J.C. Gallagher, Prevention and treatment of postmenopausal osteoporosis, *The Journal of steroid biochemistry and molecular biology* 142 (2014) 155–170.
- [50] E.D. Deeks, Denosumab: A Review in Postmenopausal Osteoporosis, *Drugs & aging* 35 (2) (2018) 163–173.
- [51] M.F. Kaiser, U. Heider, M. Mieth, C. Zang, I. von Metzler, O. Sezer, The proteasome inhibitor bortezomib stimulates osteoblastic differentiation of human osteoblast precursors via upregulation of vitamin D receptor signalling, *Eur J Haematol* 90 (4) (2013) 263–272.
- [52] G. Guzik, Oncological and functional results of the surgical treatment of vertebral metastases in patients with multiple myeloma, *BMC Surg* 17 (1) (2017) 92.
- [53] S. Utzschneider, H. Schmidt, P. Weber, G.P. Schmidt, V. Jansson, H.R. Dürr, Surgical therapy of skeletal complications in multiple myeloma, *Int Orthop* 35 (8) (2011) 1209–1213.
- [54] B. Barlogie, F. van Rhee, J.D. Shaughnessy Jr, et al., Seven-year median time to progression with thalidomide for smoldering myeloma: partial response identifies subset requiring earlier salvage therapy for symptomatic disease, *Blood* 112 (8) (2008) 3122–3125.
- [55] P. Gimsing, K. Carlson, I. Tureson, et al., Effect of pamidronate 30 mg versus 90 mg on physical function in patients with newly diagnosed multiple myeloma (Nordic Myeloma Study Group): a double-blind, randomised controlled trial, *Lancet Oncol* 11 (10) (2010) 973–982.
- [56] G.J. Morgan, F.E. Davies, W.M. Gregory, et al., Effects of induction and maintenance plus long-term bisphosphonates on bone disease in patients with multiple myeloma: the Medical Research Council Myeloma IX Trial, *Blood* 119 (23) (2012) 5374–5383.
- [57] T.E. Witzig, K.M. Laumann, M.Q. Lacy, et al., A phase III randomized trial of thalidomide plus zoledronic acid versus zoledronic acid alone in patients with asymptomatic multiple myeloma, *Leukemia* 27 (1) (2013) 220–225.
- [58] J.S. Miguel, K. Weisel, P. Moreau, et al., Pomalidomide plus low-dose dexamethasone versus high-dose dexamethasone alone for patients with relapsed and refractory multiple myeloma (MM-003): a randomised, open-label, phase 3 trial, *Lancet Oncol* 14 (11) (2013) 1055–1066.
- [59] R. García-Sanz, A. Oriol, M.J. Moreno, et al., Zoledronic acid as compared with observation in multiple myeloma patients at biochemical relapse: results of the randomized AZABACHE Spanish trial, *Haematologica* 100 (9) (2015) 1207–1213.
- [60] I.J. Diehl, J.J. Body, A.T. Stopeck, et al., The role of denosumab in the prevention of hypercalcaemia of malignancy in cancer patients with metastatic bone disease, *Eur J Cancer* 51 (11) (2015) 1467–1475.
- [61] P. Moreau, M.V. Mateos, J.R. Berenson, et al., Once weekly versus twice weekly carfilzomib dosing in patients with relapsed and refractory multiple myeloma (A.R.R.O.W.): interim analysis results of a randomised, phase 3 study, *Lancet Oncol* 19 (7) (2018) 953–964.
- [62] E. Terpos, E. Kastritis, I. Ntanasis-Stathopoulos, et al., Consolidation therapy with the combination of bortezomib and lenalidomide (VR) without dexamethasone in multiple myeloma patients after transplant: Effects on survival and bone outcomes in the absence of bisphosphonates, *Am J Hematol* 94 (4) (2019) 400–407.
- [63] R. Fazzi, I. Petrini, N. Giuliani, et al., Phase II Trial of Maintenance Treatment With IL2 and Zoledronate in Multiple Myeloma After Bone Marrow Transplantation: Biological and Clinical Results, *Front Immunol* 11 (2020), 573156.
- [64] S.Y. Huang, S.S. Yoon, K. Shimizu, et al., Denosumab Versus Zoledronic Acid in Bone Disease Treatment of Newly Diagnosed Multiple Myeloma: An International, Double-Blind, Randomized Controlled Phase 3 Study-Asian Subgroup Analysis, *Adv Ther* 37 (7) (2020) 3404–3416.
- [65] B. Diamond, N. Korde, A.M. Lesokhin, et al., Dynamics of minimal residual disease in patients with multiple myeloma on continuous lenalidomide maintenance: a single-arm, single-centre, phase 2 trial, *Lancet Haematol* 8 (6) (2021) e422–e432.
- [66] Z. Mbese, B.A. Aderibigbe, Bisphosphonate-Based Conjugates and Derivatives as Potential Therapeutic Agents in Osteoporosis, Bone Cancer and Metastatic Bone Cancer, *International journal of molecular sciences* 22 (13) (2021).
- [67] O.L. Lee, N. Horvath, C. Lee, et al., Bisphosphonate guidelines for treatment and prevention of myeloma bone disease, *Internal medicine journal* 47 (8) (2017) 938–951.
- [68] A. Alegre, M. Gironella, A. Bailén, P. Giraldo, Zoledronic acid in the management of bone disease as a consequence of multiple myeloma: a review, *Eur J Haematol* 92 (3) (2014) 181–188.
- [69] A. Guzzdar, C. Costello, Supportive Care in Multiple Myeloma, *Curr Hematol Malig Rep* 15 (2) (2020) 56–61.
- [70] J.A. Snowden, S.H. Ahmedzai, J. Ashcroft, et al., Guidelines for supportive care in multiple myeloma 2011, *British journal of haematology* 154 (1) (2011) 76–103.
- [71] R. Lahtinen, M. Laakso, I. Palva, P. Virkkunen, I. Elomaa, Randomised, placebo-controlled multicentre trial of clodronate in multiple myeloma, Finnish Leukaemia Group, *Lancet* 340 (8827) (1992) 1049–1052.
- [72] E. Terpos, G. Morgan, M.A. Dimopoulos, et al., International Myeloma Working Group Recommendations for the Treatment of Multiple Myeloma-Related Bone Disease, *Journal of Clinical Oncology* 31 (18) (2013) 2347–2357.
- [73] D.E. Robinson, M.S. Ali, N. Pallares, et al., Safety of Oral Bisphosphonates in Moderate-to-Severe Chronic Kidney Disease: A Binational Cohort Analysis, *J Bone Miner Res* 36 (5) (2021) 820–832.
- [74] E. Zamagni, M. Cavo, B. Fakhri, R. Vij, D. Roodman, Bones in Multiple Myeloma: Imaging and Therapy, *American Society of Clinical Oncology Educational Book* 38 (2018) 638–646.
- [75] S. Rasch, T. Lund, J.T. Asmussen, et al., Multiple Myeloma Associated Bone Disease, *Cancers (Basel)* 12 (2020) 8.
- [76] A.D. Anastasilakis, P. Makras, M.P. Yavropoulou, G. Tabacco, A.M. Naci, A. Palermo, Denosumab Discontinuation and the Rebound Phenomenon: A Narrative Review, *Journal of Clinical Medicine* 10 (1) (2021) 152.
- [77] V. Piechotta, T. Jakob, P. Langer, et al., Multiple drug combinations of bortezomib, lenalidomide, and thalidomide for first-line treatment in adults with transplant-ineligible multiple myeloma: a network meta-analysis, *Cochrane Database Syst Rev* 2019 (11) (2019).
- [78] M. Mohty, F. Malard, B. Mohty, B. Savani, P. Moreau, E. Terpos, The effects of bortezomib on bone disease in patients with multiple myeloma, *Cancer* 120 (5) (2014) 618–623.
- [79] S.P.E. Jayaweera, S.P. Wanigasinghe Kanakanamge, D. Rajalingam, G.N. Silva, Carfilzomib: A Promising Proteasome Inhibitor for the Treatment of Relapsed and Refractory Multiple Myeloma, *Front Oncol* 11 (2021), 740796.
- [80] Roussel M, Lauwers-Cances V, Robillard N, et al. Frontline Therapy with Carfilzomib, Lenalidomide, and Dexamethasone (KRd) Induction Followed By Autologous Stem Cell Transplantation, Krd Consolidation and Lenalidomide Maintenance in Newly Diagnosed Multiple Myeloma (NDMM) Patients: Primary Results of the Intergrroupe Francophone Du Myélome (IFM) Krd Phase II Study. *Blood* 2016; 128: 1142-.
- [81] Zimmerman T, Raj N, Vij R, et al. Final Results of a Phase 2 Trial of Extended Treatment (tx) with Carfilzomib (CFZ), Lenalidomide (LEN), and Dexamethasone (KRd) Plus Autologous Stem Cell Transplantation (ASCT) in Newly Diagnosed Multiple Myeloma (NDMM). *Blood* 2016; 128: 675-.
- [82] J.K. Jasielc, T. Kubicki, N. Raj, et al., Carfilzomib, lenalidomide, and dexamethasone plus transplant in newly diagnosed multiple myeloma, *Blood* 136 (22) (2020) 2513–2523.
- [83] D. Toscani, M. Bolzoni, M. Ferretti, C. Palumbo, N. Giuliani, Role of Osteocytes in Myeloma Bone Disease: Anti-sclerostin Antibody as New Therapeutic Strategy, *Front Immunol* 9 (2018) 2467.
- [84] M.M. McDonald, J. Delgado-Calle, Sclerostin: an Emerging Target for the Treatment of Cancer-Induced Bone Disease, *Current osteoporosis reports* 15 (6) (2017) 532–541.
- [85] J. Delgado-Calle, J. Anderson, M.D. Cregor, et al., Genetic deletion of Sost or pharmacological inhibition of sclerostin prevent multiple myeloma-induced bone disease without affecting tumor growth, *Leukemia* 31 (12) (2017) 2686–2694.
- [86] J. Delgado-Calle, A.Y. Sato, T. Bellido, Role and mechanism of action of sclerostin in bone, *Bone* 96 (2017) 29–37.
- [87] M.M. McDonald, M.R. Reagan, S.E. Youtlen, et al., Inhibiting the osteocyte-specific protein sclerostin increases bone mass and fracture resistance in multiple myeloma, *Blood* 129 (26) (2017) 3452–3464.
- [88] S. Gooding, S.W.Z. Olechnowicz, E.V. Morris, et al., Transcriptomic profiling of the myeloma bone-lining niche reveals BMP signalling inhibition to improve bone disease, *Nat Commun* 10 (1) (2019) 4533.
- [89] R. Desikan, B. Barlogie, R. Sethi, et al., Infection—an underappreciated cause of bone pain in multiple myeloma, *British journal of haematology* 120 (6) (2003) 1047–1050.
- [90] S.F. Yu, C.C. Lui, S.N. Pei, J.W. Liu, T.T. Cheng, Unsuspected multiple myeloma presenting as Escherichia coli infectious spondylitis: a case report, *Int J Rheum Dis* 13 (4) (2010) e55–e58.
- [91] M. Mohan, S.C. Shalin, A. Kothari, J.C. Rico, K. Caradine, M. Burgess, Lasiodiplodia species fungal osteomyelitis in a multiple myeloma patient, *Transpl Infect Dis* 18 (5) (2016) 761–764.

- [92] S.S. Park, S.E. Lee, C.K. Min, Empysematous osteomyelitis due to *Escherichia coli* in multiple myeloma, *Blood Res* 51 (4) (2016) 224.
- [93] T. Webber, M. Lawlor, T. Balach, *Streptococcus pneumoniae* Osteomyelitis in a 25-Year-Old Man as the Initial Presentation of Multiple Myeloma: A Case Report, *JBJS Case Connect* 7 (3) (2017) e72.
- [94] R. Cohen, T. Finn, F. Babushkin, et al., Disseminated “*Haemophilus quentini*” infection in a patient with multiple myeloma – A case report and review of the literature, *Diagn Microbiol Infect Dis* 94 (3) (2019) 293–296.
- [95] J. Sassine, D.P. Kontoyiannis, A 77-Year-Old Man with Multiple Myeloma and a Lytic Bone Lesion, *Am J Med* 134 (7) (2021) 860–862.
- [96] R. Roque, L. Machado, D. Flor, F. Cunha, Oligosecretory multiple myeloma: a devastating presentation of a difficult diagnosis, *BMJ Case Rep* 14 (4) (2021).
- [97] M. Yildirim, M. Baykara, Differentiation of Multiple Myeloma and Lytic Bone Metastases: Histogram Analysis, *Journal of Computer Assisted Tomography* 44 (6) (2020) 953–955.
- [98] S.Y. Kristinsson, M. Tang, R.M. Pfeiffer, et al., Monoclonal gammopathy of undetermined significance and risk of infections: a population-based study, *Haematologica* 97 (6) (2012) 854–858.
- [99] M.T. Drayson, S. Bowcock, T. Planche, et al., Levofloxacin prophylaxis in patients with newly diagnosed myeloma (TEAMM): a multicentre, double-blind, placebo-controlled, randomised, phase 3 trial, *The Lancet Oncology* 20 (12) (2019) 1760–1772.
- [100] M.M. Oken, C. Pomeroy, D. Weisdorf, J.M. Bennett, Prophylactic antibiotics for the prevention of early infection in multiple myeloma, *Am J Med* 100 (6) (1996) 624–628.
- [101] C. Kasperk, I. Grafe, Osteoplastic procedures for the treatment of vertebral complications in multiple myeloma patients, *Recent Results Cancer Res* 183 (2011) 293–306.
- [102] O. Nicolatou-Galitis, M. Schiødt, R.A. Mendes, et al., Medication-related osteonecrosis of the jaw: definition and best practice for prevention, diagnosis, and treatment, *Oral Surg Oral Med Oral Pathol Oral Radiol* 127 (2) (2019) 117–135.
- [103] D.J. Heath, A.D. Chantry, C.H. Buckle, et al., Inhibiting Dickkopf-1 (Dkk1) removes suppression of bone formation and prevents the development of osteolytic bone disease in multiple myeloma, *J Bone Miner Res* 24 (3) (2009) 425–436.
- [104] F. Zhou, S. Meng, H. Song, F.X. Claret, Dickkopf-1 is a key regulator of myeloma bone disease: opportunities and challenges for therapeutic intervention, *Blood Rev* 27 (6) (2013) 261–267.
- [105] S. Pozzi, M. Fulcinitti, H. Yan, et al., In vivo and in vitro effects of a novel anti-Dkk1 neutralizing antibody in multiple myeloma, *Bone* 53 (2) (2013) 487–496.
- [106] M. Fulcinitti, P. Tassone, T. Hideshima, et al., Anti-DKK1 mAb (BHQ880) as a potential therapeutic agent for multiple myeloma, *Blood* 114 (2) (2009) 371–379.
- [107] S. Yaccoby, W. Ling, F. Zhan, R. Walker, B. Barlogie, J.D. Shaughnessy Jr., Antibody-based inhibition of DKK1 suppresses tumor-induced bone resorption and multiple myeloma growth in vivo, *Blood* 109 (5) (2007) 2106–2111.
- [108] S.P. Iyer, J.T. Beck, A.K. Stewart, et al., A Phase IB multicentre dose-determination study of BHQ880 in combination with anti-myeloma therapy and zoledronic acid in patients with relapsed or refractory multiple myeloma and prior skeletal-related events, *British journal of haematology* 167 (3) (2014) 366–375.
- [109] H. Eda, L. Santo, M.N. Wein, et al., Regulation of Sclerostin Expression in Multiple Myeloma by Dkk-1: A Potential Therapeutic Strategy for Myeloma Bone Disease, *J Bone Miner Res* 31 (6) (2016) 1225–1234.
- [110] J.J. Yin, K. Selander, J.M. Chirgwin, et al., TGF-beta signaling blockade inhibits PTHrP secretion by breast cancer cells and bone metastases development, *J Clin Invest* 103 (2) (1999) 197–206.
- [111] J. Paton-Hough, S. Tazzyman, H. Evans, et al., Preventing and Repairing Myeloma Bone Disease by Combining Conventional Antiresorptive Treatment With a Bone Anabolic Agent in Murine Models, *J Bone Miner Res* 34 (5) (2019) 783–796.
- [112] T.C. Kouroukis, F.G. Baldassarre, A.E. Haynes, K. Imrie, D.E. Reece, M.C. Cheung, Bortezomib in multiple myeloma: systematic review and clinical considerations, *Curr Oncol* 21 (4) (2014) e573–e603.
- [113] A. Field-Smith, G.J. Morgan, F.E. Davies, Bortezomib (Velcade<sup>®</sup>) in the Treatment of Multiple Myeloma, *Ther Clin Risk Manag* 2 (3) (2006) 271–279.
- [114] J.S. Nyman, A.R. Merkel, S. Uppuganti, et al., Combined treatment with a transforming growth factor beta inhibitor (1D11) and bortezomib improves bone architecture in a mouse model of myeloma-induced bone disease, *Bone* 91 (2016) 81–91.
- [115] S. Roux, X. Mariette, The high rate of bone resorption in multiple myeloma is due to RANK (receptor activator of nuclear factor-kappaB) and RANK Ligand expression, *Leuk Lymphoma* 45 (6) (2004) 1111–1118.
- [116] N. Giuliani, S. Colla, V. Rizzoli, New insight in the mechanism of osteoclast activation and formation in multiple myeloma: focus on the receptor activator of NF-kappaB ligand (RANKL), *Exp Hematol* 32 (8) (2004) 685–691.
- [117] M.G. Kang, E.J. Won, H.W. Choi, et al., Serum parathyroid hormone is a new potential risk factor in multiple myeloma, *Biomed Res Int* 2014 (2014), 804182.
- [118] L. Notarfranchi, V. Marchica, B. Dalla Palma, et al., Concomitant Primary Hyperparathyroidism in Patients with Multiple Myeloma: A Possible Link? *Acta Haematologica* 144 (3) (2021) 302–307.

## **2. Murine models of orthopaedic infection featuring *Staphylococcus aureus* biofilm**

Chapter 2 describes our newly developed murine osteomyelitis model using needle insertion surgery (NIS) and *S. aureus* biofilm inoculation. This research article has been accepted for publication (Journal of Bone and Joint Infection, IF: 2.33) and has been included in manuscript format.

### **Reference:**

**Dao A**, O'Donohue AK, Vasiljevski ER, Bobyn JD, Little DG, Schindeler A. Murine models of orthopedic infection featuring *Staphylococcus aureus* biofilm. 2023. *Journal of Bone and Joint Infection*

### **Statement of Contribution:**

AD and AS conceptualised the experiments. AD, AS, and DGL developed the methodology for the experiments. AD, JDB and DGL performed the surgeries with the assistance of AKO and ERV. AD conducted the analysis and prepared all the tables and figures. AD and AS validated the results. AD wrote the original draft of the manuscript with editing by AS. Supervision, project management and funding acquisition were done by AS. All Authors have read and approved this final manuscript.



# Murine models of orthopedic infection featuring *Staphylococcus aureus* biofilm

Aiken Dao <sup>1,2,3</sup>, Alexandra K O'Donohue <sup>1,2,3</sup>, Emily R Vasiljevski <sup>1,2</sup>, Justin D Bobyn <sup>1,2</sup>, David G. Little  
5 <sup>1,2</sup>, Aaron Schindeler <sup>1,2,3§</sup>

1 Orthopaedic Research and Biotechnology Unit, the Children's Hospital at Westmead, Westmead, NSW, Australia

2 The Children's Hospital at Westmead Clinical School, Faculty of Medicine and Health, University of Sydney, Sydney, NSW, Australia

3 Bioengineering & Molecular Medicine Laboratory, the Westmead Institute for Medical Research, Westmead, NSW,  
10 Australia

§ Correspondence to: A/Prof Aaron Schindeler ([aaron.schindeler@sydney.edu.au](mailto:aaron.schindeler@sydney.edu.au))

## Abstract

**Introduction:** Osteomyelitis remains a major clinical challenge. Many published rodent fracture infection models are costly  
15 compared to murine models for rapid screening and proof-of-concept studies. We aimed to develop a dependable and cost-effective murine bone infection model that mimics bacterial bone infections associated with biofilm and metal implants.  
**Methods:** Tibial drilled hole (TDH) and needle insertion surgery (NIS) infection models were compared in C57BL/6 mice (female, N=150). Metal pins were inserted selectively into the medullary canal adjacent to the defect sites on the metaphysis. Free *Staphylococcus aureus* (ATCC-12600) or biofilm suspension (ATCC-25923) was locally inoculated. Animals were  
20 monitored for physiological or radiographic evidence of infection without prophylactic antibiotics for up to 14 days. At the endpoint, bone swabs, soft-tissue biopsies, and metal pins were taken for cultures. X-ray and micro-CT scans were performed along with histology analysis. **Results:** TDH and NIS both achieved a 100% infection rate in tibiae when a metal implant was present with free bacteria injection. In the absence of an implant, inoculation with a bacterial biofilm still induced a 40-50% infection rate. In contrast, freely suspended bacteria and no implant consistently showed lower or negligible infection rates.  
25 Micro-CT analysis confirmed that biofilm infection caused local bone loss even without a metal implant as a nidus. Although a metal surface permissive for biofilm formation is impermeable to create progressive bone infections in animal models, the metal implant can be dismissed if a bacterial biofilm is used. **Conclusion:** These models have a high potential utility for modelling surgery-related osteomyelitis, with NIS being simpler to perform than TDH.

## 30 1. Introduction

Open fractures, surgical implantation, and prosthetic joint replacements have high associated comorbidity of osteomyelitis (Zimmerli, 2014). While a range of bacterial pathogens can result in bone infection, *Staphylococcus aureus* is the most prevalent cause of osteomyelitis and post-surgical infection (Brinkman et al., 2019). Prophylactic antibiotics are not always effective due to the widespread and increasing incidence of antimicrobial resistance (Urish and Cassat, 2020). Surgical site infection in orthopedic implants has a high disease burden, with high rates of hospitalization and treatment costs (Shah et al., 2017). Clinical trials are the gold standard for assessing the efficacy of interventions to minimize the impact of orthopedic infection. However, such trials can be expensive, difficult to coordinate, and require large patient numbers (Reizner et al., 2014). In contrast, preclinical rodent models represent a valuable first-pass research tool to screen new therapies (Schindeler et al., 2018). While rat models can have more relevant biomechanical outcomes, murine (mouse) models are more economical and accessible. Despite a range of established models for bone healing (Schindeler et al., 2018), there remain no universally accepted preclinical protocols for modeling orthopedic trauma and combined infection. Moreover, models of bacterial inoculation in mice (Windolf et al., 2014; Windolf et al., 2013), rats (Mills et al., 2018; Mills et al., 2020), and sheep (Boot et al., 2021) all typically recapitulate implant-associated infection.

We aimed to iteratively develop and test orthopedic infection models in mice with a focus on localized bone defects. This was framed in the context of investigating the role of bacterial biofilm – the layer of microbial cells and extracellular matrix that forms on solid surfaces (Rodríguez-Merchán et al., 2021). Our first research question was the importance of implants and implant surfaces in the establishment of a persistent bone infection. Our second research question was to compare the impact of inoculation with a suspension of free bacteria versus bacteria grown as part of a biofilm. Ultimately, this work sought to establish reproducible and detailed protocols for implant-containing and implant-free bone infection models in mice.

50

## 2. Methods

### 2.1. Bacterial and Biofilm Culture

Two strains of *S. aureus* were sourced from the American Type Culture Collection: ATCC-12600 (used in prior rat infection models) (Mills et al., 2018; Mills et al., 2020) and a high biofilm forming strain (ATCC-25923). Bacteria suspensions were prepared by overnight growth of a single picked colony, with bacterial numbers calculated from spectrophotometry (Cary 300 UV-Vis, Agilent, Las Vegas, NV) with an OD<sub>600</sub> of 1 representing  $1 \times 10^9$  colony-forming units (CFU)/milliliter (mL). For inoculation, bacteria were resuspended in injectable saline (0.9% sodium chloride) and dosed at  $10^6$  CFU/mL (in 200  $\mu$ L for systemic injection) or  $1 \times 10^5$  CFU (in 5  $\mu$ L for local injection). For biofilm preparation, single colonies were picked for culture in tryptic soya broth (TSB) with 20% glucose in a six-well plate one week prior to surgical inoculation. A piece of sterile stainless-steel foil ( $1 \times 1$  mm) was added to the culture media (2 mL of TSB + 20% glucose) to provide a metal surface for

60

biofilm formation and media refreshed thrice per week. For inoculation, biofilm removed from the stainless-steel foil surface with a sterile swab, triturated in saline, and dosed at  $1 \times 10^5$  CFU (in 5  $\mu$ L for local injection).

## 2.2. Animal husbandry and ethics

65 Female C57BL/6 mice (8-12 weeks old) were purchased from the Australian BioResources (Moss Vale, NSW, Australia) or the Animal Resources Centre (Canning Vale, WA, Australia), co-housed up to 5 per cage with access to food and water *ad libitum* and allowed to acclimatize for at least one week prior to surgery. The study was approved by the local Animal Ethics Committee (K339) and carried out in accordance with the Australian Code for the care and use of animals for scientific purposes (2013).

70

## 2.3. Study Design

The animals were randomized in groups (summarized in **Table 1**). Three preliminary studies were carried out (1A: Trialing bone defect site location, 1B: Trialing alternate surgical methods, 1C: Trialing a high biofilm forming *S. aureus* variant) and a larger study comparing surgical approaches (Comprehensive testing of TDH and NIS model variants).

75

## 2.4. Surgery and Anesthesia

Analgesia was provided by injecting buprenorphine (0.1 mg/kg) subcutaneously one hour before surgery and post-surgery as required. Anesthesia was induced using ketamine (75mg/kg) and xylazine (10mg/kg) by intraperitoneal injection and animals were maintained on inhaled isoflurane (2-3% per 1.5-2 L oxygen). The right leg of each animal was shaved and cleaned with  
80 a povidone-iodine solution prior to surgery.

For TDH surgery, a medial parapatellar approach was used to access the right proximal tibia. A hole (0.5 mm in diameter) was made at the right tibial metaphysis (below the growth plate) using a surgical drill (Stryker® 5100-15-250 Straight, Kalamazoo, USA), exposing the medullary canal adjacent to the drilled hole for bacterial infection. For the pin insertion, a 38 mm  $\times$  0.25 mm stainless-steel pin (Australian Entomological Supplies Pty Ltd, South Murwillumbah, Australia) was inserted through the  
85 subchondral bone at the knee, adjacent to the hole defect. For NIS, a 25G needle was manually twisted to puncture the cortical bone of the metaphysis, and the stainless-steel pin inserted through the hole into the medullary canal (Videos 1 and 2). For local inoculation, bacterial suspension was injected directly into the defect with a Hamilton needle and syringe (Hamilton Company, Nevada, USA) immediately after pin-insertion. For the hematogenous systemic infection groups, bacterial suspension was administered into the bloodstream via the lateral tail-vein.

90 Baseline radiographs were taken at the time of surgery after the drill hole or pin insertion to confirm the drill hole and pin positions. Readjustment is given before closing the incision to minimize complications (e.g., pin-slip and fracture). The



incision was closed with 5-0 Vicryl (Ethicon LLC, Puerto Rico, USA), and no dressings applied to the wound. Animals were allowed to recover on a heated pad after surgery and given saline subcutaneously (1 mL) to aid in rehydration, and analgesia was maintained for at least the first 72 hrs.

95

## **2.5. X-ray and Post-Surgical Monitoring**

Animals were monitored daily by experienced staff and had twice-weekly radiographs performed under anesthesia (inhaled isoflurane) using digital X-ray (Faxitron Bioptics, Tuscan, AZ, United States) at 25 kV for five seconds with  $\times 2$  magnification. X-ray images were assessed by expert researchers and a facility veterinarian; all were blinded to treatment. The Mouse Grimace Scale (MGS) was also used to score the animals for monitoring pain and severity. As an ethical end point, animals showing overt physiological and/or radiological evidence of localized or systemic infection judged by declining overall health (loss of body weight, lethargy, pyrexia, poor coat condition, non-weight bearing, and inflammation of the surgical site) and/or radiological evidence of persistent infection (local osteolysis at the tibia joint) were euthanized. The remaining mice were euthanized two weeks postoperatively.

105

## **2.6. Specimen Collection and Bacterial Assays**

Blood samples were taken immediately after euthanasia via cardiac puncture, and swabs were taken from the bone (drilled hole), soft tissue adjacent to the drilled hole, and the metal pin. Pus (if present) was also collected by swab. Blood and swabs were immediately agitated in 1 mL sterile LB and cultured overnight at 37°C. They were reported as either positive (turbid) or negative (clear), and then quantified using a spectrophotometer (SpectraMax ® iD3, Molecular Devices, San Jose, USA) at 600 nm. A positive infection was defined by a positive bacterial culture from the bone swab and pin swab with an absorbance ( $OD_{600}$ )  $> 0.1$ . The right tibiae were harvested for radiographic and histological studies.

110

## **2.7. Radiographic Analysis**

Tibiae were fixed in 10% formalin for 24 hours and transferred to 70% ethanol before being scanned with a SkyScan 1272 micro-computed tomography (micro-CT) scanner (SkyScan, Kontich, Belgium). All samples were scanned in 70% ethanol-soaked kimwipe at 50 kV and 200  $\mu$ A using a 0.5 mm aluminium filter with 2500 ms of exposure. Images were scanned at a pixel resolution of 10  $\mu$ m, reconstructed with NRecon, straightened using DataViewer and analyzed with CTAn software (SkyScan). A global threshold to define bone tissue was set at 0.4 g/cm<sup>3</sup> calcium hydroxyapatite, calibrated using two phantom samples of known density. Bone morphometric outcomes included bone volume (mm<sup>3</sup>), tissue volume (mm<sup>3</sup>), and bone tissue mineral density (g/cm<sup>3</sup>). Three-dimensional reconstructions were generated using CTVox software (Skyscan).

120

## 2.8. Paraffin Histology

After micro-CT scanning, the specimens were stored in 70% ethanol until ready for decalcification. The tibiae were decalcified in 0.34M EDTA (pH 8.0) solution at 4°C on a shaker for two weeks, with solution changes twice weekly. Following decalcification, samples were embedded in paraffin and sectioned coronally through the tibial drilled hole at a thickness of five microns. Mounted sections were stained with hematoxylin and eosin (H&E) and scanned digitally using the Aperio CS2 digital pathology slide scanner (Leica Biosystems, Wetzlar, Germany) and reviewed with Aperio ImageScope software.

## 2.9. Statistical Analyses

Statistical power calculations and analyses were performed using GraphPad Prism (GraphPad Software, La Jolla, CA, USA) and the cutoff for significance for all tests was set to  $p < 0.05$ . *In vivo* studies were powered to infection rate and were compared using Fisher's exact test. The micro-CT data analyzed with Dunn's and Kruskal-Wallis tests.

## 3. Results

### 3.1. TDH surgery led to fracture when holes were generated in the tibial midshaft

In Study 1A, it was speculated that infection risk may differ between the trabecular bone of the metaphysis and the cortical bone of the diaphysis. Following the creation of a 0.5 mm diameter drilled hole by tibial drilled hole (TDH) surgery, animals were locally inoculated with *S. aureus*. No fractures occurred within the metaphyseal defects, however 47% (7/15) midshaft (diaphyseal) defects led to premature tibial fracture within 24 hours. For the metaphyseal defects, few animals showed evidence of persistent orthopedic infection (0-10%), despite inoculation with *S. aureus*.

### 3.2. Metal surfaces and biofilms are essential to achieve high infection rates in the TDH model

In Study 1B, an intramedullary pin was pushed through the tibial plateau into the intramedullary space apposed to the drill hole defect. This led to frequent infection (80%, 4/5) compared to mice receiving an equivalent bacterial inoculation in the absence of a pin (0%, 0/5) (**Figure 1A**).

In Study 1C, *S. aureus* was cultured for a week to form a biofilm, which was scraped from the surface and directly added (in suspension) to bone defects in the absence of a pin. Biofilms were grown from the original ATCC-12600 strain as well as a second ATCC-25923 *S. aureus* clinical isolate known to produce robust biofilms. In both cases, the biofilms were able to create bone defect infection (30% vs. 70% respectively) even in the absence of a metal surface (**Figure 1B**).

### 3.3. NIS is a less complex procedure than TDH

Study 1B also trialed an alternative surgical procedure utilizing needle insertion (NIS) as an alternative to the tibial drill hole (TDH) that did not require specialized orthopedic equipment. The NIS generated a slightly smaller hole ( $< 0.5$  mm diameter). The metal pin was inserted via the unicortical defect rather than through the tibial condyle (**Figure 2**). This contrasted with the TDH model, where insertion through the knee risked infection and/or retrograde movement of the pin (causing knee pain). Hence, the NIS procedure was gauged to be superior in these respects. Operators also reported the NIS method to be simpler and more rapid to perform. As with the TDH model, inclusion of the metal pin in the NIS model increased the infection rate compared to no pin.

### 3.4. Establishing reproducible murine models of bone defect infection

Study 2 was a large cohort study (8 groups,  $N=10$  per group) that addressed the impact of surgical technique (TDH and NIS models), metal implant or biofilm use, and the *S. aureus* strain (ATCC-12600, ATCC-25923). The primary outcomes were the infection rate and bacterial load, both judged based on the optical density (600 nm) of broth cultures following a swab of the defect site. In all groups featuring inoculation and a metal pin, 100% (10/10) defects were infected. Rates were lower in the absence of a pin. However, the ATCC-25923 biofilm still achieved 50% (5/10) and 40% (4/10) infection in the TDH and NIS models respectively (**Figure 3**). While a cutoff method was used to determine whether a specimen was infected ( $ABS\ 600 > 0.1$ ), the samples remained below maximal absorbance at the time of reading, thus the data was analyzed as a surrogate measure of bacterial load (**Figure 4**). The ATCC-12600 and pin combination showed a higher load than other groups in both the TDH and NIS models. Notably, no bacteria were recovered in blood for all animals, and no evidence of infection was seen in the uninoculated negative control groups.

A secondary outcome of the study was regenerate bone volume (BV) as quantified by micro-CT. Both TDH and NIS models showed a reduction of regenerate bone volumes in the tibial drilled holes of the infected groups compared to the uninfected controls. The micro-CT reconstructions revealed that the infection induced a characteristic response in the bone regenerate, and there remained abundant disorganized woven bone compared to uninfected defects that had the neocortex restored (**Figure 5**). The micro-CT data was quantified in terms of new regenerate in the defect (**Figure 6**). ATCC-25923 biofilm infections reduced the regenerate BV by ~50%. ATCC-12600 free bacterial infections BV was reduced by a similar amount but only when metal pins were present.

Descriptive histology was performed on bone specimens TDH and NIS procedures, with and without infection. In the control groups that were not inoculated, the drilled hole showed abundant regeneration after two weeks and had no evidence of infection (**Figure 7A**, black arrow). For the NIS procedure, as metal pins were inserted through the tibial plateau, the medial condyle appeared normal (**Figure 7B**, blue arrow). Profound effects were seen in TDH and NIS specimens that were inoculated and went on to develop infection. Disorganised bone formation was seen concomitant with bone infection (**Figures 7C, 7D**,

185 black arrows), and disruption of the cortical bone often resulted in structural deformation (**Figure 7C**, yellow arrow). This was the case for both TDH and NIS models, however the growth plate was more greatly affected by infection with the TDH model where the pin disrupted the knee (**Figures 7C vs 7D**, blue arrows).

4. Discussion

190 While many orthopedic model papers focus on the final surgical method, this report discusses the iterative approach taken to develop and refine a surgical model. It highlights some of the challenges and pitfalls associated with creating a consistent bone infection model in mice. While limited compared to rats and larger animal models, the use of mice increases accessibility with modest housing requirements.

A notable and unexpected finding was the extremely low infection rates in the initial defect models lacking either implants or  
195 biofilm bacteria. Prior models performed by our team in rats all featured metal implants, such as intramedullary pins or titanium knee implants (Mills et al., 2018; Mills et al., 2020). Upon addition of a pin adjacent to the tibial defect, the high infection rates were once again achieved. This is consistent with clinical observations that implants can act as a nidus for infection. However, such implant-dependent models are restrictive for mimicking infection in the absence of an implant, e.g. (Funk and Copley, 2017; Mcneil, 2020; Thakolkaran and Shetty, 2019), chronic osteomyelitis, and osteolytic lesions-associated  
200 osteomyelitis (Cha et al., 2012; Mukkamalla and Malipeddi, 2021; Gau et al., 2022). Biofilm infection emerged as an alternative method for achieving higher rates of infection in the absence of a metal pin. The use of *S. aureus* is applicable, as *S. aureus* and *S. epidermidis* are the most common bacterial pathogens associated with biofilm formation on biotic or abiotic surfaces (Schilcher and Horswill, 2020; Reffuveille et al., 2018).

We trialed two similar surgical approaches to generate a localized defect in the tibia – a drilled hole and a needle insertion  
205 defect. TDH model uses an orthopedic drill that is comparable to those used by surgeons. However, the drill is expensive and requires specialized training to use, making it less feasible for small laboratories. In contrast, the NIS method is simpler and more cost-effective for large scale proof-of-concepts studies. The NIS halves the surgical time by reducing the complexity of the procedure. It also makes pin-reposition easier, and it is more forgiving for minor inaccuracy. The NIS method applies less lateral force on the tibia when pushing the pin into the medullary canal, making it less likely to cause cortical bone damage  
210 and fracture. From a practical point of view, the NIS method also increases the accuracy of the hole placement by implementing the drilling manually, improving hand sensation, which is helpful for defecting a small bone. While not necessarily related to use of a needle for defect creation, for the NIS procedure we shifted to inserting the pin through the defect hole. Disruption of the tibial condyle and the damage to the patella tendon increased the risk of complications (e.g., fracture, joint swelling, inflammation, and retrograde movement of the pin). In some cases, pin movement led to slips that had to be managed by  
215 surgical intervention or euthanasia.

This paper compares a wide range of factors speculated to affect the efficiency of the model including bacterial pathogen, dose, surgical approach, and outcome measures. Nevertheless, the number of factors and combinations were limited based on practicality and animal numbers/ethics. To minimize the risk of sepsis, a mild static inoculation dose was used, and this never led to hematogenous infection; this is a clinical challenge in more severe cases, but one that may be ethically challenging to perform and manage in mice. Another limitation was the use of radiography and cultures as the primary methods to examine infection; future studies could employ measures such as neutrophil count, erythrocyte sedimentation rate (ESR) and C-reactive protein (CRP). The studies also were limited to *S. aureus* as a pathogen, although two different strains were tested. The model could be readily adapted for other strains including methicillin-resistant *S. aureus*, *Streptococcus spp*, *P. aeruginosa*, and *E. coli* (Lienard et al., 2021; Cassano et al., 2020; Foong et al., 2021; Pliska, 2020; Gornitzky et al., 2020). Other expanded variations that could be tested include the effects of mouse age, systemic inoculation reminiscent of a hematogenous infection, and the ability to model chronic osteomyelitis (Alstrup et al., 2021; Billings and Anderson, 2022; Jensen et al., 2017; Joyce et al., 2021; Lüthje et al., 2020; Roux et al., 2021).

## 5. Conclusion

This report describes the iterative development of bone defect infection models. Detailed methods (**Supplementary Protocols**) are provided for the NIS-pin and NIS-biofilm orthopedic murine models based on the outcomes of Study 2. Both models are considered to have different utilities – for modeling implant and non-implant associated infection respectively. These simplified and cost-effective methods are suitable for conducting preclinical trials and proof-of-concept studies for interventions to prevent and treat osteomyelitis.

## Ethical Statement

This study involved no human participants or specimens and did not require institutional human ethics approval. Animal experiments were approved by the Children’s Hospital at Westmead & Children’s Medical Research Institute Animal Ethics Committee (Approval K339). Animal studies were conducted in alignment with the Australian code for the care and use of animals for scientific purposes (EA28).

## Code/Data availability

The authors confirm that the data supporting the findings of this study are available within the article and its supplementary materials.

## Author contribution statement

AD and AS conceptualized the experiments. AD, AS, and DGL developed the methodology for the experiments. AD, JDB and DGL performed the surgeries with the assistance of AKO and ERV. AD conducted the analysis and prepared all the tables and figures. AD and AS validated the results. AD wrote the original draft of the manuscript with editing by AS. Supervision, project management and funding acquisition were done by AS. All Authors have read and approved this final manuscript.

**Competing interests**

The authors declare that they have no known competing financial interests or personal relationships that could have appeared to influence the work reported in this paper.

**References**

Alstrup, A. K. O., Jensen, S. B., Nielsen, O. L., Jødal, L., and Afzelius, P.: Preclinical Testing of Radiopharmaceuticals for the Detection and Characterization of Osteomyelitis: Experiences from a Porcine Model, *Molecules*, 26, 10.3390/molecules26144221, 2021.

Billings, C. and Anderson, D. E.: Role of Animal Models to Advance Research of Bacterial Osteomyelitis, *Front Vet Sci*, 9, 879630, 10.3389/fvets.2022.879630, 2022.

Boot, W., Schmid, T., D'Este, M., Guillaume, O., Foster, A., Decosterd, L., Richards, R. G., Eglin, D., Zeiter, S., and Moriarty, T. F.: A Hyaluronic Acid Hydrogel Loaded with Gentamicin and Vancomycin Successfully Eradicates Chronic Methicillin-Resistant *Staphylococcus aureus* Orthopedic Infection in a Sheep Model, *Antimicrob Agents Chemother*, 65, 10.1128/aac.01840-20, 2021.

Brinkman, C. L., Schmidt-Malan, S. M., Karau, M. J., and Patel, R.: A novel rat model of foreign body osteomyelitis for evaluation of antimicrobial efficacy, *J Exp Appl Anim Sci*, 3, 7-14, 10.20454/jeas.2019.1555, 2019.

Cassano, P., Ciprandi, G., and Passali, D.: Acute mastoiditis in children, *Acta Biomed*, 91, 54-59, 10.23750/abm.v91i1-S.9259, 2020.

Cha, J. G., Yoo, J. H., Kim, H. K., Park, J. M., Paik, S. H., and Park, S. J.: PET/CT and MRI of intra-osseous haemangioma of the tibia, *Br J Radiol*, 85, e94-98, 10.1259/bjr/35251836, 2012.

Foong, B., Wong, K. P. L., Jeyanthi, C. J., Li, J., Lim, K. B. L., and Tan, N. W. H.: Osteomyelitis in Immunocompromised children and neonates, a case series, *BMC Pediatr*, 21, 568, 10.1186/s12887-021-03031-1, 2021.

Funk, S. S. and Copley, L. A.: Acute Hematogenous Osteomyelitis in Children: Pathogenesis, Diagnosis, and Treatment, *Orthop Clin North Am*, 48, 199-208, 10.1016/j.jocl.2016.12.007, 2017.

Gau, Y. C., Yeh, T. J., Hsu, C. M., Hsiao, S. Y., and Hsiao, H. H.: Pathogenesis and Treatment of Myeloma-Related Bone Disease, *Int J Mol Sci*, 23, 10.3390/ijms23063112, 2022.

Gornitzky, A. L., Kim, A. E., O'Donnell, J. M., and Swarup, I.: Diagnosis and Management of Osteomyelitis in Children: A Critical Analysis Review, *JBJS Rev*, 8, e1900202, 10.2106/jbjs.Rvw.19.00202, 2020.

Jensen, L. K., Johansen, A. S. B., and Jensen, H. E.: Porcine Models of Biofilm Infections with Focus on Pathomorphology, *Front Microbiol*, 8, 1961, 10.3389/fmicb.2017.01961, 2017.

Joyce, K., Sakai, D., and Pandit, A.: Preclinical models of vertebral osteomyelitis and associated infections: Current models and recommendations for study design, *JOR Spine*, 4, e1142, 10.1002/jsp2.1142, 2021.

Lienard, A., Hosny, M., Jneid, J., Schuldiner, S., Cellier, N., Sotto, A., La Scola, B., Lavigne, J. P., and Pantel, A.: *Escherichia coli* Isolated from Diabetic Foot Osteomyelitis: Clonal Diversity, Resistance Profile, Virulence Potential, and Genome Adaptation, *Microorganisms*, 9, 10.3390/microorganisms9020380, 2021.

Lüthje, F. L., Jensen, L. K., Jensen, H. E., and Skovgaard, K.: The inflammatory response to bone infection - a review based on animal models and human patients, *Apmis*, 128, 275-286, 10.1111/apm.13027, 2020.

McNeil, J. C.: Acute Hematogenous Osteomyelitis in Children: Clinical Presentation and Management, *Infect Drug Resist*, 13, 4459-4473, 10.2147/idr.S257517, 2020.

Mills, R., Cheng, T. L., Mikulec, K., Peacock, L., Isaacs, D., Genberg, C., Savage, P. B., Little, D. G., and Schindeler, A.: CSA-90 Promotes Bone Formation and Mitigates Methicillin-resistant *Staphylococcus aureus* Infection in a Rat Open Fracture Model, *Clin Orthop Relat Res*, 476, 1311-1323, 10.1097/01.blo.0000533624.79802.e1, 2018.

Mills, R. J., Boyling, A., Cheng, T. L., Peacock, L., Savage, P. B., Tägil, M., Little, D. G., and Schindeler, A.: CSA-90 reduces periprosthetic joint infection in a novel rat model challenged with local and systemic *Staphylococcus aureus*, *Journal of Orthopaedic Research*, 38, 2065-2073, <https://doi.org/10.1002/jor.24618>, 2020.

295 Mukkamalla, S. K. R. and Malipeddi, D.: Myeloma Bone Disease: A Comprehensive Review, *Int J Mol Sci*, 22, 10.3390/ijms22126208, 2021.

Pliska, N. N.: *Pseudomonas Aeruginosa* as the Main Causative Agent of Osteomyelitis and its Susceptibility to Antibiotics, *Drug Res (Stuttg)*, 70, 280-285, 10.1055/a-1150-2372, 2020.

Reffuveille, F., Josse, J., Velard, F., Lamret, F., Varin-Simon, J., Dubus, M., Haney, E. F., Hancock, R. E. W., Mongaret, C., and Gangloff, S. C.: Bone Environment Influences Irreversible Adhesion of a Methicillin-Susceptible *Staphylococcus aureus* Strain, *Front Microbiol*, 9, 2865, 10.3389/fmicb.2018.02865, 2018.

300 Reizner, W., Hunter, J. G., O'Malley, N. T., Southgate, R. D., Schwarz, E. M., and Kates, S. L.: A systematic review of animal models for *Staphylococcus aureus* osteomyelitis, *Eur Cell Mater*, 27, 196-212, 10.22203/ecm.v027a15, 2014.

Rodríguez-Merchán, E. C., Davidson, D. J., and Liddle, A. D.: Recent Strategies to Combat Infections from Biofilm-Forming Bacteria on Orthopaedic Implants, *Int J Mol Sci*, 22, 10.3390/ijms221910243, 2021.

305 Roux, K. M., Cobb, L. H., Seitz, M. A., and Priddy, L. B.: Innovations in osteomyelitis research: A review of animal models, *Animal Model Exp Med*, 4, 59-70, 10.1002/ame2.12149, 2021.

Schilcher, K. and Horswill, A. R.: *Staphylococcal Biofilm Development: Structure, Regulation, and Treatment Strategies*, *Microbiol Mol Biol Rev*, 84, 10.1128/mmbr.00026-19, 2020.

Schindeler, A., Mills, R. J., Bobyn, J. D., and Little, D. G.: Preclinical models for orthopedic research and bone tissue engineering, *Journal of Orthopaedic Research*, 36, 832-840, <https://doi.org/10.1002/jor.23824>, 2018.

310 Shah, M. Q., Zardad, M. S., Khan, A., Ahmed, S., Awan, A. S., and Mohammad, T.: Surgical Site Infection In Orthopaedic Implants And Its Common Bacteria With Their Sensitivities To Antibiotics, In *Open Reduction Internal Fixation*, *J Ayub Med Coll Abbottabad*, 29, 50-53, 2017.

Thakolkaran, N. and Shetty, A. K.: Acute Hematogenous Osteomyelitis in Children, *Ochsner J*, 19, 116-122, 10.31486/toj.18.0138, 2019.

315 Urish, K. L. and Cassat, J. E.: *Staphylococcus aureus* Osteomyelitis: Bone, Bugs, and Surgery, *Infect Immun*, 88, 10.1128/iai.00932-19, 2020.

Windolf, C. D., Lögters, T., Scholz, M., Windolf, J., and Flohé, S.: Lysostaphin-coated titan-implants preventing localized osteitis by *Staphylococcus aureus* in a mouse model, *PLoS One*, 9, e115940, 10.1371/journal.pone.0115940, 2014.

320 Windolf, C. D., Meng, W., Lögters, T. T., MacKenzie, C. R., Windolf, J., and Flohé, S.: Implant-associated localized osteitis in murine femur fracture by biofilm forming *Staphylococcus aureus*: a novel experimental model, *J Orthop Res*, 31, 2013-2020, 10.1002/jor.22446, 2013.

Zimmerli, W.: Clinical presentation and treatment of orthopaedic implant-associated infection, *J Intern Med*, 276, 111-119, 10.1111/joim.12233, 2014.

**Table 1:** The study plan of TDH and NIS bone infection models.

Group	Study	Surgery	Site	Injection	N=
1	1A	TDH (no pin)	Metaphysis	Sterile saline	5
2	1A	TDH (no pin)	Diaphysis	Sterile saline	5
3	1A	TDH (no pin)	Metaphysis	Local ( $10^5$ CFU <i>S. aureus</i> )	5
4	1A	TDH (no pin)	Diaphysis	Local ( $10^5$ CFU <i>S. aureus</i> )	5
5	1A	TDH (no pin)	Metaphysis	Systemic ( $10^6$ CFU <i>S. aureus</i> )	5
6	1A	TDH (no pin)	Diaphysis	Systemic ( $10^6$ CFU <i>S. aureus</i> )	5
7	1B	TDH-pin	Metaphysis	Sterile saline	5
8	1B	TDH (no pin)	Metaphysis	<i>S. aureus</i> (ATCC-12600) ( $10^5$ CFU)	5
9	1B	TDH-pin	Metaphysis	<i>S. aureus</i> (ATCC-12600) ( $10^5$ CFU)	5
10	1B	NIS-pin	Metaphysis	<i>S. aureus</i> (ATCC-12600) ( $10^5$ CFU)	5
11	1C	TDH (no pin)	Metaphysis	ATCC-12600 biofilm	10
12	1C	TDH (no pin)	Metaphysis	ATCC-25923 biofilm	10
13	2	TDH-pin	Metaphysis	Sterile saline	10
14	2	TDH-pin	Metaphysis	<i>S. aureus</i> (ATCC-12600)	10
15	2	TDH-pin	Metaphysis	<i>S. aureus</i> biofilm (ATCC-25923)	10
16	2	TDH (no pin)	Metaphysis	<i>S. aureus</i> (ATCC-12600)	10
17	2	TDH (no pin)	Metaphysis	<i>S. aureus</i> biofilm (ATCC-25923)	10
18	2	NIS-pin	Metaphysis	Sterile saline	10
19	2	NIS-pin	Metaphysis	<i>S. aureus</i> (ATCC-12600)	10
20	2	NIS (no pin)	Metaphysis	<i>S. aureus</i> biofilm (ATCC-25923)	10
<b>Total</b>					150



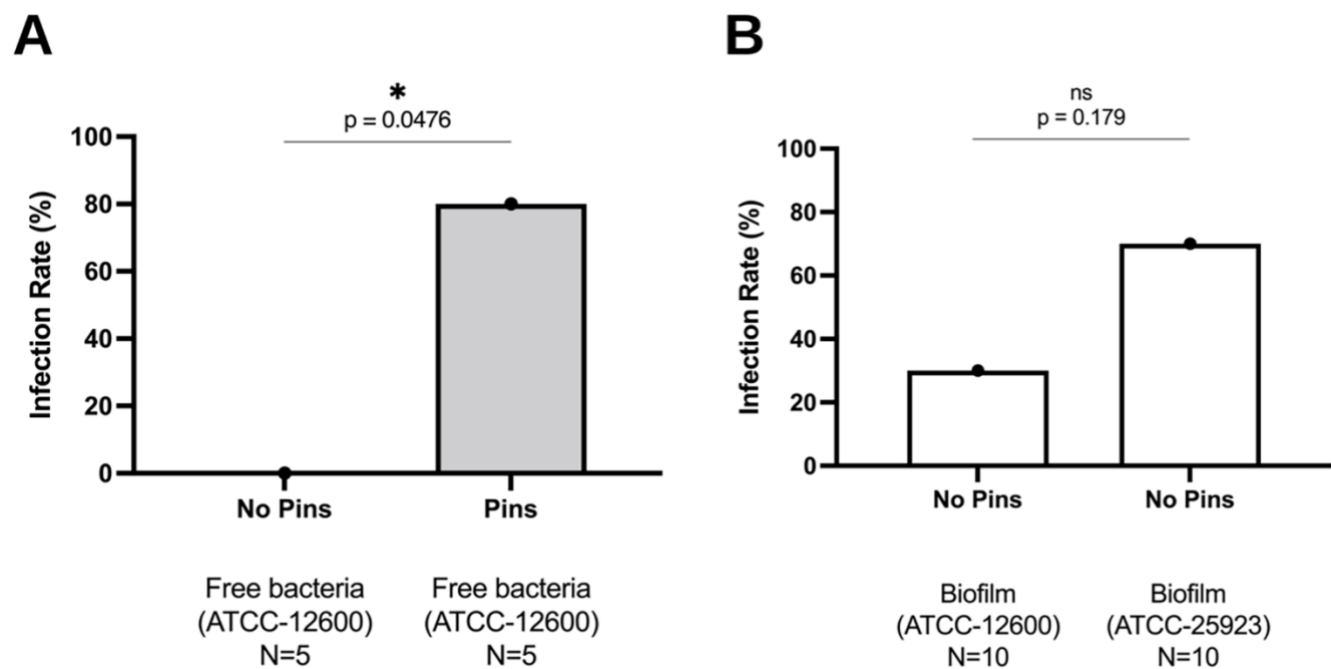


**Figure 1:** [Study 1B] The bone infection rates (%) in mice that received TDH surgery and *S. aureus* inoculation. (A) Comparison of inoculation with ATCC-12600 free bacteria with/without metal pins. (B) Comparison of inoculation with biofilm suspensions of ATCC-12600 and ATCC-25923, without metal pins. The p-values were determined by Fisher's exact test from individual experiments.

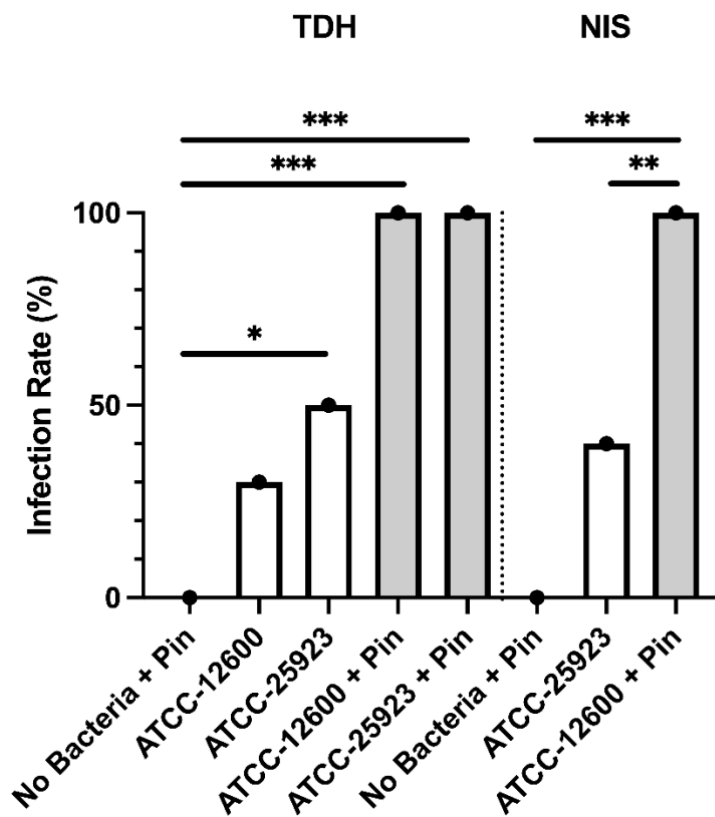


**TDH**



**NIS**

340 **Figure 2:** [Study 1B] XR images illustrating the lack of disruption of the tibial condyle (white arrows) by pin insertion through the defect site (red circles) featured in the NIS model. This latter method of insertion minimized retrograde movement of the pin at the knee.



345 **Figure 3:** [Study 2] The infection rate (%) of the TDH and NIS bone infection models inoculated with free bacteria (ATCC-12600) or biofilm (ATCC-25923) with/without metal pins. (p-values: \*  $\leq 0.05$  and  $> 0.01$ , \*\*  $\leq 0.01$  and  $> 0.001$ , and \*\*\*  $\leq 0.001$ ).

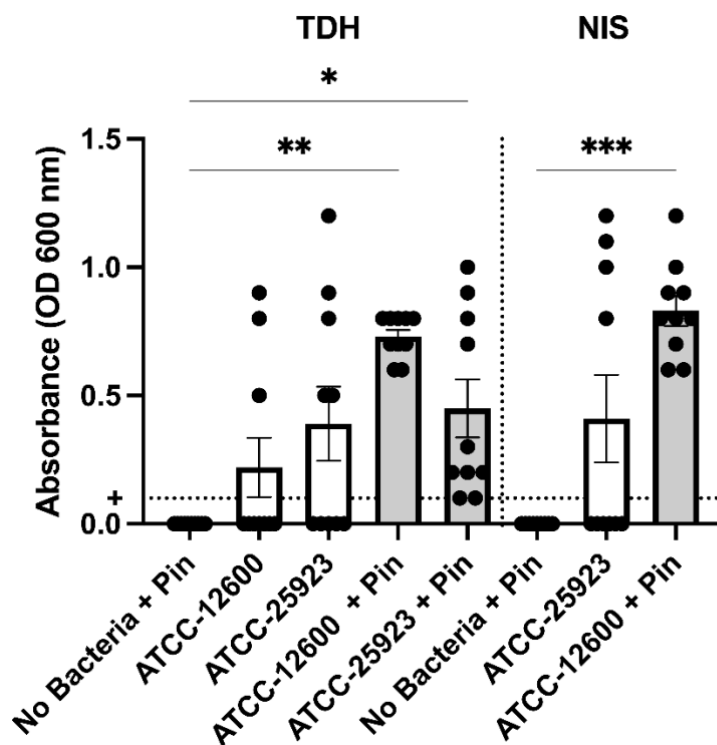


**Figure 4:** [Study 2] The optical density (600 nm absorbance) readings following culture from bone swabs are shown as a surrogate measure of bacterial load. For the purposes of determining ‘infection’ positivity or negativity, a cutoff of 0.1 was used. Significantly higher readings were seen with ATCC-12600 and a pin in the TDH and NIS models. (p-values: \*  $\leq 0.05$  and  $> 0.01$ , \*\*  $\leq 0.01$  and  $> 0.001$ , and \*\*\*  $\leq 0.001$ ).

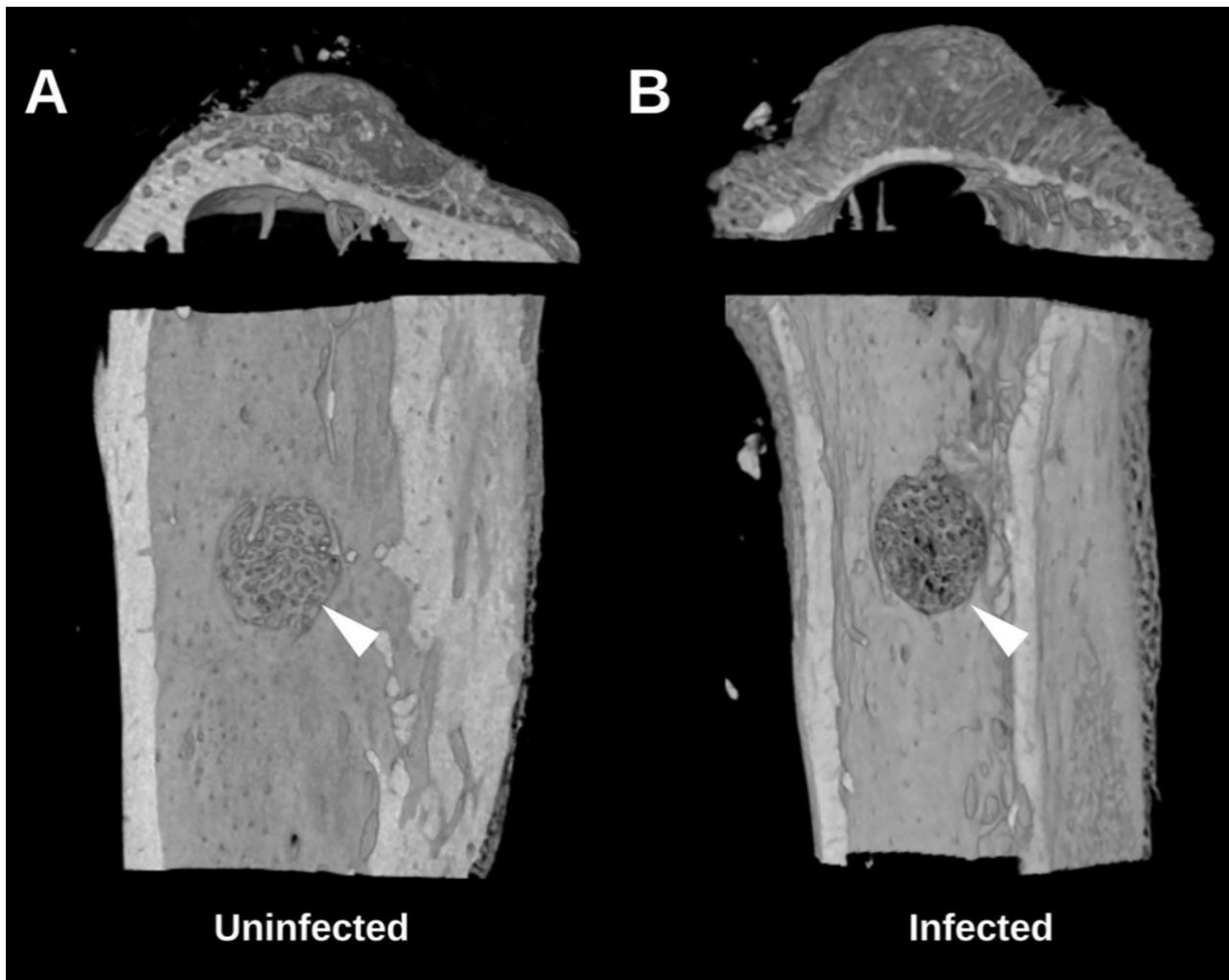


**Figure 5:** [Study 2] Micro-CT reconstructions from the TDH model of the (A) uninfected and (B) infected tibia showing the reduced bone regenerate associated with infection at the defect site (white arrow).

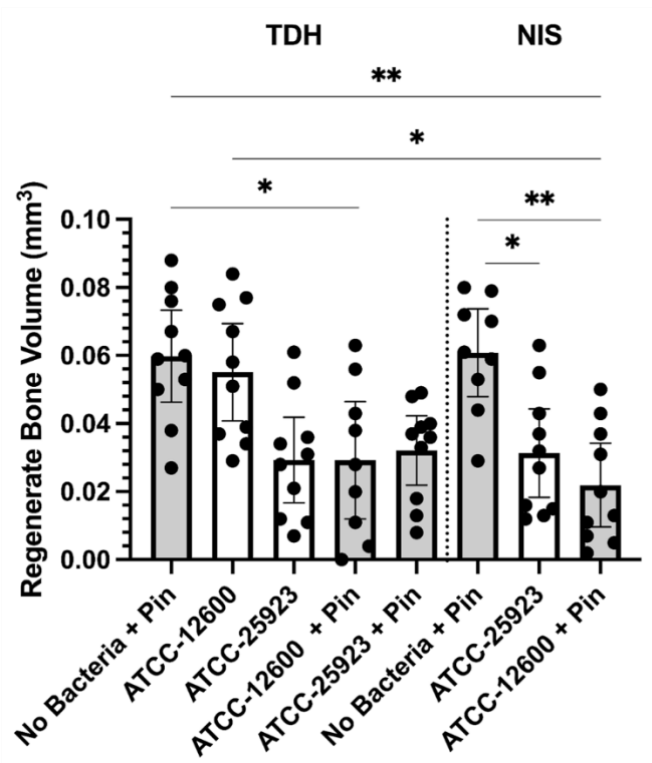
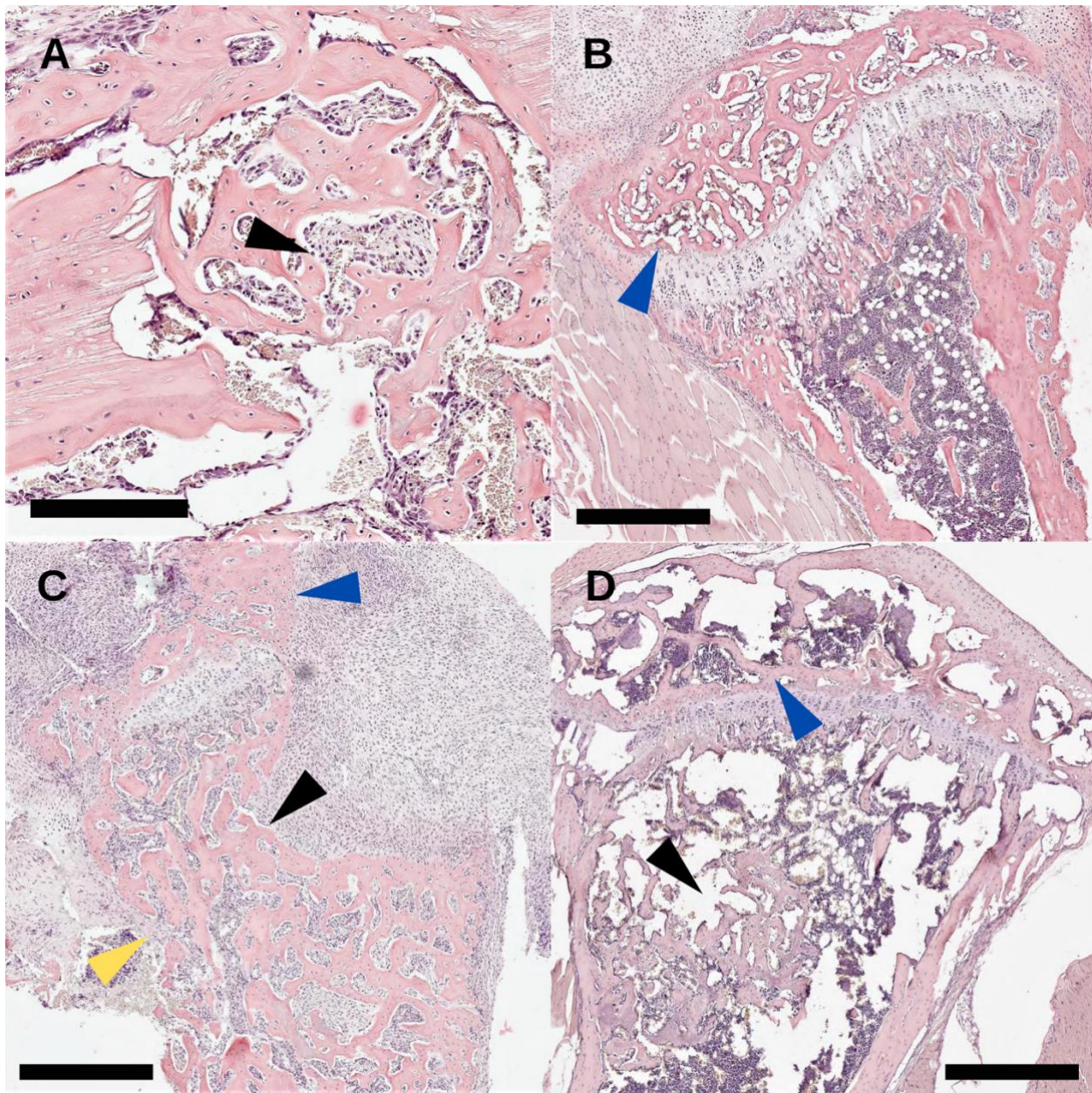


**Figure 6:** [Study 2] The regenerate bone volumes (mm<sup>3</sup>) of the tibial metaphyseal drilled hole quantified by micro-CT analysis in the TDH and NIS models. (p-values: \* ≤0.05 and >0.01, \*\* ≤0.01 and >0.001, and \*\*\* ≤0.001).





365 **Figure 7:** [Study 2] Histology sections with H&E staining (scale bar: 500  $\mu$ m) of (A): an uninfected drilled hole (black  
 370 arrow) with >90% healing two weeks post-surgery; (B): an uninfected tibial condyle (blue arrow) with >90 healing  
 from pin disruption; (C): an infected tibia with TDH-pin insertion, severe osteolysis (back arrow) of the anterior tibia  
 was seen, and the tibial condyle was woven by re-absorption (blue arrow), and the cortical bone (yellow arrow)  
 structure was breaking down; and (D) an NIS infected tibia where the tibial condyle (blue arrow) was less affected  
 than the TDH model, and the healing of the bone defect (black arrow) was less efficient.

## Appendix: Supplementary protocol

Based on our research findings, we proposed the supplementary methods of the needle-insertion surgery (NIS) to induce osteomyelitis in murine. These protocols should increase the reliability and reproducibility of the model for preclinical trials.

### 1. Materials

#### 1.1. Animals

For the NIS-biofilm and NIS-pin bone infection models, we recommend using female C57BL/6 mice at the age of 8-12 weeks. However, other mouse strains, age and gender can be amended for the need of the experiment. Genetically modified (GM) mice are also suitable for this surgery, however, there may be additional risk of fracture and other complication if the phenotype reduces the bone mineral density or mechanical feature of the animal bone.

#### 1.2. Bacterial strains

For general studies, we strongly recommend using a high biofilm forming *S. aureus* strains (e.g., ATCC-25923) for the NIS models. If other pathogens are being tested, a biofilm-forming strain of that pathogen should be employed.

#### 1.3. Lysogeny broth (LB)

1. Mix tryptone powder (5 g), yeast extract (2.5 g), sodium chloride (5 g) and dH<sub>2</sub>O water (500 mL) in a reagent media bottle.
2. Autoclave the dissolved medium at 15 lbs pressure (121°C) for 15-30 minutes.

#### 1.4. Lysogeny broth agar (LB agar)

1. Mix tryptone powder (5 g), yeast extract (2.5 g), sodium chloride (5 g), agar A (7.5 g) and MilliQ water (500 mL) in a reagent media bottle.
2. Autoclave the dissolved medium at 15 lbs pressure (121°C) for 15-30 minutes.
3. Pour the agar (10 mL) to a Petri dish and let it cool down at room temperature using antiseptic technique.



**1.5. Tryptic Soy Broth (TSB) + 10% glucose (for NIS-biofilm model)**

1. Mix 15 g of tryptic soy broth power (Mediatech Inc, Manassas, VA, Germany) with 1.5 g of glucose and 500 mL of MiliQ water.
- 400 2. Autoclave the dissolved medium at 15 lbs pressure (121°C) for 15-30 minutes.

**1.6. Drugs**

- Ketamine (75 mg/kg)
- Xylazine (10 mg/kg)
- 405 • Buprenorphine (0.1 mg/kg)
- Isoflurane (2-3% per 1.5-2L oxygen)

**1.7. Surgical equipment**

**1.7.1. NIS-biofilm model**

- 410 • Scalpel handle #3
- Surgical blade #15
- Needle holder
- Hamilton syringe and needle
- 25G needle
- 415 • 5-0 Vicryl Rapide ® coated sutures
- Isoflurane Vaporizer with a nose cone

**1.7.2. NIS-pin model**

- Scalpel handle #3
- Surgical blade #15
- 420 • Needle holder
- Hamilton syringe and needle
- 25G needle
- Stainless-steel pin (0.5 mm diameter/size 000)
- Wire pliers
- 425 • 5-0 Vicryl Rapide ® coated sutures
- Isoflurane Vaporizer with a nose cone

2. Methods

2.1. Free bacterial culture (for NIS-pin model)

- 430
- 435
1. Streak the bacterial culture (e.g., ATCC-25923 *S. aureus*) from glycerol stock  $-80^{\circ}\text{C}$ ) onto a lysogeny broth (LB) agar plate.
  2. Incubate the plate at  $37^{\circ}\text{C}$  overnight.
  3. From the streaked plate, pick a single colony and resuspend it in 1 mL of LB broth in a 10 mL falcon tube.
  4. Incubate at  $37^{\circ}\text{C}$  overnight on a shaker.
  5. Quantify the bacteria with a spectrophotometer at 600 nm (absorbance of 0.3 should be equivalent to  $3 \times 10^8$  CFU/mL).
  6. Perform a serial 10-fold dilution in injectable saline (0.9% sodium chloride) to reach a bacterial concentration of  $10^6$  to  $10^7$  colony forming unit (CFU) for inoculation.

Also see Figure S1.

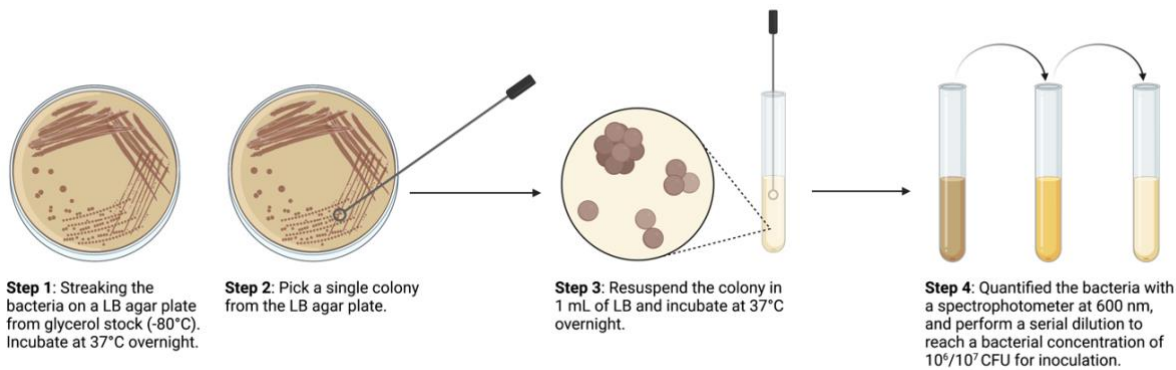


**Figure S1:** The proposed protocol of free bacterial culture for local inoculation.

**Note:** the bacterial concentration is adjustable with serial dilution. For NIS-Pin model, the bacterial concentration can be as low as  $10^4$  to  $10^5$  CFU for inoculation.

## 2.2. Bacterial biofilm culture (for NIS-biofilm model)

1. Streak the bacterial culture (e.g., ATCC-25923 *S. aureus*) from glycerol stock (−80°C) onto a lysogeny broth (LB) agar plate.
- 450 2. Incubate the plate at 37°C overnight.
3. From the streaked plate, pick a single colony from the streak plate and resuspend it in 1 mL of LB broth.
4. Incubate at 37°C overnight on a shaker.
5. Place a piece of sterile stainless-steel/titanium foil (1 cm × 1 cm) in a well of a 24-well plate.
6. Pipette 100 µL bacteria into the well.
- 455 7. Add 900 µL of tryptic soy broth (TSB) with 10% glucose to the well.
8. Incubate at 37°C for 5-7 days (change the media daily).
9. To change the media, pipette out all the media without disturbing the foil, and add fresh 1 mL of TSB with 10% glucose to the well.
10. Scrape the biofilm off the foil with a sterile swab
- 460 11. Resuspend the biofilm in 1 mL of normal saline.
12. Quantify the biofilm with a spectrophotometer at 600 nm (absorbance of 0.3 should be equivalent to  $3 \times 10^8$  CFU/mL).
13. Perform a serial 10-fold dilution to reach a biofilm concentration of  $10^6$  to  $10^7$  colony forming unit (CFU) for inoculation.

Also see Figure S2.

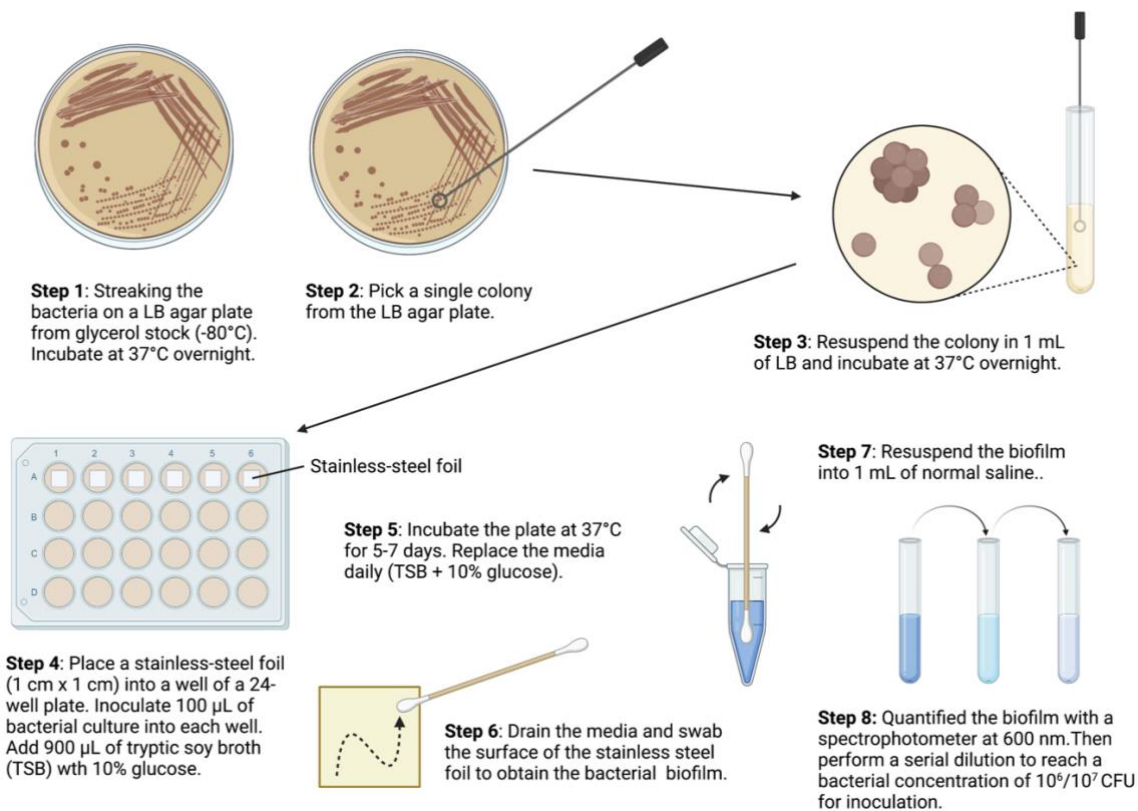


**Figure S2:** The proposed protocol of bacterial biofilm culture for local inoculation.

**Note:** the bacterial concentration is adjustable with serial dilution. For NIS-Pin model, the bacterial concentration can be as low as  $10^4$  to  $10^5$  CFU for inoculation.

### 2.3. Pain relief, anesthesia and preparation

1. Give 0.1 mg/kg buprenorphine or pain relief subcutaneously (SC) at least one hour before surgery.
2. Before surgery, inject ketamine (75mg/kg) and xylazine (10mg/kg) by intraperitoneal (IP) injection for anesthesia.
3. Shave the animal's right leg.
- 475 4. Sterilize the surgical area with a povidone-iodine solution.
5. If required, give isoflurane (2-3% per 1.5-2 L oxygen) through a nose cone during the procedure to maintain anesthesia.
6. Check the paw pinch reflex before incision.

### 480 2.4. NIS-biofilm model

1. Make a medial parapatellar incision to access the right proximal tibia.
2. Use a 25G needle to drill a hole on the tibial metaphysis (below the growth plate), exposing the medullary canal.
3. Inject 5  $\mu$ L of  $10^{6-7}$  CFU of biofilm suspension with a Hamilton syringe into the drill hole.
4. Perform a full/lower-body XR (25 kV for 15 seconds) scan to examine the drilled hole.
- 485 5. Close the incision with 5-0 Vicryl Rapide ® coated sutures.
6. Apply no dressings to the wound.

Also see Figure S3 and Video 1.

**Note:** since biofilm alone does not induce osteomyelitis very efficiently without a metal surface, a higher dose ( $>10^7$  CFU)  
490 can be used to increase the infection rate if 100% infection rate is not achieved.

## 2.5. NIS-pin model

1. Make a medial parapatellar incision to access the right proximal tibia.
2. Use a 25G needle to drill a hole on the tibial metaphysis (below the growth plate), exposing the medullary canal.
- 495 3. Inject 5  $\mu$ L of  $10^5$  CFU of biofilm suspension with a Hamilton syringe into the drill hole.
4. Insert a stainless-steel pin through the drilled-hole defect into the medullary canal of the tibia until it reaches the end of the canal.
5. Band the pin at  $90^\circ$  to prevent the pin from slipping out.
6. Cut the pin off with the wire pliers
- 500 7. Perform a full/lower-body XR (25 kV for 15 seconds) scan to monitor the drilled hole.
8. Close the incision with 5-0 Vicryl Rapide <sup>®</sup> coated sutures.
9. Apply no dressings to the wound.

Also see Figure S4 and Video 2.

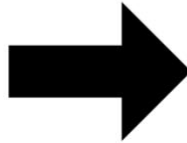
505 **Note:** since free bacteria induce osteomyelitis efficiently when a metal surface is present, a lower dose ( $<10^5$  CFU) can be used to reduce the severity of the bone infection.

**Step 1: Pain Relief**  
Buprenorphine/pain relief (SC)  
One hour before surgery



**C57BL/6 mice** ♀  
(8-12 weeks old)

**Step 2: Anesthetics**  
Ketamine/Xylazine (IP)  
Isoflurane to maintain  
Prep for surgery



**Step 3: Incision**  
Expose the right tibia



**Step 7: Monitoring**  
X-ray (thrice-weekly)  
Buprenorphine/pain relief  
post-surgery  
(every 12 hours, up to 3 days)

**Step 6: Close the wound**  
5-0 Vicryl suture  
0.9% saline injection (SC) for  
rehydration



**Step 4: Needle Insertion**  
Use a 25G needle to  
drill a small hole  
( $r = 250\ \mu\text{m}$ , metaphysis)

**Step 5: Bacterial Inoculation**  
Biofilm local injection  
with a hamilton syringe  
( $1\text{E}6$ - $1\text{E}7$  CFU in  $5\ \mu\text{L}$ )

**Figure S3:** The proposed protocol of the NIS biofilm bone infection model.

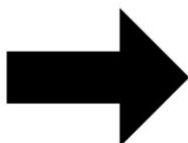


**Step 1: Pain Relief**  
Buprenorphine/pain relief (SC)  
One hour before surgery



**C57BL/6 mice** ♀  
(8-12 weeks old)

**Step 2: Anesthetics**  
Ketamine/Xylazine (IP)  
Isoflurane to maintain  
Prep for surgery



**Step 3: Incision**  
Expose the right tibia



**Step 7: Monitoring**  
X-ray (thrice-weekly)  
Buprenorphine/pain relief  
post-surgery  
(every 12 hours, up to 3 days)

**Step 6: Close the wound**  
5-0 Vicryl suture  
0.9% saline injection (SC) for  
rehydration



**Step 4: Needle Insertion**  
Use a 25G needle to  
drill a small hole  
( $r = 250\ \mu\text{m}$ , metaphysis)

**Step 5: Bacterial Inoculation**  
Insert a pin through the hole  
Planktonic bacterial local injection  
with a hamilton syringe  
( $1\text{E}5\ \text{CFU}$  in  $5\ \mu\text{L}$ )

**Figure S4:** The proposed protocol of the NIS-pin bone infection model.

515 **2.6. Post-Surgical Recovery**

1. Inject 1 mL of saline (0.9% sodium chloride) subcutaneously into the mouse for rehydration.
2. Let the animal recover within a box/cage on a heating pad with soft bedding for 30 mins or until it recovers from anesthesia.
3. Monitor breathing and heart rate every 3-5 minutes.
- 520 4. If the breathing is too shallow and slow or the heart rate is too rapid, provide 100% oxygen. (Normal HR: 310-840 beats/min and RR: 80-230 breaths/min for mice)
5. Check for righting reflex and motor recovery.

**2.7. Post-Surgical Monitoring and Pain Relief**

- 525 1. Give buprenorphine subcutaneously every 12 hours (for at least three days). (Note: pain relief should also be given when the animal is in pain, use Mouse Grimace scales to evaluate animals for pain).
2. Perform a lower-half body XR scan (25 kV for 15 seconds) thrice weekly to monitor the infection progression and complication (e.g., osteolysis, fracture).
3. Other forms of pain relief (approved by ethics) can substitute buprenorphine to minimize its side effects.

530

### 3. Ion-assisted plasma polymerisation and CSA-90 coating for orthopaedic implants

Chapter 3 demonstrates the novel ion-assisted plasma polymerisation (IPP) technology for orthopaedic implant coating. We have performed *in vitro* and *in vivo* (mouse model) experiments to determine the efficacy of PP- and PP + CSA-90-coated 3D implants to prevent osteomyelitis associated with *Staphylococcus aureus*. This study was written initially as a traditional thesis chapter. However, later we prepared a manuscript for publication (submitted to ACS Applied Materials & Interfaces; IF: 10.38), so the manuscript is attached to this chapter in the appendix.

#### Reference:

**Dao A.**, Gaitanos C., Kamble S., Tan RP., Wise, SG., Cheung TLY., Bilek M., Savage PB., Schindeler S. Antibacterial plasma polymer coatings on 3D materials for orthopedic applications. 2023. *ACS Applied Materials & Interfaces*

#### Statement of contribution:

Dr Behnam Akhavan and his team (School of Physics, University of Sydney) completed the ion-assisted plasma polymerisation surface coating. Dr Justin Bobyn and I completed animal surgeries. The supplementary data (Table 3.1 and Figures S3.1-S.3.3) were unpublished data from Mr Denis Sylvester for his honours project (2018). I contributed to the study design and data analysis.

### 3. Ion-assisted plasma polymerisation and CSA-90 coating for orthopaedic implants

#### 3.1. Introduction

##### 3.1.1. Implant-related osteomyelitis is a clinical challenge

Implant-related osteomyelitis is a great clinical challenge globally <sup>1</sup>, with procedures that involve open fracture fixation or joint replacement surgery carrying an increased risk of developing osteomyelitis <sup>2,3</sup>. Biofilm contamination and bacterial colonisation on the surface of an orthopaedic implant are key risk factors associated with implant-related osteomyelitis <sup>4,5</sup>, posing enormous risk to patient welfare. Metal surfaces, such as those found in orthopaedic implants, can act as a nidus for biofilm formation. In our prior characterisation of mouse models of osteomyelitis, the presence of a metal implant greatly increased the rate of infection (Thesis Chapter 2).

Biofilm bone infections can be particularly difficult to treat with antibiotics, as they often struggle to effectively penetrate a biofilm matrix <sup>6,7</sup>. Biofilm infection can also lead to implant failure, deep tissue infection, haematogenous infection (e.g., bacteraemia and sepsis), and chronic osteomyelitis (e.g., ulcer and diabetic foot osteomyelitis) <sup>8-10</sup>. Such complications can have major implications to the patient, increasing the likelihood of multiple revision surgery to correct implants or multiple operations to remove sequestra (dead bones) and osteonecrotic bone tissue (i.e., surgical debridement) <sup>11-13</sup>. In some cases, severe osteomyelitis can lead to amputation and prolonged intravenous antibiotic treatment (up to six months or longer) <sup>14-17</sup>. Such clinical outcomes can be life threatening and require prolonged intervention to treat; even if the infection is resolved, poor healing can lead to long-term impairments <sup>18,19</sup>. Orthopaedic infection places a considerable economic and operational burden on the healthcare system, estimated to cost more than 8.6 billion USD annually in the United States <sup>20,21</sup>.

Implantation of orthopaedic device requires patients to undergo surgery in a clinical setting. Patients are often hospitalised and need a long time of recovery. Nosocomial bacterial infection, also known as hospital-acquired infection, is a common complication among patients with prolonged hospitalisation and repeat exposure to the hospital environment <sup>22,23</sup>. Nosocomial infections can be difficult to contain and treat, as they are often associated with highly antimicrobial-resistant (AMR) bacteria <sup>24</sup> such as methicillin-resistant *Staphylococcus aureus* (MRSA) and methicillin-resistant *S. epidermidis* (MRSE) <sup>25</sup>. These bacteria can also form biofilms on orthopaedic implants, and in recent years, MRSA has become an increasingly

common causative agent of surgical site infections (SSIs) and infections after fracture fixation (IAFFs) <sup>26-31</sup>.

Despite advances in orthopaedic procedures, there are many complications that arise during and after fixation. Issues involving delayed union, mal-union, non-union, osteomyelitis, and compartment syndrome <sup>32-36</sup>. Non-healing fractures and bone defects caused by bacterial infections are regarded as one of the major clinical challenges facing by orthopaedic surgeons <sup>37</sup>. Currently, there is no gold standard for treating orthopaedic implant-related osteomyelitis, and many antibiotics lack the capacity to target bone infection sites <sup>38,39</sup>. Therefore, preventing the occurrence of orthopaedic infection is paramount to ensure rapid and vigorous recovery after orthopaedic surgery.

### **3.1.2. The current limitations on drug delivery systems and implant coatings**

Biofilms can greatly complicate the treatment of orthopaedic implant-related infection. Deposition of extracellular polymeric substances on a metallic implant and can limit the host immune response and reduce the antibiotic efficacy by nearly 1000-fold <sup>40</sup>. The utility of intravenous antibiotics can be further complicated by systemic toxicity associated with higher doses of some drugs. Treatment of implant-related infections typically requires removal of the implant, which requires additional invasive procedures. Implant removal associated with a postoperative spinal surgery infection can cause life-threatening complications and is often a last resort because it can destabilise the spine, <sup>41</sup>.

Local delivery of antibiotics with high concentrations via substances (e.g., beads, antibiotic powder application and antibiotic-impregnated polymethylmethacrylate cement) can be used to prevent and treat chronic osteomyelitis or implant-related bone infection. Surgeons have recently attempted to increase local antibiotic concentrations by either application of antibiotic powder to the wound prior to closure, or by the addition of antibiotics to polymethylmethacrylate (PMMA) cement, that is often used as a mechanical grout to secure implants to bone <sup>42</sup>.

Antibiotic powder application has a short lifetime within the soft tissue (~ 24-72 hours), after which it no longer has any antimicrobial affect <sup>43</sup>. While antibiotic-loaded bone cement has shown increased efficacy compared to IV antibiotics, it has several intrinsic limitations <sup>44</sup>. Since PMMA undergoes an exothermic reaction as it sets, so only a narrow list of thermally stable antibiotics can be used. A typical mix includes 1 g of vancomycin and 1 g of gentamicin

or tobramycin per bag of PMMA. However, the antibiotic elution only lasts for a few days <sup>45,46</sup>. Furthermore, as the amount of antibiotics added to the PMMA increases, the structural properties of the cement begin to degrade, limiting the antibiotic dose <sup>47,48</sup>. The poor release kinetics of antibiotics from PMMA makes it difficult to control and ensure that the appropriate minimum inhibitory concentrations (MICs) of antibiotics are reaching the wound bed for clinically significant amount of time <sup>42</sup>. Besides, the PMMA remains an inert porous material that can paradoxically become a nidus for persistent pathogens to form biofilms the surgical site <sup>49</sup>.

Antimicrobial implant coatings have emerged as a conceptual method for protecting the surface of implant from bacterial colonisation and locally delivering antimicrobials at high concentrations for extended durations. Traditionally, iodine- and silver-containing implant coatings have been used for orthopaedic implants. Despite rigorous testing to determine the ability of these coatings to sustain controlled release above minimum inhibitory concentrations (MICs) *in vivo*, this remains relatively unknown and there are concerns over toxicity and safety with no detrimental effect on osseointegration <sup>50-52</sup>. Although silver-containing coatings for orthopaedic implants decrease postoperative infection rate, silver nanoparticles (sizes between 50 nm and 3  $\mu$ m) exhibit cytotoxic effects on osteoblasts and osteoclasts. The cytotoxicity is primarily mediated by a size-dependent release of Ag (+). Such adverse effects on osteoblasts and osteoclast survival have deleterious effects on the biocompatibility of orthopaedic implants <sup>53</sup>.

For surface biofunctionalisation, a range of agents have been trailed including inorganic (e.g., silver, copper, zinc oxide) and organics (e.g., small molecule antibiotics antimicrobial peptides and polymers) compounds, as well as modification of the surface texture (e.g., nano-texturisation and micro-texturisation) <sup>54</sup>. While bioactive organic agents can have a high potency against infection, there remains considerable scope to develop new methods for surface attachment <sup>55</sup>. Simple adsorption methods can result in burst release and a lack of sustained protection. Agents can also be embedded in soluble polymer or hydrogel matrices that can be used for surface coating, which yields challenges with controlling degradation rates and negative biological effects of breakdown products <sup>56,57</sup>. In contrast, methods for covalent linkage to an implant surface allow for rapid and sustained biological activity that is more suitable for drug coating on orthopaedic implants <sup>58</sup>.

Conventionally, covalent attachment of bioactive molecules on surfaces have been achieved using methods relying on wet-chemical steps, such as linker chemistry methods that are

typically based on salinisation, PEGylation, and heparinisation reactions<sup>58-60</sup>. However, these methods are typically substrate-dependent, meaning they are only applicable to a particular surface chemistry. For instance, silanisation is commonly used chemical linker-mediated immobilisation approach to biofunctionalised orthopaedic substrates. However, it is limited to only hydroxylated substrates bearing a high concentration of OH groups<sup>61,62</sup>. Similarly, the wet-chemical methods for covalent biofunctionalisation can be time-consuming and complex, requiring multi-step processes. For example, the processing time for linker-mediated protein immobilisation approaches is in the order of days. Another undesirable aspect of wet-chemical methods is the extensive amounts of waste produced in the process, making them environmentally questionable. Also, multiple side reactions may occur during the multi-step processes, producing unneeded by-products that may reduce the overall reproducibility and introduce significant challenges to obtain regulatory approvals<sup>58</sup>.

Although there are more traditional coatings incorporating antibiotics currently under investigation<sup>63-68</sup>, no implant coating has yet successfully made it to market. Part of the challenge is that the selection of antimicrobials for coating is imperative to the avoidance of selection pressures leading to bacterial resistance, whereas some implant coatings may require a fundamental change in the implant manufacturing process. Additionally, an implant coated with antimicrobial during manufacturing would be reclassified as a drug-delivery device, which imposes different regulatory requirements and the shelf life may be affected<sup>21</sup>.

### **3.1.3. Preclinical models for implant-related infections**

Preclinical trials are essential for testing novel therapies, but animal models remain scarce with large lab animals (e.g., rats, rabbits, sheep, and pigs)<sup>69-77</sup>. Although the size of these animals is more convenient for surgery, it is usually difficult and expensive for conducting large animal trials with these animals due to a lack of space in facilities for housing. In contrarily, laboratory mice are more manageable for housing in large quantity, but they are smaller in size than rats and are therefore more complex and challenging to operate on. Murine implantation infection models have been established<sup>78,79</sup>. However, the surgery is often complicated, time consuming and challenging to repeat consistently in other laboratory settings. The design and preparation of metal implants can also be complex to replicate.

The tibial drilled-hole pin-insertion model (TDH-pin) as demonstrated previously (Thesis Chapter 2) has been shown as a simple, reliable, and cost-effective model to test proof-of-concept prophylaxis and therapies. It also shortens the duration of experiment to only 14 days.

It is speculated that the TDH-pin murine model would be comparable to the fracture-implant infection models in larger animals.

#### 3.1.4. IPP technology and its potential clinical applications

Ion-assisted plasma polymerisation (IPP/PP) is a versatile method that enables the biofunctionalisation of surfaces. Previously, IPP methods for conjugating functional molecules to metal surfaces have focused on 2D methods, and *in vitro* experiments (unpublished data) have shown rapid and sustaining release of antibiotic (CSA-90) when the drug is coated on titanium and stainless-steel foils (Figure S3.1). IPP is a relatively novel technology, and it was identified that new methods would be required to coat complex 3D structure like orthopaedic implants.

IPP technology creates a radical-rich, polymeric-like layer on target surfaces using an organic precursor monomer such as acetylene, while the substrate is negatively biased in a pulse manner<sup>80-84</sup>. Pulse biasing the substrate during the IPP process facilitates the energetic ion bombardment of the coating as it grows, and results in the formation of a high concentration of reactive radicals buried within the plasma polymer structure. These radicals stabilize in pi-conjugated nanoclusters that migrate to the surface where they enable the covalent attachment of a wide range of organic and inorganic bioactive compounds<sup>85</sup>. In contrast to competing wet-chemical methods, the covalent attachment is carried out in a single step and at room temperature without the need of additional reagents. This reagent-free immobilisation approach also permits control of the density and orientation of molecules on the surface by simply applying an external electric field and tuning the solution pH containing the biomolecules<sup>86</sup>. Surface-embedded radicals created by enhanced ion bombardment of polymeric substrates can also enable reagent-free polymerisation to enable covalent attachment of hydrogel layers<sup>87</sup>.

Although it is not limited to these applications, IPP can be potentially used for coating Kirshner wires, screws, and locking plates that are commonly used for fracture fixation to prevent osteomyelitis<sup>88</sup>. IPP technology can also be used to coat the surface of a femoral stem that are often used for total hip arthroplasty<sup>89</sup>. In recent years, smart orthopaedic implants that can measure physical parameters *in vivo*, including pressure, force, strain, displacement, proximity, and temperature have been developed. These implants can be used for knee and hip arthroplasties, spine fusion, fracture fixation, and others<sup>90</sup>. IPP technology can also be used on these devices.



### 3.1.5. Ceragenins (CSAs) as bioactive molecules for IPP coating

In the context of orthopaedic implants, CSAs were hypothesized to be ideal candidates for surface delivery. CSAs are a class of small molecule antimicrobial agents that disrupt bacterial membranes and are bactericidal against a wide range of Gram-positive and Gram-negative bacteria <sup>91</sup>. They act in a manner alike to cationic antimicrobial peptides (CAMPs) but have a comparatively lower cytotoxicity and higher *in vivo* stability <sup>92</sup>. In addition, CSA-90 and other CSA-13 subclass ceragenins are known as pro-osteogenic, which promote fracture healing and increase alkaline phosphatase (ALP) activities in pre-osteoblasts. Additionally, local CSA-90 delivery has been shown to prevent *S. aureus*, methicillin-resistant *S. aureus* (MRSA) and methicillin-resistant *S. epidermidis* (MRSE) infections in small animal orthopaedic models <sup>71,93,94</sup>.

In this study, we present a new IPP process using a rotating cage made of an electrically conductive mesh that is negatively biased and rotates while being immersed in RF plasma. We hypothesised that this strategy would enable the deposition of radical-rich polymeric coatings onto 3D surfaces for their subsequent biofunctionalisation. The efficacy of IPP as a surface modification method is tested with our previously developed TDH-pin bone infection model (Thesis Chapter 2), using CSA-90 as an active antimicrobial that is potentially used as a coating to prevent implant-related osteomyelitis.

### 3.1.6. Aims and hypotheses

AIM 1: To test the *in vitro* influence of plasma polymerisation treatment on bacterial growth with and without CSA-90 immobilisation on 3D surfaces.

AIM 2: To determine whether IPP-CSA-90 coating on stainless-steel pins can prevent or ameliorate *in vivo* osteomyelitis in mice.

## 3.2. Materials and Methods

### 3.2.1. Materials

Silica beads (1 mm diameter) were purchased from Sigma-Aldrich. Double-side polished silicon wafers (10 mm × 10 mm) were ultrasonicated in acetone and ethanol each for 10 mins followed by drying using a stream of nitrogen gas prior to film deposition. Stainless steel (SS)

Kirshner wires (1.1 mm in diameter) cut to 1 cm segments referred here to as SS pins were obtained from Zimmer, Warsaw, Indiana, USA. Stainless-steel pins (size 000) were purchased from the Australian Entomological Supplies Pty Ltd (South Murwillumbah, Australia). CSA-90 was obtained from Prof Paul Savage (Brigham-Young University, Provo UT, United States). Approximately 6 ml of Milli-Q water was added to 9.6 mg of CSA-90 to produce a clear solution.

### 3.2.2. Ion-assisted plasma polymerisation on silica beads and metal pins

The plasma polymerisation treatment was prepared by Dr Behnam Akhavan (School of Physics) and his team at the University of Sydney. In brief, ion-assisted plasma polymerized films were deposited on silica beads, stainless-steel pins, and silicon wafer substrates using a retrofitted plasma polymerisation system equipped with a rotating cage (Figure 3.1). The plasma polymerisation system, without the rotating cage, has been described in detail previously<sup>81,95</sup>. The rotating cage coupled to a pulse generator was installed into the side of the chamber to enable homogenous plasma polymerisation of IPP films on the 3D objects, i.e., silica beads and stainless-steel pins. The cage contained a stainless-steel mesh outer lining, supported by two inner rods. The plasma polymerisation system was equipped with a radio frequency (RF) electrode and a DC pulsed voltage source connected to the rotating cage. For each deposition, approximately 450 silica beads and 20 SS pins were used. In each batch, a silicon wafer (10mm × 10mm) was attached to the inner rod of the rotating cage. The pulsed voltage source applied to the rotating cage was generated by a RUP-6 pulse generator (GBS-Electronik) at a frequency of 3 kHz and a pulse duration of 20 μs. The cage rotation motor was set to 2.5 V, providing 10 revolutions per minute, for each deposition. Prior to ion-assisted plasma polymerisation and once the chamber base pressure was below  $5.0 \times 10^{-5}$  Torr, the silica beads or SS pins, silicon wafer, and the cage were cleaned using argon plasma [Ar flow rate = 40 standard cubic centimetre per minute (sccm)] at 75 W and -500 V pulsed bias for 10 minutes. Then, a mixture of 5 sccm acetylene and 25 sccm argon was injected into the chamber and the pressure was adjusted to 110 mTorr. The pulse bias voltage was varied from 0 to 1000 V, while the RF input power was kept unchanged at 50 W. The polymerisation time was 15 minutes unless otherwise stated.

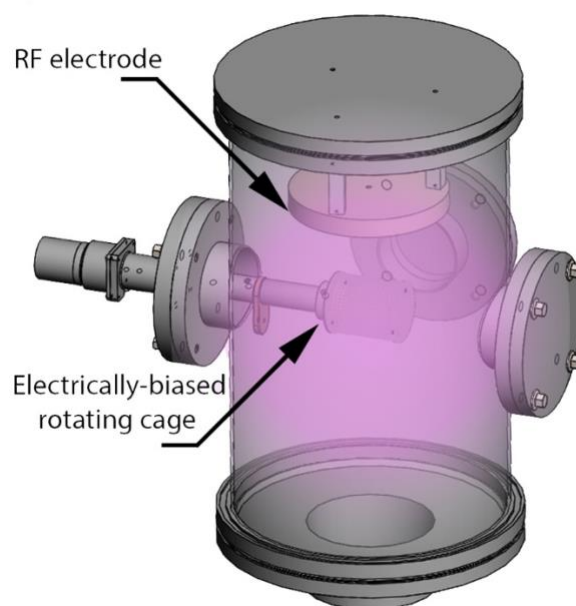


**Figure 3.1:** Schematic illustration of a retrofitted plasma polymerisation chamber equipped with a rotating cage to create IPP coatings onto 3D materials.

### 3.2.3. Beads and antimicrobial coating for *in vitro* assay

Silica beads (1mm) were modified by various coatings: IPP coating only, IPP coating with CSA-90, CSA-90 without IPP coating, and IPP coating with CSA-90 washed with 5% sodium dodecyl sulphate (SDS) at 70°C for one hour. For CSA-90 coating processes, 60 uncoated or IPP-coated silica beads were covered for 12 hours at room temperature with 300  $\mu\text{L}$  of CSA-90 solution (1 mg/mL). The CSA-90 solution was then removed, and the samples were rinsed three times with copious amount of Milli-Q water. The coated silica beads were then placed in either lysogeny broth (LB) with  $10^3$  CFU of *Staphylococcus aureus* (*S. aureus*; Figure 3.2A), or sterile LB after inoculating  $10^4$  CFU of *S. aureus* on the surface and air dried for ten minutes (Figure 3.2B).

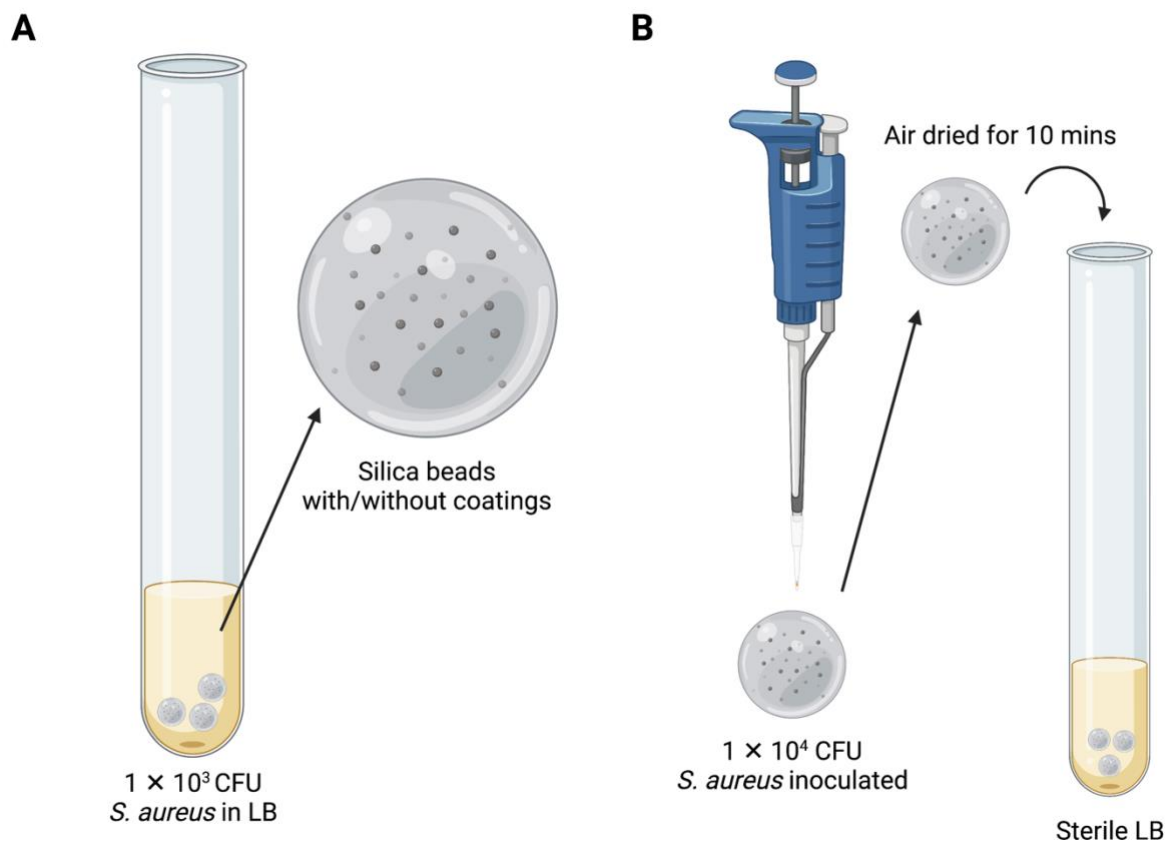


**Figure 3.2.** A schematic showing the *in vitro* assay used for testing the antimicrobial properties of coated silica beads.

#### 3.2.4. Covalent attachment of CSA-90 on stainless-steel pins

For *in vitro* validation of the coating, stainless-steel Kirshner wires (Zimmer, Warsaw, Indiana, USA) cut to 1 cm segments (1.1 mm in diameter) was used. For surgery, stainless-steel pins (size 000) were coated by plasma-polymerisation as previously described prior to drug coating. Pins were then bathed in a 1 mg/mL CSA-90 solution on a petri dish for 12 hours on a shaker, and subsequently air-dried in a 37 °C incubator overnight and then stored at room temperature.

#### 3.2.5. Bacterial culture

Patient-derived *Staphylococcus aureus* (American Type Culture Collection-12600) stored at -80°C in glycerol stocks was grown overnight on LB agar plates at 37°C, and single colonies were picked for culture in LB the day prior to surgical inoculation. Bacteria was quantified using a spectrophotometer (Cary 300 UV-Vis, Agilent, Las Vegas, NV) at 600 nm with an optical density of 1 representing  $1 \times 10^9$  colony-forming unit (CFU)/millilitre (mL). Colonies

were picked the day before surgery, enabling 12-hour growth in LB broth to ensure accurate quantification of live/active bacteria from broth culture for inoculation.

### 3.2.6. Animal ethics and study design

C57BL/6 12-week-old female mice (n=30) were purchased from the Australian BioResources (Moss Vale, NSW, Australia). They were group housed 5-6 per cage with access to food and water *ad libitum*. Mice were acclimatised for a week prior to surgery. Animal work was approved by the local Animal Ethics Committee (K339) and carried out in accordance with the Australian Code for the Care and Use of Animals for Scientific Purposes (2013). Prior to surgery, mice were randomly assigned to 3 groups (n=10 per group) to be surgically implanted with stainless steel pins that were (i) uncoated, (ii) coated by IPP, or (iii) IPP/CSA-90 coated.

### 3.2.7. Preclinical orthopaedic surgical model with implantation

Surgical anaesthesia was induced with intraperitoneal ketamine (75 mg/kg) and xylazine (10 mg/kg) and maintained with inhaled isoflurane (2-3% per 1.5-2L oxygen) as required. The right leg of each animal was shaved and treated with a topical povidone-iodine solution prior to surgery. Buprenorphine (0.1 mg/kg) was given subcutaneously 1 hour prior to surgery and then every 12 hours for 3 days for postoperative analgesia.

A medial parapatellar approach was used to access the right proximal tibia. A hole (0.5 mm in diameter) was made at the right tibial metaphysis (below the growth plate) using a surgical drill (Stryker ® 5100-15-250 Straight, Kalamazoo, USA), exposing the medullary canal adjacent to the drilled hole for bacterial infection. A stainless-steel pin was inserted through the subchondral bone at the knee, adjacent to the drilled-hole defect. After that,  $1 \times 10^6$  CFU *S. aureus* was injected in 5 µL directly into the drilled hole with a Hamilton syringe and needles (Hamilton Company, Nevada, USA) immediately after the pin-insertion. The incision was closed with 5-0 Vicryl (Ethicon LLC, Puerto Rico, USA), and no dressings were applied to the wound. Baseline radiographs were taken at the time of surgery. Animals recovered on a heated pad after surgery and were given subcutaneous saline (200 µL).

Animals were monitored daily by experienced staff and had twice-weekly radiographs performed under anaesthesia (inhaled isoflurane) using digital X-ray (Faxitron Bioptics, Tuscan, AZ) at 25 kV (five seconds) with  $\times 2$  magnification. X-ray images were assessed by orthopaedic surgeons and veterinarian blinded to treatment. To minimize animal pain and

distress, animals showing overt physiological and/or radiological evidence of infection judged by declining overall health (loss of body weight, lethargy, pyrexia, poor coat condition, non-weight bearing, and inflammation of the surgical site) or radiological evidence of worsening infection (localized osteolysis at the tibia and joint) were prematurely euthanized to avoid sepsis. The remaining mice were euthanized by carbon dioxide inhalation three weeks postoperatively.

### **3.2.8. Specimen collection and analysis**

At endpoint, a biopsy of the soft tissue adjacent to the bone defect was taken after the incision under aseptic conditions. The surgical pin was pulled out from the joint by a sterile needle holder. All specimens were then placed in LB (1 mL) for bacterial culture. A bone swab was collected at the defect site and resuspended in the broth for 15 seconds. Pus samples (if present) were also collected by swab for bacterial culture. The bacterial culture was incubated overnight at 37°C. Positive and negative results were determined by the media turbidity and quantified using a plate spectrophotometer (SpectraMax® iD3, Molecular Devices, San Jose, USA) at 600 nm.

The right tibiae were also harvested for micro-computed tomography (micro-CT) or histology. For micro-CT, the right tibiae were fixed in 10% formalin for 24 hours and transferred to 70% ethanol before being scanned with a SkyScan 1272 micro-CT scanner (SkyScan, Kontich, Belgium). All samples were scanned in 70% ethanol-soaked kimwipe at 50 kV and 200  $\mu$ A using a 0.5 mm aluminium filter. Images were scanned at a pixel resolution of 9  $\mu$ m, reconstructed with NRecon, straightened using DataViewer and analyzed with CTAn software (SkyScan). The region of interest (ROI) was drawn within the cortical bone defect (0.5 mm in diameter). A global threshold to define bone tissue was set at 0.4 g/cm<sup>3</sup> calcium hydroxyapatite, calibrated using two phantom samples of a known density. Bone morphometric outcomes included bone volume (mm<sup>3</sup>), tissue volume (mm<sup>3</sup>), and bone tissue mineral density (g/cm<sup>3</sup>). Three-dimensional reconstructions were generated using CTVox software (Skyscan).

### **3.2.9. Histology**

The tibiae were decalcified in 0.34M EDTA (pH 8.0) solution at 4°C on a shaker for two weeks with solution changes twice a week. Following decalcification, samples were embedded in paraffin and sectioned coronally through the tibial drilled hole at a thickness of five microns.

Mounted sections were stained with haematoxylin and eosin (H&E) to differentiate bone and show the bone defect region.

### 3.2.10. Statistical analysis

Statistical power calculations and analyses were performed in GraphPad Prism (La Jolla, California), with the cut-off for significance set at  $p < 0.05$ . The infection rate was analysed using the Fisher's exact test. The micro-CT data from the *in vivo* study were analysed using a Kruskal-Wallis and Dunn's test for multiple groups, followed by a non-parametric post-hoc Mann-Whitney U-test to compare groups pairwise. The *in vitro* bacterial loads data were analysed using a 2-way ANOVA with Turkey's test and an unpaired t-test.

## 3.3. Results

### 3.3.1. IPP biofunctionalised 3D surfaces for antimicrobial coating

AIM 1: To validate and optimise IPP biofunctionalisation on 3D surfaces for CSA-90 coating

IPP biofunctionalisation on 2D metal surfaces were validated by *in vitro* assays. The PP-coated titanium (Ti) and stainless-steel (SSt) foils showed significant reductions in *S. aureus* (ATCC-12600) adherence (Figures S3.1 and S3.2). Two-tailed non-paired t-test of CFU/mL counts was performed for Ti and SSt foils (N=10) incubated for 24 or 72 hours. Uncoated Ti and SSt foils were found to contain significantly higher proportion bacteria when compared to PP-coated foils. Subsequently, to test the antimicrobial activity of a particular batch of CSA-90 (~0.7 mg/mL) immobilised on PP-coated surfaces, a Kirby-Bauer (KB) assay was conducted on an agar plate incubated with *S. aureus* (ATCC-12600) for 24 hours. The resulting zone of inhibition (ZOI) of untreated, PP-coated and PP + CSA-90-coated was compared with gentamicin (10 µg/mL). The ZOI for gentamicin and PP + CSA-90-coated foils (Ti/SSt) were measured (Table S3.1) and observed (Figure S3.3). Results suggest that the CSA-90 on the PP-coated surface remains active as an antimicrobial agent against *S. aureus* on 2D surfaces.

Next, *in vitro* experiments simulated the exposure of 3D-orthopaedic implants (a spherical silica bead and Kirshner-wire pin) to sources of infection (i.e., bacteria) after implantation. The 3D surface acts as a nidus for bacterial growth and biofilm formation. Reducing the capacity of bacteria adhesion and survival on an implant surface would prove the concept of utilising IPP technology for reducing infection risk. However, 3D surfaces are more challenging to coat.

To functionally optimise the IPP technology on 3D surfaces and assess the antimicrobial effects of CSA-90 coating, IPP-coated and control uncoated silica beads were exposed to *S. aureus* (ATCC-12600). The inoculated bacteria were allowed to air-dry onto the surface, and then the beads were placed in a solution of LB. As controls, PP-coated beads alone and unwashed PP + CSA-90-coated beads were included, which gave positive and negative signals for bacterial growth, respectively. Beads where CSA-90 was adsorbed to the surface in the absence of plasma polymerisation, and then washed with sodium dodecyl sulphate solution (SDS) did not impair bacterial growth, suggesting that CSA-90 was rapidly lost when washed. Conversely, PP + CSA-90 beads washed with SDS still showed potent antimicrobial activity in this assay (Figure 3.3A). Next, stainless-steel Kirshner-wire wire segments (1 cm length), with and without PP + CSA-90 coating, were tested for antimicrobial activity. Even with a higher (10-fold) inoculation dose of *S. aureus*, PP + CSA-90 coated wires showed a potent antimicrobial activity when grown in LB (Figure 3.3B).

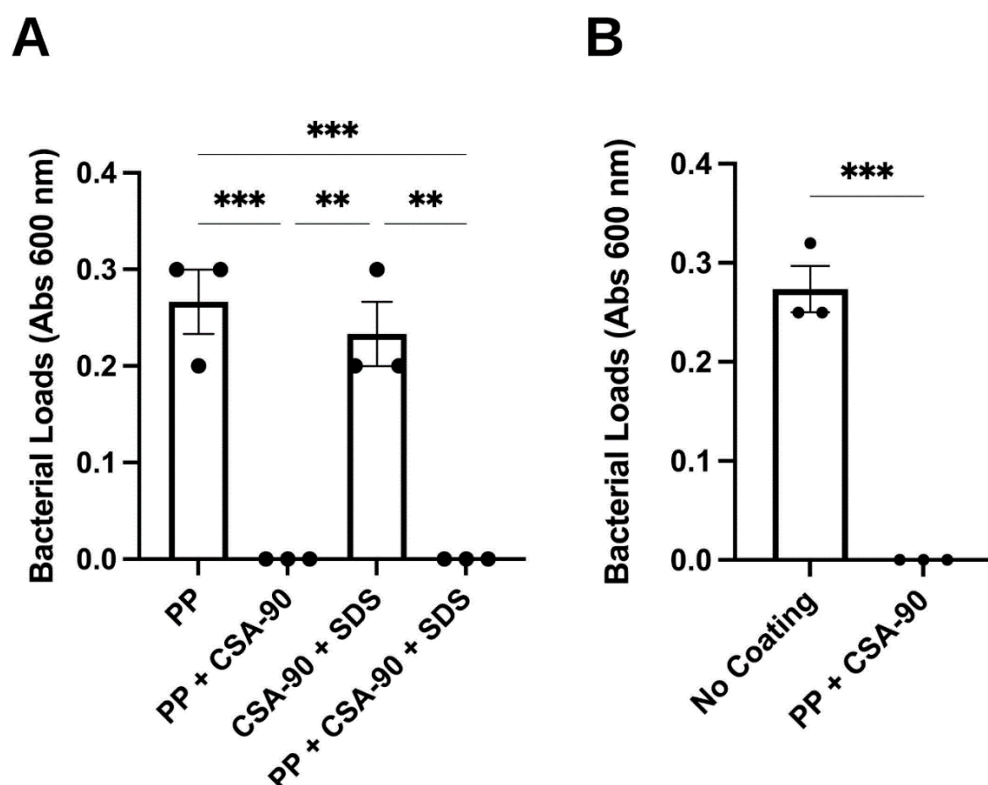


**Figure 3.3:** (A) The bacterial loads (absorbance at 600 nm) recovered from the silica beads with *S. aureus* ( $1 \times 10^4$  CFU) inoculated and air dried. (B) The bacterial loads (absorbance at 600 nm) recovered from stainless-steel Kirshner-wire (1 cm in length) with *S. aureus* ( $1 \times 10^5$  CFU) inoculated on the surface. (Error bars: mean and SEM; Statistical analysis was completed using (A) 2-way ANOVA and Turkey's Test and (B) unpaired t-test; \*\* p-value  $\leq 0.01$  and  $\geq 0.001$ ; \*\*\* p-value  $\leq 0.001$ ).



### 3.3.2. IPP+CSA-90 coating reduces bacterial loads in bones and soft-tissues

A preclinical murine orthopaedic infection model (TDH-pin method) was performed where a localized bone defect was made in the proximal tibia and a stainless-steel pin inserted into the intramedullary space as a nidus for biofilm formation and infection. Prior model development showed that a foreign surface adjacent to the bone defect (i.e., a metal pin) is important to achieve reliable and progressive infection (Thesis Chapter 2).

In the positive control group without any infection control measures, 80% (8/10) of animals developed pyogenic infections (pus present) and 80% (8/10) were positive for bacteria by swab test (bone defect site) at the study end point. Those with PP-coating only (i.e., no CSA-90) had 50% (5/10) with pus, but 90% (9/10) were tested positive for bacteria by swab test, suggesting the tissue inflammation was less severe in the PP-coated group, but the infection was not cleared without antimicrobial interventions. Subsequently, the PP + CSA-90 coating group showed 50% (5/10,  $p = 0.35$ , uncoated vs. PP + CSA-90) with pus, and 40% (4/10,  $p = 0.17$ , uncoated vs. PP + CSA-90) were tested positive for bacteria by swab test. Although it did not reach statistical significance, the PP + CSA-90 group had reduced the bone infection rate by nearly 50% (Table 3.1).

**Table 3.1:** The summary of infection rate in the preclinical trial.

Group	Bone Swab + (%)	Pus + (%)
No coating	8/10	8/10
PP	9/10	5/10
PP + CSA-90	4/10	5/10

However, quantified data showed that the bacterial loads were the lowest in the PP + CSA-90-coated group for swabs from the bones (Figure 3.3A,  $p \leq 0.05$ ), soft tissues (Figure 3.3B,  $p \leq 0.01$ ) and pins (Figure 3.3C). The data also revealed that without CSA-90, the PP-coated pins were able to reduce the bacterial loads on the bones, soft tissues, and pins even without CSA-90.

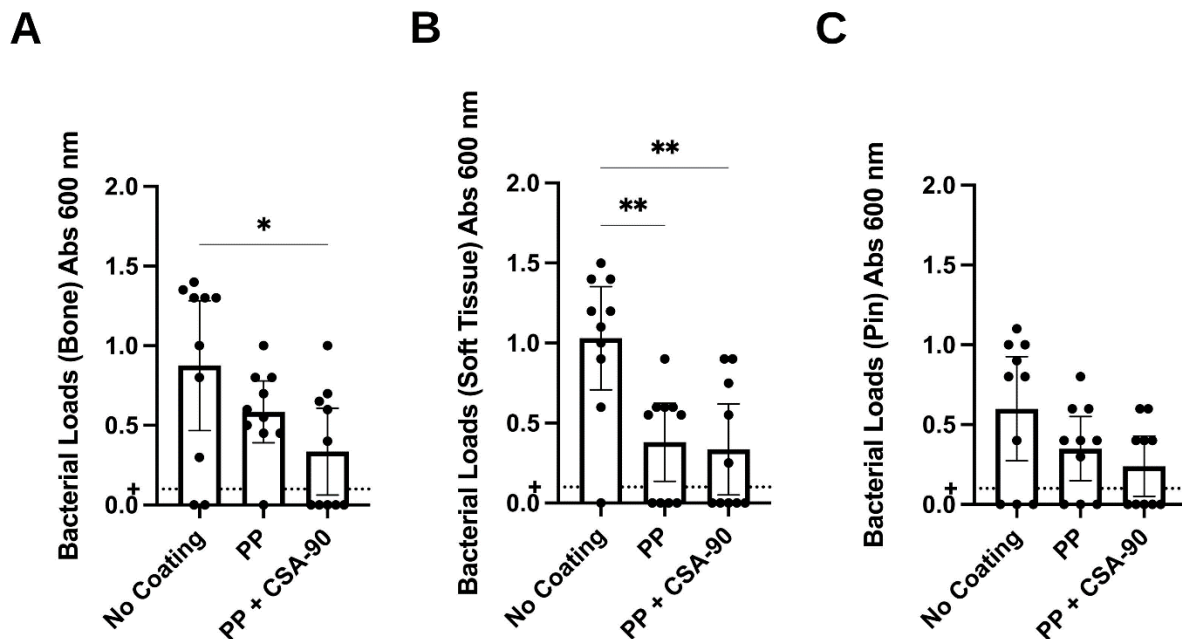


**Figure 3.4:** Semi-quantitative analysis of relative bacterial load (absorbance at 600 nm) from **(A)** bone swabs, **(B)** intramedullary steel pins, and **(C)** soft tissue adjacent to the defect site. (Error bars show mean and SEM; p-value: \* <0.05 and >0.01).

The PP + CSA-90 group had the lowest bacterial loads in bones compared to the no coating positive control group and PP-coating (no CSA-90) group (Figure 3.3A; p-values: <0.05). The PP-coating and PP + CSA-90 coatings had a reduction of bacterial load in soft-tissues (Figure 3.3B; p-values: <0.05). There was a trend for reduced bacterial loads on the pin surface for the PP-coating and PP+CSA-90-coating groups, but this did not reach statistical significance (Figure. 3.3C).

### 3.3.3. IPP + CSA-90 coating reduced bone loss and promote bone healing

Radiographs were used to assess osteolytic bone loss associated with infection. In uncoated pins, considerable bone loss was seen compared to the PP-coated pins and PP+CSA-90 coated pins, which showed superior healing (Figure 3.4). Bone loss was quantified using micro-CT and this supported the descriptive radiography (Figure 3.5). The micro-CT reconstruction images showed substantial healing of the tibial drilled-hole defect in PP-coated and PP+CSA-90 coated groups. Representative images were selected as having the median bone volume (BV) for an experimental group as assessed by quantitative micro-CT (Figure 3.5A). In addition, the PP-coated and PP + CSA-90 coated groups had an increased regenerate BV (Figure 3.5B). Although the regenerate BVs between the uncoated and PP-coated groups did not reach

statistical significance ( $p = 0.319$ , no coating vs. PP; and  $p = 0.4313$ , PP vs. PP+CSA-90), the regenerate BVs between uncoated and PP+CSA-90 coated was significant ( $p \leq 0.05$ ).



**Figure 3.5:** Radiographs (X-ray images) showing **(A)** osteolytic bone loss in infected tibiae (white arrows) with uncoated pins, and bone healing in select tibiae from groups with **(B)** PP coated pins, and **(C)** PP + CSA-90 coated pins. Radiographs show images before (left) and after (right) pin removal. The white arrows point to osteolytic lesions on XR.

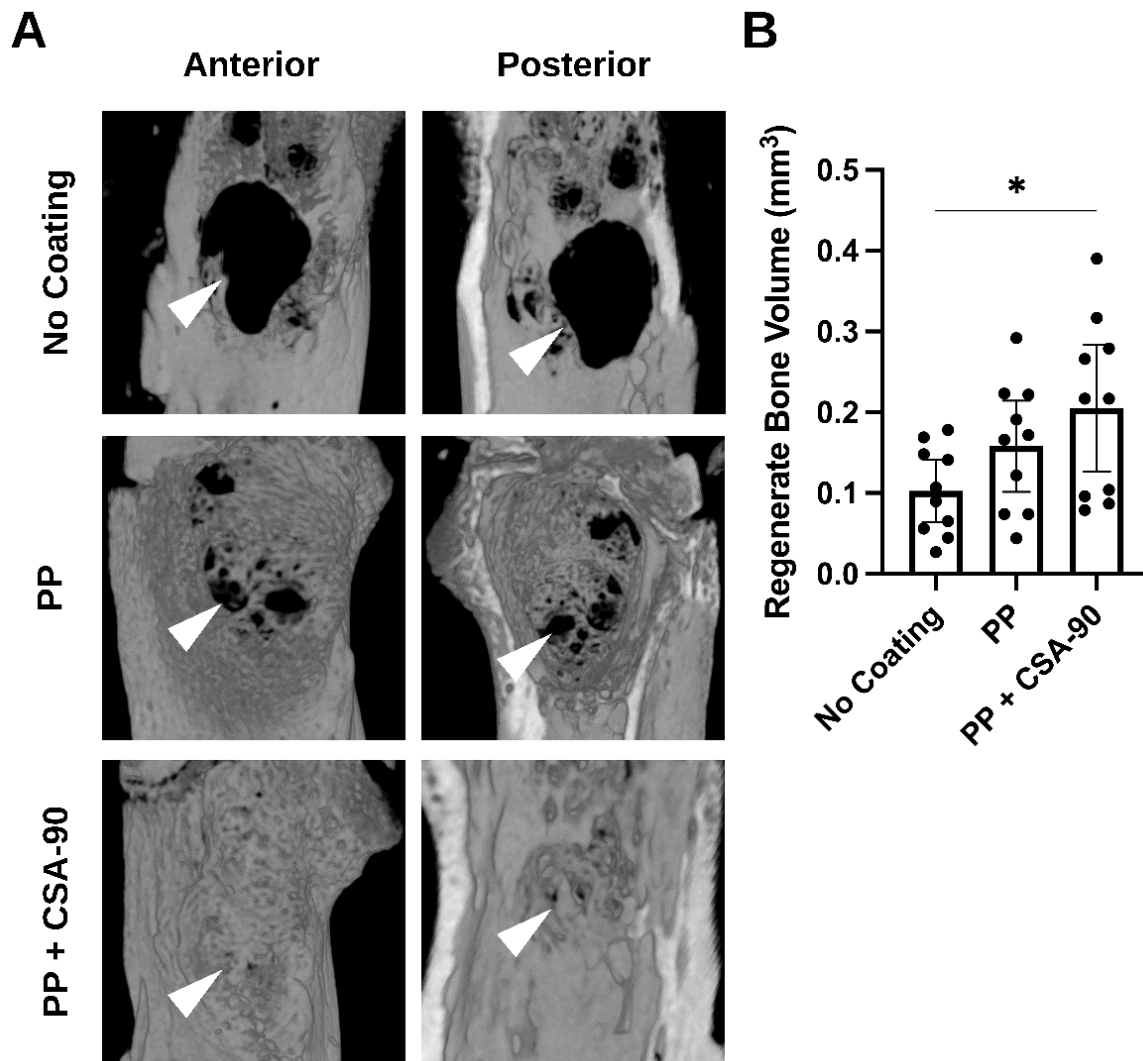


**Figure 3.6: (A)** Micro-CT reconstructions of tibial defects showing improved healing with PP+CSA-90 implant coating. **(B)** Micro-CT analysis of bone volume (mm<sup>3</sup>) in the tibial drilled hole after 2 weeks. There was significantly improved regenerate BV in the PP+CSA-90 group ( $p < 0.05$ ). BV in the PP group did not reach statistical significance with the other groups ( $p = 0.319$ , no coating vs. PP; and  $p = 0.4313$ , PP vs. PP+CSA-90). The white arrows point to the site of the original bone defects. It was shown that the defects were healed in the PP + CSA-90 group.

To complement the micro-CT analysis, descriptive histology was performed on specimens from each group. In the no coating group, the infected drilled hole persisted (Figure 3.7A) and the defect in the marrow was infiltrated with inflammatory macrophages and lymphocytes (Figure 3.7B; yellow arrows). It is found that infection leads to both bone resorption and subsequent woven bone formation all around the defect site affected the entire proximal metaphysis (Figures 3.7A, C and D, black arrows). However, the bone resorption was most severe in the infected bones without treatment, whereas the groups that received PP-coated or



PP + CSA-90-coated pins showed new bone formation with no histological evidence of persistent infection (Figures 3.7C and D).

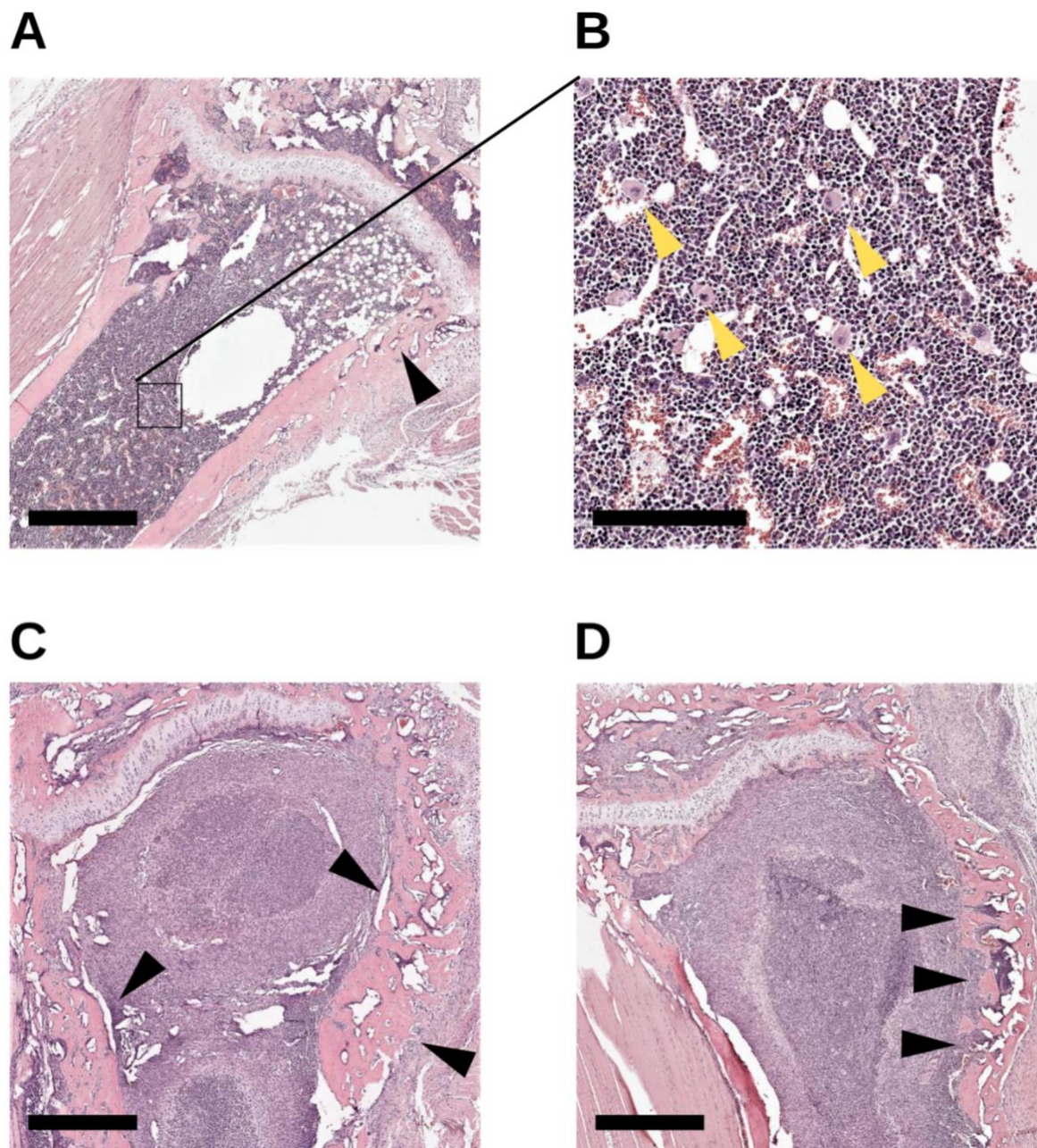


**Figure 3.7:** H&E-stained sections of the tibial drilled-hole defects in **(A-B)** no coating, **(C)** IPP-coated and **(D)** IPP+CSA-90 groups. Scale bars represent 600  $\mu\text{m}$  (**A**, **C-D**) and 200  $\mu\text{m}$  (**B**). Black arrows represent woven cortical bones; yellow arrows represent inflammatory macrophages and lymphocytes.

### 3.4. Discussion

Treatment for implant-related osteomyelitis has historically been a clinical challenge. Apart from implant removal and replacement, there are few options currently available to treat or prevent the formation of biofilm on metallic implant surfaces. Intravenous antibiotics are not typically effective against these types of infections, meaning patients sometimes need to tolerate systemic toxicity, limiting dosing for treatment. Consequently, novel strategies are needed to decrease the risk of implant-related infection utilising safer and more reliable methods of local antibiotic delivery.

In this study, we challenged the IPP + CSA-90 coating on 3D surfaces with bacterial exposure. Our preliminary *in vitro* data show similar antimicrobial effects on silica beads and Kirshner-wires. The function of CSA-90 remains active after immobilisation, reflecting the effects observed in 2D surfaces. The *in vitro* experiment also demonstrates that the CSA-90 on a PP-coated surface can tolerate SDS washes and the concentration remains sufficient to kill bacteria, suggesting a synergistic effect of IPP and CSA-90 as implant coating agents. These findings are also supported by the animal trial data. The *in vivo* data confirmed the profound osteogenic property of CSA-90 as well as the anti-adhesive feature of PP-coating for bacterial cells. The reduction of infection rate and bacterial loads on bones and soft tissues in the IPP + CSA-90 coating group suggest that CSA-90 provides protection against *S. aureus*.

Based on the observation of burst release, there is limited evidence to suggest whether the immobilisation of CSA-90 on the IPP-coated surface involves covalent linkage. However, due to the high efficacy of CSA-90 at low concentration, perhaps there is sufficient CSA-90 attached on the surface to have a lasting antifouling effect. The mechanism requires further investigations to improve drug release and sustainability. Nonetheless, the *in vivo* findings suggest that the IPP coating itself can be advantageous to prevent implant-related bone infections, and such effect can be enhanced by osteogenic CSA-90.

In contrast, the decreased bacterial loads on bones, soft tissues, and pins in the IPP-coating group (no CSA-90) highlight the importance of bacterial adhesion on a metal surface to bone infections. Without a metal surface to act as a nidus, bacterial growth and biofilm formation are inhibited, which potentially reduce the severity of infection even without the presence of antibiotics, even though the bacteria are still detectable from swab tests. While the exact mechanisms by which inhibition occurs is currently unknown, one possible explanation is that the IPP-coating composition containing hydrogen, carbon, nitrogen, and argon elements, which

are not conducive to bacterial adhesion<sup>80,83</sup>. Nevertheless, these results align with previous findings on 2D metal surfaces.

One limitation of this study is that we only tested one CSA-90 concentration on the coating. Although CSA-90 was known to be effective against multiple *S. aureus* strains in low-concentration, the IPP + CSA-90 coating group did not prevent osteomyelitis in all animals, suggesting the dosage of CSA-90 for coating is not optimised. Previous trials with rats have suggested that CSA-90 can be used in conjunction with routine systemic antibiotic prophylaxis to prevent periprosthetic joint infections<sup>93,94</sup>. Subsequently, there is no validation on how much CSA-90 can be immobilised on IPP-coated surfaces. There may be reduced amount of CSA-90 on the surface due to a wash-off effect or it may be affected by other *in vivo* biological factors that have not been considered in previous *in vitro* experiments. Future studies can use our model to test higher concentrations of CSA-90 or assess the efficacies of other ceragenins like CSA-131 (the second generation of CSA-13) that has similar molecular structure to CSA-90.

CSA-131 has been approved by Food and Drug Administration (FDA) in the United States for clinical endotracheal tube coating, suggesting that it may also be a feasible candidate for orthopaedic implant coating. Additionally, other CSAs in the CSA-13 subgroups (e.g., CSA-13 and CSA-131) are also known to be pro-osteogenic like CSA-90 and have bactericidal and antibiofilm activities against orthopaedic pathogens. The applications of IPP technology are not limited to delivering CSAs only, but also a variety of bioactive agents including proteins like bone-morphogenetic protein-2 (BMP-2), peptides such as MEL4 and caspofungin, and other antimicrobials that do not result in drug resistance from long-term exposure, and it opens the opportunity to nearly unlimited innovations and interventions<sup>80,83</sup>.

Although we have utilised IPP technology to coat surfaces other than metal (e.g., silica beads) *in vitro*, we have not performed any *in vivo* experiments to examine the efficacy of PP + CSA-90 coating on non-metal implants or evaluate the drug-release effect of CSA-90 using silica beads. Polymethylmethacrylate (PMMA) beads have been used to treat bone and wound infections over the last 30 years<sup>96</sup>. Therefore, future studies could also test the IPP technology on PMMA beads or other non-metal implants.

Another limitation of this study is that we only tested one monoclonal *S. aureus* strain (ATCC-12600) in this model, whereas clinically osteomyelitis can be multiclonal and polymicrobial. Other bacterial pathogens (e.g., methicillin-resistant *S. aureus*, *S. epidermidis*, *Propionibacterium acnes*, *Escherichia coli*, *Streptococcus*, and *Pseudomonas aeruginosa*) can

also be tested with the current model or using our newly developed NIS-Pin model as an alternative. In addition, ATCC-12600 *S. aureus* is not a high biofilm forming strain like ATCC-25923, so future experiments can also challenge the efficacy of PP-coating with a biofilm infection model. Furthermore, future experiments can also consider using bioluminescent bacteria (e.g., Xen36 *S. aureus*) to detect and track progressions of *in vivo* bone infections. IVIS scanning can perform on *in vitro* implants to validate bacterial inhibition and bactericidal activity of PP-coating and CSA-90 respectively.

One of the advantages of using IPP coating is that it does not require modification of the implant manufacturing process. Potentially, it can be prepared on any 3D surfaces that require antibiotic coating, and it is highly flexible for the applications from a clinical point of view, as it can be applied at the point-of-care before surgery, and it does not affect the shelf life of the implant.

Poly(ethylene glycol)-polyallyl mercaptan (PEG-PAM) coating method also features as a biodegradable implant coating technology <sup>21</sup>. PEG-PAM is a unique polymer formulation derived from PEG and poly(propylene sulphide) that carries antimicrobial compounds with a single layer, rapid polymerisation design that can deliver and release therapeutics <sup>97-100</sup>. The copolymer PEG-PAM requires just a few minutes to coat the implant in the operation room and has demonstrated antimicrobial efficacy <sup>21</sup>. It was suggested that a variety of antibiotics such as vancomycin, ceftriaxone, cefazolin, cefepime, tobramycin, piperacillin, and tazobactam, clindamycin, linezolid, rifampin and various combination of these antibiotics can be encapsulated in the PEG-PAM coating without losing their efficacy. These antibiotics can be passively released over two weeks to maintain the MIC during the perioperative period. While there is potential to use IPP with these antibiotics on orthopaedic implants, those antibiotics do not have osteogenic property, and may not be as advantageous as ceragenins (CSAs) combined with IPP coating to reduce the likelihood and impact of antibiotic resistance. Furthermore, CSAs are effective against bacterial biofilms, which is a unique feature that many traditional antibiotics lack <sup>101-103</sup>. Therefore, it is speculated that the application of CSA-90 for orthopaedic implant coating will be more advantageous compared to other conventional antibiotics. Nonetheless, the local delivery of antibiotic for orthopaedic implanted-related osteomyelitis remains challenging and require further research and development.

Further preclinical trials should be performed on a larger scale with higher concentrations of CSA-90 or other ceragenins. There is also no limitation for using multiple drugs for implant coating. For example, CSA-90/CSA-131 combined with vancomycin could be feasible. Future



studies should determine synergistic effects and applications using ceragenins as a conjugate prophylaxis with other antimicrobials.

In the context of orthopaedic implants, we regard IPP as an alternative technology to biofunctionalise surfaces of metal implants. Although IPP technology can potentially apply to any orthopaedic implant, we speculate that the IPP coating would be most benefit if used on screws, Kirshner-wires, and surgical locking plates that are used for internal fixation, as these implants have relatively unified 3D structures and are most used in fracture surgery and treatment.

Although a range of bioactive substrates have the potential to improve clinical outcomes. Ceragenins would be ideal candidates for surface delivery due to their active bactericidal and antibiofilm activities *in vitro* and *in vivo*. Using osteogenic CSAs as a coating agent should also be more advantageous than coatings with other bioactive substrates as it can promote fracture reunion. Studies have also demonstrated that it is difficult for bacterial and fungal pathogen to develop antimicrobial resistance against ceragenins, suggesting routine and prolonged exposure would not deteriorate the risk and incidence of AMR infections. In addition, gold nanoparticle (AuNP) conjugates with ceragenins were found to reduce *in vivo* toxicity and adverse effect and should be considered for implant coating<sup>104-106</sup>.

### 3.5. Conclusion

These studies have examined the utility of IPP for the biofunctionalisation of surfaces and demonstrates proof-of-principle that the IPP technology previously adapted for 2D surfaces can be optimised for 3D surfaces. This study focuses on applying IPP to create CSA-90 coated pins that were tested in our TDH-pin murine bone infection model. The data strongly shows the benefits of PP + CSA-90 coating as an antimicrobial suppression tool, but notably raises the potential of PP-coating itself as having antimicrobial qualities. Moving forward, the potential of IPP biofunctionalised coatings is extremely broad and could be adapted for other molecules including osteogenic factors, bone antiresorptives, or alternative antimicrobial drugs.

### 3.6. Supplementary Data

**Table S3.1:** Average measured ZOI (mm) of substances incubated for 24h with *S. aureus*.

Incubated Substances (24 hours)	Average ZOI (mm)
PP + CSA-90 Ti foil	22
PP + CSA-90 SSt foil	24
Gentamicin disc	17

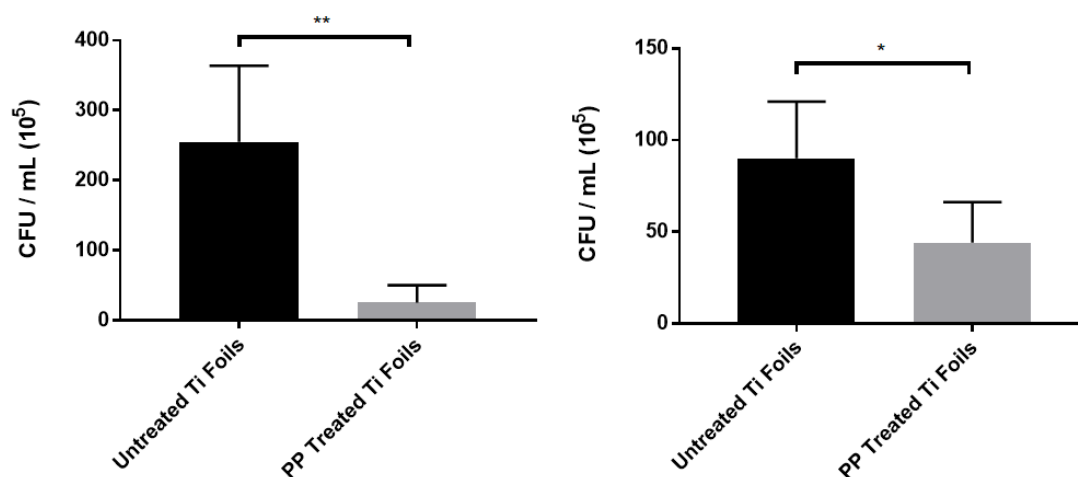


**Figure S3.1:** CFU/mL count of untreated and PP treated Ti foil surfaces (n=10) after bacterial adhesion assay and incubation at 37 °C for (A) 24 hours ( $p = 0.0062$ ) and (B) 72 hours ( $p = 0.0139$ ).

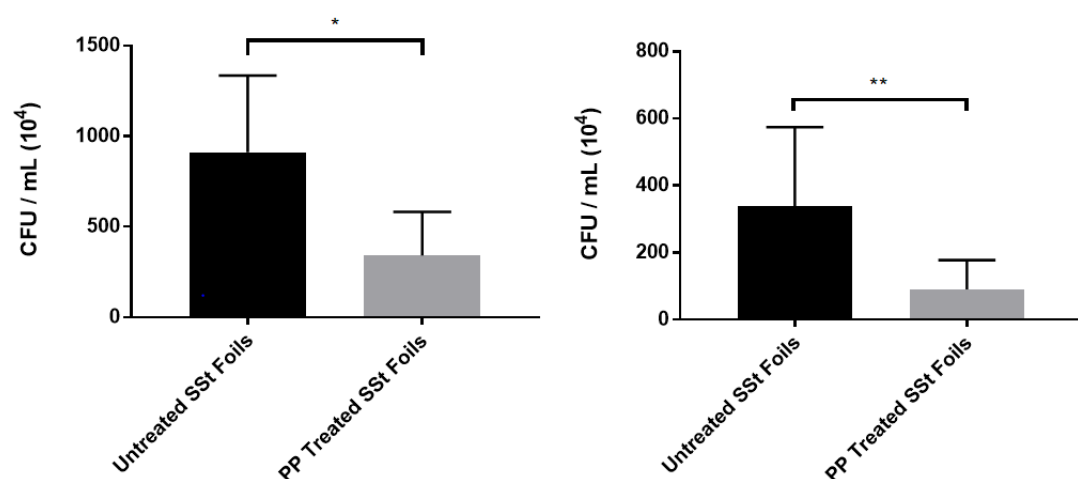


**Figure S3.2:** CFU/mL count of untreated and PP treated SSt foil surfaces (n=10) after bacterial adhesion assay and incubation at 37 °C for (A) 24 hours ( $p = 0.0162$ ) and (B) 72 hours ( $p = 0.0060$ ).

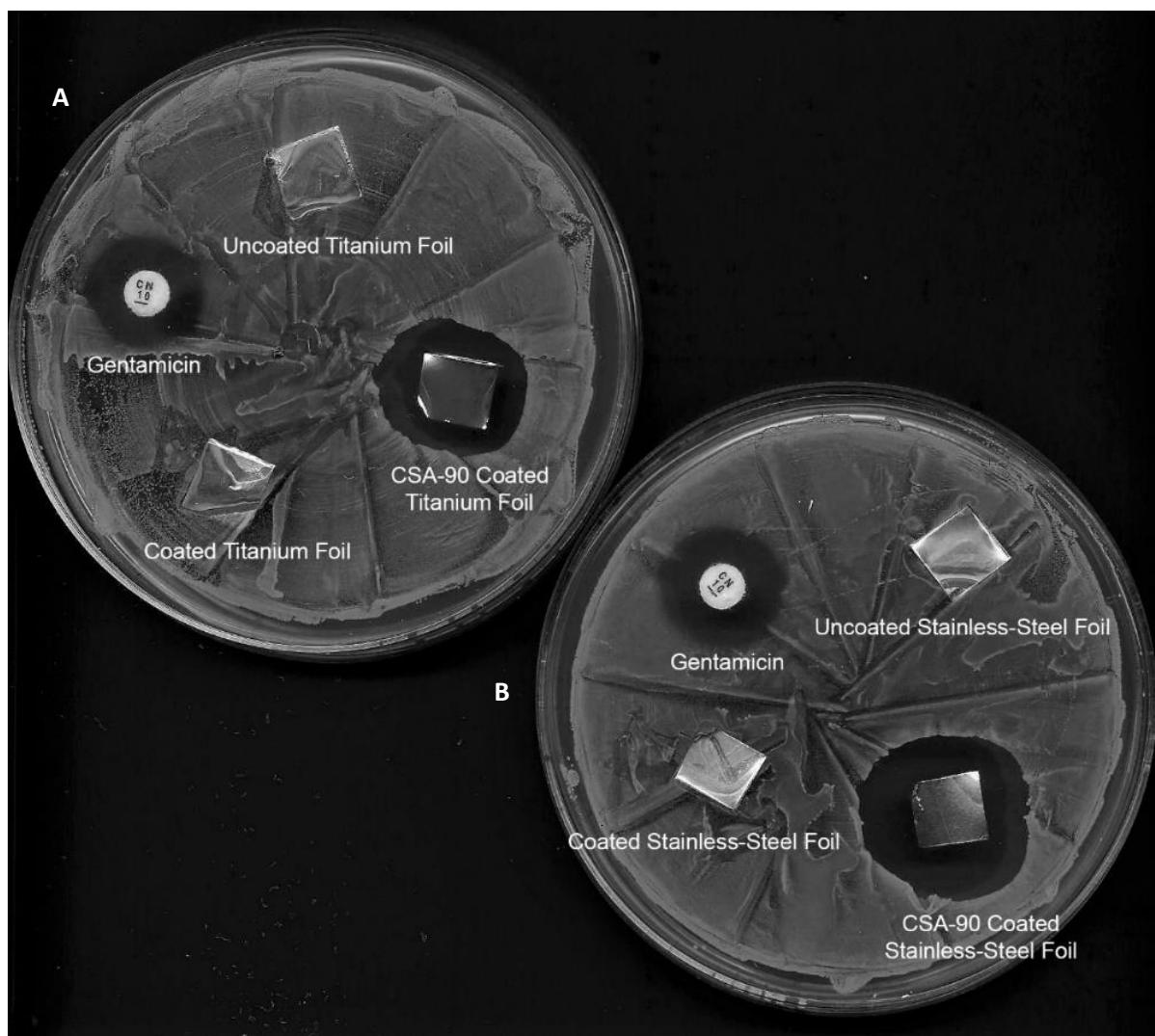


**Figure S3.3:** Kirby-Bauer diffusion susceptibility test incorporating CSA-90 (0.7 mg/mL) immobilised PP treated surfaces incubated in *S. aureus* at 37 °C for 24 hours. (A) Ti surfaces (B) Stainless-steel surfaces.

### References

1. Metsemakers WJ, Kuehl R, Moriarty TF, et al. Infection after fracture fixation: Current surgical and microbiological concepts. *Injury* 2018; **49**(3): 511-22.
2. Lewandowski LR, Potter BK, Murray CK, et al. Osteomyelitis Risk Factors Related to Combat Trauma Open Femur Fractures: A Case-Control Analysis. *Journal of orthopaedic trauma* 2019; **33**(4): e110-e9.
3. Tande AJ, Gomez-Urena EO, Berbari EF, Osmon DR. Management of Prosthetic Joint Infection. *Infectious disease clinics of North America* 2017; **31**(2): 237-52.
4. Singh S, Tan CL, Ahmad AR. Explaining Osteomyelitis and Prosthetic Joint Infections (PJI) in terms of Biofilm - A Review. *Malaysian orthopaedic journal* 2021; **15**(2): 1-8.
5. Zimmerli W, Sendi P. Orthopaedic biofilm infections. *APMIS : acta pathologica, microbiologica, et immunologica Scandinavica* 2017; **125**(4): 353-64.
6. Cobb LH, McCabe EM, Priddy LB. Therapeutics and delivery vehicles for local treatment of osteomyelitis. *Journal of orthopaedic research : official publication of the Orthopaedic Research Society* 2020; **38**(10): 2091-103.
7. Walter G, Kemmerer M, Kappler C, Hoffmann R. Treatment algorithms for chronic osteomyelitis. *Deutsches Arzteblatt international* 2012; **109**(14): 257-64.

8. Masters EA, Trombetta RP, de Mesy Bentley KL, et al. Evolving concepts in bone infection: redefining "biofilm", "acute vs. chronic osteomyelitis", "the immune proteome" and "local antibiotic therapy". *Bone research* 2019; **7**: 20.
9. Morgenstern M, Post V, Erichsen C, et al. Biofilm formation increases treatment failure in Staphylococcus epidermidis device-related osteomyelitis of the lower extremity in human patients. *Journal of orthopaedic research : official publication of the Orthopaedic Research Society* 2016; **34**(11): 1905-13.
10. Rao N, Ziran BH, Lipsky BA. Treating osteomyelitis: antibiotics and surgery. *Plastic and reconstructive surgery* 2011; **127 Suppl 1**: 177s-87s.
11. Bury DC, Rogers TS, Dickman MM. Osteomyelitis: Diagnosis and Treatment. *American family physician* 2021; **104**(4): 395-402.
12. Dekker AP, Uzoho C, Scammell B. Do Antibiotic-impregnated Calcium Sulfate Beads Improve the Healing of Neuropathic Foot Ulcers With Osteomyelitis Undergoing Surgical Debridement? *Wounds : a compendium of clinical research and practice* 2019; **31**(6): 145-50.
13. Hatzenbuehler J, Pulling TJ. Diagnosis and management of osteomyelitis. *American family physician* 2011; **84**(9): 1027-33.
14. Boffeli TJ, Luer SA, Brett KM, Chang HC. A Review of Consecutive Cases to Identify the Rate of Underlying Osteomyelitis in Patients Undergoing Surgical Treatment of Gangrene of the Forefoot and Impact of Acute Infection on Outcome Following Amputation. *The Journal of foot and ankle surgery : official publication of the American College of Foot and Ankle Surgeons* 2022; **61**(2): 286-92.
15. Grady JF, Winters CL. The Boyd amputation as a treatment for osteomyelitis of the foot. *Journal of the American Podiatric Medical Association* 2000; **90**(5): 234-9.
16. Miller W, Berg C, Wilson ML, Heard S, Knepper B, Young H. Risk Factors for Below-the-Knee Amputation in Diabetic Foot Osteomyelitis After Minor Amputation. *Journal of the American Podiatric Medical Association* 2019; **109**(2): 91-7.
17. Nizamani R, Heisler S, Chrisco L, Campbell H, Jones SW, Williams FN. Osteomyelitis Increases the Rate of Amputation in Patients With Type 2 Diabetes and Lower Extremity Burns. *Journal of burn care & research : official publication of the American Burn Association* 2020; **41**(5): 981-5.
18. J. F, M. M, D. S. THE FINANCIAL BURDEN OF TREATING OSTEOMYELITIS IN THE UK. *Orthopaedic Proceedings* 2019; **101-B**(SUPP\_14): 65-.
19. Shirley R, Fazekas J, McNally M, Ramsden A. Costs and remuneration of osteomyelitis treatment involving free flaps: implications of return to theatre. *J Bone Joint Infect* 2018; **3**(1): 15-9.
20. Geraghty T, LaPorta G. Current health and economic burden of chronic diabetic osteomyelitis. *Expert review of pharmacoeconomics & outcomes research* 2019; **19**(3): 279-86.
21. Xi W, Hegde V, Zoller SD, et al. Point-of-care antimicrobial coating protects orthopaedic implants from bacterial challenge. *Nature Communications* 2021; **12**(1): 5473.
22. Horino T, Hori S. Metastatic infection during Staphylococcus aureus bacteremia. *Journal of infection and chemotherapy : official journal of the Japan Society of Chemotherapy* 2020; **26**(2): 162-9.
23. Schattner A, Drahy Y. Nosocomial Vertebral Osteomyelitis. *The American journal of medicine* 2017; **130**(7): e309-e10.
24. Khan A, Miller WR, Arias CA. Mechanisms of antimicrobial resistance among hospital-associated pathogens. *Expert review of anti-infective therapy* 2018; **16**(4): 269-87.
25. Xu Z, Cave R, Chen L, et al. Antibiotic resistance and molecular characteristics of methicillin-resistant Staphylococcus epidermidis recovered from hospital personnel in China. *Journal of global antimicrobial resistance* 2020; **22**: 195-201.
26. Adapa AR, Linzey JR, Daou BJ, et al. Evaluating the role of methicillin-resistant Staphylococcus aureus (MRSA)-specific antibiotic prophylaxis for neurosurgical patients. *Clinical neurology and neurosurgery* 2021; **200**: 106353.
27. Craxford S, Marson BA, Oderuth E, Nightingale J, Agrawal Y, Ollivere B. Methicillin-resistant Staphylococcus aureus in hip fracture. *The bone & joint journal* 2021; **103-b**(1): 170-7.
28. Goyal N, Miller A, Tripathi M, Parvizi J. Methicillin-resistant Staphylococcus aureus (MRSA): colonisation and pre-operative screening. *The bone & joint journal* 2013; **95-b**(1): 4-9.

29. Lin S, Melki S, Lisgaris MV, Ahadizadeh EN, Zender CA. Post-operative MRSA infections in head and neck surgery. *American journal of otolaryngology* 2017; **38**(4): 417-21.
30. Thakkar V, Ghobrial GM, Maulucci CM, et al. Nasal MRSA colonization: impact on surgical site infection following spine surgery. *Clinical neurology and neurosurgery* 2014; **125**: 94-7.
31. Zhou J, Wang R, Huo X, Xiong W, Kang L, Xue Y. Incidence of Surgical Site Infection After Spine Surgery: A Systematic Review and Meta-analysis. *Spine* 2020; **45**(3): 208-16.
32. Janssen SJ, Kloen P. Supercutaneous locking compression plate in the treatment of infected non-union and open fracture of the leg. *Archives of orthopaedic and trauma surgery* 2021.
33. Munir MA, Tandiabang PA, Prihantono. Internal fixation of delayed union of fracture with chronic osteomyelitis due to Staphylococcus epidermidis: A case report. *Annals of medicine and surgery (2012)* 2020; **56**: 56-60.
34. Pouwels S, De Jongh F, Willems WF, Nguyen T, Rhemrev SJ. Complications in the Treatment of Delayed Union and Underlying Chronic Osteomyelitis After Right Crural Fracture Treated With Anterolateral Thigh Flap and Double-Barrelled Vascularized Fibula Graft. *Cureus* 2021; **13**(9): e17923.
35. Tarng YW, Lin KC. Management of bone defects due to infected non-union or chronic osteomyelitis with autologous non-vascularized free fibular grafts. *Injury* 2020; **51**(2): 294-300.
36. Baddula AR, Yalamanchili RK, Vuthpala VM. A Case Report of Osteomyelitis of Lower End of Tibia and Fibula as a Complication of Elastic Rubber Band Syndrome (Dhaga Syndrome). *Journal of orthopaedic case reports* 2021; **11**(4): 56-8.
37. Jiang N, Wang BW, Chai YM, et al. Chinese expert consensus on diagnosis and treatment of infection after fracture fixation. *Injury* 2019; **50**(11): 1952-8.
38. Kusejko K, Auñón Á, Jost B, et al. The Impact of Surgical Strategy and Rifampin on Treatment Outcome in Cutibacterium Periprosthetic Joint Infections. *Clinical infectious diseases : an official publication of the Infectious Diseases Society of America* 2021; **72**(12): e1064-e73.
39. Hickok NJ, Shapiro IM. Immobilized antibiotics to prevent orthopaedic implant infections. *Advanced drug delivery reviews* 2012; **64**(12): 1165-76.
40. Olsen MA, Mayfield J, Laurysen C, et al. Risk factors for surgical site infection in spinal surgery. *Journal of neurosurgery* 2003; **98**(2 Suppl): 149-55.
41. Strowitzki M, Vastmans J, Vogel M, Jaksche H. Complex 360°-reconstruction and stabilization of the cervical spine due to osteomyelitis. *European spine journal : official publication of the European Spine Society, the European Spinal Deformity Society, and the European Section of the Cervical Spine Research Society* 2011; **20 Suppl 2**(Suppl 2): S248-52.
42. van de Belt H, Neut D, Schenk W, van Horn JR, van der Mei HC, Busscher HJ. Infection of orthopedic implants and the use of antibiotic-loaded bone cements. A review. *Acta orthopaedica Scandinavica* 2001; **72**(6): 557-71.
43. Johnson JD, Nessler JM, Horazdovsky RD, Vang S, Thomas AJ, Marston SB. Serum and Wound Vancomycin Levels After Intrawound Administration in Primary Total Joint Arthroplasty. *The Journal of arthroplasty* 2017; **32**(3): 924-8.
44. Jiranek WA, Hanssen AD, Greenwald AS. Antibiotic-loaded bone cement for infection prophylaxis in total joint replacement. *The Journal of bone and joint surgery American volume* 2006; **88**(11): 2487-500.
45. Slane J, Gietman B, Squire M. Antibiotic elution from acrylic bone cement loaded with high doses of tobramycin and vancomycin. *Journal of orthopaedic research : official publication of the Orthopaedic Research Society* 2018; **36**(4): 1078-85.
46. Stevens CM, Tetsworth KD, Calhoun JH, Mader JT. An articulated antibiotic spacer used for infected total knee arthroplasty: a comparative in vitro elution study of Simplex and Palacos bone cements. *Journal of orthopaedic research : official publication of the Orthopaedic Research Society* 2005; **23**(1): 27-33.
47. Gallo J, Kolár M, Florschütz AV, Novotný R, Pantůček R, Kesselová M. In vitro testing of gentamicin-vancomycin loaded bone cement to prevent prosthetic joint infection. *Biomedical papers of the Medical Faculty of the University Palacky, Olomouc, Czechoslovakia* 2005; **149**(1): 153-8.
48. Dunne NJ, Hill J, McAfee P, Kirkpatrick R, Patrick S, Tunney M. Incorporation of large amounts of gentamicin sulphate into acrylic bone cement: effect on handling and mechanical properties, antibiotic release, and biofilm formation. *Proceedings of the Institution of Mechanical Engineers Part H, Journal of engineering in medicine* 2008; **222**(3): 355-65.

49. Howlin RP, Brayford MJ, Webb JS, Cooper JJ, Aiken SS, Stoodley P. Antibiotic-loaded synthetic calcium sulfate beads for prevention of bacterial colonization and biofilm formation in periprosthetic infections. *Antimicrobial agents and chemotherapy* 2015; **59**(1): 111-20.
50. Tsuchiya H, Shirai T, Nishida H, et al. Innovative antimicrobial coating of titanium implants with iodine. *Journal of orthopaedic science : official journal of the Japanese Orthopaedic Association* 2012; **17**(5): 595-604.
51. Brennan SA, C NF, Devitt BM, O'Mahony FJ, Brabazon D, Walsh A. Silver nanoparticles and their orthopaedic applications. *The bone & joint journal* 2015; **97-b**(5): 582-9.
52. Romanò CL, Scarponi S, Gallazzi E, Romanò D, Drago L. Antibacterial coating of implants in orthopaedics and trauma: a classification proposal in an evolving panorama. *Journal of orthopaedic surgery and research* 2015; **10**: 157.
53. Albers CE, Hofstetter W, Siebenrock KA, Landmann R, Klenke FM. In vitro cytotoxicity of silver nanoparticles on osteoblasts and osteoclasts at antibacterial concentrations. *Nanotoxicology* 2013; **7**(1): 30-6.
54. Liu Z, Liu X, Ramakrishna S. Surface engineering of biomaterials in orthopedic and dental implants: Strategies to improve osteointegration, bacteriostatic and bactericidal activities. *Biotechnology journal* 2021; **16**(7): e2000116.
55. Ghimire A, Song J. Anti-Periprosthetic Infection Strategies: From Implant Surface Topographical Engineering to Smart Drug-Releasing Coatings. *ACS applied materials & interfaces* 2021; **13**(18): 20921-37.
56. Bohara S, Suthakorn J. Surface coating of orthopedic implant to enhance the osseointegration and reduction of bacterial colonization: a review. *Biomater Res* 2022; **26**(1): 26.
57. Pangli H, Vatanpour S, Hortamani S, Jalili R, Ghahary A. Incorporation of Silver Nanoparticles in Hydrogel Matrices for Controlling Wound Infection. *Journal of burn care & research : official publication of the American Burn Association* 2021; **42**(4): 785-93.
58. Stewart C, Akhavan B, Wise SG, Bilek MMM. A review of biomimetic surface functionalization for bone-integrating orthopedic implants: Mechanisms, current approaches, and future directions. *Progress in Materials Science* 2019; **106**: 100588.
59. Altmann SD-CD, Pfeiffer JDD-C. The Hydrolysis/Condensation Behaviour of Methacryloyloxyalkylfunctional Alkoxysilanes: Structure-Reactivity Relations. *Monatshefte für Chemie / Chemical Monthly* 2003; **134**: 1081-92.
60. Hanawa T. A comprehensive review of techniques for biofunctionalization of titanium. *Journal of periodontal & implant science* 2011; **41**(6): 263-72.
61. Alagem-Shafir M, Kivovich E, Tzchori I, et al. The formation of an anti-restenotic/anti-thrombotic surface by immobilization of nitric oxide synthase on a metallic carrier. *Acta biomaterialia* 2014; **10**(5): 2304-12.
62. Fang K, Song W, Wang L, et al. Immobilization of chitosan film containing semaphorin 3A onto a microarc oxidized titanium implant surface via silane reaction to improve MG63 osteogenic differentiation. *International journal of nanomedicine* 2014; **9**: 4649-57.
63. Schaer TP, Stewart S, Hsu BB, Klivanov AM. Hydrophobic polycationic coatings that inhibit biofilms and support bone healing during infection. *Biomaterials* 2012; **33**(5): 1245-54.
64. Chen J, Howell C, Haller CA, et al. An immobilized liquid interface prevents device associated bacterial infection in vivo. *Biomaterials* 2017; **113**: 80-92.
65. Gilchrist SE, Lange D, Letchford K, Bach H, Fazli L, Burt HM. Fusidic acid and rifampicin co-loaded PLGA nanofibers for the prevention of orthopedic implant associated infections. *Journal of controlled release : official journal of the Controlled Release Society* 2013; **170**(1): 64-73.
66. Qin L, Dong H, Mu Z, Zhang Y, Dong G. Preparation and bioactive properties of chitosan and casein phosphopeptides composite coatings for orthopedic implants. *Carbohydrate polymers* 2015; **133**: 236-44.
67. van Hengel IAJ, Riool M, Fratila-Apachitei LE, et al. Selective laser melting porous metallic implants with immobilized silver nanoparticles kill and prevent biofilm formation by methicillin-resistant *Staphylococcus aureus*. *Biomaterials* 2017; **140**: 1-15.
68. Jennings JA, Carpenter DP, Troxel KS, et al. Novel Antibiotic-loaded Point-of-care Implant Coating Inhibits Biofilm. *Clinical orthopaedics and related research* 2015; **473**(7): 2270-82.

69. Klein K, Schweizer TA, Siwy K, et al. Establishment of a localized acute implant-associated Staphylococcus aureus bone infection model in sheep. *Pathogens and disease* 2021; **79**(6).
70. Odekerken JC, Brans BT, Welting TJ, Walenkamp GH. (18)F-FDG microPET imaging differentiates between septic and aseptic wound healing after orthopedic implant placement: a longitudinal study of an implant osteomyelitis in the rabbit tibia. *Acta Orthop* 2014; **85**(3): 305-13.
71. Schindeler A, Yu NY, Cheng TL, et al. Local delivery of the cationic steroid antibiotic CSA-90 enables osseous union in a rat open fracture model of Staphylococcus aureus infection. *The Journal of bone and joint surgery American volume* 2015; **97**(4): 302-9.
72. Shiels SM, Bedigrew KM, Wenke JC. Development of a hematogenous implant-related infection in a rat model. *BMC Musculoskelet Disord* 2015; **16**: 255.
73. Boot W, Schmid T, D'Este M, et al. A Hyaluronic Acid Hydrogel Loaded with Gentamicin and Vancomycin Successfully Eradicates Chronic Methicillin-Resistant Staphylococcus aureus Orthopedic Infection in a Sheep Model. *Antimicrobial agents and chemotherapy* 2021; **65**(4).
74. Croes M, van der Wal BCH, Vogely HC. Impact of Bacterial Infections on Osteogenesis: Evidence From In Vivo Studies. *Journal of orthopaedic research : official publication of the Orthopaedic Research Society* 2019; **37**(10): 2067-76.
75. Odekerken JC, Arts JJ, Surtel DA, Walenkamp GH, Welting TJ. A rabbit osteomyelitis model for the longitudinal assessment of early post-operative implant infections. *Journal of orthopaedic surgery and research* 2013; **8**: 38.
76. Stadelmann VA, Potapova I, Camenisch K, Nehrass D, Richards RG, Moriarty TF. In Vivo MicroCT Monitoring of Osteomyelitis in a Rat Model. *Biomed Res Int* 2015; **2015**: 587857.
77. Tomizawa T, Nishitani K, Ito H, et al. The limitations of mono- and combination antibiotic therapies on immature biofilms in a murine model of implant-associated osteomyelitis. *Journal of orthopaedic research : official publication of the Orthopaedic Research Society* 2021; **39**(2): 449-57.
78. Windolf CD, Meng W, Lögters TT, MacKenzie CR, Windolf J, Flohé S. Implant-associated localized osteitis in murine femur fracture by biofilm forming Staphylococcus aureus: a novel experimental model. *Journal of orthopaedic research : official publication of the Orthopaedic Research Society* 2013; **31**(12): 2013-20.
79. Windolf CD, Lögters T, Scholz M, Windolf J, Flohé S. Lysostaphin-coated titan-implants preventing localized osteitis by Staphylococcus aureus in a mouse model. *PloS one* 2014; **9**(12): e115940.
80. Akhavan B, Bakhshandeh S, Najafi-Ashtiani H, et al. Direct covalent attachment of silver nanoparticles on radical-rich plasma polymer films for antibacterial applications. *Journal of materials chemistry B* 2018; **6**(37): 5845-53.
81. Akhavan B, Croes M, Wise SG, et al. Radical-functionalized plasma polymers: Stable biomimetic interfaces for bone implant applications. *Applied Materials Today* 2019; **16**: 456-73.
82. Akhavan B, Michl TD, Giles C, et al. Plasma activated coatings with dual action against fungi and bacteria. *Applied Materials Today* 2018; **12**: 72-84.
83. Croes M, Akhavan B, Sharifahmadian O, et al. A multifaceted biomimetic interface to improve the longevity of orthopedic implants. *Acta biomaterialia* 2020; **110**: 266-79.
84. Stewart CAC, Akhavan B, Hung J, et al. Multifunctional Protein-Immobilized Plasma Polymer Films for Orthopedic Applications. *ACS biomaterials science & engineering* 2018; **4**(12): 4084-94.
85. Bilek MM, Bax DV, Kondyurin A, et al. Free radical functionalization of surfaces to prevent adverse responses to biomedical devices. *Proceedings of the National Academy of Sciences of the United States of America* 2011; **108**(35): 14405-10.
86. Martin LJ, Akhavan B, Bilek MM. Electric fields control the orientation of peptides irreversibly immobilized on radical-functionalized surfaces. *Nat Commun* 2018; **9**(1): 357.
87. Walia R, Akhavan B, Kosobrodova E, et al. Hydrogel–Solid Hybrid Materials for Biomedical Applications Enabled by Surface-Embedded Radicals. *Advanced Functional Materials* 2020; **30**(38): 2004599.
88. Costa ML, Achten J, Rangan A, Lamb SE, Parsons NR. Percutaneous fixation with Kirschner wires versus volar locking-plate fixation in adults with dorsally displaced fracture of distal radius: five-year follow-up of a randomized controlled trial. *The bone & joint journal* 2019; **101-b**(8): 978-83.

89. Emara AK, Ng M, Krebs VE, Bloomfield M, Molloy RM, Piuze NS. Femoral Stem Cementation in Hip Arthroplasty: The Know-How of a "Lost" Art. *Current reviews in musculoskeletal medicine* 2021; **14**(1): 47-59.
90. Ledet EH, Liddle B, Kradinova K, Harper S. Smart implants in orthopedic surgery, improving patient outcomes: a review. *Innovation and entrepreneurship in health* 2018; **5**: 41-51.
91. Lai XZ, Feng Y, Pollard J, et al. Ceragenins: cholic acid-based mimics of antimicrobial peptides. *Accounts of chemical research* 2008; **41**(10): 1233-40.
92. Vaara M. New approaches in peptide antibiotics. *Current opinion in pharmacology* 2009; **9**(5): 571-6.
93. Mills R, Cheng TL, Mikulec K, et al. CSA-90 Promotes Bone Formation and Mitigates Methicillin-resistant Staphylococcus aureus Infection in a Rat Open Fracture Model. *Clinical orthopaedics and related research* 2018; **476**(6): 1311-23.
94. Mills RJ, Boyling A, Cheng TL, et al. CSA-90 reduces periprosthetic joint infection in a novel rat model challenged with local and systemic Staphylococcus aureus. *Journal of orthopaedic research : official publication of the Orthopaedic Research Society* 2020; **38**(9): 2065-73.
95. Akhavan B, Wise SG, Bilek MMM. Substrate-Regulated Growth of Plasma-Polymerized Films on Carbide-Forming Metals. *Langmuir* 2016; **32**(42): 10835-43.
96. El-Ghannam A, Jahed K, Govindaswami M. Resorbable bioactive ceramic for treatment of bone infection. *Journal of Biomedical Materials Research Part A* 2010; **94A**(1): 308-16.
97. Ernest M, Hunja C, Arakura Y, et al. The Toll-Like Receptor 2 agonist PEG-Pam(2)Cys as an immunochemoprophylactic and immunochemotherapeutic against the liver and transmission stages of malaria parasites. *International journal for parasitology Drugs and drug resistance* 2018; **8**(3): 451-8.
98. Jia Y, Wang C, Zheng J, et al. Novel nanomedicine with a chemical-exchange saturation transfer effect for breast cancer treatment in vivo. *Journal of nanobiotechnology* 2019; **17**(1): 123.
99. Wang C, Du L, Zhou J, et al. Elaboration on the Distribution of Hydrophobic Segments in the Chains of Amphiphilic Cationic Polymers for Small Interfering RNA Delivery. *ACS applied materials & interfaces* 2017; **9**(38): 32463-74.
100. Zhao M, Li J, Chen D, Hu H. A Valid Bisphosphonate Modified Calcium Phosphate-Based Gene Delivery System: Increased Stability and Enhanced Transfection Efficiency In Vitro and In Vivo. *Pharmaceutics* 2019; **11**(9).
101. Latorre MC, Pérez-Granda MJ, Savage PB, et al. Endotracheal tubes coated with a broad-spectrum antibacterial ceragenin reduce bacterial biofilm in an in vitro bench top model. *The Journal of antimicrobial chemotherapy* 2021; **76**(5): 1168-73.
102. Paprocka P, Durnaś B, Mańkowska A, et al. New  $\beta$ -Lactam Antibiotics and Ceragenins - A Study to Assess Their Potential in Treatment of Infections Caused by Multidrug-Resistant Strains of Pseudomonas aeruginosa. *Infection and drug resistance* 2021; **14**: 5681-98.
103. Tokajuk J, Deptuła P, Chmielewska SJ, et al. Ceragenin CSA-44 as a Means to Control the Formation of the Biofilm on the Surface of Tooth and Composite Fillings. *Pathogens (Basel, Switzerland)* 2022; **11**(5).
104. Chmielewska SJ, Skłodowski K, Depciuch J, et al. Bactericidal Properties of Rod-, Peanut-, and Star-Shaped Gold Nanoparticles Coated with Ceragenin CSA-131 against Multidrug-Resistant Bacterial Strains. *Pharmaceutics* 2021; **13**(3).
105. Piktel E, Oscilowska I, Suprewicz Ł, et al. Peanut-Shaped Gold Nanoparticles with Shells of Ceragenin CSA-131 Display the Ability to Inhibit Ovarian Cancer Growth In Vitro and in a Tumor Xenograft Model. *Cancers* 2021; **13**(21).
106. Skłodowski K, Chmielewska SJ, Depciuch J, et al. Ceragenin-Coated Non-Spherical Gold Nanoparticles as Novel Candidacidal Agents. *Pharmaceutics* 2021; **13**(11).



### Antibacterial plasma polymer coatings on 3D materials for orthopedic applications

Aiken Dao <sup>1,2,3</sup>, Christale Gaitanos <sup>4,5</sup>, Sumedh Kamble <sup>1,2</sup>, Omid Sharifahmadian <sup>4,6</sup>, Richard P. Tan <sup>7,8</sup>, Steven G. Wise <sup>7,8,9</sup>, Tiffany Lai Yun Cheung <sup>4,5</sup>, Marcela Bilek <sup>4,5,7,9</sup>, Paul B. Savage <sup>10</sup>, Aaron Schindeler <sup>1,2,3</sup>, Behnam Akhavan <sup>4,5,7,11,12\*</sup>

- 1 *Bioengineering & Molecular Medicine, The Children's Hospital at Westmead, Westmead, NSW, Australia*
- 2 *The Children's Hospital at Westmead Clinical School, Faculty of Medicine and Health, The University of Sydney, Sydney, NSW, Australia*
- 3 *Bioengineering & Molecular Medicine, The Westmead Institute for Medical Research, Westmead, NSW, Australia*
- 4 *School of Physics, Faculty of Science, The University of Sydney, Sydney, NSW 2006, Australia*
- 5 *School of Biomedical Engineering, University of Sydney, Sydney, NSW 2006, Australia*
- 6 *Coating Department, Centre for Functional and Surface Functionalized Glass, Alexander Dubcek University of Trencin, 91150 Trencin, Slovakia"*
- 7 *The University of Sydney Nano Institute, The University of Sydney, Sydney, NSW 2006, Australia*
- 8 *School of Medical Sciences, Faculty of Medicine and Health, The University of Sydney, Sydney, NSW 2006, Australia*
- 9 *Charles Perkins Centre, University of Sydney, Sydney, NSW 2006, Australia*
- 10 *Department of Chemistry and Biochemistry, Brigham Young University, C100 BNSN, Provo, UT 84602, USA*
- 11 *School of Engineering, University of Newcastle, Callaghan, NSW 2308, Australia*
- 12 *Hunter Medical Research Institute (HMRI), Precision Medicine Program, New Lambton Heights NSW 2305, Australia*

\* Corresponding author:

Dr Behnam Akhavan

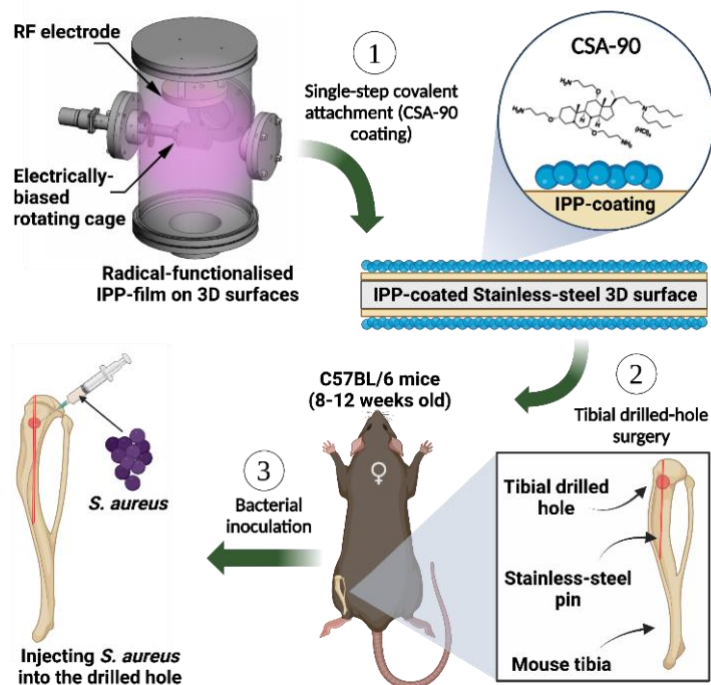
[Behnam.Akhavan@newcastle.edu.au](mailto:Behnam.Akhavan@newcastle.edu.au)

[behnam.akhavan@sydney.edu.au](mailto:behnam.akhavan@sydney.edu.au)

## Abstract

Covalent biofunctionalization of implant surfaces using antimicrobial agents is a promising approach to reducing bone infection and implant failure. Radical-rich, ion-assisted plasma polymerized (IPP) coatings enable surface covalent biofunctionalization in a single, reagent-free step; but until now, they have been limited to only 2D surfaces. Here we demonstrate a new technology to create homogenous IPP coatings on 3D materials using a rotating, conductive cage that is negatively biased while immersed in RF plasma. We provided evidence that under controlled energetic ion bombardment, this technology enables the formation of highly robust and homogenous radical-rich coatings on 3D objects for subsequent covalent attachment of antimicrobial agents. To functionally apply this technology, the broad-spectrum antimicrobial CSA-90 was attached to the surfaces, where it retained potent antibacterial activity against *Staphylococcus aureus*. CSA-90 covalent functionalization of stainless-steel pins used in a murine model of orthopedic infection revealed the highly promising potential of this coating system to reduce *S. aureus* infection-related bone loss. This study takes the previous research on plasma-based covalent functionalization of 2D surfaces a step further, with important implications for ushering in a new dimension in the biofunctionalization of 3D structures for applications in bone implants and beyond.

## Graphical Abstract:



**Keywords:** Plasma polymerization; Biofunctionalization; Antimicrobials; Bone infection; Orthopedic implant coating; Surface engineering

## 1. Introduction

Bone infection is a major clinical problem and can be of exceptionally high risk for open fractures and surgeries <sup>1</sup>. Although re-operation and debridement combined with systemic antibiotic treatment can often resolve an initial superficial infection, deep infections are often refractory to intervention <sup>2</sup>. Treating the resultant non-unions can be challenging and costly <sup>3,4</sup>. Orthopedic implants can act as a nidus for biofilm formation, making them particularly prone to infection. Joint replacement or total joint arthroplasty is a high-volume, high-cost surgery where preventable post-operative complications are significant cost drivers <sup>5</sup>. Infection rates are particularly high in joint replacement revisions, even when implants are being revised for complications not previously associated with infection. Hence, there is a growing trend toward establishing antimicrobial coatings for medical implants, particularly those implanted in the bone <sup>6</sup>.

In terms of surface biofunctionalization, agents that have been trialed can be broadly classified into inorganics (e.g., silver, copper, and zinc oxide), organics (e.g., small molecule antibiotics, antimicrobial peptides, polymers), as well as modification of surface texture (e.g., nano-texturization, micro-texturization) <sup>7</sup>. While bioactive organic agents can have high potency against infection, there remains considerable scope to develop new methods for surface attachment <sup>8</sup>. Simple adsorption methods can result in burst release and a lack of sustained protection. Agents can also be embedded in soluble polymer or hydrogel matrices that can be used for surface coating. This approach can yield challenges with controlling degradation rates and the negative biological effects of breakdown products. In contrast, methods for covalent linkage to an implant surface allow for rapid and sustained biological activity.

Covalent attachment of bioactive molecules on surfaces has been traditionally achieved using methods relying on wet-chemical steps <sup>9</sup>. Examples of these approaches include linker chemistry methods based on salinization <sup>10</sup>, PEGylation <sup>11</sup>, and heparinization <sup>12</sup>. However, these methods are typically substrate-dependent, meaning they apply to only a particular surface chemistry. For example, salinization, a commonly used chemical linker-mediated immobilization approach to biofunctionalize orthopedic substrates, is limited to only hydroxylated substrates bearing a high concentration of OH groups <sup>13,14</sup>. Further, the wet-chemical methods for covalent biofunctionalization are often time-consuming and complex, requiring multi-step processes. For example, the processing time for linker-mediated protein immobilization approaches is typically in the order of days <sup>9</sup>. Another undesirable aspect of such wet-chemistry methods is the extensive waste produced in the process, making them environmentally questionable. In addition, many side reactions may occur during the multi-step processes, producing by-products that may reduce the overall reproducibility and introduce significant challenges to obtaining regulatory approvals <sup>9</sup>.

We have recently introduced ion-assisted plasma polymerization (IPP) as a versatile, alternative method to biofunctionalize surfaces. In this technology, a radical-rich, polymeric-like layer is created on the surface using an organic precursor monomer such as acetylene, while the substrate is negatively biased in a pulse manner <sup>15-18</sup>. Pulse biasing the substrate during the IPP process facilitates the energetic ion bombardment of the coating as it grows, resulting in the formation of a high concentration of reactive radicals buried within the plasma polymer structure. These radicals, stabilized in pi-conjugated nanoclusters, migrate to the surface, where they enable the covalent attachment of a wide range of organic and inorganic bioactive compounds <sup>19</sup>. The covalent attachment is carried out in a single step and at room temperature without needing additional reagents. Such a reagent-free immobilization approach also permits control of the density and orientation of molecules on the surface by simply applying an external electric field and/or tuning the solution pH containing the biomolecules <sup>20</sup>. Surface-embedded radicals created by enhanced ion bombardment of polymeric substrates can also enable the reagent-free polymerization of hydrogel layers that are covalently attached to the surface <sup>21</sup>.

In the context of bone implants, a range of bioactive substrates has the potential to improve clinical outcomes. It is speculated that CSA antibiotics would be ideal candidates for surface immobilization. CSAs are a class of small molecule agents that disrupt bacterial membranes and are bactericidal against Gram-positive and Gram-negative bacteria <sup>22</sup>. They act in a manner similar to antimicrobial peptides but have comparatively reduced cytotoxicity and greater *in vivo* stability <sup>23</sup>. Local CSA-90 delivery has been shown to prevent *S. aureus* infection in small animal orthopedic models <sup>24-26</sup>. However, IPP coating can be used to immobilize and present a variety of bioactive agents, including proteins such as BMP2 <sup>17</sup>, peptides such as MEL4 and caspofungin <sup>16</sup>, and silver nano-particles <sup>15</sup>.

Despite all these intriguing potential applications of the IPP technology in biomimetic surface engineering; to date, it has been limited to only 2D substrates. As almost all biomedical devices are in 3D form, to achieve homogenous and robust coatings on 3D surfaces, new technologies with bespoke reactor designs and geometries are needed. As schematically illustrated in Figure 1, here we present a new ion-assisted plasma polymerization process using a rotating cage made of an electrically conductive mesh that is negatively biased and rotates while immersed in RF plasma. We hypothesized that this strategy enables the deposition of radical-rich polymeric coatings onto 3D surfaces for their subsequent covalent biofunctionalization in a single-step, reagent-free process. IPP's efficacy as a surface modification method using CSA-90 was tested for antimicrobial potential using both *in vitro* assays and an *in vivo* model of stainless-steel pin infection.

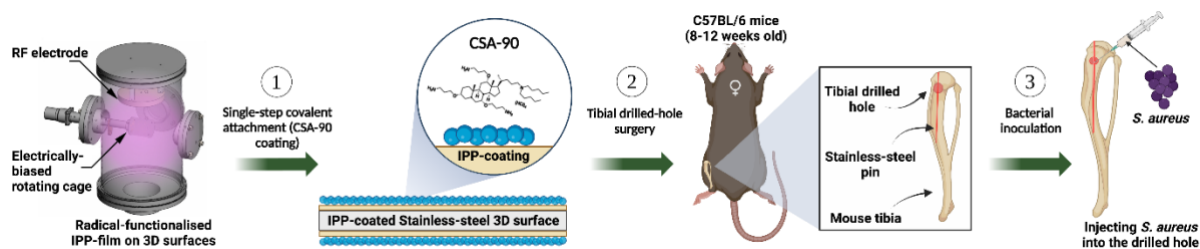


Figure 1. Schematic illustration of the ion-assisted plasma polymerization process to form radical-rich coatings on 3D materials for CSA-90 covalent biofunctionalization. The antibacterial efficacy of the coatings to reduce *S. aureus* infection-related bone loss was evaluated in a murine model of orthopedic infection.

## 2. Materials and Methods

### 2.1. Materials

Silica beads (1 mm diameter) were purchased from Sigma-Aldrich. Double-side polished silicon wafers (10 mm × 10 mm) were ultrasonicated in acetone and ethanol each for 10 min, then dried using a stream of nitrogen gas before film deposition. Stainless-steel (SS) Kirshner-wires (1.1 mm in diameter) cut to 1 cm segments referred to as SS rods were obtained from Zimmer, Warsaw, Indiana, USA. Stainless steel pins (size 000) were purchased from the Australian Entomological Supplies Pty Ltd (South Murwillumbah, Australia). CSA-90 was obtained from Prof Paul Savage (Brigham-Young University, Provo, Utah, United States). Approximately 6 ml of Milli-Q water was added to 9.6 mg of CSA-90 to produce a clear solution.

### 2.2. Ion-assisted plasma polymerization on 3D substrates

Ion-assisted plasma polymerized films were deposited on silica beads, stainless-steel pins and silicon wafer substrates using a retrofitted plasma polymerization system (Figure 2A) equipped with a rotating cage (Figure 2B). The plasma polymerization system, without the rotating cage, has been described in detail previously<sup>16,27,28</sup>. The rotating cage coupled to a pulse generator was installed into the side of the chamber to enable homogenous plasma polymerization of IPP films on the 3D objects, i.e., silica beads and stainless-steel pins. The cage contained a stainless-steel mesh outer lining supported by two inner rods. The plasma polymerization system was equipped with a radio frequency (RF) electrode and a DC-pulsed voltage source connected to the rotating cage. Approximately 450 silica beads, or 20 SS pins were used for each deposition. In each batch, a silicon wafer (10 mm × 10 mm) was attached to the inner rod of the rotating cage. The bias voltage pulses applied to the rotating cage were generated by a

RUP-6 pulse generator (GBS-Electronik) at 3 kHz for a pulse duration of 20  $\mu$ s. The cage rotation motor was set to 2.5 V, providing ten revolutions per minute. Prior to ion-assisted plasma polymerization and once the chamber base pressure was below  $5.0 \times 10^{-5}$  Torr, the silica beads or SS pins, silicon wafer, and the cage were cleaned using argon plasma (Ar flow rate = 40 standard cubic centimeters per minute (sccm)) at 75 W and -500 V pulsed bias applied to the cage for 10 minutes. Then, a mixture of 5 sccm acetylene and 25 sccm argon was injected into the chamber, and the pressure was adjusted to 110 mTorr. The pulse bias voltage was varied from 0 to 1000 V, while the RF input power was kept unchanged at 50 W. The polymerization time for each coating process was 15 minutes unless otherwise stated.

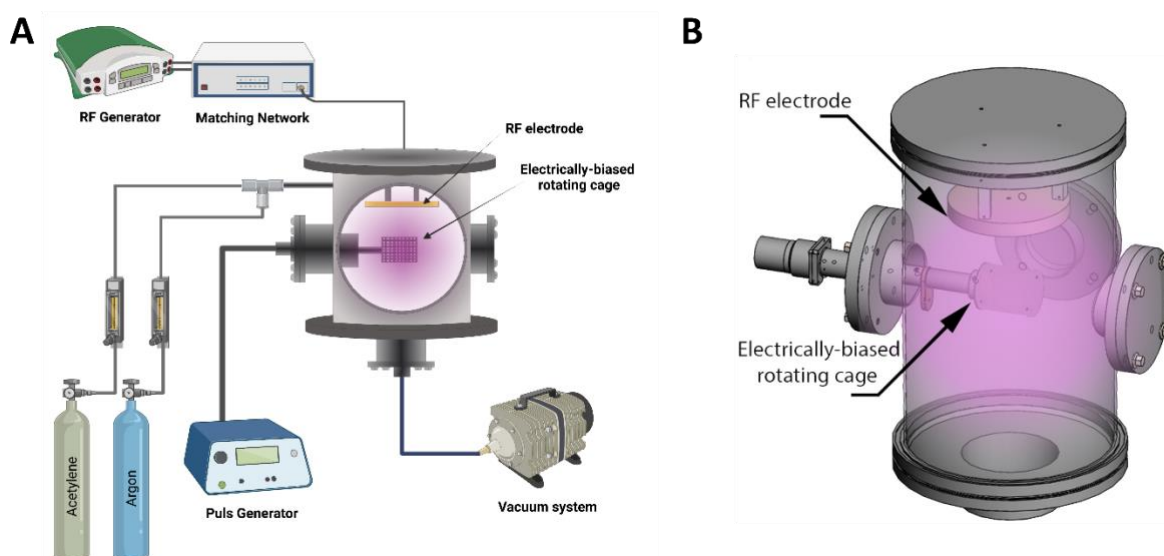


**Figure 2:** (A) Schematic illustration of a retrofitted plasma polymerization system equipped with (B) a negatively biased rotating cage to create IPP coatings on 3D materials.

### 2.3. X-ray photoelectron spectroscopy (XPS)

The surface chemistry of IPP-coated materials was analyzed using a SPECS FlexMod spectrometer within 24 hours after deposition. The spectrometer was equipped with a hemispherical analyzer (PHOIBOS 150), an MCD9 electron detector, and a monochromatic X-ray source, operating at 10 kV and 20 mA (AlK $\alpha$ ,  $h\nu = 1486.7$  eV). The samples were mounted on the holder using double-sided, conductive carbon tape. Each sample was measured at a take-off angle of 90 degrees once the base pressure was below  $5.0 \times 10^{-8}$  mbar. The survey spectra were obtained at a pass energy of 30 eV (0.5 eV resolution) over an energy range of 0-1000 eV. The carbon high-resolution (C1s) spectra were collected at pass energy of 20 eV and 0.1 eV resolution. Calculations of the atomic concentrations of

elements and curve fittings of high-resolution spectra were carried out using CASA XPS software (version 2.3.14).

### 2.4. Time of flight secondary ion mass spectrometry (ToF-SIMS)

ToF-SIMS data were obtained using a nanoTOF instrument (PHI TRIFT V, Chanhassen, MN) with a 30 eV pulsed liquid ( $^{79}\text{Au}^+$ ) metal primary ion source (LMIG). All measurements were carried out in the positive mode of SIMS at the base pressure below  $5 \times 10^{-6}$  Pa. Dual charge compensation was achieved by employing an electron flood gun and  $\text{Ar}^+$  ions at 10 eV. The raster size was recorded for at least six spots with areas of  $100 \mu\text{m} \times 100 \mu\text{m}$  per sample. WincadenceN software (version 1.8.1, Physical Electronics) was utilized for all spectral analyses.

### 2.5. Spectroscopic Ellipsometry

To estimate the cross-linking degree of the IPP coatings deposited on silicon wafers, their refractive indices were measured using a J.A. Woollam spectroscopic ellipsometer (EC-400 light source). Measurements were carried out at incidence angles of 65, 70 and 75 degrees and the data were analyzed using the WVASE32 software. All measurements were taken within a wavelength range of 200–1000 nm with 5 nm steps. A Cauchy model was applied to obtain a fit of the data to calculate the thicknesses and refractive indices.

### 2.6. Electron paramagnetic resonance (EPR) spectroscopy

An ADANI SPINSCAN X EPR device was used to assess the concentration of radicals embedded in the coatings on the IPP-coated silica beads. The silica beads were placed in a 3 mm diameter quartz tube and secured with a Teflon holder approximately 9.5 cm from the middle of the sample cavity. The central magnetic field was set to 336 mT, and the modulation amplitude was 200  $\mu\text{T}$ . The data from an average of 10 scans were reported.

### 2.7 Stability evaluation in Tyrode's simulated body fluid (SBF)

Tyrode's solution was used as a biologically relevant medium to evaluate the robustness of the IPP coatings deposited on silica beads. IPP-coated silica beads were placed in a falcon tube and covered with 0.5 ml of Tyrode's solution with the chemical composition listed elsewhere<sup>27</sup>. After one month (at  $37 \pm 1^\circ\text{C}$ ), the SBF solution was removed, and each sample was rinsed with 1 ml of MilliQ water

three times, followed by drying with a stream of nitrogen gas. XPS spectra of the washed samples and SEM images were obtained within 24 hours.

### 2.8. Scanning electron microscopy (SEM)

The physical stability of the IPP-coated silica beads incubated in SBF solution (1 month at  $37 \pm 1^\circ\text{C}$ ) was evaluated using SEM micrographs. The SEM images were obtained using a Phenom Table-top SEM at a vacuum pressure of 60 Pa, an acceleration voltage of 10 kV and a working distance of 7 mm.

### 2.9. AF488 antibody covalent attachment and fluorescence imaging

To confirm attachment and demonstrate the homogenous distribution of attached biomolecules on the IPP-coated 3D materials (silica beads and SS pins), we used Alexa Fluor 488-conjugated IgG antibody (4  $\mu\text{g}/\text{ml}$ , Abcam, USA) as an example biomolecule. The materials were incubated in the AF488 antibody solution for one hour at room temperature. Pre-wash images were taken by imaging the surfaces using an upright fluorescence microscope (Zeiss Z1, Oberkochen, Germany) with a  $5\times$  objective and an exposure time of 200 ms. Samples were then individually transferred to 50 mL falcon tubes filled with 5% sodium dodecyl sulfate (SDS, Sigma-Aldrich, USA) in sterile MilliQ water and allowed to rotate for four hours at room temperature to desorb unbound AF488 antibody from the implant surface. The samples were then re-imaged using the same imaging protocols to obtain post-wash images.

### 2.10. Bacterial culture

Patient-derived *Staphylococcus aureus* (American Type Culture Collection-12600) stored at  $-80^\circ\text{C}$  in glycerol stocks was grown overnight on lysogeny broth (LB) agar plates at  $37^\circ\text{C}$ , and single colonies were picked for culture in lysogeny broth (LB) the day prior to surgical inoculation. Bacteria were quantified using a spectrophotometer (Cary 300 UV-Vis, Agilent, Las Vegas, NV) at 600 nm with an optical density of 1 representing  $1 \times 10^9$  colony-forming unit (CFU)/milliliter (mL). Colonies were picked the day before surgery and enabled 12-hour growth in LB broth to ensure accurate quantification of live/active bacteria from broth culture for inoculation.

### 2.11. Beads and antimicrobial coating *in vitro* assay

Silica beads (1 mm) were modified by various coatings: IPP coating only, IPP coating with CSA-90, CSA-90 without IPP coating, and IPP coating with CSA-90 washed with 5% sodium dodecyl sulphate



(SDS) at 70°C for 1 hr. For CSA 90 coating processes, 60 uncoated or IPP-coated silica beads were covered for 12 hours at room temperature with 300 µl of CSA-90 solution (1 mg/ml). The CSA-90 solution was removed, and the samples were rinsed with copious amounts of MilliQ water three times. The coated silica beads were then placed in either LB with  $10^3$  CFU of *S. aureus* (Figure 3A) or sterile LB after inoculating  $10^4$  CFU of *S. aureus* on the surface and air-dried for ten minutes (Figure 3B).

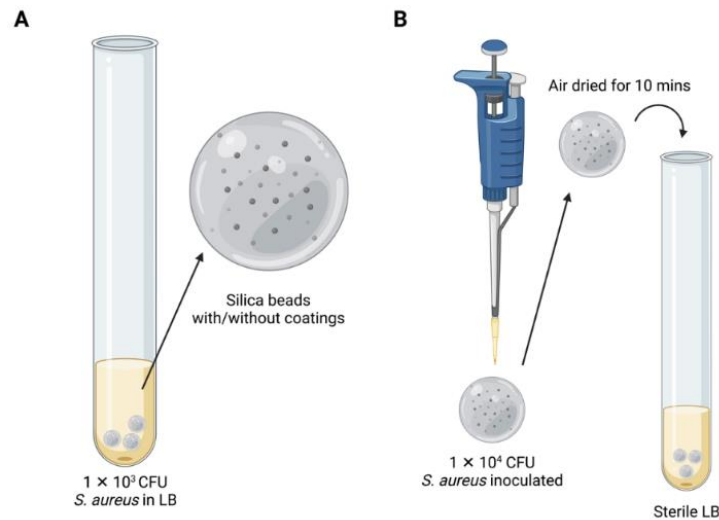


**Figure 3:** Schematic illustration showing the *in vitro* assay used for testing the antimicrobial properties of coated glass beads.

### 2.12. Covalent attachment of CSA-90 on stainless steel pins

For *in vitro* validation of the coating on metallic implants, stainless steel (SS) Kirshner-wire (Zimmer, Warsaw, Indiana, USA) cut to 1 cm segments (1.1 mm in diameter) was used. For surgery, stainless-steel pins (size 000) were purchased from the Australian Entomological Supplies Pty Ltd (South Murwillumbah, Australia). The SS surfaces were coated by IPP as described in 2.2 prior to drug coating. Pins were then bathed in a 1 mg/mL CSA-90 solution in a petri dish for 12 hours on a shaker, subsequently air-dried in an incubator (37 °C) overnight and stored at room temperature.

### 2.13. Animal ethics and study design

C57BL/6 12-week-old female mice (n=30) were purchased from the Australian BioResources (Moss Vale, NSW, Australia). They were group-housed 5-6 per cage with access to food and water *ad libitum*. Mice could acclimatize for a week prior to surgery. Animal work was approved by the local Animal Ethics Committee (K339) and carried out in accordance with the Australian Code for the Care and Use of Animals for Scientific Purposes (2013). Prior to surgery, mice were randomly assigned to 3 groups

(n=10 per group) to be surgically implanted with stainless-steel pins that were (i) uncoated, (ii) coated by ion-assisted plasma polymerization (IPP), or (iii) coated by IPP and subsequently incubated in CSA-90.

### 2.14. Orthopedic Surgical Model

Surgical anesthesia was induced with intraperitoneal ketamine (75 mg/kg) and xylazine (10 mg/kg) and maintained with inhaled isoflurane (2-3% per 1.5-2L oxygen) as required. The right leg of each animal was shaved and treated with a topical povidone-iodine solution before surgery.

A medial parapatellar approach was used to access the right proximal tibia. A hole (0.5 mm in diameter) was made at the right tibial metaphysis (below the growth plate) using a surgical drill (Stryker® 5100-15-250 Straight, Kalamazoo, USA), exposing the medullary canal adjacent to the drilled hole for bacterial infection. A stainless-steel pin was inserted through the subchondral bone at the knee, adjacent to the hole defect. After that,  $1 \times 10^6$  CFU *S. aureus* in 5 µL was injected directly into the drilled hole with a Hamilton syringe and needles (Hamilton Company, Nevada, USA) immediately after the pin insertion. The incision was closed with 5-0 Vicryl (Ethicon LLC, Puerto Rico, USA), and no dressings were applied to the wound. Baseline radiographs were taken at the time of surgery. Animals recovered on a heated pad after surgery and were given normal saline (200 µL) subcutaneously for rehydration. Buprenorphine (0.1 mg/kg) was given subcutaneously one hour prior to surgery and then every 12 hours for three days for post-operative analgesia.

Animals were monitored daily by experienced staff and had twice-weekly radiographs performed under anesthesia (inhaled isoflurane) using digital X-ray (Faxitron Bioptics, Tuscan, AZ) at 25 kV (five seconds) with  $\times 2$  magnification. X-ray images were assessed by orthopedic surgeons and veterinarians blinded to treatment. To minimize animal pain and distress, animals showing overt physiological and/or radiological evidence of infection judged by declining overall health (loss of body weight, lethargy, pyrexia, poor coat condition, non-weight bearing, and inflammation of the surgical site) or radiological evidence of worsening infection (localized osteolysis at the tibia and joint) were prematurely euthanized to avoid sepsis. The remaining mice were euthanized by carbon dioxide inhalation at three weeks postoperatively.

### 2.15. Sample collection and analysis

A biopsy of the soft tissue adjacent to the bone defect was taken after the incision under aseptic conditions. The surgical pin was pulled out from the joint by a sterile needle holder. All specimens were placed in Luria-Bertani (LB) broth (1 mL) for bacterial culture. A bone swab was collected at the defect site and resuspended in the LB broth for 15 seconds. Pus samples (if present) were also collected by

swab for bacterial culture. The right femora and tibiae were harvested. The bacterial culture was incubated overnight at 37°C. Positive and negative results were determined by the media turbidity and quantified using a plate spectrophotometer (SpectraMax® iD3, Molecular Devices, San Jose, USA) at 600 nm.

For micro-CT, the right tibiae were fixed in 10% formalin for 24 hours and transferred to 70% ethanol before being scanned with a SkyScan 1272 micro-computed tomography (micro-CT) scanner (SkyScan, Kontich, Belgium). All samples were scanned in 70% ethanol-soaked kimwipe at 50 kV and 200  $\mu$ A using a 0.5 mm aluminium filter. Images were scanned at a pixel resolution of 9  $\mu$ m, reconstructed with NRecon, straightened using DataViewer and analyzed with CTAn software (SkyScan). A global threshold to define bone tissue was set at 0.4 g/cm<sup>3</sup> calcium hydroxyapatite, calibrated using two phantom samples of a known density. Bone morphometric outcomes included bone volume (mm<sup>3</sup>), tissue volume (mm<sup>3</sup>), and bone tissue mineral density (g/cm<sup>3</sup>). Three-dimensional reconstructions were generated using CTVox software (Skyscan).

### 2.16. Decalcification and paraffin histology

The tibiae were decalcified in 0.34M EDTA (pH 8.0) solution at 4°C on a shaker for two weeks with solution changes twice a week. Samples were next embedded in paraffin and sectioned coronally through the tibial drilled hole at a thickness of five microns. Mounted sections were stained with hematoxylin and eosin (H&E) to differentiate bone and show the bone defect region.

### 2.17. Statistical analysis

Statistical power calculations and analyses were performed using GraphPad Prism (La Jolla, California), and the cut-off for significance was set at  $p < 0.05$ . The micro-CT data from the *in vivo* study were analyzed using a Kruskal-Wallis test for multiple groups, followed by a non-parametric post-hoc Mann-Whitney U test to compare individual groups.

## 3. Results and Discussion

### 3.1. Ion-assisted plasma polymerization on 3D objects

Plasma polymerization has been predominantly applied to coat planar substrates with negligible to moderate curvatures. However, almost all structures of interest for biomedical engineering applications, such as implantable medical devices, are three-dimensional. To deposit robust and homogeneous IPP coatings on 3D surfaces, we exploited a new strategy using an electrically conductive mesh connected to a high-voltage power supply that rotates while immersed in the RF plasma of a polymerizable gas.

We hypothesized that this novel design would permit homogenous deposition of radical-rich IPP coatings on 3D objects while also accelerating plasma ions towards the 3D objects, thus achieving strong substrate-coating adhesion and significant concentrations of radicals embedded in the coating. To verify this hypothesis, we initially used silica beads as simple, model 3D substrates and evaluated the role of the applied bias voltage ( $V_b$ ) in producing the IPP coatings for subsequent covalent attachment of biomolecules. Figure 4A shows the XPS surface chemical composition of IPP films as a function of pulsed bias voltage ( $V_b$ ). The uncoated silica beads show surface atomic concentrations of approximately 25%, 48% and 26% for silicon, oxygen, and carbon, respectively. XPS results showed that by the deposition of IPP coatings on the beads, the atomic concentration of carbon increased to ( $80 \pm 3$ )%, while those of silicon and oxygen decreased to ( $5 \pm 1$ )% and ( $13 \pm 2$ )%, respectively. Such changes in the surface chemistry indicate the presence of IPP coatings on the surfaces, resulting from successful ion-assisted plasma polymerization of the acetylene and argon mixture on the beads. The deposited IPP coating reduces the silicon and oxygen signals originating from the underlying substrate, thus resulting in a drop of their atomic concentrations.

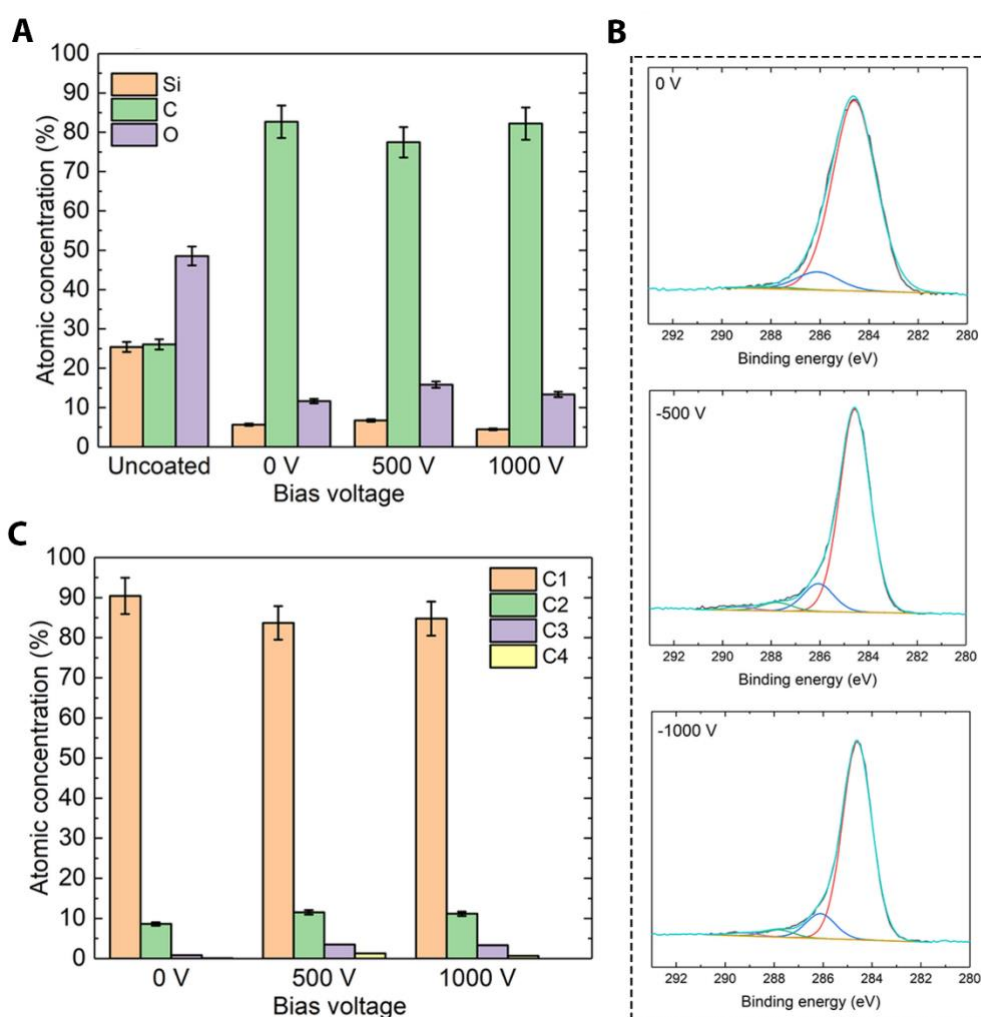


**Figure 4:** XPS Surface chemistry of IPP coatings deposited on silica beads as model 3D substrates (A) XPS elemental composition of uncoated and IPP-coated silica beads as a function of bias voltage. (B) XPS C 1s high-resolution spectra of IPP films. The spectra are curve-fitted using three components: C1: C–C/C–H, C2: C–O, C3: C=O, and C4: COOH. (C) Area percentage for carbon-containing components (C1 – C4) fitted in C1s high-resolution spectra as a function of bias voltage.

To further evaluate the chemistry of IPP coatings, we curve-fitted the C1s high-resolution spectra, as shown in Figure 4B. Three peaks associated with C–C/C–H at binding energy (BE)  $\sim$  284.6 eV, C–O at BE  $\sim$  286.5 eV, C=O at BE  $\sim$  287.5 eV, COOH at BE  $\sim$  289 eV were fitted in the C1s high-resolution spectra with their area percentage values plotted in Figure 4C. As the bias voltage increases, the C1s peak becomes narrower. The highest concentration of C1 compounds and the lowest concentration of C2 and C3 groups are observed for the coating prepared using the bias voltage of 0 V. These results suggest that a higher concentration of oxygenated carbon-containing moieties is formed on the surfaces for higher applied bias voltages. Such an increase in the concentration of oxygenated groups at higher bias voltages is explained by the greater ion bombardment that occurred on the growing film, resulting in the formation of a high concentration of radicals susceptible to post-deposition oxidation. The post-deposition oxidation of plasma polymer films, also referred to as auto-oxidation<sup>29</sup>, is an inevitable process that has also been previously observed for other hydrocarbon precursor monomers such as 1,7-octadiene<sup>30,31</sup> and thiophene<sup>32,33</sup>.

We used electron paramagnetic resonance (EPR) spectroscopy to evaluate the differences in the number of electron spins, i.e., the concentration of radicals created in the IPP coatings. The EPR spectra of the IPP coatings deposited using the V<sub>b</sub> values of 0, –500, and –1000 V are plotted in Figure 5. The EPR spectra, measured ten days post deposition, are broad and show single resonance peaks. The resonance peak intensity increases by increasing the applied bias voltage, indicating that higher concentrations of radicals are embedded within the IPP structure. During the growth of plasma polymers, the film-forming compounds on the surface are continuously bombarded by photons, electrons, as well as positively charged ions<sup>34</sup>. These interactions between the growing coating and the reactive species present in the plasma phase produce radicals that can be trapped within the coating structure. In the case of IPP coatings polymerized using a rotating cage, higher bias voltages applied to the cage result in greater degrees of energetic ion bombardment onto the 3D materials. This strategy, in turn, increases the fragmenting chance of acetylene molecules, bond cleavage, and chain scission, resulting in the formation of higher concentrations of reactive radicals within the growing IPP coating. Using 2D substrates, such as titanium and stainless steel, we have previously shown that such radicals are mobile and migrate from sub-surface reservoirs to the surface in a thermally activated manner, where they facilitate the covalent attachment of bioactive molecules<sup>20</sup>. The EPR results shown here underpin the

importance of bias voltage applied to the rotating cage in producing high concentrations of radicals for subsequent covalent biomolecule functionalization onto 3D objects.

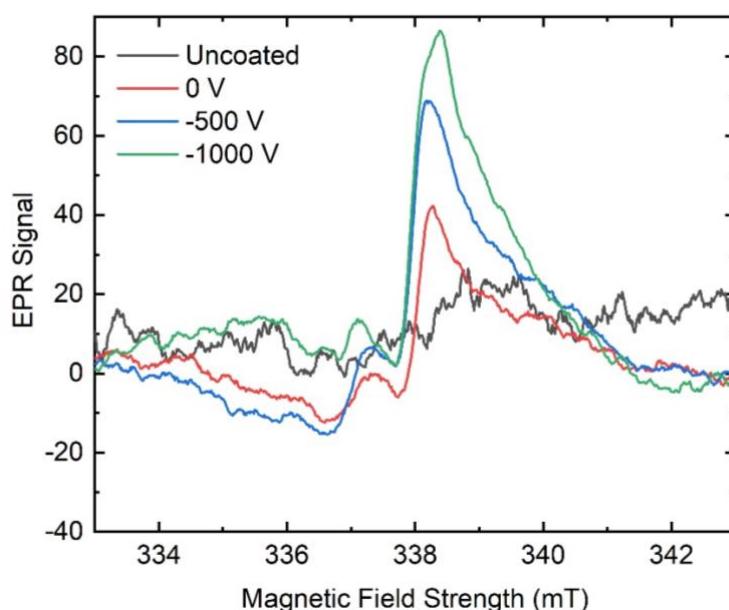


**Figure 5:** EPR spectra of IPP coatings deposited on silica beads using bias voltages of 0, –500, and –1000 V.

The chemical stability of the IPP coatings is an essential factor for their application in the surface engineering of biomedical devices, particularly for orthopedic implants. Extensive oxidation of a polymeric coating once exposed to aqueous media can result in the deterioration of its integrity<sup>35</sup>. The degradation rate of a polymeric coating exposed to biological media depends on the diffusion rate of oxygen and water molecules throughout the film thickness and the availability of reactive sites for the formation of metastable compounds during the early stages of oxygen uptake<sup>34</sup>. To investigate the role of ion bombardment on the stability of the IPP films deposited on silica beads, we examined their XPS surface chemistry after incubation in Tyrode's Simulated Body Fluid (SBF) at 37 °C for one month. Tyrode's salt-balanced solution has been commonly used in the testing of biomaterials<sup>36-39</sup>. The XPS elemental composition of the coatings after SBF incubation is shown in Fig 6A. These results indicate that the coating deposited at the highest voltage bias of -1000 V shows the lowest chemical stability as indicated by the highest variations in its surface chemistry after SBF incubation, where the most significant increase in oxygen and decrease in carbon atomic concentrations are observed. These changes in surface chemistry are consistent with the peak-fitted XPS high-resolution C1s spectra (Figure 6B) and the changes in the calculated area percentage of various carbon-containing components presented in Figure 6C. The XPS data show that the most significant changes in the concentrations of C = O and COOH groups are observed for the coating deposited at – 1000 V. The higher oxidation rate observed for the IPP coating deposited at -1000 V is explained by its greater content of embedded

radicals, as indicated by EPR spectra (Figure 5). This observation is also in good agreement with other works in which it has been shown that plasma polymer films containing higher concentrations of radicals suffer from a greater degree of oxidation and hydrolysis<sup>34,40,41</sup>.

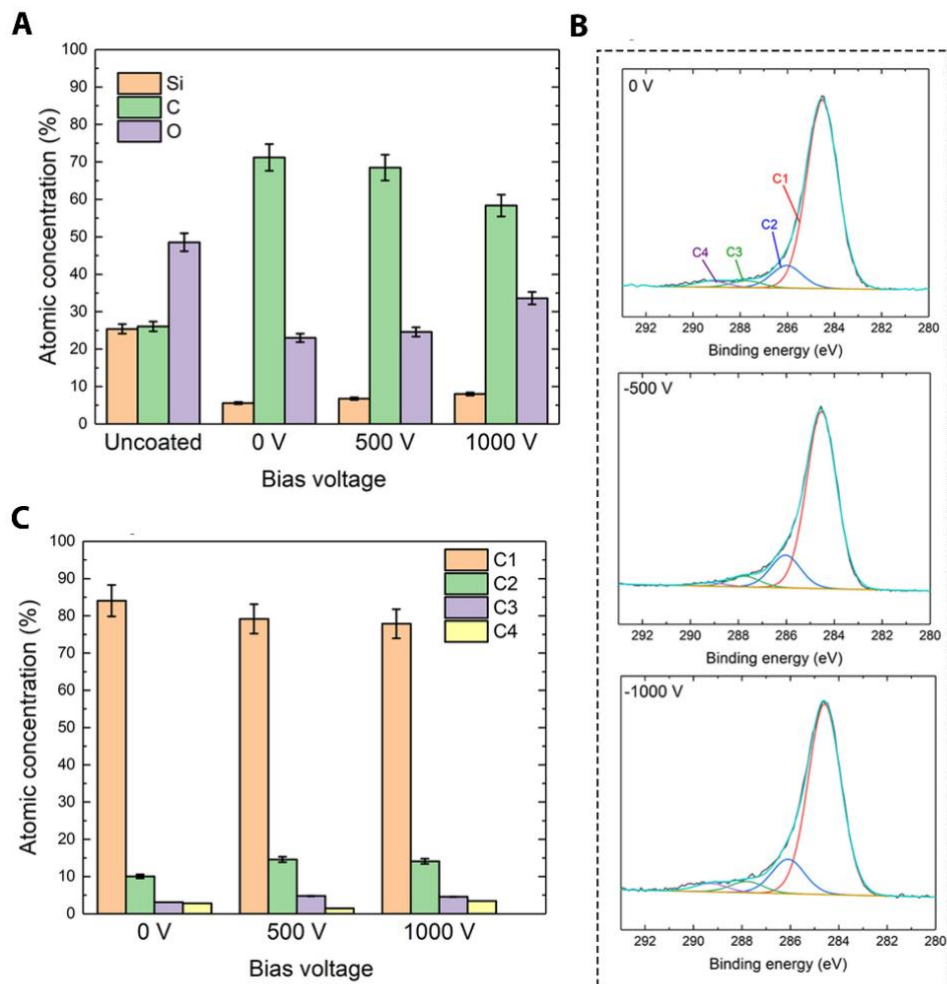


**Figure 6:** Surface chemistry of IPP coatings after incubation in SBF at 37°C for 1 month. **(A)** XPS elemental composition of IPP-coated silica beads as a function of bias voltage after incubation in SBF. **(B)** XPS C 1s high-resolution spectra of IPP films after incubation in SBF solution. The spectra are curve-fitted using three components: C1: C–C/C–H, C2: C–O, C3: C=O, and C4: COOH. **(C)** Area percentage for carbon-containing components (C1 – C4) fitted in C1s high-resolution spectra as a function of bias voltage.

In addition to the initial density of radicals embedded within the IPP structure, the cross-linking degree of the coating is also an essential factor that can regulate oxidation kinetics. To evaluate the cross-linking degree of the IPP coatings deposited at varied bias voltages, we used spectroscopic ellipsometry and measured their refractive indices at 630 nm, plotted in Figure 7A. The refractive index of a polymer is correlated with its degree of cross-linking and density<sup>42,43</sup>. The coatings deposited using bias voltages



of 0 and  $-500\text{ V}$  showed refractive indices of approximately 1.6, whereas a refractive index of approximately 1.7 was achieved for the coating deposited using a bias voltage of  $-1000\text{ V}$ . The higher refractive index measured for the  $-1000\text{ V}$  IPP coating is attributed to the higher fluxes of energetic ions arriving at the substrate, thus, greater fragmentation and recombination of deposited species, yielding highly cross-linked structures. In previous work carried out on flat titanium and silicon wafer surfaces, we observed that the oxidation kinetics could be moderated in an extremely dense and highly cross-linked IPP structure with an  $n$  value of as high as 1.8<sup>44</sup>. Such highly cross-linked structures limit the oxygen diffusion into the surface and the mobility of structural elements, including the secondary radicals, e.g.,  $\text{C-O-O}\cdot$ , generated from oxidation. In the current work on 3D substrates, however, a maximum refractive index of 1.7 was achieved, leaving the high concentration of reactive radicals as the primary factor for regulating the oxidation kinetics.

All the IPP coatings deposited using negative bias voltages of  $0 - 1000\text{ V}$  showed excellent physical stability upon incubation in the SBF solution, as indicated by SEM micrographs obtained before and after incubation, shown in Figure 7B. From the SEM images, no evidence of physical failure in delamination, cracking or buckling was witnessed, indicating that sufficient adhesion between the IPP coatings and the underlying substrate has been achieved. Informed by these surface characterization results and based on the criteria of chemical stability and concentration of embedded reactive radicals, we used the IPP coating deposited at  $V_b = -500\text{ V}$  for all subsequent experiments.

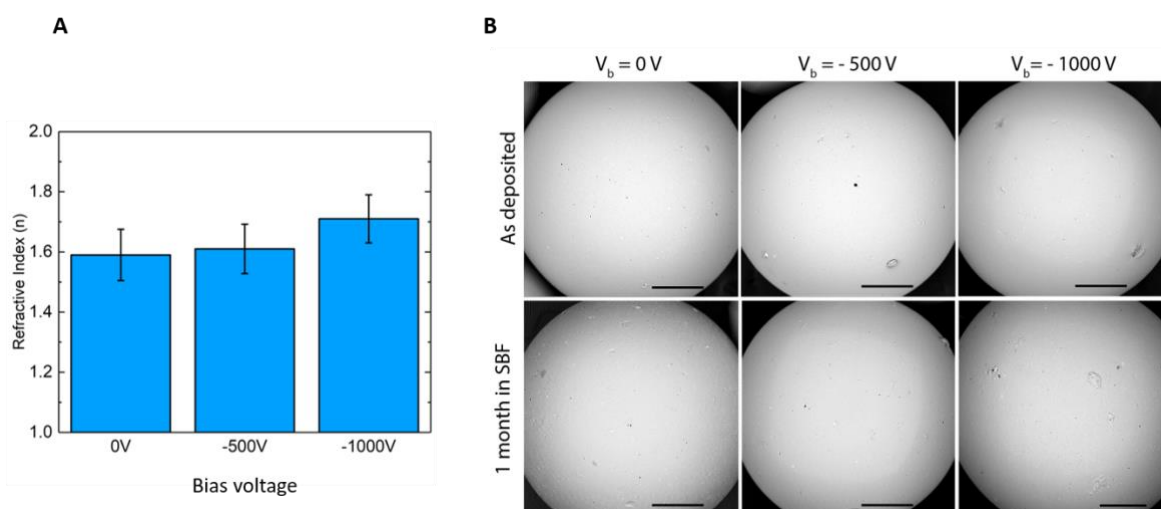


**Figure 7:** (A) Refractive indices of IPP coatings (at 630 nm) obtained using spectroscopic ellipsometry. The coatings were deposited on silicon wafers using various bias voltages as indicated. (B) SEM images of IPP coatings deposited on silica beads using applied bias voltages of 0,  $-500$ , and  $-1000\text{ V}$  before and after 1 month incubation in SBF. Scale bar =  $200\text{ }\mu\text{m}$ .



To evaluate the influence of ion-assisted plasma polymerization time on the surface chemistry, and homogeneity of the coatings, we varied the deposition time from 0 to 20 minutes while the bias voltage was kept constant at  $-500$  V. The XPS atomic concentrations of uncoated and IPP-coated silica beads as a function of polymerization time are shown in Figure 8A. An increase in the polymerization time resulted in an increase in carbon atomic concentration and a decrease in the concentrations of silicon and oxygen. The increase of carbon atomic concentration versus deposition time is due to the polymerization and deposition of more hydrocarbon fragments from the acetylene precursor onto the silica bead surfaces. The decrease of silicon and oxygen concentrations, on the other hand, is due to the reduction of the signals originating from the underlying substrate. For a polymerization time of 25 minutes, no contribution of silicon in the XPS surface chemistry was detected, indicative of the formation of IPP coating with a thickness larger than the sampling depth of XPS that is 8 -10 nm <sup>45</sup>. The absence of silicon signals also suggests that the IPP coating deposited for 25 min is conformal and continuous, fully concealing the silica bead substrate. While no oxygen was present in the precursor gas mixture (acetylene + Ar), ~8% oxygen was measured on the surface of this sample due to auto-oxidation, as previously explained.

The changes in XPS surface chemistry correlate well with ToF-SIMS normalized positive counts obtained for IPP coatings deposited at various deposition times, as shown in Figure 8B. The ToF-SIMS data demonstrate that by increasing the polymerization time, the counts of hydrocarbon species increase, whereas those of Si decrease. The major changes in ToF-SIMS positive counts are recorded for deposition times of up to 15 min, with no marked changes observed by increasing the deposition time to 25 minutes. These changes in surface chemistry indicate that at polymerization times longer than 15 minutes, the IPP coatings formed on the silica beads are thicker than the sampling depth of ToF-SIMS, which is in the range of 1-2 nm <sup>46</sup>. These changes in surface chemistry can also be visually observed from the ToF-SIMS imaging data shown in Figure 8C. The increase of C<sub>2</sub>H<sub>3</sub><sup>+</sup> counts, shown here as representative hydrocarbon species present on the IPP-coated surfaces, is evident from these ion distribution maps. Altogether from the XPS and ToF-SIMS results, we chose the ion-assisted plasma polymerization time of 25 minutes for all the subsequent experiments to ensure sufficiently thick coatings are formed on the 3D substrates including stainless-steel pins.

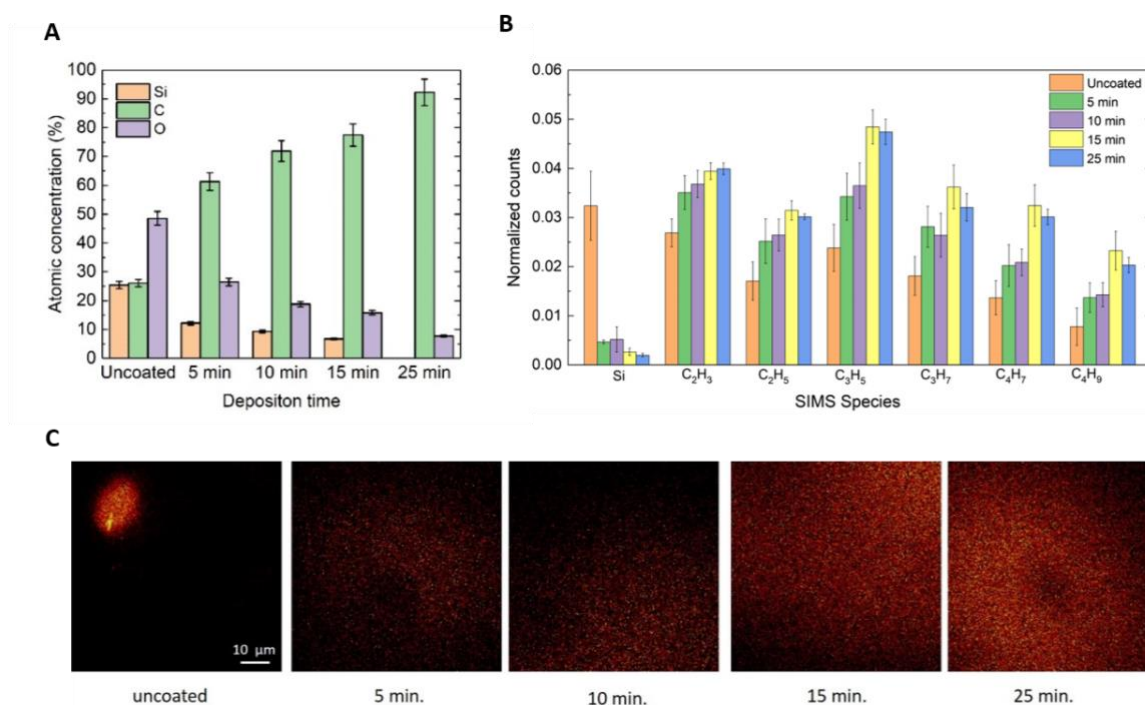


**Figure 8:** (A) Surface chemistry of the IPP-coated silicon beads deposited at -500V as a function of deposition time. (B) Surface chemistry results from ToF-SIMS showing normalized Si and hydrocarbon positive counts for various deposition times (C) ToF-SIMS distribution maps of C<sub>2</sub>H<sub>3</sub><sup>+</sup> obtained for IPP coatings prepared using various plasma polymerization times.

### 3.2 Covalent bio-functionalization of IPP-coated 3D objects

Fluorescently labelled IgG was used as a model molecule to image the homogeneity of covalent biofunctionalization achieved on silica beads and stainless-steel pins. Detergents such as SDS remove physically attached molecules but cannot remove covalently attached molecules<sup>47,48</sup>. From the images shown in Figure 9, homogenous covalent attachment of fluorescently labelled IgG onto the 3D surfaces is confirmed. The data show that the molecules were resistant to SDS detergent washing in the IPP-coated group, whereas most of the physically adsorbed IgG was removed from the uncoated surfaces.

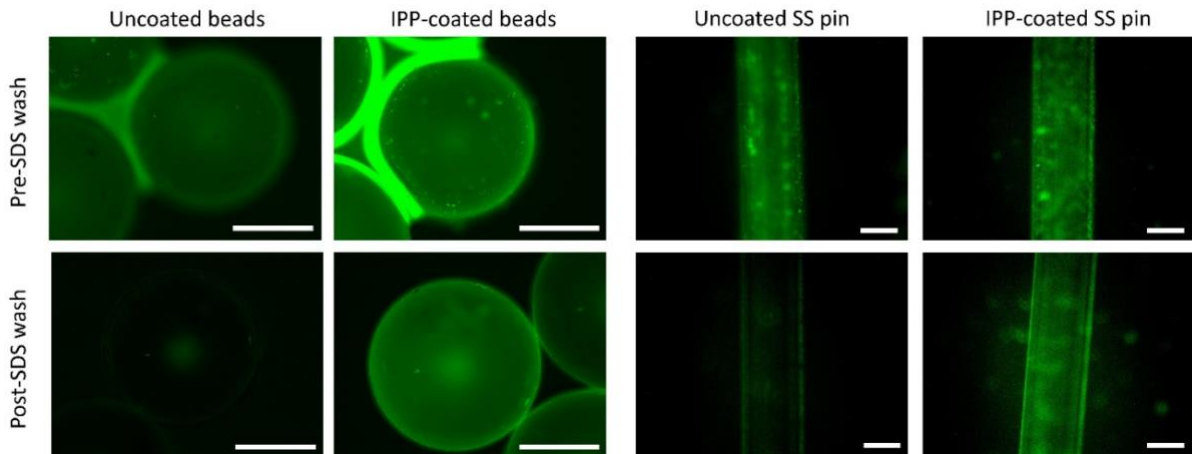


**Figure 9:** Alexa Fluor 488-conjugated IgG antibody on uncoated and IPP-coated silica beads and pins before and after SDS wash. Scale bar: 500  $\mu\text{m}$ .

### 3.3. CSA-90 functionalization

To functionally assess the antimicrobial effects of antimicrobial treatments, coated silica beads were exposed to *S. aureus*. The inoculated bacteria were allowed to air dry on the surface, and then beads were placed in a solution of nutrient media. As controls, PP-coated beads alone and unwashed PP + CSA-90 coated beads were included, giving positive and negative signals for bacterial growth. Beads where CSA-90 was adsorbed to the surface without plasma polymerization and then washed with a sodium dodecyl sulfate (SDS) solution did not impair bacterial growth, suggesting that CSA-90 was rapidly lost when washed. In contrast, PP + CSA-90 beads washed with SDS still showed potent antimicrobial activity in this assay (Figure 10A).

Next, 1 cm stainless-steel wire segments (analogous to those used in later mouse surgery) were tested for antimicrobial activity with and without PP + CSA-90 coating. Even with a higher inoculation dose of *S. aureus*, PP + CSA-90 coated wires showed a potent antimicrobial activity when grown in nutrient broth (Figure 10B).

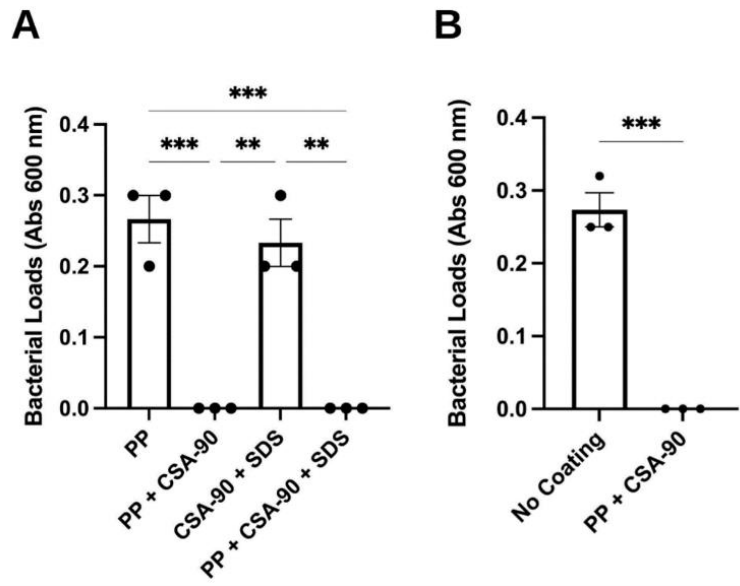


**Figure 10:** (A) The bacterial loads (absorbance at 600 nm) recovered from the silicon beads with *S. aureus* ( $1 \times 10^4$  CFU) inoculated and air dried. (B) The bacterial loads (absorbance at 600 nm) recovered from stainless-steel K-wire (1 cm in length) with *S. aureus* ( $1 \times 10^5$  CFU) inoculated on the surface. (Error bars: mean and SEM; Statistical analysis was completed using (A) 2way ANOVA and Turkey's Test and (B) unpaired t-test; \*\* p-value  $\leq 0.01$  and  $\geq 0.001$ ; \*\*\* p-value  $\leq 0.001$ )

### 3.4. Antibacterial activity in an infected fracture model

A preclinical murine orthopedic infection model was performed, where a localized bone defect was made in the proximal tibia and a stainless-steel pin was inserted into the intramedullary space as a nidus for biofilm formation and infection. Prior model development showed that a foreign surface adjacent to the bone defect (i.e., a metal pin) is required for reliable and progressive infection.

In the control group without any infection control measures, 8/10 developed pyogenic infections (pus present) and 8/10 were positive for bacteria by swab test at the study endpoint. Those with PP-coating only (no CSA-90) had 5/10 with pus, but 9/10 were positive for bacteria by swab test. The PP + CSA-90 group showed 5/10 with pus ( $p = 0.35$ ) and 4/10 with bacteria by swab test ( $p = 0.16$ ). While this did not reach statistical significance, bone loss imaged by radiography (Figure 11) and micro-CT (Figure 12A) suggested worse infection in the group featuring uncoated pins. Indeed, the quantification of bone loss in the drilled hole defects showed a more significant amount of regenerated bone with PP + CAS-90 coating compared to no coating, and it is higher than PP-coating alone (Figure 12B).

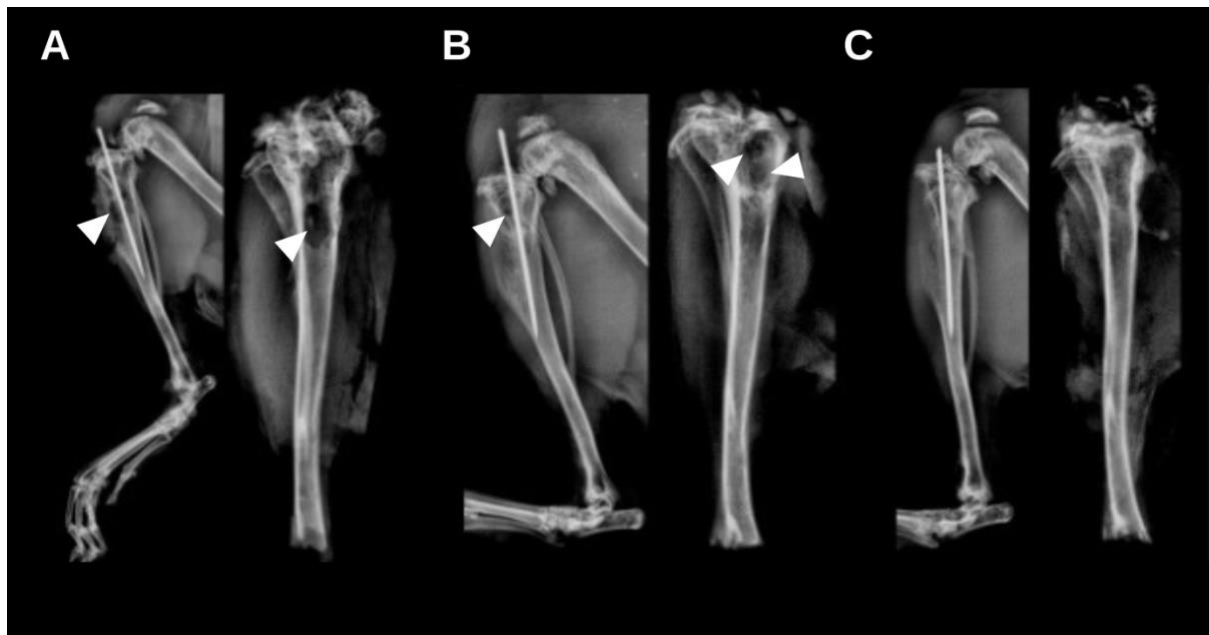


**Figure 11:** Radiographs (X-ray images) (A-C) showing osteolytic bone loss in infected tibiae with uncoated pins (A) and bone healing in select tibiae from groups with PP coated pins (B) and PP + CSA-90 coated pins (C). Radiographs show images before (left) and after (right) pin removal. The white arrows point to the osteolytic lesions of the tibial drilled hole due to infections.

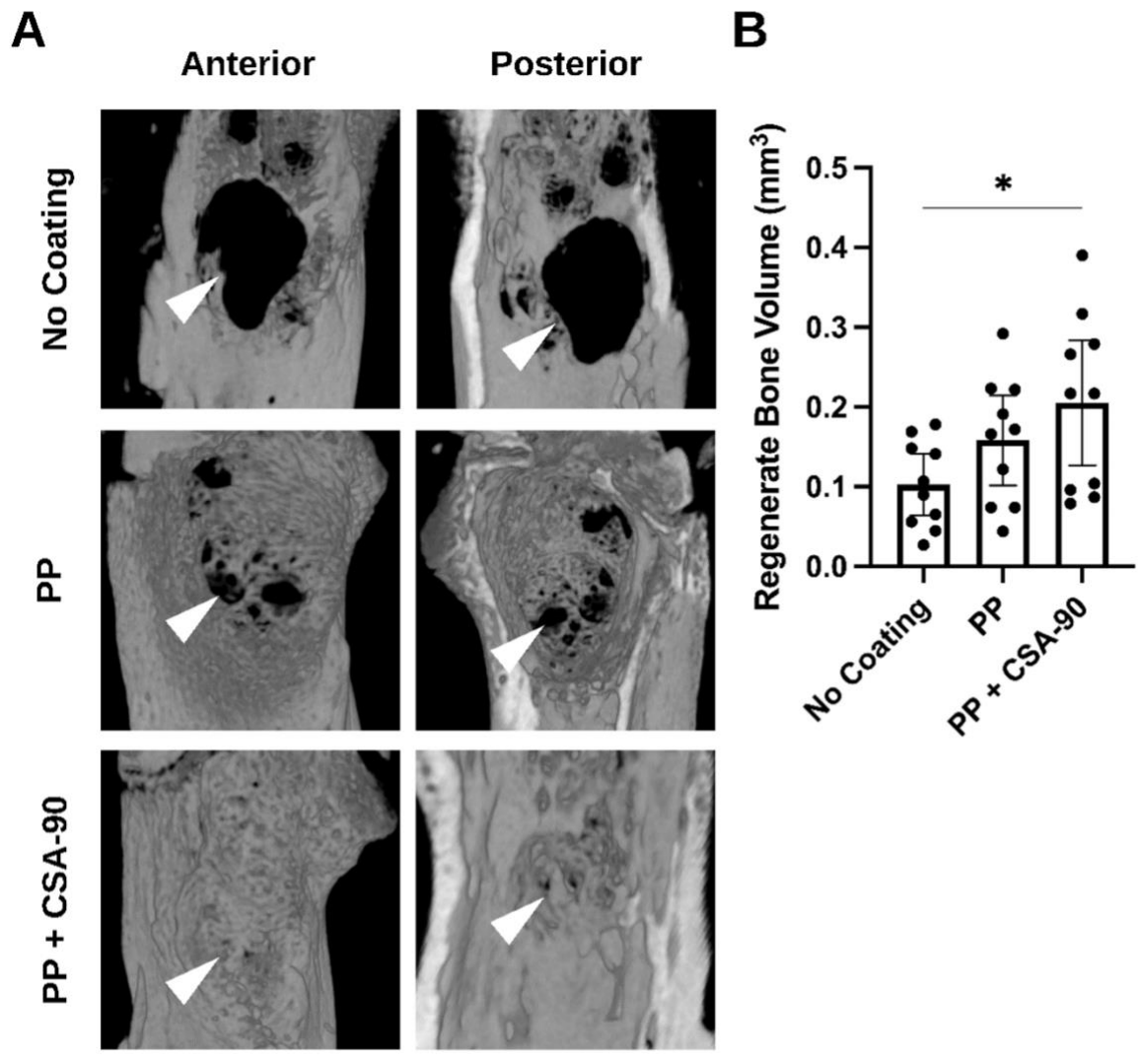


**Figure 12:** (A) Micro-CT reconstructions. (B) Micro-CT data showing bone volume (mm<sup>3</sup>) in the tibial drilled hole. There was significantly improved defect repair in the PP + CSA-90 group ( $p < 0.05$ ). BV was increased in the PP group, but this did not reach statistical significance ( $p = 0.319$ , no coating vs. PP; and  $p = 0.4313$ , PP vs. PP + CSA-90). The white arrows point to the non-union osteolytic lesions of the tibial drilled holes.

Semi-quantitation measurements of bacterial load from the infection site grown in nutrient broth were compared at the bone defect (swab), the cultured removed pin, and soft tissue excised adjacent to the defect. Across the specimens, there was a trend towards reduced bacteria densities with no coating > PP > PP + CSA-90. From the local bone swabs, PP + CSA-90 showed significantly fewer bacteria than uncoated ( $p < 0.05$ ). From the soft tissue sample cultures, PP and PP + CSA-90 both showed significantly fewer bacteria than uncoated ( $p < 0.01$ ) (Figure 13).

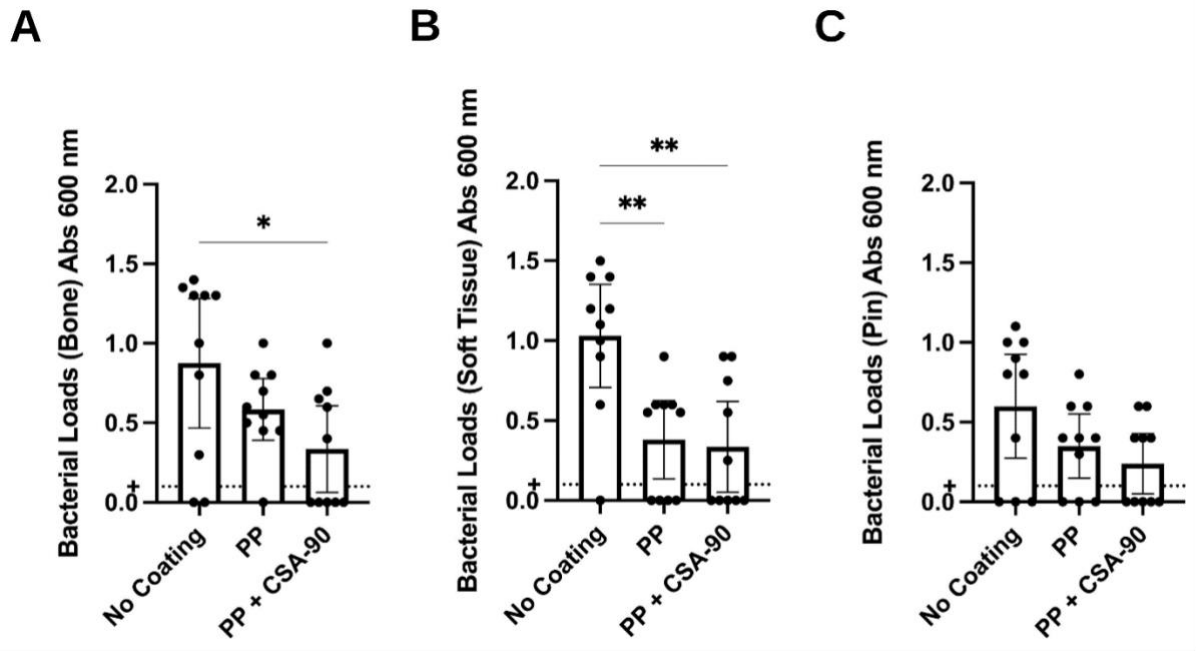


**Figure 13:** Semi-quantitative analysis of relative bacterial load (absorbance at 600 nm) from (A) bone swabs, (B) intramedullary steel pins, and (C) soft tissue adjacent to the defect site. (Error bars show mean and SEM; p-value: \* <0.05 and >0.01).

To complement the micro-CT analysis, descriptive histology was performed on specimens from each group. In the no-coating group, the infected drilled hole persisted (Figure 14A), and the defect in the marrow was infiltrated with inflammatory macrophages and lymphocytes (Figure 14B; yellow arrows). All groups showed evidence of new woven bone formation in the metaphyseal bone at or adjacent to the defect site (Figures 14A, C-D; black arrows). Specimens that featured CSA-90 delivered by PP-coating showed no histological evidence of persistent infection and showed superior bone repair (Figure 14D). Taken together, from these results it can be concluded that CSA-90 molecules retain their activity after covalent immobilization on the IPP-coated surfaces. In summary, our findings suggest that radical-rich IPP coatings on 3D objects, fabricated through a new technology presented here, hold great potential to open new avenues in simple and reagent-free surface biofunctionalization of antibacterial implantable medical devices, in particular bone implants.



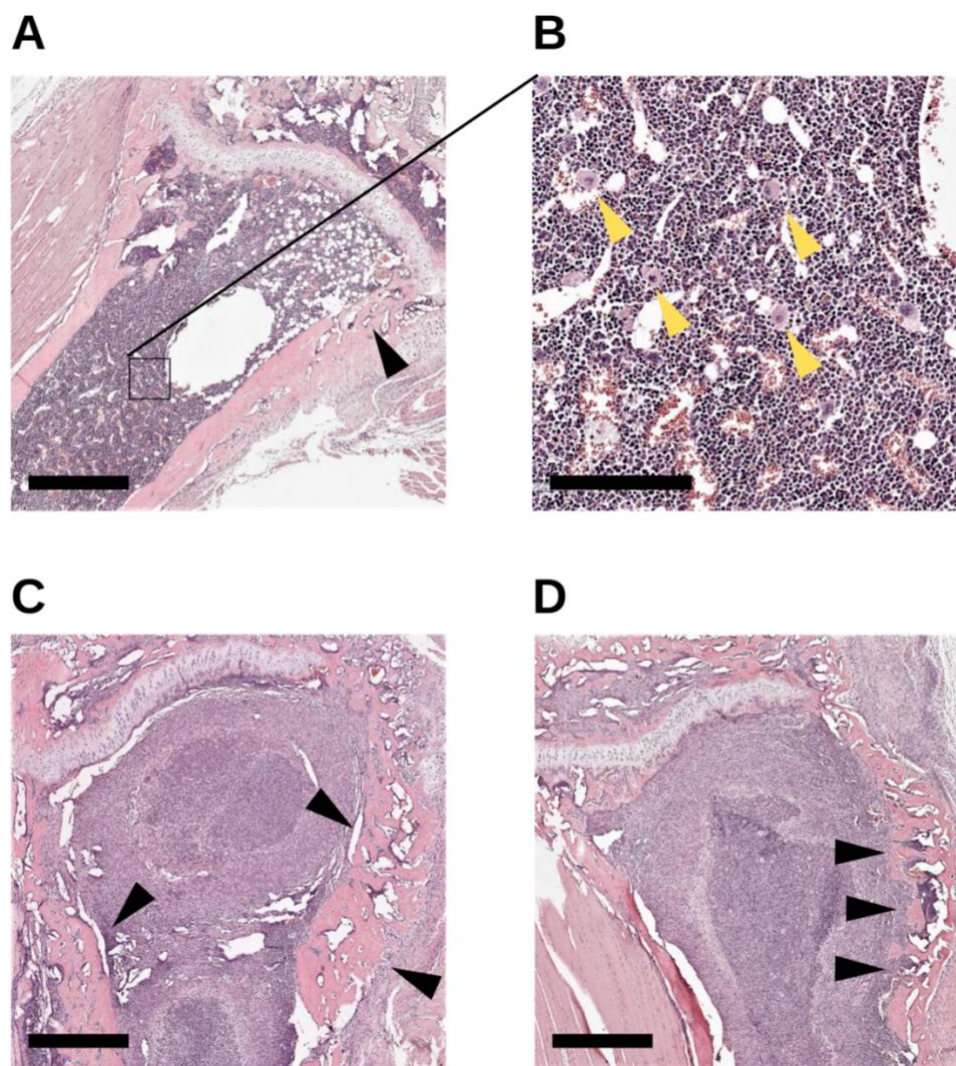


**Figure 14:** H&E-stained sections illustrating the healing of the bone defects in (A-B) no coating, (C) PP-coated and (D) PP + CSA-90 groups. Scale bars equal to 600  $\mu\text{m}$  (A, C and D) and 200  $\mu\text{m}$  (B). (Black arrows: woven cortical bones; yellow arrows: inflammatory macrophages and lymphocytes).

### 3.5. Conclusions

We have developed an ion-assisted plasma polymerization (IPP) technology to generate radical-rich, organic coatings for sing-step covalent functionalization, which has numerous potential applications for developing biomimetic and antimicrobial interfaces on real-world 3D objects. We demonstrated that this technology, previously adapted for 2D surfaces, can be re-engineered to modify 3D materials. Notably, using a combination of spectroscopic data and fluorescent labelled antibody attachment and imaging, we provided evidence that the IPP coatings are uniformly formed on 3D materials and are robust, with no evidence of failure after incubation in a simulated body fluid at 37°C for up to one month. The reactivity, uniformity and robustness of these coatings make them ideal for the surface



engineering of biomaterials in various applications. In this study, we showcased one application and demonstrated its excellent potential in creating antibacterial 3D interfaces using CSA-90 as a model antimicrobial molecule. The CSA-90-functionalized pins were permissive for healing in an infected bone defect model. These findings support the potential of this dry and environmentally friendly plasma technology to affix and retain antimicrobials on implants, mainly where antibacterial prophylaxis is advisable. Considering the substrate-independent nature of the IPP process, it can be applied to modify other 3D objects used in tissue engineering and regenerative medicine applications, including implantable medical devices.

### Acknowledgements

The authors gratefully acknowledge the financial support of the Australian Research Council (ARC) through the Discovery Early Career Researcher Award (DECRA) program (DE210100662). The authors acknowledge the facilities, scientific and technical assistance of Microscopy Australia at the University of South Australia, a facility that is funded by the University of South Australia, the State and Federal Governments.

### Data Availability

The authors declare that all data supporting the findings of this study are available within the article or from the corresponding author upon request.

### References

1. Im GI, Tae SK. Distal metaphyseal fractures of tibia: a prospective randomized trial of closed reduction and intramedullary nail versus open reduction and plate and screws fixation. *The Journal of trauma* 2005; **59**(5): 1219-23; discussion 23.
2. Yusof NM, Halim AS. Outcomes of infected grade IIIB open tibial fractures. *Singapore medical journal* 2012; **53**(9): 591-4.
3. Tay WH, de Steiger R, Richardson M, Gruen R, Balogh ZJ. Health outcomes of delayed union and non-union of femoral and tibial shaft fractures. *Injury* 2014; **45**(10): 1653-8.
4. Wu N, Lee, Wilcox, Boulanger, Murray, Segina. Economic burden of illness among US patients experiencing fracture non-union. *Orthopedic Research and Reviews* 2013; **2013**: 21.
5. Peel TN, Cheng AC, Liew D, et al. Direct hospital cost determinants following hip and knee arthroplasty. *Arthritis care & research* 2015; **67**(6): 782-90.
6. Chen L, Song X, Xing F, et al. A Review on Antimicrobial Coatings for Biomaterial Implants and Medical Devices. *Journal of biomedical nanotechnology* 2020; **16**(6): 789-809.

7. Liu Z, Liu X, Ramakrishna S. Surface engineering of biomaterials in orthopedic and dental implants: Strategies to improve osteointegration, bacteriostatic and bactericidal activities. *Biotechnology journal* 2021; **16**(7): e2000116.
8. Ghimire A, Song J. Anti-Periprosthetic Infection Strategies: From Implant Surface Topographical Engineering to Smart Drug-Releasing Coatings. *ACS applied materials & interfaces* 2021; **13**(18): 20921-37.
9. Stewart C, Akhavan B, Wise SG, Bilek MMM. A review of biomimetic surface functionalization for bone-integrating orthopedic implants: Mechanisms, current approaches, and future directions. *Progress in Materials Science* 2019; **106**: 100588.
10. Altmann SD-CD, Pfeiffer JDD-C. The Hydrolysis/Condensation Behaviour of Methacryloyloxyalkylfunctional Alkoxysilanes: Structure-Reactivity Relations. *Monatshefte für Chemie / Chemical Monthly* 2003; **134**: 1081-92.
11. Hanawa T. A comprehensive review of techniques for biofunctionalization of titanium. *Journal of periodontal & implant science* 2011; **41**(6): 263-72.
12. Sakiyama-Elbert SE. Incorporation of heparin into biomaterials. *Acta biomaterialia* 2014; **10**(4): 1581-7.
13. Alagem-Shafir M, Kivovich E, Tzchori I, et al. The formation of an anti-restenotic/anti-thrombotic surface by immobilization of nitric oxide synthase on a metallic carrier. *Acta biomaterialia* 2014; **10**(5): 2304-12.
14. Fang K, Song W, Wang L, et al. Immobilization of chitosan film containing semaphorin 3A onto a microarc oxidized titanium implant surface via silane reaction to improve MG63 osteogenic differentiation. *International journal of nanomedicine* 2014; **9**: 4649-57.
15. Akhavan B, Bakhshandeh S, Najafi-Ashtiani H, et al. Direct covalent attachment of silver nanoparticles on radical-rich plasma polymer films for antibacterial applications. *Journal of materials chemistry B* 2018; **6**(37): 5845-53.
16. Akhavan B, Michl TD, Giles C, et al. Plasma activated coatings with dual action against fungi and bacteria. *Applied Materials Today* 2018; **12**: 72-84.
17. Croes M, Akhavan B, Sharifahmadian O, et al. A multifaceted biomimetic interface to improve the longevity of orthopedic implants. *Acta biomaterialia* 2020; **110**: 266-79.
18. Stewart CAC, Akhavan B, Hung J, et al. Multifunctional Protein-Immobilized Plasma Polymer Films for Orthopedic Applications. *ACS biomaterials science & engineering* 2018; **4**(12): 4084-94.
19. Bilek MM, Bax DV, Kondyurin A, et al. Free radical functionalization of surfaces to prevent adverse responses to biomedical devices. *Proceedings of the National Academy of Sciences of the United States of America* 2011; **108**(35): 14405-10.
20. Martin LJ, Akhavan B, Bilek MMM. Electric fields control the orientation of peptides irreversibly immobilized on radical-functionalized surfaces. *Nature communications* 2018; **9**(1): 357.
21. Walia R, Akhavan B, Kosobrodova E, et al. Hydrogel–Solid Hybrid Materials for Biomedical Applications Enabled by Surface-Embedded Radicals. *Advanced Functional Materials* 2020; **30**(38): 2004599.
22. Lai XZ, Feng Y, Pollard J, et al. Ceragenins: cholic acid-based mimics of antimicrobial peptides. *Accounts of chemical research* 2008; **41**(10): 1233-40.
23. Vaara M. New approaches in peptide antibiotics. *Current opinion in pharmacology* 2009; **9**(5): 571-6.
24. Schindeler A, Yu NY, Cheng TL, et al. Local delivery of the cationic steroid antibiotic CSA-90 enables osseous union in a rat open fracture model of Staphylococcus aureus infection. *The Journal of bone and joint surgery American volume* 2015; **97**(4): 302-9.
25. Mills R, Cheng TL, Mikulec K, et al. CSA-90 Promotes Bone Formation and Mitigates Methicillin-resistant Staphylococcus aureus Infection in a Rat Open Fracture Model. *Clinical orthopaedics and related research* 2018; **476**(6): 1311-23.
26. Mills RJ, Boyling A, Cheng TL, et al. CSA-90 reduces periprosthetic joint infection in a novel rat model challenged with local and systemic Staphylococcus aureus. *Journal of orthopaedic research : official publication of the Orthopaedic Research Society* 2020; **38**(9): 2065-73.

27. Akhavan B, Wise SG, Bilek MMM. Substrate-Regulated Growth of Plasma-Polymerized Films on Carbide-Forming Metals. *Langmuir : the ACS journal of surfaces and colloids* 2016; **32**(42): 10835-43.
28. Akhavan B, Bilek M. Controlled deposition of plasma activated coatings on zirconium substrates: SPIE; 2015.
29. Stewart CAC, Akhavan B, Santos M, et al. Cellular responses to radical propagation from ion-implanted plasma polymer surfaces. *Applied Surface Science* 2018; **456**: 701-10.
30. Akhavan B, Jarvis K, Majewski P. Tuning the hydrophobicity of plasma polymer coated silica particles. *Powder Technology* 2013; **249**: 403-11.
31. Akhavan B, Jarvis K, Majewski P. Evolution of Hydrophobicity in Plasma Polymerised 1,7-Octadiene Films. *Plasma Processes and Polymers* 2013; **10**(11): 1018-29.
32. Akhavan B, Jarvis K, Majewski P. Development of negatively charged particulate surfaces through a dry plasma-assisted approach. *RSC Advances* 2015; **5**(17): 12910-21.
33. Akhavan B, Jarvis K, Majewski P. Plasma polymerization of sulfur-rich and water-stable coatings on silica particles. *Surface and Coatings Technology* 2015; **264**: 72-9.
34. Gengenbach TR, Vasic ZR, Chatelier RC, Griesser HJ. A multi-technique study of the spontaneous oxidation of N-hexane plasma polymers. *Journal of Polymer Science Part A: Polymer Chemistry* 1994; **32**(8): 1399-414.
35. Gengenbach TR, Griesser HJ. Deposition conditions influence the postdeposition oxidation of methyl methacrylate plasma polymer films. *Journal of Polymer Science Part A: Polymer Chemistry* 1998; **36**(6): 985-1000.
36. Yu S, Yu Z, Wang G, Han J, Ma X, Dargusch MS. Biocompatibility and osteoconduction of active porous calcium-phosphate films on a novel Ti-3Zr-2Sn-3Mo-25Nb biomedical alloy. *Colloids and surfaces B, Biointerfaces* 2011; **85**(2): 103-15.
37. Liu C, Xin Y, Tang G, Chu PK. Influence of heat treatment on degradation behavior of bio-degradable die-cast AZ63 magnesium alloy in simulated body fluid. *Materials Science and Engineering: A* 2007; **456**(1): 350-7.
38. Feinberg AW, Alford PW, Jin H, et al. Controlling the contractile strength of engineered cardiac muscle by hierarchical tissue architecture. *Biomaterials* 2012; **33**(23): 5732-41.
39. Hongpaisan J, Winters CA, Andrews SB. Strong calcium entry activates mitochondrial superoxide generation, upregulating kinase signaling in hippocampal neurons. *The Journal of neuroscience : the official journal of the Society for Neuroscience* 2004; **24**(48): 10878-87.
40. Ruiz J-C, St-Georges-Robillard A, Thérésy C, Lerouge S, Wertheimer MR. Fabrication and Characterization of Amine-Rich Organic Thin Films: Focus on Stability. *Plasma Processes and Polymers* 2010; **7**(9-10): 737-53.
41. Gengenbach TR, Griesser HJ. Aging of 1,3-diaminopropane plasma-deposited polymer films: Mechanisms and reaction pathways. *Journal of Polymer Science Part A: Polymer Chemistry* 1999; **37**(13): 2191-206.
42. Akhavan B, Menges B, Förch R. Inhomogeneous Growth of Micrometer Thick Plasma Polymerized Films. *Langmuir : the ACS journal of surfaces and colloids* 2016; **32**(19): 4792-9.
43. Robertson J. Diamond-like amorphous carbon. *Materials Science and Engineering: R: Reports* 2002; **37**(4): 129-281.
44. Akhavan B, Croes M, Wise SG, et al. Radical-functionalized plasma polymers: Stable biomimetic interfaces for bone implant applications. *Applied Materials Today* 2019; **16**: 456-73.
45. Lau K, Akhavan B, Lord MS, Bilek MM, Rnjak-Kovacina J. Dry Surface Treatments of Silk Biomaterials and Their Utility in Biomedical Applications. *ACS biomaterials science & engineering* 2020; **6**(10): 5431-52.
46. Vickerman JCB. ToF-SIMS : surface analysis by mass spectrometry. Chichester; Manchester: IM : SurfaceSpectra; 2001.
47. Feng M, Morales AB, Poot A, Beugeling T, Bantjes A. Effects of Tween 20 on the desorption of proteins from polymer surfaces. *Journal of biomaterials science Polymer edition* 1995; **7**(5): 415-24.
48. Vandenberg ET, Krull UJ. The prevention of adsorption of interferents to radiolabelled protein by Tween 20. *Journal of biochemical and biophysical methods* 1991; **22**(4): 269-77.

#### 4. Testing BBA-1 *in vivo* to prevent osteomyelitis and myeloma bone

Chapter 4 demonstrates the potential of our synthesised bone-binding antimicrobial, BBA-1, as prophylactic therapy for osteomyelitis. We have determined the efficacy of BBA-1 with our murine bone infection model and attempted to develop a bone infection model in multiple myeloma mice for future preclinical trials.

This chapter is written as a traditional thesis chapter. We recognised that our data from this chapter are still preliminary, so there is no manuscript for publication to be presented.

This chapter is also submitted for emergency assessment due to the COVID-19 outbreak and lockdown in 2021 (June-October). The lockdown has disrupted some experiments due to limited access to the Garvan Institute of Medical Research facility. We acknowledged the limitation of our study in the extended discussion, and the hypothetical results are discussed.

The University of Sydney has accepted the emergency assessment application for this thesis.

##### **Statement of contribution:**

The synthesis of BBA-1 was conducted by Prof Paul Savage (Brigham Young University) and Dr Sumedh Kamble (University of Sydney). I conducted the *in vivo* efficacy testing of BBA-1 and developed the multiple myeloma-related bone infection animal models with A/Prof Michelle McDonald at the Garvan Institute of Medical Research. I performed animal surgeries with the assistance of Dr Justin Bobyn and Ms Ya Xiao. A/Prof Aaron Schindeler contributed to the conception of the study.

## 4. Testing BBA-1 *in vivo* to prevent osteomyelitis and myeloma bone disease

### 4.1. Introduction

#### 4.1.1. The clinical challenges of using intravenous antibiotics to treat osteomyelitis

Osteomyelitis and deep surgical site infections (SSIs) can be challenging to manage <sup>1</sup>. The high morbidity of osteomyelitis is partially attributed to the limited antibiotic options. This is due to a lack of antimicrobials targeting bone infections and an increasing prevalence of antibiotic-resistant bacterial strains <sup>2-4</sup>. Meanwhile, trauma, open fractures, and prosthetic joint replacement are conditions prone to high risk of infection in orthopaedic and clinical settings <sup>5-8</sup>. The current infection rates range from 4.3% for general orthopaedic trauma to 16% for high-risk fracture <sup>9</sup>. Treatment failure after deep surgical site infection is common in orthopaedics, especially if the infection is polymicrobial or associated with IIIB/C fracture and implantation <sup>10</sup>. Further, treatments will likely fail if the infection cannot be eradicated in the first series of surgeries and antibiotics.

Chronic osteomyelitis usually persists with multiple clinical failures and relapses after periods of quiescence and successful treatment <sup>11</sup>. Chronic osteomyelitis can lead to severe complications and significantly impacts the quality of life in patients and healthcare system costs. Although systemic antibiotics can resolve acute osteomyelitis, chronic osteomyelitis can remain recalcitrant even with high and sustained antibiotic doses. Also, systemic antibiotic delivery to the bone to treat osteomyelitis has always been a clinical challenge, especially if pus, sequestra (dead bones), gangrenes, and antibiotic-resistant bacterial strains or biofilm are involved <sup>12,13</sup>. Therefore, while surgical debridement and systemic antibiotic therapies remain typical treatments for acute osteomyelitis, local antibiotic delivery and oral antibiotics treatment are often used to manage chronic osteomyelitis.

Bacterial biofilms are self-produced extracellular matrices that resist antimicrobial treatments and are associated with chronic osteomyelitis and diabetic foot osteomyelitis (DFO). Biofilms provide extracellular protection by preventing exposure of the bacteria to antibiotics. The poor efficacy of systemic antibiotic treatment is due to vascular insufficiency, poor antibiotic penetration into the bone, and the complexity of the bone microenvironment. Overall, the penetration of antibiotics into bone tissue is low, achieving a bone-to-serum concentration ratio of a maximum of 0.3 for the majority of antibiotics <sup>11</sup>.

### 4.1.2. The generation of bone-binding antimicrobials

The broad-spectrum potent antimicrobial activity and pro-osteogenic effects of CSA-90 are appealing for use in orthopaedic settings to prevent and treat bone infections<sup>14</sup>. The concept behind the synthesis of BBA-1 was to conjugate CSA-90 with a bisphosphonate (alendronate) via a PEG-based heterobifunctional NHS-PEG-COOH linker (Figure 4.1). BBA-1 aimed to achieve higher targeted delivery to bone and sustained delivery from the bone surface<sup>14</sup>.

Kamble et al (2020) used infra-red spectroscopy, NMR spectroscopy, and HPLC-GS chromatograms to characterise the synthesised BBA-1<sup>14</sup>. The structure of BBA-1 was later confirmed by mass spectrometry (MS), and the antimicrobial activity of BBA-1 was confirmed by Kirby-Bauer disk diffusion susceptibility testing. The *in vitro* Kirby-Bauer assay demonstrated comparable bactericidal activity for BBA-1 and CSA-90 at equivalent molarities. BBA-1 was effective against *S. aureus*, and methicillin-resistant *S. aureus* (MRSA). The minimum bactericidal concentration (MBC) against *S. aureus* and MRSA was 3 µg/mL<sup>14</sup>. Like CSA-90, BBA-1 was pro-osteogenic demonstrated by the alkaline phosphatase assay and yielded synergistic effects when used in combination with recombinant human bone morphogenetic protein-2 (rhBMP-2)<sup>14,15</sup>.

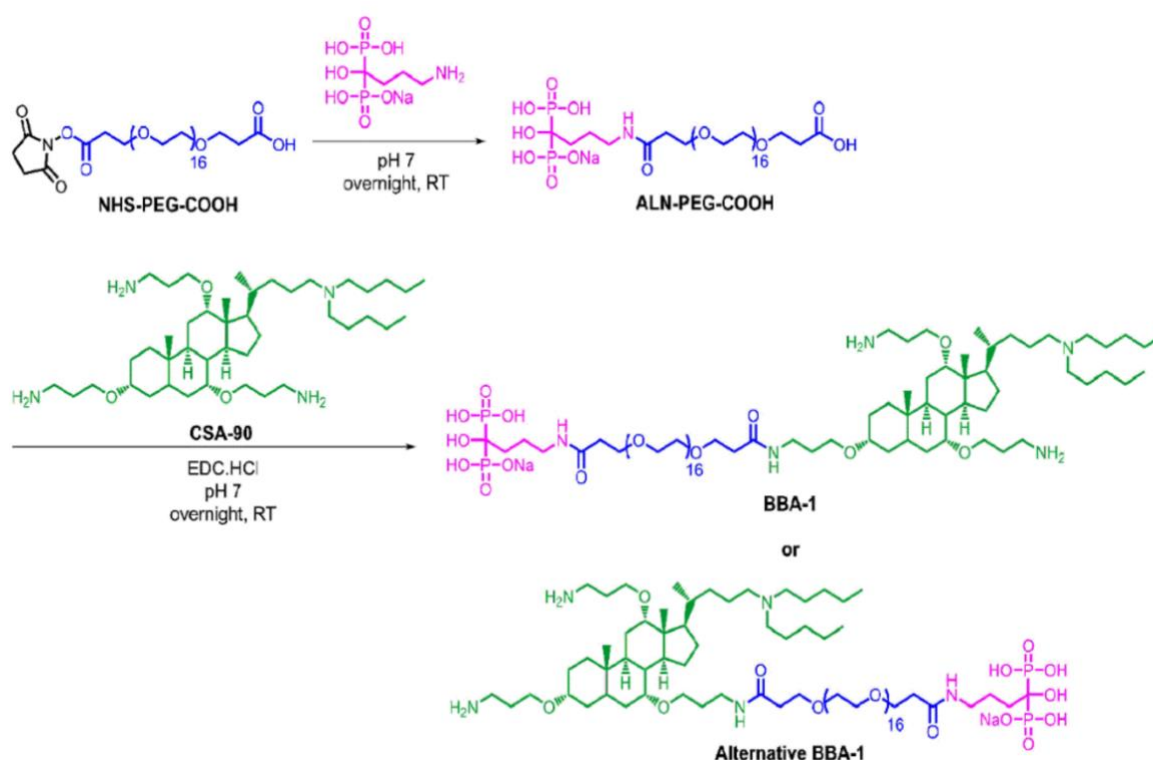


Figure 4.1: Synthesis of bone-binding antibiotic (BBA-1) by conjugating alendronate (ALN) and CSA-90 using the NHS-PEG-COOH linker (Kamble, et al. 2020).

While CSA-90 has been trialled to prevent and treat osteomyelitis *in vivo* <sup>16,17</sup>, the efficacy of BBA-1 has not yet been tested *in vivo*. Based on the *in vitro* data, it was shown that BBA-1 retains a similar antimicrobial potency as CSA-90, but BBA-1 has the advantage of homing to and persisting on the bone surface. This could allow it to prevent osteomyelitis as an intravenous prophylactic antimicrobial.

Previously, our team has demonstrated that local CSA-90 given at lower doses was ineffective in treating established infections <sup>16</sup>. Its utility was greater when used as a prophylactic agent to prevent infection. In addition, it is recognised that the clinical application of BBA-1 is not limited to orthopaedic surgery. It could also be useful for medical situations that feature an elevated risk of bone infections, such as myeloma bone disease. Thus, our animal trial (Study 4A) aimed to focus on testing BBA-1 as an infection prophylactic instead of a therapeutic.

#### 4.1.3. Developing a MM-related bone infection murine model

Multiple myeloma (MM) is the second most prevalent haematological malignancy and is responsible for 2.1% of all cancer deaths <sup>18</sup>. MM develops from the plasma cells, and the cause is still unknown <sup>19-21</sup>. Nearly 80-90% of MM patients develop myeloma bone disease (MBD), and the 5-year survival rate falls to 46% <sup>20</sup>. MBD is the presence of one or more osteolytic bone lesions or diffused osteoporosis with compression fracture attributable to the underlying clonal plasma cell disorder. While these lesions can lead to fractures, neurological deficits, and mobility issues, they are also highly prone to infection (osteomyelitis), dramatically worsening the prognosis of affected individuals <sup>22</sup>. Since BBA-1 has the potential to provide sustained protection on bone surfaces, we hypothesised that BBA-1 can prevent osteolytic lesions and bone infections in MM.

Although no previous animal trials have particularly focused on MM-related bone infections, various models exist to study MBD and osteolytic lesions *in vivo* <sup>18</sup>. The 5TMM-derived C57BL/KaLwRij mouse model was established by serial transplantation of the bone marrow of tumour-bearing mice into young syngeneic recipient C57BL/KaLwRij mice. It resembles features of the human benign monoclonal gammopathy of undetermined significance (MGUS) stage, and several mouse myeloma cell lines can be used, including 5T33MM, 5TGM1 and 5T2MM <sup>23</sup>. The 5TGM1 cell is a subsequent subclone of the 5T33 line and was established via serial *in vivo* passage of the 5T33MM. The 5TGM1-cells injection is a cost-effective and reproducible method to study MBD due to its short latency period and pronounced osteolytic lesion formation <sup>18,23</sup>. It has been previously shown that systemic injection of 5TGM1-GFP

cells into C57BL/KaLwRij mouse allowed tracing of individual myeloma cells and showed that they colonize the endothelial niche, entering a dormant stage. The dormant stage can be switched on by bone line cells or osteoblasts and switched off by osteoclasts <sup>24</sup>. Later, it was discovered that injecting 5TGM1 to naïve C57BL6/KaLwRij female mice could produce small extracellular vesicles, increase osteolysis, and reduce the trabecular bone volume <sup>25</sup>.

To develop a murine multiple myeloma-related bone infection model, we adopted the 5TGM1-MMBD model featured by osteolysis and bone lesions <sup>23,24</sup>. The rationale of our model development is to trial inducing bone infections in 5T cell-bearing female mice (MM-mice) with a systemic mono-dose of *S. aureus*.

Additionally, we decided to use a bioluminescent *S. aureus* strain (Xen36) for the bacterial inoculation. The bioluminescent bacteria provide a non-invasive and effective solution to this challenge. The bioluminescent bacterial strain *S. aureus* Xen36 (PerkinElmer, Hopkinton, MA) is a derivative of a patient strain (ATCC-29525). It contains a bioluminescent operon (luxABCDE) integrated into the bacterial genome <sup>26,27</sup>. When the Xen36 *S. aureus* (Xen36) strain is metabolically active, it emits a blue-green light with a maximal emission wavelength of 490 nm. Xen36 *S. aureus* allows longitudinal monitoring of infection burden in animal models <sup>28-31</sup>.

We speculated that the local bone lesions would act as a nidus for biofilm formation and lead to localised osteomyelitis following haematogenous infection. Moreover, based on prior work with a rat knee implant model, a low dose of *S. aureus* via systemic inoculation was surmised sufficient to infect lesions <sup>17</sup>. Therefore, in Study 4B, we aimed to develop a murine MM-related bone infection model to determine the efficacy and advantages of using BBA-1 for MBD.

## 4.2. Methods

### 4.2.1. Study 4A design: *in vivo* testing of BBA-1 in an orthopaedic model

For Study 4A, C57B/6 mice (10-week-old, female, N=30) were divided into three groups (Table 4.1). All animals received a tibial drilled-hole surgery (TDH) with a stainless-steel pin insertion through the medullary canal through the tibial condyle. While group 1 received no local bacterial injection (negative control), group 2 and 3 both received a single dose of bacterial injection locally into the bone defect. Group 2 received no treatment, whereas group



3 received a single dose prophylaxis of BBA-1 (10 mg/kg) one hour before surgery. Table 4.1 summarises the study design.

**Table 4.1: Study 4A**

Group	Surgery	Local Infection ( $10^5$ CFU)	Treatment	N=
1	TDH + Pin	Nil	Nil	10
2	TDH + Pin	ATCC-12600 <i>S. aureus</i>	Nil	10
3	TDH + Pin	ATCC-12600 <i>S. aureus</i>	BBA-1 prophylaxis	10
<b>Total</b>				<b>30</b>

#### 4.2.2. Study 4B design: development of a MM infection model

For Study 4B, C57BL/KaLwRijHsd (BKAL) mice (6-8 weeks old) were divided into four groups (Table 4.2). Group 4 only received  $2 \times 10^6$  5TGM1-eGFP MM cells intravenously (day 0) without the Xen36 bacteria. Group 5 received the bacterial injection (day 14) without the MM cells. Group 6 received the MM cell injection (day 0) and the bacterial injection (day 14). Group 7 did not receive a cell injection but had a bone defect on the right tibia by needle insertion surgery (NIS) as previously described and a Xen36 bacterial injection (day 14). The purpose of this was to validate bone lesion infection prior to any therapeutic rescue experiments utilising BBA-1.

**Table 4.2: Study 4B**

Group	IV MM Cell Injection (Day 0)	Surgery and Bacterial Injection (Day 14)	N=
4	$2 \times 10^6$ 5TGM1-eGFP MM cells	Nil	2
5	Nil	IV Xen36 injection ( $1 \times 10^6$ CFU)	2
6	$2 \times 10^6$ 5TGM1-eGFP MM cells	IV Xen36 injection ( $1 \times 10^6$ CFU)	2
7	Nil	NIS + local Xen36 injection ( $1 \times 10^6$ CFU)	2
<b>Total</b>			<b>8</b>

#### 4.2.3. Bacterial and biofilm culture

For Study 4A, a strain of clinical-derived *Staphylococcus aureus* (American Type Culture Collection-12600) was cultured from  $-80^\circ\text{C}$  glycerol stocks onto lysogeny broth (LB) agar at

incubated for 24 hours at 37°C. For Study 4B, the bioluminescent *S. aureus* strain (Xen36) was cultured using the same methods.

After 24 hours of incubation, a single colony was selected and resuspended from the LB agar plate into LB (1 mL), incubated at 37°C overnight. The bacterial suspension was then quantified using a spectrophotometer (Cary 300 UV-Vis, Agilent, Las Vegas, NV) at 600 nm. The spectrophotometer was calibrated by an optical density of 1 representing  $1 \times 10^9$  colony-forming unit (CFU)/millilitre (mL). A final solution with a concentration of  $2 \times 10^7$  CFU was diluted by injectable saline (0.9% sodium chloride).

#### 4.2.4. Cell culture and injection

For Study 4B, 5TGM1-eGFP myeloma cells were cultured in RPMI-1640 supplemented with 10% foetal calf serum (FCS) and 1% penicillin–streptomycin and incubated in 5% CO<sub>2</sub> at 37 °C<sup>32</sup>. A total of  $2 \times 10^6$  5TGM1-eGFP murine myeloma cells were labelled with the lipid dye 1,1'-dioctadecyl-3,3,3',3'-tetramethylindodicarbocyanine (DiD) and injected intravenously into six-to-eight-week-old C57BL/KaLwRijHsd (BKAL) female mice (Harlan, Netherlands) in 200 µL PBS. The MM cells were negative for mycoplasma.

#### 4.2.5. Animal husbandry and ethics

For Study 4A, female C57BL/6 mice (8-10 weeks old) were purchased from Australian BioResources (Moss Vale, NSW, Australia). They were co-housed up to 6 per cage with access to food and water *ad libitum* and allowed to acclimatize for at least one week prior to surgery. Animal experiments were approved by the local Animal Ethics Committee (K339) and carried out in accordance with the Australian Code for the care and use of animals for scientific purposes (2013).

For Study 4B, the C57BL/KaLwRijHsd (BKAL) mice were bred in-house at the Garvan Institute of Medical Research (Sydney, Australia). Animal experiments were approved by the Garvan Institute of Medical Research Animal Ethics Committee (ARA18/03)<sup>32-34</sup>.

#### 4.2.6. Surgery and anaesthesia

Analgesia was provided using buprenorphine (0.1 mg/kg) given subcutaneously one hour before surgery. Anaesthesia was induced using ketamine (75 mg/kg) and xylazine (10 mg/kg)

given by intraperitoneal injection and animals were maintained on inhaled isoflurane (2-3% per 1.5-2 L oxygen) as required using a nose cone during the procedure. The right leg of each animal was shaved and wiped with a povidone-iodine solution prior to surgery.

For Study 4A, a medial parapatellar approach was used to access the right proximal tibia. A hole (0.5 mm in diameter) was made at the right tibial metaphysis (below the growth plate) using a surgical drill (Stryker ® 5100-15-250 Straight, Kalamazoo, USA), exposing the medullary canal adjacent to the drilled hole for bacterial infection. A 38 mm × 0.25 mm stainless-steel pin (Australian Entomological Supplies Pty Ltd, South Murwillumbah, Australia) was inserted through the subchondral bone at the knee, adjacent to the drilled-hole defect. The pin provides a metal surface for bacterial mounting and encourages biofilm formation.

For Study 4B, a 25G needle was used to puncture through the unicortical bone of the metaphysis to create a bone defect. No stainless-steel pin was inserted for this model.

The incisions were closed with 5-0 Vicryl (Ethicon LLC, Puerto Rico, USA), and no dressings applied to the wound. Baseline radiographs were taken at the time of surgery. Animals were recovered on a heated pad after surgery and given subcutaneous normal saline (1 mL) to aid in rehydration. Buprenorphine (0.1 mg/kg) was given subcutaneously every 12 hours post-surgically and whenever required during monitoring.

#### **4.2.7. Surgical or post-surgical bacterial inoculation**

For Study 4A, the ATCC-12600 *S. aureus* was locally injected (5 µL with  $1 \times 10^5$  CFU bacterial dilution) directly into the hole with a Hamilton syringe and needles (Hamilton Company, Nevada, USA) intraoperatively, immediately after the pin-insertion.

For study 4B, group 6 received a tail-vein bacterial systemic injection of Xen36 (100 µL with  $1 \times 10^6$  CFU) on day-14 (post-surgery), whereas group 7 received a local interoperative injection of Xen36 (5 µL with  $1 \times 10^6$  CFU).

#### **4.2.8. X-ray and IVIS imaging and monitoring**

For Study 4A and 4B, animals were monitored daily by experienced staff and had twice-weekly radiographs performed under anaesthesia (inhaled isoflurane) using digital X-ray (Faxitron Bioptics, Tuscan, AZ) at 25 kV for five seconds with ×2 magnification. X-ray (XR) images were assessed by expert researchers and a facility veterinarian; all were blinded to treatment.

For ethical reasons, animals showing overt physiological and/or radiological evidence of infection judged by declining overall health (loss of body weight, lethargy, pyrexia, poor coat condition, non-weight bearing, and inflammation of the surgical site) and/or radiological evidence of persistent infection (local osteolysis at the tibia joint) were euthanized. The remaining mice were euthanized by carbon dioxide inhalation at study end point.

For Study 4B, a bioluminescent IVIS scan was added to monitor the infection of Xen36 *S. aureus* (for the infected groups only). The IVIS ® Spectrum *in vivo* imaging system (PerkinElmer, Waltham, MA) was used to obtain bioluminescent images representative of infectious burden on postoperative and day 0, 1, 3, 5, 7, 10 and 14. Data were quantified as total flux (photons per second per cm<sup>2</sup> per steradian [p/sec/cm<sup>2</sup>/sr]).

#### 4.2.9. Specimen Collection and Bacterial Assay

After cull, a blood sample was taken from the heart, and swabs were taken from the bone (drilled hole), soft tissue adjacent to the drilled hole, and the metal pin. The soft tissue surrounding the drilled-hole and any pus (if present) were also collected. The right tibiae were harvested. Blood and swabs were immediately agitated in 1 mL sterile LB and cultured overnight at 37°C. They were reported as either positive (turbid) or negative (clear), and then quantified using a spectrophotometer (SpectraMax ® iD3, Molecular Devices, San Jose, USA) at 600 nm. A positive infection was defined as a positive bacterial culture from the bone swab and pin swab with an absorbance (OD<sub>600</sub>) over 0.1.

#### 4.2.10. Radiographic Analysis and Paraffin Histology

The tibiae were fixed in 10% formalin for 24 hours before being transferred to 70% ethanol. The specimens were wrapped with a kimwipe soaked with 70% ethanol and placed in a plastic tube for scanning. The radiographic scanning was conducted using a SkyScan 1272 micro-computed tomography (micro-CT) scanner (SkyScan, Kontich, Belgium). All samples were scanned at 50kV and 200 µA using a 0.5 mm aluminium filter with 2500 ms of exposure. Images were scanned at a pixel resolution of 10 µm, reconstructed with NRecon, straightened using DataViewer and analysed with CTAn software (SkyScan). The region of interest (ROI) was drawn within the cortical bone defect (0.5 mm in diameter). A global threshold to define bone tissue was set at 0.4 g/cm<sup>3</sup> calcium hydroxyapatite, calibrated using two phantom samples with known densities. Bone morphometric outcomes included bone volume (mm<sup>3</sup>), tissue

volume (mm<sup>3</sup>), and bone tissue mineral density (g/cm<sup>3</sup>). Three-dimensional reconstructions were generated using CTVox software (Skyscan).

#### 4.2.11. Statistical Analyses

Statistical power calculations and analyses were performed using GraphPad Prism® (GraphPad Software, La Jolla, CA, USA) and the cut-off for significance for all tests was set to  $p < 0.05$ . *In vivo* studies were powered to infection rate and defect union based on means and variances from previously published studies<sup>15-17</sup> and were compared using Fisher's exact test. The micro-CT data were analysed by Kruskal-Wallis testing and post-hoc Dunn's multiple comparison test.

### 4.3. Results

#### 4.3.1. BBA-1 showed limited *in vivo* antimicrobial activities and osteogenic property

*AIM 1: To determine the in vivo efficacy of BBA-1 of preventing osteomyelitis*

In Study 4A, mice injected with BBA-1 intravenously had survived throughout the trial without showing any adverse reactions to the antibiotic. Meanwhile, one mouse (from the control group) had a complication during surgery and was euthanised immediately as per ethics requirement on Day 0. Other than that, no animals had died before the experimental end point. Additionally, the BBA-1 dosage (10 mg/kg) was selected based on the speculated maximal tolerated physiological dose.

The data showed that BBA-1 significantly reduced soft-tissue infections in mice by 50% (5/10) (Figure 4.1A). In contrast, there were 10% less blood and bone infections in the BBA-1 treated group compared to the infected and untreated group (Figure 4.1B and 4.1C). Meanwhile, the negative control (uninfected) group had zero number of infections, suggesting the risk of contamination during surgery and specimen collection was low.

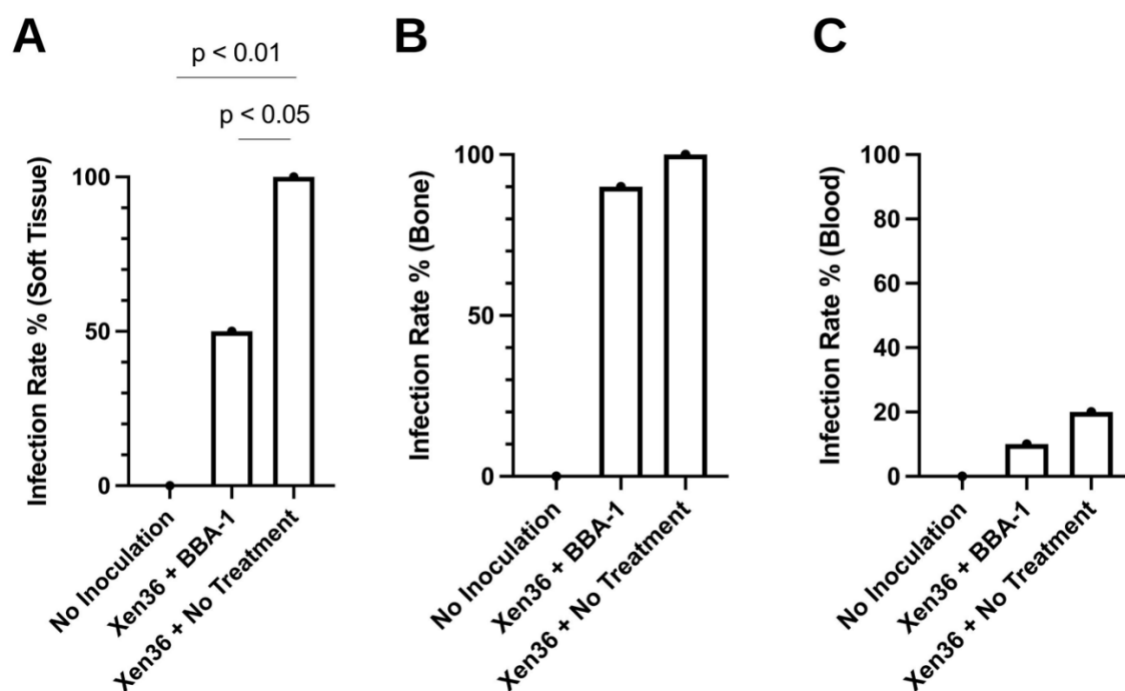


Figure 4.2: [Study 4A] The infection rate in tibial drill holes inoculated with *S. aureus* (%) of (A) soft-tissue infections, (B) bone infections, and (C) blood infections (N=10 per group).

Micro-CT quantification indicated that BBA-1 increased osteogenesis and promoted healing of the bone defects. There was an increase of bone volumes (Figure 4.2A) and bone surfaces (Figure 4.2B) at the bone defect sites in the BBA-1 treated group that was higher than the infected group but lower than the uninfected group. Also, the progression of bone healing was visualized by 3D-reconstruction (Figure 4.3).

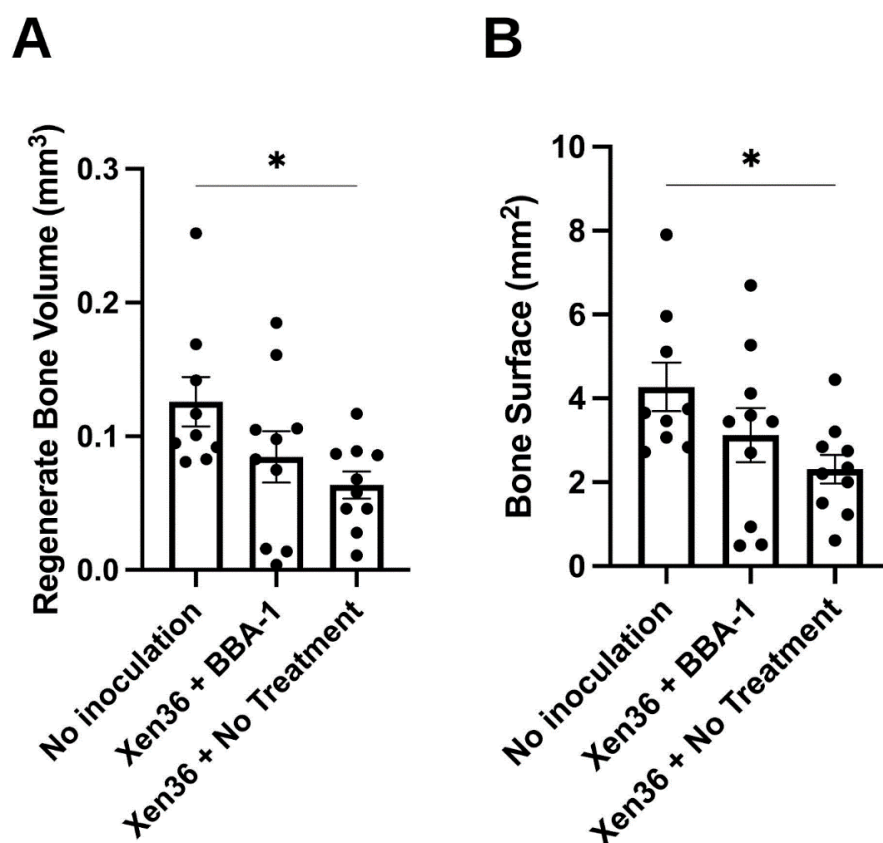


Figure 4.3: [Study 4A] (A) The regenerate bone volumes (mm<sup>3</sup>) of the tibial metaphyseal drilled hole quantified by micro-CT analysis in the TDH and NIS models. (B) The bone surface (mm<sup>2</sup>) of the defect site. The micro-CT data analysed with Kruskal-Wallis testing and post-hoc Dunn's multiple comparison test (error bars: mean and SEM; p-values: \*  $\leq 0.05$  and  $> 0.01$ ).

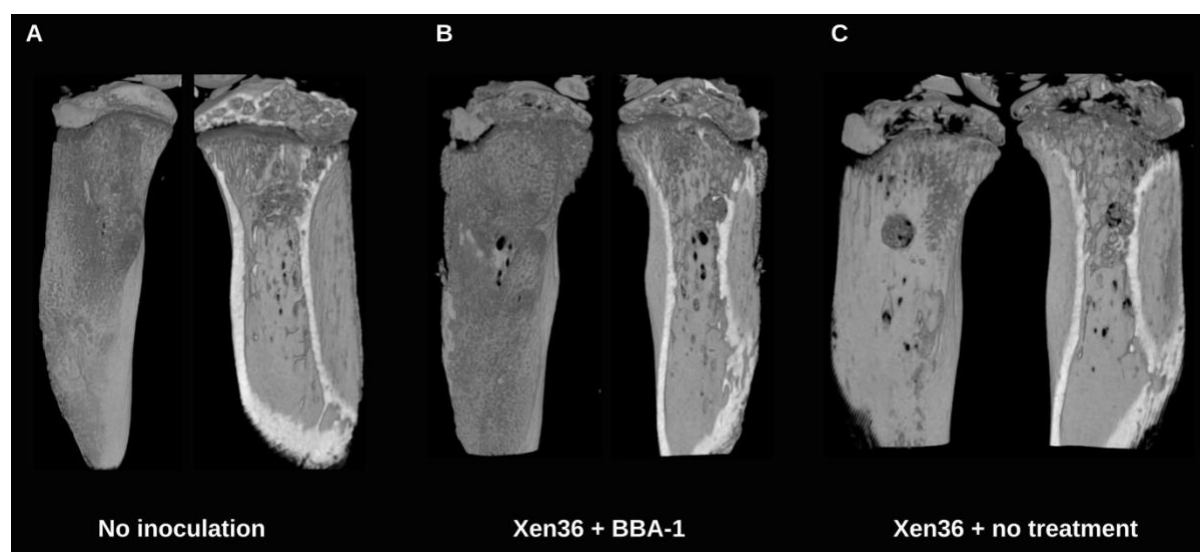


Figure 4.4: The anterior (left) and posterior (right) micro-CT 3D-reconstructions of the (A) no inoculation negative control group, (B) Xen36 + BBA-1 group, and (C) Xen36 + no treatment group. The median of bone volume representatives was selected from each group (Study 4A).

### 4.3.2. The pilot trial of modelling bone infection in MM mice

*AIM 2: To develop a multiple myeloma-related osteomyelitis model in murine.*

In Study 4B, the C57BL/KaLwRijHsd (BKAL) mice group 4 and 6 (N=2 per group) received a single dose of 5TGM1-eGFP MM cells ( $2 \times 10^6$  cells) intravenously two weeks prior to bacterial inoculation. Two weeks later, group 5-7 received a single dose of planktonic Xen36 ( $10^5$  CFU) intravenously to simulate a low-level haematogenous infection. In results, all mice (4/4) receiving the MM-cells injection (Group 4 and 6) developed tail weakness in week 3 and 4. The affected mice were euthanised before they developed weaknesses in their lower limbs (an early sign of paralysis). However, at the end point, no animals that received the MM-cell injection had developed an osteolytic lesion in the tibia. Only the mice (2/2) that received the NIS and local inoculation of Xen36 (Group 7) developed bone infections. These mice were euthanised as soon as they developed signs of bone infections. The mice (2/2) that received Xen36 only (Group 5) did not develop bone infection and were monitored till the end of the experiment. Table 4.3 summarises the outcome of this preliminary trial.

Table 4.3: [Study 4B] The bacterial assays of the MM-related bone infection model.

Group	Procedures	ID	Bacterial Assays	
			Bone	Blood
4	MM-cells only	7204	-	-
		7205	-	-
5	Xen36 only	7216	-	-
		7217	-	-
6	MM-cells + Xen36	7197	-	-
		7198	-	-
7	NIS + Xen36	7218	+	-
		7219	+	-

The x-ray scans revealed no osteolytic lesions in the MM-cells injected mice (Figure 4.5A), and the NIS-Xen36 group had a bone defect (0.5 mm in diameter) on the metaphysis of the tibia with sign of osteolysis surrounding the unicortical drilled-hole defect (Figure 4.5B).



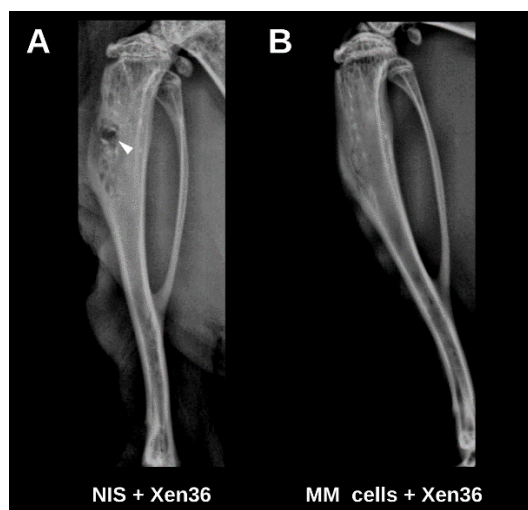


Figure 4.5: [Study 4B] The radiograph (XR) of a mouse tibia that received (A) a NIS drilled hole (white arrow) and local inoculation of Xen36 and (B) 5TGM1-eGFP MM and systemic inoculation of Xen36.

The *ex vivo* IVIS scanning revealed the bioluminescent Xen36 *S. aureus* ( $\sim 1 \times 10^8$  CFU) in the mice (Figure 4.6). The image showed two separated high bioluminescent signals under the skin ( $> 6 \times 10^6$  p/sec/cm<sup>3</sup>/sr) when Xen36 *S. aureus* was injected subcutaneously. However, in our preliminary MM-related bone infection trial, there was no bioluminescent signal detected in any mice.

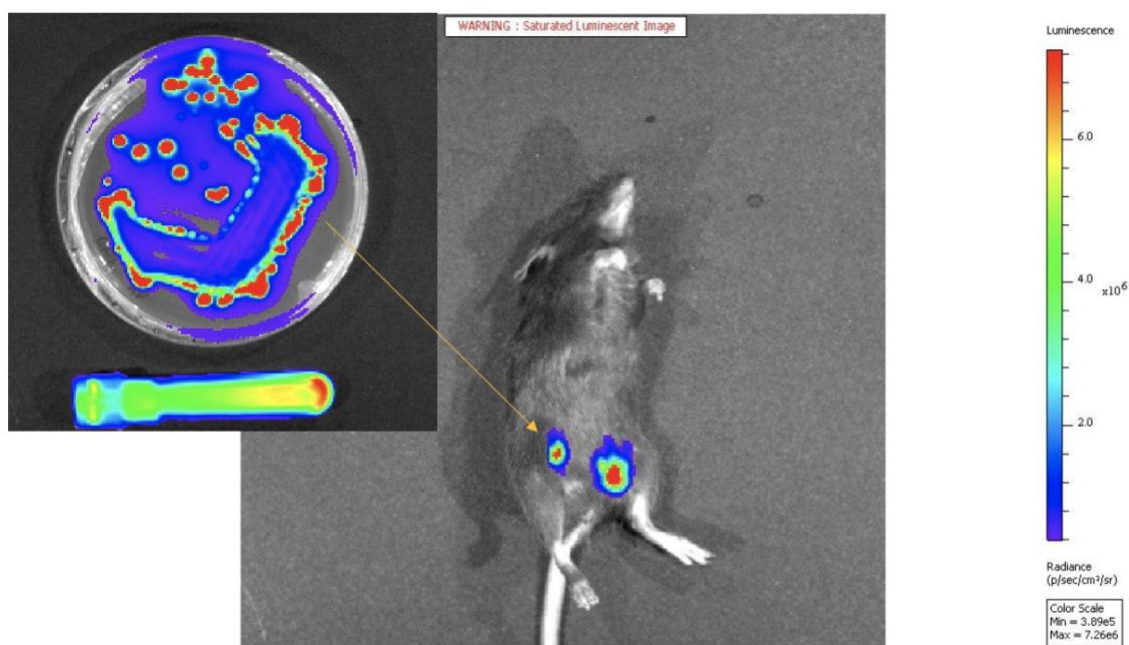


Figure 4.6: [Study 4B] An *in vitro* IVIS scanned image of the bacterial cells (Xen36 *S. aureus*) in a petri-dish and 10 mL falcon tube (left), and the *in vivo* IVIS scanned image of the bioluminescent bacterial cells (Xen36 *S. aureus*) injected subcutaneously into a mouse.

## 4.4. Extended Discussion

### 4.4.1. Study 4A: BBA-1 requires further trials and development

This is the first preclinical trial testing the *in vivo* efficacy of BBA-1 for the prevention of bone infection. Using our established murine bone infection model (TDH-pin method), we examined the effect of BBA-1 on preventing bone infections in mice. The current data show that BBA-1 cannot prevent bone infections in mice. Furthermore, the reduction of soft tissue infection may indicate some underlying antimicrobial activities from BBA-1. However, the data are inconclusive from the preclinical trial to suggest that BBA-1 is more advantageous than CSA-90 as a prophylactic antimicrobial agent.

In contrast, although the micro-CT data appear to show a trend of increased regenerate bone volumes in the BBA-1 group, the quantification did not generate statistical significance. Nevertheless, micro-CT reconstructions show substantial bone healing from BBA-1 in the bone defects without clearing the bone infection. This suggests BBA-1 may be osteogenic, but the current data are underpowered to determine the significance.

TDH-pin infection can lead to severe bone loss without treatment, based on our previous findings from the PP + CSA-90-coated implants animal trial (thesis Chapter 3). However, in the BBA-1 animal trial, despite the pins being uncoated, and all animals from the treatment group had only been given a single dose of BBA-1 (10 mg/kg) before surgery, the BBA-1 was able to promote bone formation even with the presence of infection. This shows that BBA-1 has a high potential to be used as an adjuvant therapeutic to prevent osteomyelitis.

Our data are still preliminary at this point, there are several variables that have not been tested for our hypothesis. Nonetheless, our previous *in vitro* study has demonstrated the bactericidal activities (against *S. aureus* and MRSA) and osteogenic property of BBA-1<sup>14</sup>. One limitation of this trial is that the concentration of BBA-1 used in this experiment (10 mg/kg) was indeed empirical, as this was our first preclinical trial of BBA-1. Although the *in vitro* MIC and MBC of BBA-1 against *S. aureus*<sup>14</sup>, these findings are usually not directly transferable for *in vivo* experiments due to various biological factors that *in vitro* trials cannot mimic. The selected concentration of BBA-1 was our expected maximum tolerated concentration. Nonetheless, none of the animals had developed any adverse reactions or side effects from the BBA-1, suggesting a higher concentration can be tested in the future.

Furthermore, we only tested a single dose administration of BBA-1 throughout the 14-days period instead of multiple doses. In clinical settings, antibiotics are usually given daily and for

a prolonged period up to several weeks or months. Therefore, future trials will consider multiple doses of BBA-1 (daily/weekly) to determine the efficacy of BBA-1. The power of the preclinical trials may also be increased by having a larger group size.

Additionally, we did not investigate the side effects and adverse reactions of BBA-1 at higher concentrations. Although the current dosage seems unharmed, ceragenins are known to be haemolytic and can induce some cytotoxicity in high concentrations<sup>35,36</sup>. However, recent studies have shown evidence that the cytotoxic effect can be reduced by delivering the ceragenins with polaxamers<sup>37-41</sup>. It is speculated that polaxamers can conjugate with BBA-1 thereby reducing the toxicity in animals given higher concentrations. It is encouraging to see no adverse reactions in the preliminary animal study. The safety profile of BBA-1 may also have been an undersold property that can have clinical advantages to be used in orthopaedics. Future studies should determine the safety and potential adverse reactions of using BBA-1 at higher concentrations. We suspect that BBA-1 may have the same or less toxicity than CSA-90 due to its specific bond binding property. However, our preliminary trial is unable to determine this hypothesis.

Another limitation of the preclinical trial of BBA-1 is the presence of a metal pin. At the time of the trial, the NIS-biofilm model was not fully developed, so a metal pin was used as a nidus for bacterial inoculation and biofilm formation. However, since BBA-1 is an intravenous antimicrobial, it is speculated that the BBA-1 does not reach the bacteria on an implant surface, and therefore, cannot eliminate the bacteria. Since CSA-90 and other ceragenins from the CSA-13 and CSA-44 subgroups are known to have high antibiofilm activity, it is hypothesised that BBA-1 will also be an antibiofilm agent. Thus, future trials of BBA-1 should consider using the NIS-biofilm model (described in thesis Chapter 2) instead of a TDH/NIS-pin method.

Bioluminescent Xen36 *S. aureus* strain or other bioluminescent bacteria strains can be used as an alternative in future preclinical trials. Xen36 allows in vivo tracking of the bacteria inside the body, and the bioluminescent signal can be detected and quantified. It is particularly useful to determine the progression of bone and tissue infections, and potentially to demonstrate the bactericidal activities of CSAs and BBAs in real-time<sup>42-47</sup>. Subsequently, other common orthopaedic pathogens such as *Staphylococcus epidermidis*, *Pseudomonas aeruginosa*, and *Escherichia coli* clinical isolates will also be tested for BBA-1 susceptibility.

While the current data confirm that BBA-1 promotes osteogenesis and have advantages in orthopaedic application, we lack evidence to suggest that BBA-1 is more superior to CSA-90 and other CSAs treatments. Indeed, we would suggest the consideration of using CSA-90 as

an orthopaedic implant coating agent, adjuvant with single or multiple doses of BBA-1 before and after surgery to achieve a higher efficacy and increase the prophylactic and therapeutic impact. Subsequently, BBA-1 can be considered as an adjuvant treatment with other commonly used antibiotics (e.g., clindamycin, gentamicin, and vancomycin) to reduce the risk of implant-related infections and improve clinical outcomes.

#### 4.4.2. Study 4B: MM-related bone infection model development

Multiple myeloma (MM) is a hematologic malignancy characterised by presence of abnormal clonal plasma cells, and the disease remains incurable. MM patients often complain about bone pain, and 80-90% will develop multiple osteolytic bone lesions at some point <sup>20</sup>.

Our clinical trial and case report review (Section 1.3) highlights that the osteolytic lesions can be prone to infections, and the treatments for these conditions are mostly relying on surgical interventions and prolonged antibiotic therapies. Therefore, we speculate that our synthesised BBA-1 will bring benefits to MM patients who suffer myeloma bone disease (MBD) and prevent osteolytic bone infections. However, to prove this concept, we first needed to determine the efficacy of BBA-1 in MM mice. The first step was to create a MM mouse bone infection model (Study 4B).

The 5TGM1-eGFP MM-cell injection is a well-established method to induce MM in mice <sup>32,48</sup>. Initially, we expected that all mice would develop osteolytic lesions in their bones, and these lesions would be prone to infection by a systemic bacterial inoculation via tail-vein injection. While all MM-cell injected mice developed neurological symptoms as expected, none of the MM-cell injected mice had developed bone lesions in the following two weeks after the bacterial injections. These results suggest that systemic MM-cell injection may not induce osteolytic lesions easily within a short period of time. However, it was impossible to extend the experiment as the mice must be euthanized as soon as they develop neurological symptoms. This limitation remains a major challenge of our model development. On the other hand, without the presence of osteolytic lesions or metal surface to act as a nidus for biofilm formation, we expected the bone infection rate to be low. Although we recognised the preliminary trial to be underpowered (N=2 per group), we saw 0/2 mice bone infections in MM-cell injected mice, and 2/2 bone infections in mice that received the NIS surgery, suggesting that biofilm is also essential to induce MM-related osteomyelitis.

Although the 5TGM1-eGFP MM cells injection method is reported as a mild systemic MM model that features gradual bone loss alongside the development of neurological features, the model was not designed to cause bone lesions. A potential alternative, a intratibial MM-cell injection model by Xu et al. (2018), reported a success in inducing bone elicits osteolytic reaction in nude mice by injecting tumour cells via intratibial injection <sup>49</sup>. A similar approach for multiple myeloma has also been reported in a mouse model for studying bone metastasis and bone pain <sup>50-53</sup>. Therefore, we decided to adopt the intratibial injection of 5TGM1-eGFP MM cells method for our next model development study.

#### 4.4.3. Future iterative development and refinement of a MM-bone infection model

The next stage of model development was to conduct another trial featuring the intratibial MM-cells injection method, expected to create more robust osteolytic lesions. Our plan was to have two groups (Group 8 and 9, N=10 per group). In proposed Study 4C, groups would receive a single intratibial injection of 5TGM1-eGFP MM cells ( $10^5$  cells) on the right leg (Table 4.4). Then the mice would be monitored for two weeks (or >2 weeks until osteolytic lesions were formed). The mice would be monitored by XR thrice weekly for osteolytic lesions and physically for neurological symptoms. As soon as the osteolytic lesions were seen on the right tibia, we would inoculate the bacterial biofilm of Xen36 *S. aureus* ( $10^5$  CFU) to the right and left tibiae by intratibial injection (local inoculation).

The mouse studies were approved by the Garvan Institute ethics committee (ARA18/03), and the animals were bred for experiment. However, one week before the starting point, the plan was disrupted by the SARS-CoV-2 lockdown in New South Wales from June to October 2021. Initially, the experiment was postponed due to the lockdown, but was then cancelled as the lockdown had extended for four months, and the bred mice had to be culled. During that time, no new animal experiments were allowed to begin at the Garvan Institute, access to the facility was strictly limited, and only if necessary. Staff from other institutes with no current essential experiments were prohibited from entering the facility.

**Table 4.4: The study intratibial injection MM-related bone infection model.**

Group	MM-cells (10 <sup>5</sup> cells)	Intratibial injection (MM-cells)		Bacteria (10 <sup>5</sup> CFU)	Intratibial injection (bacterial biofilm)		N=
		Right	Left		Right	Left	
8	5TGM1-eGFP	Yes	No	Nil	No	No	10
9	5TGM1-eGFP	Yes	No	Xen36	Yes	Yes	10
<b>Total</b>							<b>20</b>

Theoretically, based on our understanding of the model, we expected the mice in Group 8 and 9 to develop local osteolytic bone lesions on the right tibiae (with MM-cells), but not on the left tibiae (no MM-cells). We hypothesised that the mice in Group 9 that receive Xen36 biofilm on both legs would only develop bone infections on the right side due to the presence of bone lesions. In contrast, we expected 0% infection rate in Group 8 (no biofilm inoculation), but osteolytic lesions would be seen on the right leg due to MM-cells injection. We expected the bacterial biofilm to be trackable by IVIS scans as we continued to employ Xen36 biofilm for local inoculation. Bioluminescent signal should have been detectable within one week after the bacterial inoculation in Group 9. Since the bacteria were to be inoculated after the osteolytic lesions, we speculated that a bioluminescent signal would be detectable on the right side, aligning with the bone lesions.

For micro-CT analysis, the mice in Group 8 should have a higher bone volume (BV) and bone mineral density (BMD) than Group 9. Since there was no treatment for the MM-mice, we would not expect any regenerate bone volume of the bone lesion; osteolysis should only occur on the right tibiae (MM-cells injected), and the left tibiae should appear normal in both groups (no MM-cells). Regarding histology, we expected to see inflammatory cells (e.g., phagocytes and lymphocytes) presence in the bone marrow of infected tibiae, where uncontrollably proliferating plasma cells should be seen in the MM-cells injected bone marrow. In Group 9, we expected to find more profound effects of infection on the right tibia than the left tibia. Osteolysis and woven bones due to bone resorption on the cortical surface should be more severe on the right side than the left side. In some cases, structural deformation may have been present on the right tibia due to disruption of the cortical bone. Subsequently, with the larger group size (N=10 per group), we expected the statistical power to be improved and sufficient.

#### 4.4.4. Preclinical testing of BBA-1 using the MM-related bone infection model

Moving forward, if we were able to develop a reliable MM-related bone infection model in mice (Study 4C), we would optimise our model and complete proposed Study 4D (Table 4.5) to determine the efficacy of BBA-1 in preventing MM-related osteomyelitis.

Similar to Study 4C, the initial plan was to induce local osteolytic bone lesions in MM-cells injected mice by intratibial injection (Group 10-12). Once the bone lesions occurred, we would inoculate local Xen36 *S. aureus* biofilm via intratibial injection in Group 10 and 11 (N=10 per group) and give the mice BBA-1 (5 mg/kg) via intravenous injection (Group 12) or normal saline (Group 11) as a no-treatment positive control. As a no-infection control group, Group 10 (N=6) would receive no Xen36 but a single dose of BBA-1 (5 mg/kg) systemically. We aimed to evaluate the osteogenic and antimicrobial effects of BBA-1 in MM and MM-infected mice.

**Table 4.5: The study plan of BBA-1 efficacy testing**

Group	Cell intratibial injection (right side)	Bacterial inoculation	IV injection	N=
10	5TGM1-eGFP MM cells ( $1 \times 10^5$ )	Nil	BBA-1 (10 mg/kg)	6
11	5TGM1-eGFP MM cells ( $1 \times 10^5$ )	Xen36 ( $1 \times 10^6$ CFU)	Nil (saline)	10
12	5TGM1-eGFP MM cells ( $1 \times 10^5$ )	Xen36 ( $1 \times 10^6$ CFU)	BBA-1 (10 mg/kg)	10

Theoretically, all groups would develop osteolytic lesions on the right tibia due to MM-cells injection and the left tibiae should appear normal. Without the protection of BBA-1, Group 11 (MM-cells + Xen36 + no treatment) would develop osteolytic lesions and bone infections in the right tibiae (positive control), whereas Group 12 (MM-cells + Xen36 + BBA-1) would have a reduced rate of bone and soft-tissue infections. Meanwhile, Group 10 (MM-cells + BBA-1) would have no bone infections at all (negative control).

For micro-CT analysis, the bone volume (BV) and bone mineral density (BMD) would be the lowest in Group 11 as no treatment is given. In group 10, we expected the bone lesions on the right tibiae would be improved by the osteogenic effect of BBA-1, and since no biofilm was inoculated, there would be efficient improvements in BV and BMD, hypothetically. In Group 12, we expected BBA-1 to prevent osteomyelitis in the right tibiae of some animals (if not all). At this stage, the efficacy of BBA-1 is not predictable, but we would expect a higher prophylactic effect to be seen in Study 4D as no metal pins were implanted. Although it has

not been fully tested with BBA-1, CSA-90 and other CSA-13 subclass ceragenins have high antibiofilm activities, so theoretically, BBA-1 would also be able to prevent biofilm infections. Regarding histologic analysis, we expected to see woven cortical bones and lesions in all MM-cells injected tibiae. Group 10 would have a higher proportion of new bone formation due to BBA-1 treatment, and Group 12 would have less bone formation due to biofilm infection. Whereas Group 11 would have no bone healing and have severe bone resorption and destruction. Proliferated MM-cells would be seen in all bone marrow cavities of MM-cells injected tibiae. High numbers of inflammatory cells would also be found in the infected groups.

## 4.5. Conclusion

The first preclinical trial determined that BBA-1 can potentially be used in orthopaedic surgery to prevent osteomyelitis. However, the minimum bactericidal concentration (MBC) of BBA-1 to eliminate *S. aureus* infection remains to be determined. Although the *in vitro* osteogenic property of BBA-1 was previously determined, our preliminary *in vivo* study provided limited evidence to demonstrate that BBA-1 can promote bone healing. Subsequently, we speculated that BBA-1 would benefit MM patients by preventing osteolytic bone infections and myeloma bone diseases. Our pilot trial showed that systemic 5TGM1-eGFP cells injection was able to produce neurological symptoms but did not cause osteolytic bone lesions or bone infections in mice. Our data suggested that bone lesions were essential to act as a nidus for biofilm formation. Therefore, future studies will develop a multiple myeloma bone infection model using intratibial injections of 5TGM1-eGFP cells and Xen36 *S. aureus* biofilm.

## References

1. Dockery DM, Allu S, Vishwanath N, et al. Review of Pre-Operative Skin Preparation Options Based on Surgical Site in Orthopedic Surgery. *Surgical infections* 2021; **22**(10): 1004-13.
2. Klenerman L. A history of osteomyelitis from the Journal of Bone and Joint Surgery: 1948 TO 2006. *The Journal of bone and joint surgery British volume* 2007; **89**(5): 667-70.
3. Conterno LO, Turchi MD. Antibiotics for treating chronic osteomyelitis in adults. *Cochrane Database of Systematic Reviews* 2013; (9).
4. Hassoun A, Linden PK, Friedman B. Incidence, prevalence, and management of MRSA bacteremia across patient populations—a review of recent developments in MRSA management and treatment. *Critical Care* 2017; **21**(1): 211.
5. Lewandowski LR, Potter BK, Murray CK, et al. Osteomyelitis Risk Factors Related to Combat Trauma Open Femur Fractures: A Case-Control Analysis. *Journal of orthopaedic trauma* 2019; **33**(4): e110-e9.



6. Tribble DR, Lewandowski LR, Potter BK, et al. Osteomyelitis Risk Factors Related to Combat Trauma Open Tibia Fractures: A Case-Control Analysis. *Journal of orthopaedic trauma* 2018; **32**(9): e344-e53.
7. Wang X, Wang S, Fu J, Sun D, Shen J, Xie Z. Risk factors associated with recurrence of extremity osteomyelitis treated with the induced membrane technique. *Injury* 2020; **51**(2): 307-11.
8. Yalikun A, Yushan M, Li W, Abulaiti A, Yusufu A. Risk factors associated with infection recurrence of posttraumatic osteomyelitis treated with Ilizarov bone transport technique-a retrospective study of 149 cases. *BMC musculoskeletal disorders* 2021; **22**(1): 573.
9. Kirchner GJ, Smith NP, Garner MR. Intra-wound vancomycin and tobramycin powder for infection prophylaxis in orthopaedic trauma surgery: Economically justifiable? *Injury* 2021; **52**(11): 3340-3.
10. Horton SA, Hoyt BW, Zaidi SMR, et al. Risk factors for treatment failure of fracture-related infections. *Injury* 2021; **52**(6): 1351-5.
11. Fantoni M, Taccari F, Giovannenze F. Systemic antibiotic treatment of chronic osteomyelitis in adults. *European review for medical and pharmacological sciences* 2019; **23**(2 Suppl): 258-70.
12. Chatzipapas C, Karaglani M, Papanas N, Tilkeridis K, Drosos GI. Local Antibiotic Delivery Systems in Diabetic Foot Osteomyelitis: A Brief Review. *The review of diabetic studies : RDS* 2021; **17**(2): 75-81.
13. Cobb LH, McCabe EM, Priddy LB. Therapeutics and delivery vehicles for local treatment of osteomyelitis. *Journal of orthopaedic research : official publication of the Orthopaedic Research Society* 2020; **38**(10): 2091-103.
14. Kamble S, Valtchev P, Dao A, et al. Synthesis and Characterization of Bone Binding Antibiotic-1 (BBA-1), a Novel Antimicrobial for Orthopedic Applications. *Molecules (Basel, Switzerland)* 2021; **26**(6).
15. Schindeler A, Yu NY, Cheng TL, et al. Local delivery of the cationic steroid antibiotic CSA-90 enables osseous union in a rat open fracture model of Staphylococcus aureus infection. *The Journal of bone and joint surgery American volume* 2015; **97**(4): 302-9.
16. Mills R, Cheng TL, Mikulec K, et al. CSA-90 Promotes Bone Formation and Mitigates Methicillin-resistant Staphylococcus aureus Infection in a Rat Open Fracture Model. *Clin Orthop Relat Res* 2018; **476**(6): 1311-23.
17. Mills RJ, Boyling A, Cheng TL, et al. CSA-90 reduces periprosthetic joint infection in a novel rat model challenged with local and systemic Staphylococcus aureus. *Journal of orthopaedic research : official publication of the Orthopaedic Research Society* 2020; **38**(9): 2065-73.
18. Mehdi SH, Nafees S, Mehdi SJ, Morris CA, Mashouri L, Yoon D. Animal Models of Multiple Myeloma Bone Disease. *Frontiers in genetics* 2021; **12**: 640954.
19. Haertle L, Barrio S, Munawar U, et al. Cereblon enhancer methylation and IMiD resistance in multiple myeloma. *Blood* 2021; **138**(18): 1721-6.
20. Cowan AJ, Green DJ, Kwok M, et al. Diagnosis and Management of Multiple Myeloma: A Review. *Jama* 2022; **327**(5): 464-77.
21. van de Donk N, Usmani SZ, Yong K. CAR T-cell therapy for multiple myeloma: state of the art and prospects. *The Lancet Haematology* 2021; **8**(6): e446-e61.
22. Shapiro YN, Peppercorn JM, Yee AJ, Branagan AR, Raje NS, Donnell EKO. Lifestyle considerations in multiple myeloma. *Blood cancer journal* 2021; **11**(10): 172.
23. Asosingh K, Radl J, Van Riet I, Van Camp B, Vanderkerken K. The 5TMM series: a useful in vivo mouse model of human multiple myeloma. *The hematology journal : the official journal of the European Haematology Association* 2000; **1**(5): 351-6.

24. Lawson MA, McDonald MM, Kovacic N, et al. Osteoclasts control reactivation of dormant myeloma cells by remodelling the endosteal niche. *Nature communications* 2015; **6**: 8983.
25. Faict S, Muller J, De Veirman K, et al. Exosomes play a role in multiple myeloma bone disease and tumor development by targeting osteoclasts and osteoblasts. *Blood cancer journal* 2018; **8**(11): 105.
26. Peetermans M, Vanassche T, Liesenborghs L, et al. Plasminogen activation by staphylokinase enhances local spreading of *S. aureus* in skin infections. *BMC Microbiol* 2014; **14**: 310.
27. Trikha R, Greig D, Sekimura T, et al. Active rheumatoid arthritis in a mouse model is not an independent risk factor for periprosthetic joint infection. *PLoS One* 2021; **16**(8): e0250910.
28. Stavrakis AI, Zhu S, Loftin AH, et al. Controlled Release of Vancomycin and Tigecycline from an Orthopaedic Implant Coating Prevents *Staphylococcus aureus* Infection in an Open Fracture Animal Model. *Biomed Res Int* 2019; **2019**: 1638508.
29. Pribaz JR, Bernthal NM, Billi F, et al. Mouse model of chronic post-arthroplasty infection: noninvasive in vivo bioluminescence imaging to monitor bacterial burden for long-term study. *Journal of orthopaedic research : official publication of the Orthopaedic Research Society* 2012; **30**(3): 335-40.
30. Hegde V, Dworsky EM, Stavrakis AI, et al. Single-Dose, Preoperative Vitamin-D Supplementation Decreases Infection in a Mouse Model of Periprosthetic Joint Infection. *The Journal of bone and joint surgery American volume* 2017; **99**(20): 1737-44.
31. Bernthal NM, Stavrakis AI, Billi F, et al. A mouse model of post-arthroplasty *Staphylococcus aureus* joint infection to evaluate in vivo the efficacy of antimicrobial implant coatings. *PLoS One* 2010; **5**(9): e12580.
32. McDonald MM, Reagan MR, Youtlen SE, et al. Inhibiting the osteocyte-specific protein sclerostin increases bone mass and fracture resistance in multiple myeloma. *Blood* 2017; **129**(26): 3452-64.
33. Diaz-delCastillo M, Kamstrup D, Olsen RB, et al. Differential Pain-Related Behaviors and Bone Disease in Immunocompetent Mouse Models of Myeloma. *JBMR plus* 2020; **4**(2): e10252.
34. Opperman KS, Vandyke K, Clark KC, et al. Clodronate-Liposome Mediated Macrophage Depletion Abrogates Multiple Myeloma Tumor Establishment In Vivo. *Neoplasia (New York, NY)* 2019; **21**(8): 777-87.
35. Hoppens MA, Sylvester CB, Qureshi AT, et al. Ceragenin mediated selectivity of antimicrobial silver nanoparticles. *ACS Appl Mater Interfaces* 2014; **6**(16): 13900-8.
36. Polat ZA, Savage PB, Genberg C. In vitro amoebicidal activity of a ceragenin, cationic steroid antibiotic-13, against *Acanthamoeba castellanii* and its cytotoxic potential. *J Ocul Pharmacol Ther* 2011; **27**(1): 1-5.
37. Nagant C, Savage PB, Dehay JP. Effect of pluronic acid F-127 on the toxicity towards eukaryotic cells of CSA-13, a cationic steroid analogue of antimicrobial peptides. *Journal of applied microbiology* 2012; **112**(6): 1173-83.
38. Hashemi MM, Holden BS, Taylor MF, et al. Antibacterial and Antifungal Activities of Poloxamer Micelles Containing Ceragenin CSA-131 on Ciliated Tissues. *Molecules (Basel, Switzerland)* 2018; **23**(3).
39. Leszczyńska K, Namiot A, Cruz K, et al. Potential of ceragenin CSA-13 and its mixture with pluronic F-127 as treatment of topical bacterial infections. *Journal of applied microbiology* 2011; **110**(1): 229-38.

40. Oyardi Ö, Savage PB, Erturan Z, Bozkurt-Guzel C. In vitro assessment of CSA-131 and CSA-131 poloxamer form for the treatment of *Stenotrophomonas maltophilia* infections in cystic fibrosis. *The Journal of antimicrobial chemotherapy* 2021; **76**(2): 443-50.
41. Paprocka P, Durnaś B, Mańkowska A, et al. New  $\beta$ -Lactam Antibiotics and Ceragenins - A Study to Assess Their Potential in Treatment of Infections Caused by Multidrug-Resistant Strains of *Pseudomonas aeruginosa*. *Infection and drug resistance* 2021; **14**: 5681-98.
42. Avci P, Karimi M, Sadasivam M, Antunes-Melo WC, Carrasco E, Hamblin MR. In-vivo monitoring of infectious diseases in living animals using bioluminescence imaging. *Virulence* 2018; **9**(1): 28-63.
43. Sweeney E, Lovering AM, Bowker KE, MacGowan AP, Nelson SM. An in vitro biofilm model of *Staphylococcus aureus* infection of bone. *Letters in applied microbiology* 2019; **68**(4): 294-302.
44. Trombetta RP, de Mesy Bentley KL, Schwarz EM, Kate SL, Awad HA. A murine femoral osteotomy model with hardware exchange to assess antibiotic-impregnated spacers for implant-associated osteomyelitis. *European cells & materials* 2019; **37**: 431-43.
45. Isogai N, Shiono Y, Kuramoto T, et al. Potential osteomyelitis biomarkers identified by plasma metabolome analysis in mice. *Scientific reports* 2020; **10**(1): 839.
46. Sheppard WL, Mosich GM, Smith RA, et al. Novel in vivo mouse model of shoulder implant infection. *Journal of shoulder and elbow surgery* 2020; **29**(7): 1412-24.
47. Klopfenstein N, Cassat JE, Monteith A, et al. Murine Models for Staphylococcal Infection. *Current protocols* 2021; **1**(3): e52.
48. Oyajobi BO, Muñoz S, Kakonen R, et al. Detection of myeloma in skeleton of mice by whole-body optical fluorescence imaging. *Molecular cancer therapeutics* 2007; **6**(6): 1701-8.
49. Xu L, Wu Z, Zhou Z, Yang X, Xiao J. Intratibial injection of patient-derived tumor cells from giant cell tumor of bone elicits osteolytic reaction in nude mouse. *Oncology letters* 2018; **16**(4): 4649-55.
50. Schueler J, Wider D, Klingner K, et al. Intratibial injection of human multiple myeloma cells in NOD/SCID IL-2R $\gamma$ (null) mice mimics human myeloma and serves as a valuable tool for the development of anticancer strategies. *PLoS One* 2013; **8**(11): e79939.
51. Fryer RA, Graham TJ, Smith EM, et al. Characterization of a novel mouse model of multiple myeloma and its use in preclinical therapeutic assessment. *PLoS One* 2013; **8**(2): e57641.
52. Hiasa M, Okui T, Allette YM, et al. Bone Pain Induced by Multiple Myeloma Is Reduced by Targeting V-ATPase and ASIC3. *Cancer research* 2017; **77**(6): 1283-95.
53. Zhang B, Li X, Qian WP, Wu D, Dong JT. Measurement of Bone Metastatic Tumor Growth by a Tibial Tumorigenesis Assay. *Bio-protocol* 2021; **11**(22): e4231.

## 5. Discussion

### 5.1. Key findings

#### 5.1.1. Development of a reliable murine bone infection model for preclinical trials

We have described the iterative development of a murine model for bone infection that utilises the tibial drilled-hole (TDH) and needle insertion surgery (NIS) methods, featuring inoculation adjacent to a metal implant or using a bacterial biofilm. These models are more cost-effective for large preclinical trials compared to larger animal models. Moreover, the methods are simple to perform and should be highly reproducible in any laboratory setting.

Traditional preclinical trials employing larger animals like sheep and pigs often require substantial housing space and research funding. It is estimated that the cost of developing a new drug ranges from 314 million to 2.8 billion USD <sup>1</sup>. Between 2009 and 2018, the estimated median capitalised research and development cost per product was 985 million USD, including the expenditures on failed trials. Using mice as subjects would reduce the cost of collecting preliminary data to support novel therapy research.

Throughout the development of our NIS-pin and NIS-biofilm models, we have found a strong association between metal implants with osteomyelitis. The underlying mechanism is linked to metal surfaces acting as a nidus for biofilm formation. Even a small dose of bacteria can cause a 100% infection rate when a metal surface is present. This is consistent with the high risk of infections after fracture fixation (IAFF) and implant-related infection (IRI) when metal implants are involved. Alternatively, local biofilm inoculation to the bone is more pathological than planktonic-free bacteria and is sufficient to induce osteomyelitis.

#### 5.1.2. Plasma polymerisation has utility in producing antimicrobial coatings

We validated that the ion-assisted plasma polymerisation (IPP) technology can conjugate functional molecules to 3D metal surfaces and potentially apply to orthopaedic implant coatings. The *in vitro* experiments strongly suggest that metal-bound CSA-90 retains its antimicrobial activity, and the IPP coating allows rapid and sustainable release of CSA-90 to inhibit bacterial growth and prevent infections. The osteogenic property of CSA-90 was also verified by the *in vivo* data of regenerate bone volumes in the tibial drilled-hole defects, supporting its unique advantage as a coating agent for orthopaedic implants. We speculate that other substantial osteogenic ceragenins in the CSA-13 and CSA-44 subclasses (i.e., CSA-13, CSA-44, CSA-131, and CSA-144) will have similar benefits.

### 5.1.3. Synthetic bone binding antimicrobial is functional

Our group synthesised a novel bone binding antimicrobial (BBA-1) by conjugating CSA-90 to the bisphosphonate alendronate via an NHS-PEG-COOH linker, and the osteogenic and antimicrobial effects of BBA-1 were tested in *in vitro* experiments <sup>2</sup>. For the *in vivo* efficacy testing, our preliminary data show that a single dose of BBA-1 (10 mg/kg) can reduce the infection rate and increase the regenerate bone volume of the bone defects on the tibia, suggesting its antimicrobial and osteogenic effects were unaffected by the synthetic process. The current dosage (10 mg/kg) is safe for mice and has no *in vivo* toxicity or adverse reactions. These findings also reinforce the need to create alternative BBAs, using other CSAs, that may have more advantageous effects than BBA-1 in future.

## 5.2. Major limitations

### 5.2.1. NIS models need optimisation and testing new variables

We have developed a cost-effective and reliable bone infection murine model utilising the NIS method, including a metal implant with or without a biofilm. The extent of bone infection was evaluated using micro-CT imaging. Our results indicated that the tibial metaphysis was predominantly affected, characterised by osteolysis and the formation of woven bone near the drill-hole site. In certain cases, the infection spread to the diaphysis of the tibia, resulting in mild osteolysis. However, sepsis or the spread of infection to other bones such as the patella and femur was not observed.

Although many variables can be tested with our models for future applications, further development and optimisation are required. For instance, only female mice were tested, but osteomyelitis is more common in men than women (behaviour related). The reason for choosing female mice was to reduce housing capacity, as female mice can be housed together (up to 5 mice per cage), whereas group housing is not recommended for male mice. The age of animals in this study were only 8-12 weeks old and were all healthy wild-type animals. Most mice reach sexual maturity (both sexes) at 4-7 weeks old, so 8-12 weeks is considered young adulthood in mice. The reason we chose this age group is that mice at this age are more likely to survive the surgery and generate bone healing within two weeks. For age-insensitive studies, we recommend using animals at this age, but further studies are needed to determine the feasibility of using older mice, mice with other illnesses (e.g., diabetes) and genetically modified mice.

Another limitation that was not fully addressed was that we did not include the NIS ATCC-25923 (*S. aureus* biofilm) + pin group in our final experiment. Since an extensive number of animals was used (N=80), this experimental group was excluded, as based on data from the TDH model, such conditions would be expected to produce a 100% infection rate. However, there could be value in using such a model to test intervention strategies featuring implants and recalcitrant biofilm infection.

Although animals were monitored and weighed frequently, we did not include their weights and body temperature as results in the study (Chapter 2). No animals had lost weight over the two weeks, and body temperature was not measured as it was not included in our animal ethics approval. Instead, the Mouse Grimace Scale was used monitoring the animals. Rectal thermometry is a standard method of measuring body temperature in rodents. It involves inserting a small-diameter temperature probe through the anus, which can be onerous in extensive animal studies. Since we were only inoculating a small dose of bacteria locally, we would not expect any animals to develop high fever, and such data were unlikely to add any significance to our finding. However, measuring body temperature would be essential for future studies when testing therapeutics.

We collected blood, bone swabs, pins, and soft tissues for bacterial culture to determine the infection rate. Our data showed that no animals developed septicaemia, and bone swab culture was used to determine the presence of bacteria in the bone defects. The pin culture data were mostly consistent with the bone culture, as the bacteria were inoculated and adhered to the metal surface. Sometimes there were bacteria only detected in pins but not in the bone defects, so the data were not used as a standard. In contrast, soft-tissue culture results were not reported due to their inconsistency as often bacteria were only detected in soft tissue when pus was present, suggesting that soft-tissue culture may only pick up severe infections and was insensitive to mild bone infections. Since our goal is to determine the infection rate of bone infections in our model, we decided to use bone swabs as the standard for determining bone infection. However, soft-tissue culture should be continued in future studies due to its relevance to local infection.

Additionally, we lacked histological data to determine the presence of bacteria at the infection site. Bacterial staining in histology was not initially considered in our study design, partially due to limitations in time and resources. Potentially, gram-staining with H&E staining in histology section would determine the presence of bacteria under the light microscope. Alternatively, electron microscopy could perform high-scale imaging and visualise the

bacterial cells with additional preparation. Nonetheless, these techniques should be considered in future studies.

Future studies could be improved by optimising the concentration of inoculating bacteria to increase the reliability of the infection rate. Other orthopaedic pathogens, such as *Staphylococcus epidermidis*, *Pseudomonas aeruginosa* and *Escherichia coli*, could be compared in terms of their *in vivo* efficacy for testing novel therapeutics. While the current NIS model focuses on local inoculation, it is speculated that systemic inoculation would be possible but would require bacterial dose optimisation.

### 5.2.2. IPP coating with ceragenins require further investigations and clinical trials

The *in vitro* bacterial assays have shown that it is possible to utilise IPP technology for 3D orthopaedic implants. Both stainless-steel wires (rods) and silica beads (spheres) can be coated with IPP technology and CSA-90. Once coated, the CSA-90 on the surface can remain active and kill bacteria.

There is a lack of quantitative data to evaluate how much CSA-90 can attach to the 3D surface and be released. From the *in vitro* studies where PP + CSA-90 surfaces were washed with water and SDS, there we observed a burst release of CSA-90 with PP-coating, suggesting the drug linkage is unlikely to be covalently bonded. The underlying mechanism is still unclear, and it requires further investigation.

Although in *in vitro* studies, PP + CSA-90 showed a statistically significant and potent antimicrobial/bactericidal action, the *in vivo* data were less convincing. Since the CSA-90 coating technology was not fully optimised, while we used the same coating method for PP + CSA-90, *in vivo* environmental factors may affect drug binding that was not noticed previously. Also, CSA-90 may be lost during the surgical procedure, due to scratches, physical insertion, and moisture from tissue reducing the delivered dose. Such variation is difficult to encounter and quantify. With the complete optimisation of our NIS model, these effects could be reduced in future studies.

Alternatively, we could use polymerase chain reaction (PCR) to measure the 16S ribosomal RNA of *S. aureus* to quantify the bacterial load more accurately, however, PCR detection cannot distinguish live and dead bacteria, and therefore, it could not reflect the bactericidal effect of CSA-90 compared to viable bacterial culture. Despite that, quantified PCR data should

be comparable to the bioluminescent signal from bioluminescent bacteria (e.g., Xen36 *S. aureus*) and can be used to determine the presence of live bacteria in future studies.

Nonetheless, our preclinical trial with mice has demonstrated the synergistic effect between IPP and CSA-90. While a PP-coated surface can reduce bacterial adhesion and strengthen the attachment of CSA-90 to the implant surface, the CSA-90 on the implant can eliminate the inoculated bacteria and prevent osteomyelitis. Our results showed that the PP + CSA-90 coating reduced the infection rate compared to PP coating only from 90% to 50% (N=10). However, the difference was not statistically significant. Interestingly, despite the presence of bacterial infection, the CSA-90 coating seemed to promote adequate bone healing in the treated groups, which further enhance the advantages of using CSA-90 as a coating agent for orthopaedic implants. Future studies can increase the sample size and the CSA-90 concentration on the implant to improve statistical significance. Subsequent testing with various CSA-90 concentrations will determine the optimal concentration for implant coating.

Our data also further supported that CSA-90 has osteogenic activity based on regenerate bone volume, however, we did not perform a bone mineral density analysis to determine the bone loss due to bacterial infection and demineralisation. We hypothesised that CSA-90 alone could promote bone formation and potentiate recombinant human bone morphogenetic protein-2 (rhBMP-2) induced osteoblast differentiation. Our study did not demonstrate such an effect, as no rhBMP-2 was used on implants. However, future studies could investigate the opportunity of using CSA-90 + rhBMP-2 combined coating. We speculate that such coating will enhance bone healing and may have other applications in orthopaedic surgery for treating other conditions (e.g., osteogenesis imperfecta).

Another limitation of the study was that we did not employ the NIS-pin model as the NIS infection model had not been optimised at that time. Further, the study did not address biofilm infections, which are more severe in clinical settings, and only the monoclonal *S. aureus* strain has been tested. We also did not examine the IPP technology for non-metal implants (e.g., silica beads). Future studies should include plans to utilise these developed models to further evaluate the efficacy of the CSA-90 implant coating.

### **5.2.3. The MM-related bone infection model demands amendments and development**

The review article on clinical trials and case studies (Section 1.3) highlights that multiple myeloma (MM) patients are at risk of developing osteolytic lesions. Nearly all MM patients



will experience bone pain due to osteolytic lesions and myeloma bone disease at some point as the disease progresses. Therefore, we have targeted the MM patients as the primary testing group for clinical trials of BBA-1. It is hypothesised that BBA-1 is advantageous in treating conditions that involve bone loss and the risk of osteomyelitis.

In the first BBA-1 preclinical trial, only a single dose of BBA-1 was administered as prophylaxis, whereas in reality, patients are often given multiple doses of antibiotics to prevent bone infections. While we did not see a statistically significant reduction of bone infections in the BBA-1 treated group, this may be due to insufficient dosing. Interestingly, BBA-1 seemed to reduce the soft-tissue infection rate in our model, we hypothesised that the BBA-1 on the periosteum may reduce bacterial load and contact to the soft-tissue surrounding the bone surface. However, the protective mechanism was not fully delineated. Future studies could investigate further to determine the drug mechanism, and trial multiple dosing of BBAs to determine the prophylactic efficacy. We speculated that multiple injections and potentially a higher dose of BBA-1 will generate improved outcomes.

Additionally, our previous studies have shown effective binding of BBA-1 to the periosteum. However, its affinity for binding to the endosteum has not been determined. One major limitation of this study was that we used the TDH-pin model, so more bacteria might remain in the medullary canal from the metal surface, whereas BBA-1 might not be efficiently binding to the endosteum. Therefore, future experiments should address the affinity of BBA-1 binding to the endosteum, and a biofilm bone infection model should be employed.

To promote the progression of bone infections in the BBA-1 trial, metal pins were employed in conjunction with TDH. Despite this, the bacteria may remain within the medullary canal, where BBA-1 may not be effectively delivered via circulation.

Currently, no animal models for multiple myeloma-related bone infections have been developed successfully. While the intravenous injection of 5TGM1-eGFP MM cells can induce neurological symptoms of MM in BKAL mice, it does not induce osteolytic lesion within the study timeframe. Without bone lesions, there is no nidus on the bone surface for bacteria to form biofilms; therefore, no bone infections occurred in the preliminary trial. It is hypothesised that an intratibial injection of 5TGM1-eGFP MM cells would be able to cause osteolytic lesions, and local intratibial inoculation of bacterial biofilm will cause bone infection from the lesions. Further development of this and other aspects of the model are still needed.

### 5.3. Results from parallel studies

The literature review article (Section 1.2) on ceragenins in orthopaedic applications only covered studies published up to 2019. Between January 2020 and June 2022, additional studies involving ceragenins have been published. Many of these studies focused on the antimicrobial and antibiofilm effects of CSA-131 and other ceragenins from the CSA-13 and CSA-44 subgroups. Some studies demonstrated the use of nanoparticles to reduce the toxicity of ceragenins and improve drug delivery and efficacy.

#### 5.3.1. The applications of ceragenins for infectious diseases

Bozkurt Güzel et al. (2020) determined that CSA-131 and CSA-138 were good candidates for carbapenem-resistant *Pseudomonas aeruginosa* infections using *in vitro* time-kill assays and minimum inhibitory concentration (MIC) or minimum bactericidal concentration (MBC) assays <sup>3</sup>. They also found that CSA-13 and CSA-131 are good alternatives for carbapenem-resistant *Acinetobacter baumannii* infections <sup>4</sup>. Chmielewska et al. (2020) separately reported that CSA-13, CSA-44 and CSA-131 may be favourable for prevention and decrease of global burden of New Delhi Metallo-beta-lactamase (NDM-1) carbapenemase-producing Enterobacteriaceae (CPE), which include *Escherichia coli* BAA-2471, *Enterobacter cloacae* BAA-2468, *Klebsiella pneumoniae* subsp. BAA-2472, and *K. pneumoniae* BAA-2473 <sup>5</sup>.

Hacioglu et al. (2020) found that CSA-90 and CSA-13 were effective agents against both mono- and multispecies (including *Candida albicans*, *Pseudomonas aeruginosa*, *Acinetobacter baumannii* and *Escherichia coli*) biofilms ( $P < 0.05$ ), whereas CSA-131 and CSA-192 were the least effective against mono- and fungal-bacterial multispecies biofilms. The study also highlighted that ceragenins were more advantageous than antimicrobial peptides (AMPs) against mono- or multispecies biofilms <sup>6</sup>. This study supports our speculation that CSA-90 can be used as a prophylactic agent to prevent implant-related osteomyelitis, as this infection is often associated with bacterial biofilms and multiple microorganisms.

Latorre et al. (2021) reported the *in vitro* antibiofilm activity of CSA-131 on endotracheal tubes (ETTs). The ETTs were coated with CSA-131 and then exposed to biofilms of clinical *Pseudomonas aeruginosa*, *Escherichia coli* and *Staphylococcus aureus* <sup>7</sup>. Paprocka et al. (2021) collected MIC/MBC values and evaluated the ability of CSA-13, CSA-44 and CSA-131 against 150 clinical isolates of *P. aeruginosa* to prevent bacterial biofilm formation. It was found that ceragenins (CSA-13 subgroup) are highly active against clinical strains of *P. aeruginosa* at low

concentrations despite their resistance mechanisms to conventional antibiotics (e.g., ceftolozane/tazobactam, ceftazidime/avibactam and meropenem/vaborbactam) <sup>8</sup>. The study also confirmed that tested CSAs have high antibiofilm activities against various pathogens. Tokajuk et al. (2022) performed an *in vitro* biofilm mass analysis using crystal violet (CV) staining, showing that CSA-44 could prevent biofilm formation and reduce the mass of biofilm formed by endodontic and periodontal pathogens, including *Enterococcus faecalis* and *Candida albicans* <sup>9</sup>. The study recognised the application of CSA-44 as an agent to combat oral pathogens and control biofilm formation on the tooth's surface and composite fillings.

Damar-Çelik et al. (2021) reported that CSA-13, CSA-131 and CSA-131P (CSA-131 formulated with a poloxamer Pluronic® F127) were effective against biofilm-producing *Achromobacter* strains <sup>10</sup>. Their results indicated that CSA-131 formulated in micelles could be therapeutic for polymicrobial and biofilm-related infections. The study also demonstrated that CSA-131P has the same antimicrobial and antibiofilm activities as CSA-13. In contrast, Oyardi et al. (2021) demonstrated that CSA-131P (5% Pluronic ® F127) had the lowest MIC, followed by CSA-131 and CSA-13, against a *Stenotrophomonas maltophilia*, which is a Gram-negative bacterium resistant to several antibiotics and is prevalent in cystic fibrosis patients <sup>11</sup>. Paprocka et al. (2021) examined the cytotoxicity of ceragenins using human erythrocyte (red blood cell) haemolysis and microscopy observations of human lung epithelial cells (A549) post-treatment. The study suggested that adding poloxamer 407 (Pluronic ® F-127) with ceragenins at concentrations ranging from 0.5-5% can reduce toxicity <sup>8</sup>. These studies all support that poloxamer 407 and other alternative drug delivery substrates can be advantageous in reducing drug side effects and adverse reactions.

Demir et al. (2022) demonstrated that CSA-13, CSA-131 and CSA-131P were effective against *Burkholderia cepacia* complex (Bcc), Gram-negative aerobic and non-fermentative bacilli, often seen in cystic fibrosis with clinical symptoms <sup>12</sup>. Although Bcc infection can be asymptomatic, it can also cause fatal pneumonia. Both first-generation (CSA-13) and second-generation (CSA-131 and CSA-131P) have significant antimicrobial effects on Bcc. The study also reported synergistic activity of CSA-13 and levofloxacin against Bcc, suggesting combining ceragenins with currently marketed antibiotics could be more advantageous in treating infections.

An *in vivo* rat implant-infection study was also published in 2020 by our team, demonstrating the capability of CSA-90 as a coating agent on porous metal implants to prevent periprosthetic joint infection (PJI) challenged with either local or systemic *Staphylococcus aureus* inoculation

<sup>13</sup>. The data showed that CSA-90 reduced the rates of PJI with local (from 100% to 30%) and systemic (from 90% to 10%) bacterial inoculations. The median survival time was also increased from 8 to 17 days (local) and 8 to 42 days (systemic). Although CSA-90 alone did not prevent infection from developing in all implants, CSA-90 can likely be used as an adjunct to routine systemic antibiotic prophylaxis, and it supports the further development of CSA-90 as a novel antimicrobial coating for orthopaedic implants.

In 2021, Chmielewska et al. demonstrated a new class of gold nanoparticles (AuNPs) were able to conjugate with CSA-131, showing high bactericidal activity against multidrug-resistant Gram-positive and Gram-negative bacteria <sup>14</sup>. This study reveals the therapeutic potential of gold nanosystems, due to their high haemocompatibility with CSA-131, meaning AuNPs may aid in the development of newer and superior systems for safe, systemic delivery of ceragenins. Prasad et al. (2021) conjugated peanut-shaped AuNPs (AuPs) with CSA-13, CSA-44 and CSA-131 (i.e., AuP@CSA-13, AuP@CSA-44 and AuP@CSA-131) and tested their efficacy against *Haemophilus influenza* (ATCC-49766), *Moraxella catarrhalis* (ATCC-25238) and *Streptococcus pneumoniae* (ATCC-49619). The study showed that all tested CSAs exerted bactericidal activity against these pathogens. However, most importantly, it was found that the conjugation of CSAs with AuPs strongly enhanced their killing efficacy, as all CSA-based nanosystems eradicated the bacterial pathogens in doses ranging from 0.5-5 µg/mL, which is significantly lower than free CSAs (0.5-10 µg/mL) <sup>15</sup>. AuP-CSAs were found to be more active than free CSAs, and CSA-131 was the most potent ceragenin among all three, with the highest efficacy in limiting the colony-forming ability of tested bacteria. Similar effects were reported in fungal infections (*Candida*) using a set of nanosystems with rod-(AuR), peanut-(AuP), and star-shaped (AuS) metal cores conjugated with CSA-13, CSA-44 and CSA-131 <sup>16</sup>.

Regarding antimicrobial resistance, it has been documented that ceragenins have a low potential for resistance development <sup>8</sup>. A similar observation was reported with *Candida*. A study showed that CSAs (CSA-13 and CSA-131) have significant candidacidal activities *in vitro* and could effectively eradicate species of yeast responsible for biofilm formation and voice prostheses failure <sup>17</sup>. Subsequently, even after different *Candida* species were subjected to CSA-13 and CSA-131 during 25 passages, no tested *Candida* strain showed a significant development of resistance.

While ceragenins are a family of synthetic, amphipathic molecules, designed to mimic the antimicrobial properties naturally found in cationic antimicrobial peptides (CAMPs), Mitchell et al. (2022) speculated that CSAs have distinct antimicrobial mechanisms. The study reported

the results of a comparative study of the bacterial (*E. coli*) responses to CAMPs (LL-37, colistin) and ceragenins (CSA-13 and CSA-131), using transcriptomic and proteomic analyses. It found that *E. coli* responded similarly to CAMPs and ceragenins by inducing a Cpx envelope stress response. Genes involved in the membrane stress response such as *spy*, *degP* and *cpxP* were upregulated by all antibiotics. However, when *E. coli* were exposed to CAMPs, increased expression of genes involved in LPS/colonic acid biosynthesis (*wzc*, *wcaE* and *cpsB*) was found, whereas if *E. coli* were exposed to CSAs, genes encoding phosphate-responsive regulators (PhoR and PhoB) were upregulated. The results indicated that different mechanisms of action could be involved between these two classes of drugs<sup>18</sup>. Pathway analysis of genes modulated by more than one compound was completed to define transcriptional responses to CAMPs and CSAs. Significant increases in mRNA abundance were seen for 86 *E. coli* genes across all conditions, with 68 and 57 genes upregulated in response to CAMP and CSA treatment, respectively. The study also highlighted that CSAs could trigger an unprecedented Cpx envelope stress response in *E. coli*, suggesting that CSA-13 and CSA-131 may act on the bacterial envelope. While the result explained why ceragenins are effective against colistin-resistant bacteria, it also suggests that the Cpx response might help bacteria survive exposure to ceragenins. Further studies should determine the mechanistic similarities between CSAs and CAMPs in other systems.

### 5.3.2. The potentials of ceragenins as anticancer agents

The opportunity of using CSAs as a cancer therapy has been explored. Piktel et al. (2020) examined the anticancer effect and haemocompatibility of nanoformulations consisting of CSA-131 united with amino silane-modified iron oxide-based magnetic nanoparticles (MNP)<sup>19</sup>. It was found that MNP-based nano-molecules increased the killing efficiency of CSA-131, decreasing the viability of selected lung and colon cancer cells *in vitro* when compared to CSA-131 alone. This study supports the idea of using CSAs as an anticancer agent and the potential of adopting the MNP nanosystems with CSA-90 and BBA-1 for treating multiple myeloma.

Although there is a growing body of scientific evidence suggesting the great potential of ceragenins as anti-cancer agents, the gathered evidence mainly was based on *in vitro* studies, and the hypothesis was never tested in animal models. However, Piktel et al. (2021) theorised that gold nanoparticles-assisted delivery of antineoplastics into cancerous cells is a practical approach for overcoming the limitations of systemic chemotherapy. While ceragenins have a high potential to be novel anti-cancer drugs, high-dose concentrations within their haemolytic

range may be required to inhibit cell proliferation in some tumours effectively. Therefore, to control the toxicity/efficiency ratio, AuPs were used to deliver CSA-131 (AuP@CSA-131) and the cytotoxicity of AuP@CSA-131 was tested against ovarian cancer (SKOV-3) cells *in vitro*. They also determined the efficacy of intravenously and intratumorally administered CSA-131 and AuP@CSA-131 *in vivo* with a xenograft ovarian cancer model. Comparative analysis revealed that AuP@CSA-131 exerted more potent antineoplastic effects than free ceragenin. Such effects were determined by enhanced ability to induce caspase-dependent apoptosis and autophagy processes via reactive oxygen species (ROS)-mediated pathways. While both CSA-131 and AuP@CSA-131 administrations prevent the inflammatory response associated with cancer development, the animal study found that AuP@CSA-131 had delayed clearance and prolonged blood circulation compared with free CSA-131<sup>20</sup>. All these findings support the possibility of utilising non-spherical gold nanoparticles as an effective way to deliver antineoplastics for the treatment of ovarian malignancy.

### 5.4. Future directions

The current clinical management of bone infections still centres on source control, tailored antibiotic therapy, and correction of medical comorbidities. Moving forward, there are numerous opportunities for future research on osteomyelitis, including understanding the pathophysiology and pathogenic mechanisms, antibiotic susceptibility patterns, novel preventive measures and treatments, and improved diagnostic tools. Subsequent to this thesis, several directions to further research have emerged and been considered, which involve optimising the preclinical bone infection model, developing new coating technology for orthopaedic implants, exploring the full potential of ceragenins as clinical agents to treat infectious diseases and cancer, and the validation of opportunistic conjugates and substrates to improve ceragenin drug efficacy, delivery, and safety.

#### 5.4.1. Antibiotic susceptibility and resistance surveillance

Recent changes in antimicrobial susceptibility have altered empirical antibiotic selection, and the treatment of osteomyelitis has been essentially unchanged over the last decades. In the clinical arena, ongoing research on interdisciplinary clinical care guidelines and severity classification will improve the quality of care locally and nationally. Since the emergence and dissemination of multi-drug resistance (MDR) or extensively drug resistance (XDR) are

significant concerns for public health <sup>21</sup>, continuous surveillance and monitoring of changes in antimicrobial susceptibility patterns are essential for public health and policy. Consistent vigilance of antimicrobial resistance will also aid decision making on empirical therapy selection.

To date, there are no reports of antibiotic resistance to ceragenins. Although it is challenging and unlikely to happen promptly, bacterial and fungal pathogens can develop mechanisms and stress responses to compromise ceragenins and other associated therapeutics (e.g., BBAs and nano-CSAs) <sup>18</sup>. Like other conventional antibiotics, regular determinations of MICs and MBCs of clinically isolated strains using the microbroth dilution method would be essential for ceragenins. The susceptibility patterns and ceragenin-resistances should be closely monitored for the CSA-13 subgroup, considering their wide clinical applications as coating, anticancer and antimicrobial agents.

Meanwhile, susceptibility testing and time-kill assays should be performed to explore the efficacy of ceragenins (like CSA-8, CSA-13, CSA-44, CSA-131 and CSA-138) against other unconsidered pathogens. Monitoring antimicrobial susceptibility patterns of ceragenins against various pathogens will also determine other potential clinical applications in specialities other than orthopaedic surgery.

Prolonged exposure can be another risk factor for antibiotic resistance development. Understanding the antimicrobial mechanism will identify new essential biological pathways of bacteria that are less prone to develop ceragenin-resistance, informing the design principles for maximising antimicrobial effects of next generation ceragenins and other synthetic CAMPs. Additional mechanistic studies are required to better understand the structure-activity relationship underlying ceragenin antimicrobial effects and uncover how new defensive mechanisms may emerge.

Several studies have reported synergistic effects of ceragenins and other conventional antibiotics and nanoparticles <sup>3,4,12,19,22</sup>. Future studies should also focus on validating and optimising combined therapies with *in vivo* trials, including the combination of CSAs and BBAs.

### 5.4.2. Optimising animal models for preclinical trials

Animal models and preclinical trials are essential for discovering new ideas and concepts for treating and preventing osteomyelitis. Standard *in vitro* antibiotic susceptibility testing is often

unable to model the complexity of bacterial physiology *in vivo* associated with abscess and biofilm formation or nutrient deprivation and tissue hypoxia<sup>23</sup>. However, such conditions can only be simulated in animal models, which implies the value of animal models for drug efficacy testing. In recent years, animal studies have also shed light on host and bacterial factors contributing to osteomyelitis's pathogenesis. Animal models can also demonstrate new therapeutic targets, drug delivery methods, and immunomodulatory therapies<sup>24</sup>.

Initially, our NIS models were designed to test novel therapies. However, there is no limitation to using our models for studying other types of bone infections, such as myeloma bone disease and diabetic-foot osteomyelitis. The NIS models should be transferable to other established animal models and study-related diseases' pathophysiology. The MM-related bone infection model attempt is one example, but many subsequent models can be developed in the future with uncountable opportunities.

With the increased interest in bioluminescent bacteria in preclinical research, we have employed Xen36 *Staphylococcus aureus* in our NIS model. Bioluminescent bacteria are a tool for cell tracking and progression monitoring and quantifying the real-time efficacy of therapeutics<sup>25,26</sup>. The bioluminescent signals can also determine bacterial bioactivity and pathogenesis with the IVIS Spectrum *in vivo* imaging system in real-time. Future studies can focus on testing other bioluminescent orthopaedic pathogens and bioluminescent biofilms.

### 5.4.3. Determining the orthopaedic applications of CSA-131

In recent years, many studies have focused on CSA-131 and CSA-131P (conjugated with AuNPs)<sup>3,5,11,14,19,20</sup>. While CSA-90 is particularly known for its osteogenic features, we speculate that CSA-131 (the second generation of CSA-13 and the cousin of CSA-90) should also have osteogenic properties. Indeed, our preliminary *in vitro* ALP assays with MC3T3-E1 mouse pre-osteoblasts (unpublished data) have suggested that CSA-131 can be equally as osteogenic as CSA-90 and have a similar synergistic effect with recombinant human BMP-2 (rhBMP-2). Although further *in vitro* and *in vivo* studies are required to consolidate our findings and determine the orthopaedic applications of CSA-131, theoretically, the next generation bone binding antimicrobials (BBAs) can be derived and synthesised from CSA-131, as both CSA-90 and CSA-131 have the same conjugating sites for the linker.

Regarding orthopaedic applications, CSA-131 is effective against a variety of bacterial and fungal pathogens and biofilms<sup>5-8,11,17,27</sup>. Meanwhile, CSA-131 conjugated with AuNPs seems



to be an efficient delivery method to enhance haemocompatibility and bactericidal effects and reduce toxicity<sup>14,16,20</sup>. Future studies should examine the osteogenic effect of AuNPs@CSA-131 and other alternatives. No studies have yet considered the possibility of synthesising BBAs conjugated with AuNPs. Since the gold nanosystems have higher haemocompatibility, which can increase the duration of circulation, and lower toxicity than free CSAs in the blood, it may be possible to combine AuNPs and BBAs to form AuNP@BBA molecules (e.g., AuP@BBA-1) to increase drug efficacy and delivery efficiency of BBAs to bones.

The Food and Drug Administration (FDA) has approved CSA-131 for endotracheal tube coating<sup>7</sup>. Future studies can determine if CSA-131 is suitable for orthopaedic implant coating. No studies have yet determined this possibility. However, a similar approach with the NIS-pin model can be used to assess CSA-131 with IPP coating technology or with other coating methods, such as nano-coating. Many variables can be considered in future studies.

Although it has not been a significant focus of the initial development of ceragenins, wide-ranging research using cancer cell lines with tremendous clinical implications has shown that CSA-13 and CSA-131 exert anticancer activity in colon cancer, breast cancer and lung adenocarcinoma<sup>22,28-30</sup>. Nonetheless, no recent studies consider the applications of CSA-13, CSA-90 and CSA-131 for osteosarcoma or metastatic bone cancer. Future studies should consider applying BBA-1, CSA-131 and other derivative molecules to prevent or treat bone cancer or cancer-related bone disease (e.g., myeloma bone disease). Preclinical trials should also be performed to demonstrate the efficacy of these therapeutics for other forms of cancer. Determining the therapeutic mechanisms of ceragenins against cancer cells will inspire future designs of cancer-targeting CSAs.

#### **5.4.4. Exploring the combined effects of BBAs and CSA-coated implants**

Clinically, it is difficult to endow implants with excellent osteogenic ability and antibacterial activity simultaneously<sup>31</sup>. Since CSA-90 is considered more effective as an adjuvant prophylactic agent with intravenous antimicrobials, rather than a monotherapy<sup>13</sup>, future studies can demonstrate the combined efficacy of osteogenic CSA-coated implants with BBAs to prevent bone infections. This concept derives from the observations that CSA-90 coating alone cannot eliminate the risk of bone infection, whereas BBA-1 is not particularly effective against implant-related infections.

To date, our preliminary trial of BBA-1 (thesis chapter 4) is the first *in vivo* study determining the efficacy of BBA-1 in animals. With our established NIS-pin and NIS-biofilm models, combining the models and assessing the effectiveness and safety of using CSA-coated pins with a single dose of BBA-1 via intravenous administration is feasible. The hypothesis is that CSA-coated pins and BBA-1 can prevent or eradicate biofilm infections and promote bone-producing bone defects. Based on our previous observation, we suspect that the adverse reactions with the current dosages would be minimal. Nonetheless, the concentrations of CSAs and BBAs can be tested as variables to determine the optimal synergistic doses of both agents. It is speculated that CSA-90 and CSA-131 would be good candidates for the implant coating, whereas BBAs with AuNP-conjugates may be even more advantageous for drug delivery than free BBAs.

Moving forward, we are also considering the idea that ceramic coated implants, which bind to bone mineral and would be expected to interact and prevent resorption, could be used with BBAs. Ceramic is more commonly used for dental implant<sup>32</sup>, but one of our recent studies has demonstrated the development and various applications of personalised baghdadite ( $\text{Ca}_3\text{ZrSi}_2\text{O}_9$ ) scaffolds in orthopaedic and dental surgery<sup>33</sup>.

### 5.4.5. Understanding the underlying osteogenic mechanisms of CSAs and BBAs

The findings of this thesis are opening opportunities to create new osteogenic ceragenins and bone binding antimicrobials that have various applications in clinical settings other than orthopaedic surgery. Future studies should continue inventing novel osteogenic and bone-targeting therapeutics using ceragenins other than CSA-90 and testing other bio-linkers. Importantly, we are creating the second generation of BBA-1 with alternative substrates and linkers, and we will continue to test the osteogenic and antimicrobial properties of new BBAs *in vitro* and *in vivo*. Previous studies have determined a synergistic osteogenic effect of CSA-90 and BBA-1 with rhBMP-2 on mouse pre-osteoblasts<sup>2,34</sup>. Our studies have also shown that even without rhBMP-2, CSA-90 and BBA-1 alone can stimulate osteogenesis in cell culture. However, the osteogenic mechanism of CSA-90 is not fully understood. Transcriptomic and proteomic analyses may reveal the underlying osteogenic mechanism at a molecular level. Future studies should determine genes or proteins responsible for the osteogenic effect. Understanding the osteogenic mechanism will help develop more osteogenic ceragenins that are more advantageous than CSA-90 and BBA-1 to promote bone healing.

### Conclusion

Osteomyelitis remains a high-burden disease and requires ongoing research to develop new technologies and novel therapeutics for prevention and clinical management. We developed several preclinical murine bone infection models featuring infected bone defects. Using one of these models, we tested the potential of CSA-90 and other ceragenins in the CSA-13 subgroup to be active orthopaedic implant coating agents, due to their broad-spectrum antimicrobial effects and osteogenic properties promoting bone healing. We also examined the potential use of IPP as an implant coating technology. Subsequently, we implemented the design of a synthetic bone-binding antimicrobial agent that has the potential to be used as a systemic antimicrobial, with similar antimicrobial and osteogenic effects to CSA-90. Although this still needs to be validated in a preclinical model, we believe that BBA-1 and other bone binding antimicrobials may have utility for preventing general osteomyelitis, osteolytic infections in fractures and bone defects, and myeloma bone disease in multiple myeloma patients. Future research will continue to focus on model optimisation, preclinical trials of CSAs and BBAs, and improving the technology of implant coating to prevent osteomyelitis.

### References

1. Wouters OJ, McKee M, Luyten J. Estimated Research and Development Investment Needed to Bring a New Medicine to Market, 2009-2018. *JAMA* 2020; **323**(9): 844-53.
2. Kamble S, Valtchev P, Dao A, et al. Synthesis and Characterization of Bone Binding Antibiotic-1 (BBA-1), a Novel Antimicrobial for Orthopedic Applications. *Molecules (Basel, Switzerland)* 2021; **26**(6).
3. Bozkurt Güzel Ç, Avci NM, Savage P. In Vitro Activities of the Cationic Steroid Antibiotics CSA-13, CSA-131, CSA-138, CSA-142, and CSA-192 Against Carbapenem-resistant *Pseudomonas aeruginosa*. *Turkish journal of pharmaceutical sciences* 2020; **17**(1): 63-7.
4. Bozkurt-Guzel C, Inci G, Oyardi O, Savage PB. Synergistic Activity of Ceragenins Against Carbapenem-Resistant *Acinetobacter baumannii* Strains in Both Checkerboard and Dynamic Time-Kill Assays. *Current microbiology* 2020; **77**(8): 1419-28.
5. Chmielewska SJ, Skłodowski K, Piktel E, et al. NDM-1 Carbapenemase-Producing Enterobacteriaceae are Highly Susceptible to Ceragenins CSA-13, CSA-44, and CSA-131. *Infection and drug resistance* 2020; **13**: 3277-94.
6. Hacıoglu M, Oyardi O, Bozkurt-Guzel C, Savage PB. Antibiofilm activities of ceragenins and antimicrobial peptides against fungal-bacterial mono and multispecies biofilms. *The Journal of antibiotics* 2020; **73**(7): 455-62.
7. Latorre MC, Pérez-Granda MJ, Savage PB, et al. Endotracheal tubes coated with a broad-spectrum antibacterial ceragenin reduce bacterial biofilm in an in vitro bench top model. *The Journal of antimicrobial chemotherapy* 2021; **76**(5): 1168-73.

8. Paprocka P, Durnaś B, Mańkowska A, et al. New  $\beta$ -Lactam Antibiotics and Ceragenins - A Study to Assess Their Potential in Treatment of Infections Caused by Multidrug-Resistant Strains of *Pseudomonas aeruginosa*. *Infection and drug resistance* 2021; **14**: 5681-98.
9. Tokajuk J, Deptuła P, Chmielewska SJ, et al. Ceragenin CSA-44 as a Means to Control the Formation of the Biofilm on the Surface of Tooth and Composite Fillings. *Pathogens (Basel, Switzerland)* 2022; **11**(5).
10. Damar-Çelik D, Mataracı-Kara E, Savage PB, Özbek-Çelik B. Antibacterial and antibiofilm activities of ceragenins against *Achromobacter* species isolated from cystic fibrosis patients. *Journal of chemotherapy (Florence, Italy)* 2021; **33**(4): 216-27.
11. Oyardi Ö, Savage PB, Erturan Z, Bozkurt-Guzel C. In vitro assessment of CSA-131 and CSA-131 poloxamer form for the treatment of *Stenotrophomonas maltophilia* infections in cystic fibrosis. *The Journal of antimicrobial chemotherapy* 2021; **76**(2): 443-50.
12. Demir ES, Oyardi O, Savage PB, Altay HO, Bozkurt-Guzel C. In vitro activity of ceragenins against *Burkholderia cepacia* complex. *The Journal of antibiotics* 2022; **75**(7): 403-9.
13. Mills RJ, Boyling A, Cheng TL, et al. CSA-90 reduces periprosthetic joint infection in a novel rat model challenged with local and systemic *Staphylococcus aureus*. *Journal of orthopaedic research : official publication of the Orthopaedic Research Society* 2020; **38**(9): 2065-73.
14. Chmielewska SJ, Skłodowski K, Depciuch J, et al. Bactericidal Properties of Rod-, Peanut-, and Star-Shaped Gold Nanoparticles Coated with Ceragenin CSA-131 against Multidrug-Resistant Bacterial Strains. *Pharmaceutics* 2021; **13**(3).
15. Prasad SV, Pikel E, Depciuch J, et al. Targeting bacteria causing otitis media using nanosystems containing nonspherical gold nanoparticles and ceragenins. *Nanomedicine (London, England)* 2021; **16**(30): 2657-78.
16. Skłodowski K, Chmielewska SJ, Depciuch J, et al. Ceragenin-Coated Non-Spherical Gold Nanoparticles as Novel Candidacidal Agents. *Pharmaceutics* 2021; **13**(11).
17. Spalek J, Daniluk T, Godlewski A, et al. Assessment of Ceragenins in Prevention of Damage to Voice Prostheses Caused by *Candida* Biofilm Formation. *Pathogens (Basel, Switzerland)* 2021; **10**(11).
18. Mitchell G, Silvis MR, Talkington KC, et al. Ceragenins and Antimicrobial Peptides Kill Bacteria through Distinct Mechanisms. *mBio* 2022; **13**(1): e0272621.
19. Pikel E, Markiewicz KH, Wilczewska AZ, et al. Quantification of Synergistic Effects of Ceragenin CSA-131 Combined with Iron Oxide Magnetic Nanoparticles Against Cancer Cells. *International journal of nanomedicine* 2020; **15**: 4573-89.
20. Pikel E, Oscilowska I, Suprewicz Ł, et al. Peanut-Shaped Gold Nanoparticles with Shells of Ceragenin CSA-131 Display the Ability to Inhibit Ovarian Cancer Growth In Vitro and in a Tumor Xenograft Model. *Cancers* 2021; **13**(21).
21. Horcajada JP, Montero M, Oliver A, et al. Epidemiology and Treatment of Multidrug-Resistant and Extensively Drug-Resistant *Pseudomonas aeruginosa* Infections. *Clin Microbiol Rev* 2019; **32**(4).
22. Wnorowska U, Fiedoruk K, Pikel E, et al. Nanoantibiotics containing membrane-active human cathelicidin LL-37 or synthetic ceragenins attached to the surface of magnetic nanoparticles as novel and innovative therapeutic tools: current status and potential future applications. *Journal of nanobiotechnology* 2020; **18**(1): 3.
23. Radlinski L, Conlon BP. Antibiotic efficacy in the complex infection environment. *Current opinion in microbiology* 2018; **42**: 19-24.
24. Urish KL, Cassat JE. *Staphylococcus aureus* Osteomyelitis: Bone, Bugs, and Surgery. *Infect Immun* 2020; **88**(7): e00932-19.

25. Kodama J, Chen H, Zhou T, et al. Antibacterial efficacy of quaternized chitosan coating on 3D printed titanium cage in rat intervertebral disc space. *The spine journal : official journal of the North American Spine Society* 2021; **21**(7): 1217-28.
26. Wang Y, Borthwell RM, Hori K, et al. In vitro and in vivo methods to study bacterial colonization of hydrogel dermal fillers. *Journal of biomedical materials research Part B, Applied biomaterials* 2022; **110**(8): 1932-41.
27. Dao A, Mills RJ, Kamble S, Savage PB, Little DG, Schindeler A. The application of ceragenins to orthopedic surgery and medicine. *Journal of orthopaedic research : official publication of the Orthopaedic Research Society* 2020; **38**(9): 1883-94.
28. Niemirowicz K, Prokop I, Wilczewska AZ, et al. Magnetic nanoparticles enhance the anticancer activity of cathelicidin LL-37 peptide against colon cancer cells. *International journal of nanomedicine* 2015; **10**: 3843-53.
29. Kuroda K, Fukuda T, Okumura K, et al. Ceragenin CSA-13 induces cell cycle arrest and antiproliferative effects in wild-type and p53 null mutant HCT116 colon cancer cells. *Anti-cancer drugs* 2013; **24**(8): 826-34.
30. Piktel E, Prokop I, Wnorowska U, et al. Ceragenin CSA-13 as free molecules and attached to magnetic nanoparticle surfaces induce caspase-dependent apoptosis in human breast cancer cells via disruption of cell oxidative balance. *Oncotarget* 2018; **9**(31): 21904-20.
31. Fu J, Zhu W, Liu X, et al. Self-activating anti-infection implant. *Nature communications* 2021; **12**(1): 6907.
32. Lacefield WR. Current status of ceramic coatings for dental implants. *Implant dentistry* 1998; **7**(4): 315-22.
33. Mirkhalaf M, Dao A, Schindeler A, Little DG, Dunstan CR, Zreiqat H. Personalized Baghdadite scaffolds: stereolithography, mechanics and in vivo testing. *Acta biomaterialia* 2021; **132**: 217-26.
34. Schindeler A, Yu NY, Cheng TL, et al. Local delivery of the cationic steroid antibiotic CSA-90 enables osseous union in a rat open fracture model of Staphylococcus aureus infection. *The Journal of bone and joint surgery American volume* 2015; **97**(4): 302-9.